PACKER ENGINEERING INC,
1950 North Washington Street,
Naperville, IL 60566

Evaluation of Three DOT 3AL 6061-T6 Cylinders to Determine the Neck Cracks Cause and Initiation Site (CIS of Neck Cracks)

FINAL REPORT

August 19, 2010

Packer Project No. 501855

Prepared for
Mark Toughiry
Office of Hazardous Materials Technology
Pipeline and Hazardous
Materials Safety Administration
U.S. Department of Transportation

Purchase Order No. DTPH56-09-D-000022

P.O. Box 353 (60566-0353)
1950 N. Washington St. (60563-1366)
Naperville, IL
630.505.5722 Fax: 630.505.1986
www.packereng.com

6304 Woodside Court
Suite 110
Columbia, MD 21046
443.545.2000 Fax: 443.545.2001
www.packereng.com

1050 Highland Drive
Suite B
Ann Arbor, MI 48108-2262
734.786.5000 Fax: 734.786.5001
www.packereng.com

Table of Contents

Cause and Initiation Site of Neck Cracks of DOT-3AL Cylinders

1.0 INTRODUCTION

Objective: - The purpose of this investigation was to analyze the cylinder heads in order to determine the crack initiation site (CIS), crack type, the extent of crack propagation and the common cause of this type of cracks.

1.1 Technical Approach

In this project a total of three (3) gas cylinders that were manufactured from aluminum alloy 6061-T6 were analyzed to determine the cause and initiation of the neck indications. All three cylinders were reportedly designed and manufactured in accordance with DOT specification 3AL listed in title 49 CFR, §178.46 DOT - 3AL. The submitted cylinders bore serial numbers AR0119524, AR0118876 and AR0120056.

Upon arrival at Packer Engineering (Packer), the general condition of the cylinders was documented. All markings on the cylinder's surface were identified and recorded. Internal observations of the indications in the neck region were performed using a borescope. The cylinders were then cut open to expose the indications in the neck and head region.

Dye penetrant inspection was performed on each of the cylinder heads. To perform this task, each cylinder head was filled with liquid dye and place in a vacuum chamber for 25 minutes to ensure deep penetration of dye. The following testing was performed based upon the results of the dye penetrant inspection:

- Cylinder # AR0119524 was selected for a sustained load cracking test. The test was conducted in accordance with Annex B of ISO 7866. This testing was performed to determine sustained load cracking resistance. Cylinder #AR0119524 was also selected for chemical analysis, fractographic analysis, metallographic analysis, Rockwell hardness testing and tensile testing.

- Cylinder # AR0118876 was selected for assessing susceptibility to inter-crystalline corrosion as per Annex A of ISO 7866.

- Cylinder # AR0120056 was only visually inspected and this cylinder was saved in case any further testing was required.

2.0 GENERAL DOCUMENTATION OF THE CYLINDER

2.1 Visual Documentation and Cylinder Specifications

All three cylinders submitted to Packer Engineering were manufactured from aluminum alloy 6061-T6, and designed and manufactured in accordance with DOT specification 3AL listed in title 49 CFR, §178.46. These cylinders were in medical oxygen service for the Miami Dade Fire Department. The compressed oxygen used was reportedly in compliance with USP (United States Pharmacopoeia). The shipping ID of on all three cylinders was UN1072. The received cylinders are shown in Figure 1. All three cylinders were manufactured by Catalina.

1) DOT-3AL AR0119524

External and internal examination photos of the DOT – 3AL cylinder with serial number AR0119524 are shown in Figure 2 to 12.

- The cylinder was identified as XXX- XXX AR0119524 O2 CLIFF DIV 12 @ 03 TC – 3AL M139.
- It was marked as MDFR
- Lot # TV12V365C
  Capacity: 4.25 liters
  Expiration date: 12- 2013
- There were no indications observed on the outer surface of the cylinder. The paint on the cylinder was scratched at several locations near the head region.
- Two indications located at 199º and 267 º were pre-identified by the DOT on the external surface in the neck region of the cylinder as shown by Figure 13.
- Internal observation of the cylinder confirmed indications starting from the last thread of the neck region and extending in the shoulder at 199º and 267º location. The indications are shown in Figures 14 to 16. The cylinder showed no signs of corrosion on the inside.

2) DOT-3AL AR0118876

External and internal examination photos of the DOT – 3AL cylinder with serial number AR0118876 are shown in Figure 17 to 27.

- The cylinder was identified as DOT –XXX AR0118876 O2 Cliff Div 12@O3 TC- 3ALM139.
- Lot # TV05V346A
  Capacity: 4.25 liters
  Expiration date: 12- 2013

- There were no indications observed on the outer surface of the cylinder. The paint on the cylinder was scratched at several locations near the head region.
- Three indications located at 116º, around 250º and at 250º were pre-identified by the DOT on the external surface in the neck region of the cylinder as shown by Figure 28 and 29.
- Internal observation of the cylinder confirmed indications starting from the last thread of the neck region and extending into the shoulder at 116º, around 250º and at 250º locations. The indications are shown in Figures 30 to 32. The cylinder showed no signs of corrosion on the inside.

3) DOT-3AL AR0120056

External and internal examination photos of the DOT – 3AL cylinder with serial number AR0120056 are shown in Figure 33 to 43.

- The cylinder is identified as XXX- XXX AR0120056 O2 CLIFF DIV12 @O3 TC-3ALM139
- It was marked as MDFR
- Lot # TV08V352A
  Capacity: 4.25 liters
  Expiration date: 12-2013
- There were no visible indications observed on the outer surface of the cylinder. The paint on the cylinder was scratched at several locations near the head region.
- Two indications located at 170º and 220º were pre-identified by the DOT on the external surface in the neck region of the cylinder as shown by Figure 44.
- Internal observation of the cylinder confirmed indications starting from the last thread of the neck region and extending into the shoulder at the 170º and 220 º locations. The indications are shown in Figures 45 and 46. The cylinder showed no signs of corrosion on the inside.

3.0 VISUAL OBSERVATION AFTER MACHINING AND DYE PENETRANT TESTING OF THE CYLINDERS

All three cylinder heads were sectioned using a liquid cooled saw to expose the indications in the neck area. Figure 47 shows the location at which each cylinder head was sectioned. Figures 48 to 63 show the indications in the neck region of the three cylinders.

Each cylinder head containing indications was filled with liquid penetrant dye and placed in a vacuum chamber for 25 minutes to ensure deep penetration of the liquid dye. This set up may be viewed in Figure 64. The tank head removed from the vacuum chamber can be seen in Figure 65. After which the excess penetrant dye was removed from the surface and developer was applied rendering the indications visible. Figures 66 to 69 shows the indications in each of the cylinder heads revealed after dye penetrant testing. In general,

the indications observed during dye penetrant inspection corresponded with forming folds in the cylinder head. Following dye penetrant inspection, the folds were evaluated in more detail using a stereomicroscope.

Stereomicroscope examination could not determine if cracks may have been present under the forming folds or if the dye penetrant testing was resulting in "false indications" due to the dye being trapped in the folds. Stereoscope images of the indications and corresponding folds in each of the cylinder head can be seen in Figures 70 to 86.

Based on the dye penetration test, cylinder# AR0119524 was selected for sustained load cracking testing, chemical analysis, fractographic analysis, Rockwell hardness testing and tensile testing. Cylinder# AR0118876 was selected for assessing susceptibility to inter-crystalline corrosion as per Annex A of ISO 7866. Cylinder # AR0120056 was only visually inspected and this cylinder was saved in case any further testing was required.

4.0 ASSESSING SUSCEPTIBILITY TO INTER-CRYSTALLINE CORROSION

4.1 Machining and Preparing Coupon Surface before Etching

Cylinder# AR0118876 was tested as per Annex A of ISO 7866 to assess susceptibility to inter-crystalline corrosion. Four test samples of size 20 mm x 30 mm were sectioned from the head, body and base of the cylinder respectively as per Figure A.1 of the Annex A. Figures 87 and 88 show the samples machined for the corrosion test. The samples from the head had green paint. And these samples were polished using a 600 grit sand paper to remove the paint and coating. Figure 89 shows the samples after removing the surface coating on the outer surface. Figure 90 shows the inside surface of the samples prior to testing.

A solution of HNO_3, HF and H_2O was prepared and heated to a temperature of 95º C. All samples were suspended in the heated solution for 1 minute using Teflon wire. The test set-up can be seen in Figure 91. Following immersion the samples were washed using deionized water. The samples were then immersed in HNO_3 for 1 minute at room temperature to remove any copper deposits which may have formed. The samples were finally rinsed with deionized water as the last step prior to corrosion testing.

4.2 Corrosion Test

The test comprises using a corrosive solution that contains 57g/L of NaCl and ~ 3g/L of H_2O_2. The amount of H_2O_2 to be added was determined by titrating of H_2O_2 with $KMNO_4$ and H_2SO_4. The corrosive solution was placed in a large beaker and heated using a mantle. The samples were suspended using Teflon wire. The samples were etched for 6 hours in the corrosive media at a temperature of 30 º C ± 1 º C. The corrosion test set-up can be seen in Figures 92 to 93. After 6 hours the samples were washed in water

for about 30 seconds in 50% dilute HNO_3 and washed again in deionized water and finally dried using compressed air. Figures 94 and 95 show the samples after the corrosion test.

4.3 Preparation of Specimens for Examination

All samples were sectioned as shown in Figure 96 and one section of each coupon was mounted in epoxy resin. The sample sections of head, body and base of the cylinder were then mechanically polished using abrasive sand paper, a diamond compound and alumina polishing compound.

4.4 Results

The outer diameter (OD) and inner diameter (ID) of all the polished samples from the head, body and base were observed under an optical microscope for signs of inter-crystalline corrosion. As per ISO 7866 Annex A, for alloys with a crystal structure oriented in one direction through cold working, the depth of corrosion into each of the two faces which make up the internal and external surfaces of the cylinder should not exceed 0.1mm. The depth of the inter-crystalline attack in all the corrosion coupons was measured using a metallograph.

No inter-crystalline attack was observed in the four samples tested from the middle body of the cylinder. Inter-crystalline attack was observed in the samples taken from the head and the base of the cylinder. However, the depth of inter-crystalline attack in both the head and the base samples was ≤ 0.1 mm. This indicates that the 6061-T6 aluminum alloy used in the manufacturing of DOT - 3AL cylinders with serial number AR0119524 is not susceptible to inter-crystalline corrosion. The results of the corrosion attack are summarized in Table I. The metallograph images of the corrosion samples from the head, middle body and base of the cylinder can be seen in Figures 97 to 159.

Table I: Inter-crystalline corrosion depth of samples from the head, body and base compared to the ISO 7866 Annex A requirement.

Sample	Inter-crystalline attack depth	ISO 7866 Annex A requirement.
Head Sample 1 ID	0.02 mm	≤ 0.1 mm
Head Sample 1 OD	None	
Head Sample 2 ID	None	
Head Sample 2 OD	0.01 mm	
Head Sample 3 ID	None	
Head Sample 3 OD	None	
Head Sample 4 ID	None	
Head Sample 4 OD	None	
Middle Body Sample 1 ID	None	
Middle Body Sample 1 OD	None	
Middle Body Sample 2 ID	None	
Middle Body Sample 2 OD	None	
Middle Body Sample 3 ID	None	
Middle Body Sample 3 OD	None	
Middle Body Sample 4 ID	None	
Middle Body Sample 4 OD	None	
Base Sample 1 ID	None	
Base Sample 1 OD	0.04mm & 0.04 mm	
Base Sample 2 ID	None	
Base Sample 2 OD	0.10 mm	
Base Sample 3 ID	None	
Base Sample 3 OD	0.01 mm	
Base Sample 4 ID	None	
Base Sample 4 OD	0.07 mm & 0.1 mm	

5.0 SUSTAINED LOAD CRACKING RESISTANCE TEST

The sustained load cracking resistance test was conducted as per ISO-7866 Annex B. A constant tension load method was used for this test. Three samples from the neck area and five samples from the wall of cylinder # AR0119524 were machined according to the compact tension sample geometry listed in ISO 7639-6. Figures 160 and 161 show the machined compact tension test samples. A fatigue pre-crack was generated in these samples using a MTS machine. After pre-cracking, the compact tension samples were loaded at a constant load for 90 days at room temperature. The test set-up at the beginning of the test is shown in Figure 162. The test set up at the end of the 90 days can be seen in Figure 163. All samples were able to hold the load for 90 days. Figures 164 to 168 show the samples unloaded at the end of the test. After the 90 day test, the samples were post-fatigued until the specimen broke into two pieces. The samples after post-

fatigue and final failure can be seen in Figure 169. The dimension of the compact tension samples, pre-crack length and actual KIAPP are as shown in Table II. Samples 1, 5 and 8 from the wall area broke during pre-fatigue cracking.

Table II: Shows the sustained load crack testing parameters

Parameter	Sample 2	Sample 3	Sample 4	Sample 6	Sample 7
Location	Neck	Neck	Wall	Neck	Wall
Thickness (B)	0.150	0.150	0.150	0.150	0.150
Net width (W)	0.300	0.300	0.300	0.300	0.300
Min total Width (C)	0.375	0.375	0.375	0.375	0.375
Half Height (H)	0.180	0.180	0.180	0.180	0.180
Hole Diameter (D)	0.075	0.075	0.075	0.075	0.075
Half distance between hole out edges (F)	0.120	0.120	0.120	0.120	0.120
Max notch width (N)	0.020	0.020	0.020	0.020	0.020
Effective notch length (l) (range)	0.075	0.075	0.075	0.075	0.075
Effective crack length (a) (range)	0.135	0.135	0.135	0.135	0.135
Crack length (a) in	0.1455	0.1400	0.1385	0.1920	0.2370
a/w	0.485	0.466	0.461	0.64	0.79
Y	9.229	8.745	8.620	16.12	38.122
K1APP (ksi/in2)	2.8	2.8	2.8	2.8	2.8
Target load p (lbs)	24.924	26.304	26.68	14.27	6.034
Actual applied load (lbs)	25	27.5	27.5	15.0	7.5
K1APP according to actual applied load	2.81	2.93	2.89	2.94	3.48

Following the post-fatigue test, the fracture surface of the samples was observed using a scanning electron microscope (SEM). SEM observation of the three samples from the neck and two samples from the wall of cylinder # AR0119524 were made between the fatigue pre-crack and post-fatigue crack interface. The distance between the pre-fatigue and post-fatigue cracks was measured. The measurements were taken perpendicular to the pre- and post-fatigue cracks at 25%, 50% and 75% thickness locations for all the specimens.

ISO-7866 Annex B states that if the average distance between the pre- and post-fatigue cracks does not exceed 0.16 mm, the sample passes the test. If all samples pass, the alloy/process is qualified. In all the 5 samples tested, no signs of dimples were observed until the final fracture region. All the samples showed presence of fatigue striations at the fatigue pre-crack interface and even beyond the 0.16 mm distance from the pre-fatigue crack. There was no demarcation between the pre-and post-fatigue crack in all the

samples. This indicates that the fatigue pre-crack didn't propagate during the 90 day constant load test.

In order to demonstrate that the fatigue pre-crack didn't propagate during the test, a line was marked on the SEM image at the fatigue pre-crack interface and another line was marked at 0.16 mm distance from the fatigue pre-crack. This was done at 75X and 200X magnifications for each sample. Also, at the pre -fatigue crack interface SEM images were taken at 650 X and 2000X magnifications to show the fatigue striations. Then the SEM was moved from the fatigue pre-fatigue crack interface by 0.16 mm and SEM images were taken at 650X and 2000X magnifications to show the fatigue striations in the post-fatigue zone. This was done at 25%, 50% and 75% thickness for all samples. The SEM images for all the samples can be seen in Figures 171 to 259.

6.0 METALLURGICAL EVALUATION

Chemical analysis and fractographic and metallographic analysis was performed on cylinder # AR0119524.

6.1 Chemical Analysis

Chemical analysis of the subject DOT-3AA cylinder with serial number AR0119524 was compared to heat treatable aluminum alloy 6061 materials authorized for DOT-3AL cylinders by the Code of Federal Regulations (CFR) 49, Chapter I –Pipeline and Hazardous Materials Safety Administration, Department of transportation Subchapter A-Specification for Packaging's, Specifications for 3AL seamless aluminum cylinders, part § 178.46. The chemical analysis results and specification are shown in Table III. The composition of DOT-3AL cylinder AR0119524 meets the specifications for 6061.

Table III: Comparison of the chemistry of the DOT -3AL cylinder AR0119524 with the heat treatable aluminum 6061 authorized for DOT-3AL cylinder as per 49 CFR part § 178.46

Elements	AR0119524 Composition (Wt %)	6061-T6 Composition (Wt %) as per CFR 49 part § 178.46
Silicon (Si)	0.62	0.4 – 0.8
Iron (Fe)	0.16	0.7 max
Copper (Cu)	0.31	0.15 - 0.40
Manganese (Mn)	0.01	0.15 max
Magnesium (Mg)	0.94	0.8 - 1.2
Chromium (Cr)	0.08	0.04 – 0.35
Lead (Pb)	<0.005	0.005 max
Zinc (Zn)	<0.1	0.25 max
Tin (Sn)	<0.1	-
Titanium (Ti)	0.1	0.15 max
Max other (each)	<0.5	0.05
Max others (total)	<0.15	0.15
Aluminum	Rest	Rest

6.2 Fractographic and Metallographic Analysis:

A section from the neck region of the cylinder AR0119524 was cut as shown in Figures 260 and 261 for fractographic analysis. In the neck region, indications were observed in the forming fold of the cylinder. Three sections identified as Sections 1 to 3 in Figure 261 were cut with each containing a forming fold. Section 1 from the neck region containing the forming fold was observed using a scanning electron microscope (SEM).

SEM examination revealed a crack coincided with the forming fold in the neck region and this may be viewed in Figures 262 to 264. To evaluate the crack in more detail, the section was back cut to expose the fracture surface. Visual and SEM examination revealed an oxide layer on the fracture surface. To understand the composition of the coating an Elemental Dispersive Spectroscopy (EDS) was performed on the fracture surface. The deposit was found to be composed of aluminum (Al), silicon (Si), Magnesium (Mg) and oxygen (O). The EDS spectra of the deposit can be viewed in Figure 265.

The fracture surface was then ultrasonically cleaned using a 100% HNO3 solution. Despite several attempts, the oxide layer was found to be too tenacious to remove without damaging the underlying fracture surface. A stereoscope image of the fracture surface following cleaning can be seen in Figure 266. The cleaned fracture surface was then observed under the SEM. SEM examination revealed the oxide layer was still obstructing most of the fracture surface. The fracture surface was found to be heavily damaged as a

result of relative movement (rubbing) between the two mating fracture surfaces. SEM images of the fracture surface can be seen in Figures 267 to 270.

Sections 2 and 3 were then cut at the locations shown in Figures 271 and 272. Each fold was cut at two locations identified as plane 1 and plane 2. These sections were then mounted and polished using standard laboratory metallography techniques. The samples were then etched using Keller's etchant. Examination of the polished and etched cross sections confirmed the presence of cracking in the forming fold at both planes 1 and 2. The cracks were found to propagate from the ID surface of the neck region towards the OD surface. The depth of the cracks ranged from 0.15 – 1.26 mm and the crack in plane 1 was deeper than that in plane 2. The microstructure images can be viewed in Figures 273 to 287.

7.0 MECHANICAL PROPERTY EVALUATION

Samples for Rockwell hardness testing and tensile testing were performed on a sample from cylinder # AR0119524

7.1 Rockwell Hardness:

Rockwell hardness testing was performed on the cylinder sample in accordance with ASTM E18-98. The results of the Rockwell hardness testing are shown in Table IV.

Table IV: Rockwell Hardness Data (HRB) of cylinder # AR0119524.

Location	Hardness (HRB)
1	57
2	57
3	55
4	56
5	58
Average	57

7.2 Tensile Test

Three tensile samples were prepared from cylinder # AR0119524 to determine the strength and elongation. The results of the tensile tests were compared to the 6061-T6 tensile properties listed by the Code of Federal Regulations (CFR) 49, Chapter I – Pipeline and Hazardous Materials Safety Administration, Department of Transportation Subchapter A- Specification for Packaging's, Specifications for 3AL Seamless aluminum cylinders, part § 178.46. Based on the comparison, the cylinder met the tensile property requirements of 6061-T6 alloy. The tensile results are presented in Table V.

Table V: Tensile Results of Cylinder # AR0119524

Property	AR0119524 Sample 1	AR0119524 Sample 2	AR0119524 Sample 3	6061-T6 property as per CFR 49 part § 178.46
Yield Strength (ksi)	49.5	53.4	50.3	38 min
Tensile Strength (ksi)	54.4	57.5	54.3	35 min
Elongation (%)	14	15	14	14%

8.0 DISCUSSION

External and internal inspection was performed on all three cylinders with serial numbers AR0119524, AR0118876 and AR0120056. In all three cylinders indications were observed in the neck area. The head of all three cylinders were cut open to expose the indication. Forming folds were observed in all three cylinders. Dye penetrant testing revealed indications corresponding with the folds in all three cylinder heads. Stereoscope examination could not conclusively determine if cracks may have been present under the forming folds or if the dye penetrant was resulting in false-indications due to dye trapped in folds.

Cylinder# AR0118876 was selected for assessing susceptibility to inter-crystalline corrosion as per Annex A of ISO. As per the standard, alloys with a crystal structure oriented in one direction through cold working, the depth of corrosion into each of the two faces which make up the internal and external surfaces of the cylinder should not exceed 0.1mm. No inter-crystalline attack was observed in the four samples tested from the middle body of the cylinder. Inter-crystalline attack was observed in the samples taken from the head and the base of the cylinder. However, the depth of inter-crystalline attack in both the head and the base samples was $\leq$ 0.1 mm. This indicates that the 6061-T6 aluminum alloy used in the manufacturing of DOT - 3AL cylinders with serial number AR0119524 was not susceptible to inter-crystalline corrosion.

Cylinder # AR0119524 was selected for sustained load cracking test. The test was conducted based on Annex B of ISO 7866. Three samples from the neck area and two samples from the wall area were tested. The standard requires that if the average distance between the pre- and post-fatigue cracks does not exceed 0.16 mm, the samples pass the test. If all samples pass, the alloy/process is qualified. No evidence of dimpled rupture fracture was observed in any of the samples tested from cylinder AR0119524 until the final fracture region. All samples showed presence of fatigue striations at the fatigue pre-crack interface and even beyond the 0.16 mm distance. There was no demarcation between the pre-and post fatigue crack in all the samples. These results indicate that the fatigue pre-crack did not propagate during the 90 day constant load test.

Cylinder #AR0119524 was also selected for chemical analysis, fractographic analysis, metallographic analysis, Rockwell hardness testing and tensile testing. The composition of the DOT-3AL cylinder # AR0119524 met the specifications for 6061 listed in CFR 49 part § 178.46. Fractographic analysis confirmed that the indications observed in the forming folds were indeed cracks. One of the cracks was opened and observed in the SEM. A tenacious oxide was adhered to the entire fracture surface which could not be removed without damaging under the underlying fracture. However, SEM examination revealed relative motion in the way of rubbing between the two mating fracture surfaces indicating the crack had been present for sometime and possibly propagating by fatigue. Metallographic sections of the crack confirmed the depth of the cracks ranged from 0.15 – 1.26 mm.

As per the information provided, the subject cylinders were back extruded, threaded and then solution aged. Following forming, the ID surface was inspected using lights and mirrors. The indications examined during the present investigation were found by DOT during their first qualifications after 5 years of service using eddy current methods. Based on the fractographic analysis, corrosion and sustained load crack testing it appears that either these cracks were pre-existing or formed due to fatigue. The folds observed in the neck region act as a source of stress-concentration and would increase the susceptibility to crack initiation during service.

ISO-7866 section 11.6 requires that all the cylinders be examined for neck folds by a suitable means (e.g. introscope, tactile, ultrasonic etc). Folds that are visible as lines running into the thread portion shall be removed by a machining operation until the lines are no longer visible. After machining, the thickness of the machined area and the thread's characteristics shall be least those required to pass all necessary testing. The whole internal shoulder area shall be re-inspected to verify that folding or its lines have been removed. However, all three cylinders with serial numbers AR0119524, AR0118876 and AR0120056 had forming folds in the neck area running into the thread portion. Hence, all the three cylinders do not meet the ISO-7866 section 11.6 requirement.

The tensile properties of the cylinder # AR0119524 meets the specifications for 6061-T6 listed in CFR 49 part § 178.46

9.0 CONCLUSIONS

Based on the above testing the following can be concluded.

- The indications observed during visual and dye penetration testing were cracks located inside of the shoulder's folds and neck of the cylinders.
- Based on ISO 7866 section A 1.7 it is permissible that the inter-crystalline attack shall not exceed 0.1 mm. Therefore, this would not constitute the alloy (aluminum alloy 6061-T6) of this cylinder to be susceptible to inter-crystalline corrosion.
- Based on ISO 7866 section B.7.3 in the samples tested for sustained load cracking, if the average measured distance between the two fatigue cracks doesn't exceed 0.16 mm, the specimen passes the test. If all specimens pass, the alloy/process is qualified. In the sustained load cracking test performed on the cylinder no evidence of dimpled rupture fracture was observed until the final fracture region. All samples showed presence of fatigue striations at the fatigue pre-crack interface and even beyond the 0.16 mm distance. There was no demarcation between the pre-and post fatigue crack in all the samples. Therefore the cylinder material (aluminum alloy 6061-T6) is not susceptible to sustained load cracking.
- The chemistry of the cylinder meets the specifications for aluminum alloy 6061 listed in CFR 49 part § 178.46.
- The tensile properties of the cylinder meets the specifications for aluminum alloy 6061-T6 listed in CFR 49 part § 178.46.
- The cracks found in the neck folds were either pre-existing or formed due to fatigue while in service.

This concludes the evaluation of three DOT-3AL 6061-T6 cylinder with serial number AR0119524, AR0118876, and ARO120056. If you have questions or need additional information, please contact the undersigned at mpareek@packereng.com or 630-577-1930.

Sincerely,

PACKER ENGINEERING, INC.

Mridula L Pareek
Engineering Technologist

Kevin L. Jones, P.E.
Director

10.0 FIGURES

Figure 1: Shows the three received DOT 3-AL cylinders with serial number AR0119524, AR0118876 and AR0120056

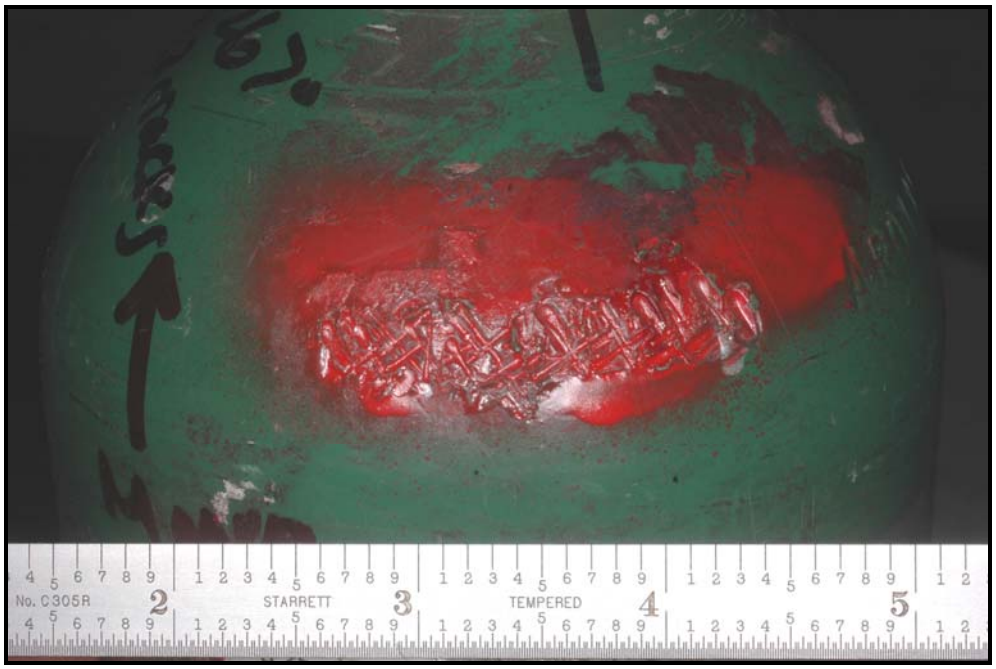

Figure 2: Indented marking on the DOT-3AL cylinder # AR0119524

Figure 3: Indented marking on the DOT-3AL cylinder # AR0119524

Figure 4: Indented marking on the DOT-3AL cylinder # AR0119524

Figure 5: Indented marking on the DOT-3AL cylinder # AR0119524

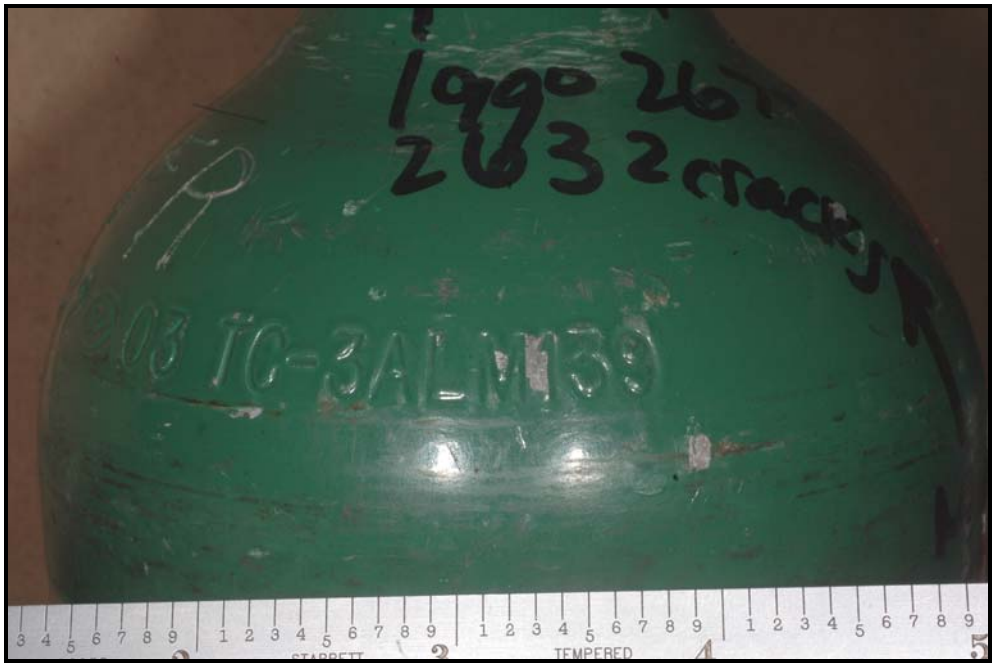

Figure 6: Indented marking on the DOT-3AL cylinder # AR0119524

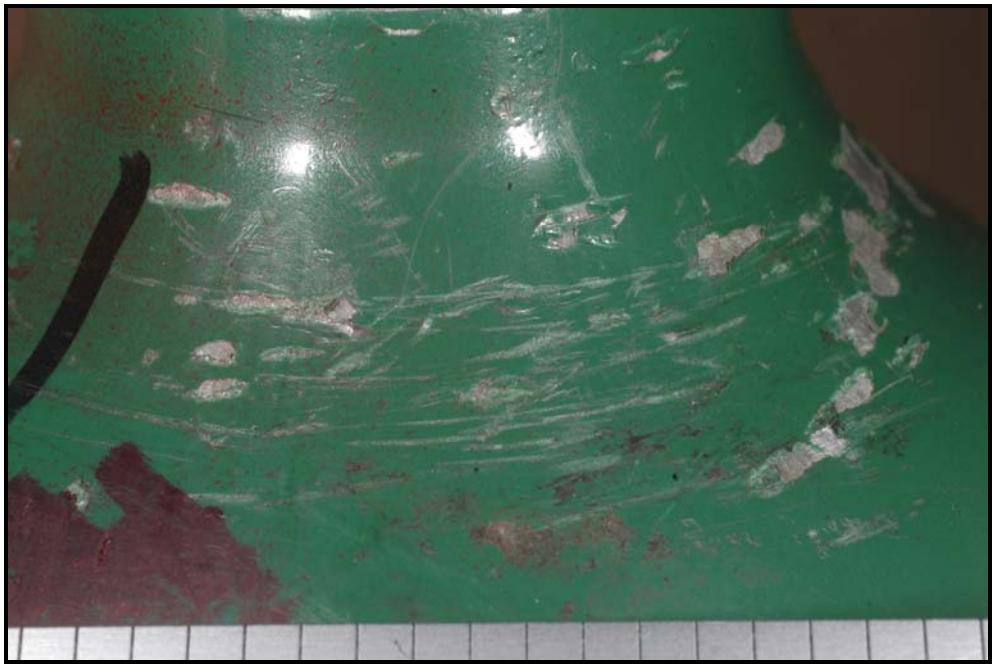

Figure 7: Shows the scratched paint on the cylinder # AR0119524.

Figure 8: Shows the inscribed letter on the cylinder # AR0119524.

Figure 9: Shows the label on the cylinder # AR0119524.

Figure 10: Shows the neck and the shoulder region of the cylinder # AR0119524.

Figure 11: Shows the labels on the cylinder # AR0119524.

Figure 12: Shows the labels on the cylinder # AR0119524.

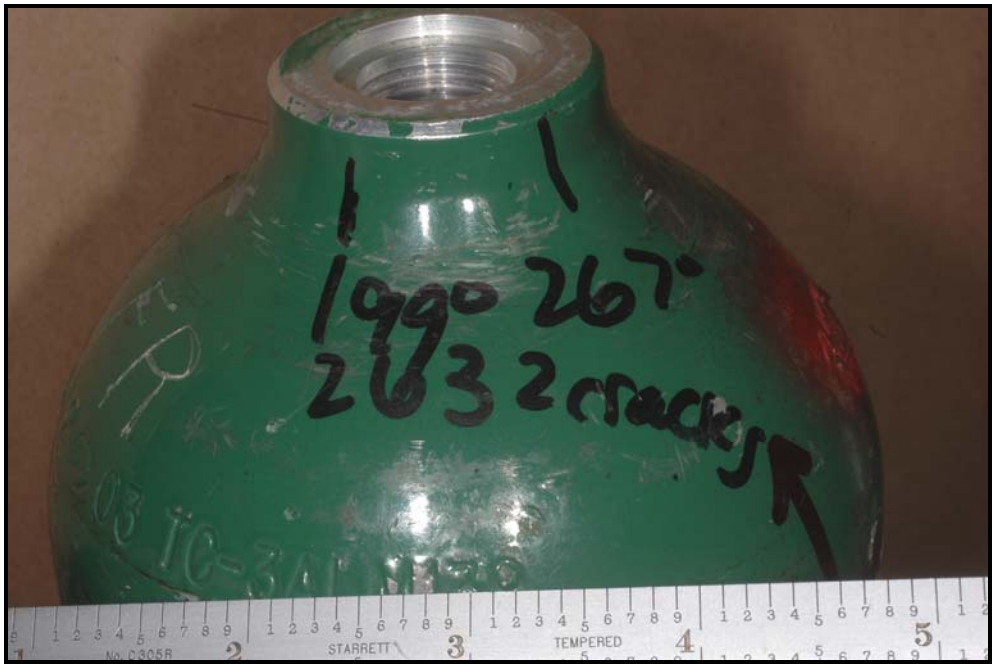

Figure 13: Shows the location of the indications pre-identified by DOT on the cylinder # AR0119524.

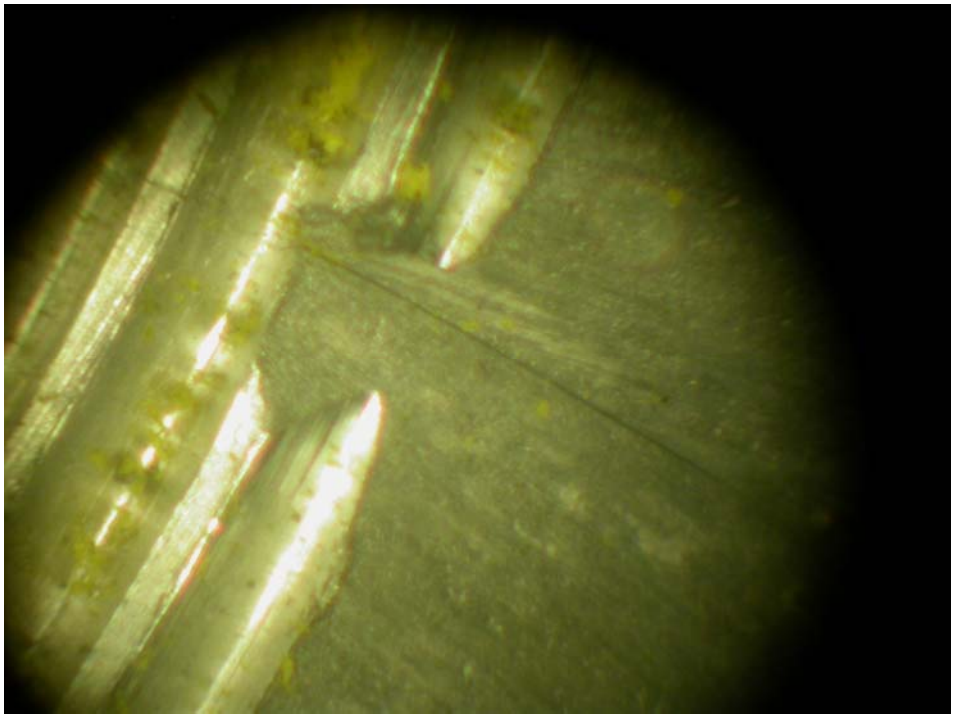

Figure 14: Shows borescope image of the indication in the shoulder area of DOT-3AL cylinder # AR0119524 at 199º location identified in Figure 13.

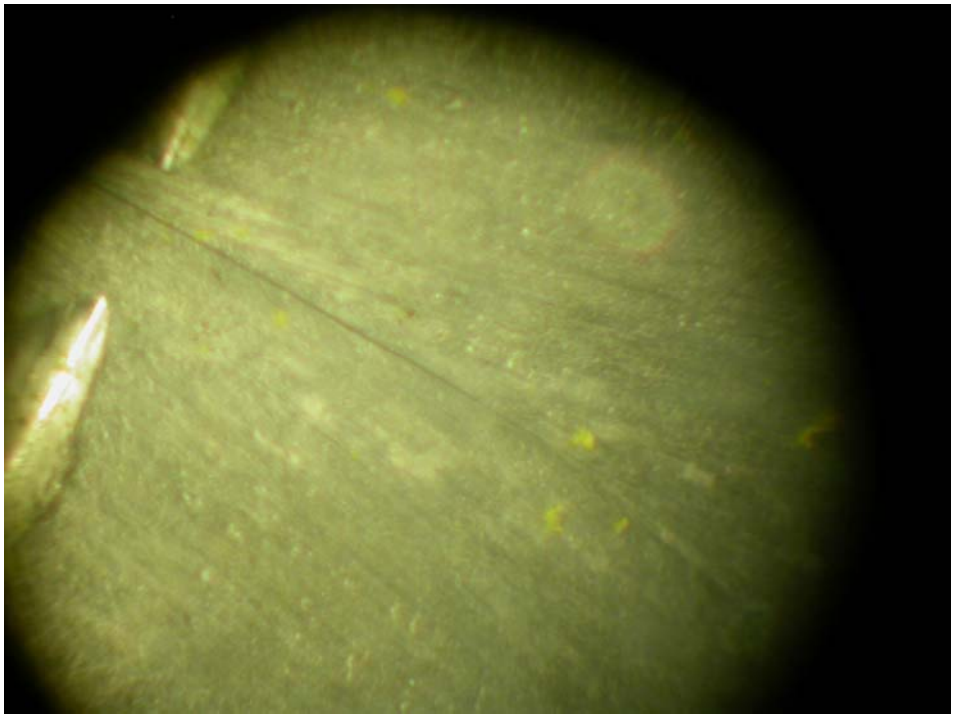

Figure 15: Shows borescope image of the indication in the shoulder area of DOT-3AL cylinder # AR0119524 at 199º location identified in Figure 13.

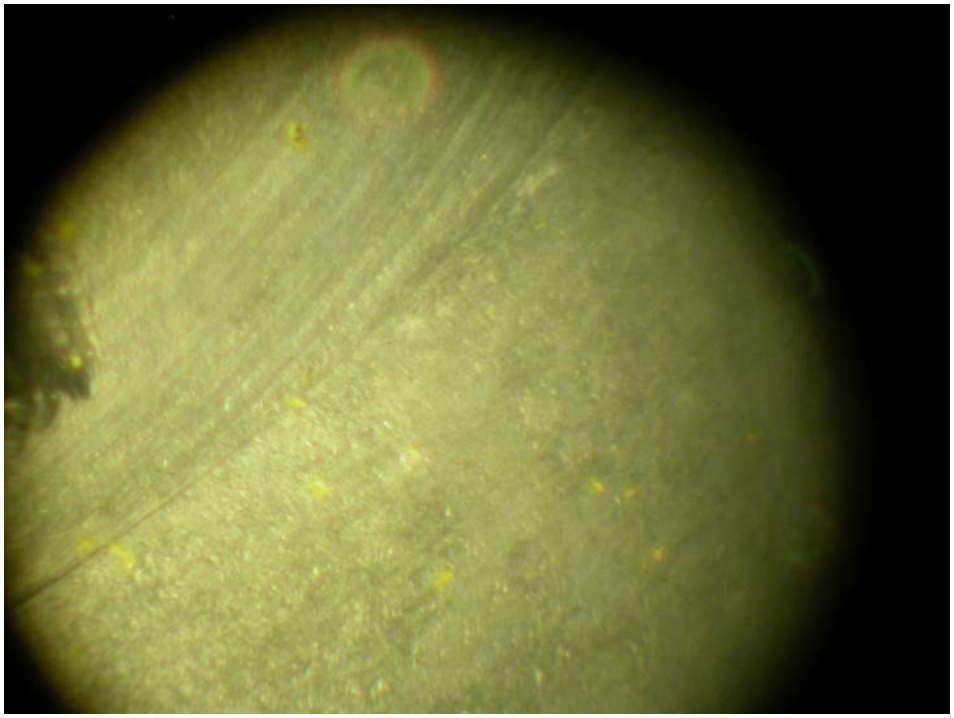

Figure 16: Shows borescope image of the indication in the shoulder area of DOT-3AL cylinder # AR0119524 at 267º location identified in Figure 13.

Figure 17: Indented marking on the DOT-3AL cylinder # AR0118876

Figure 18: Indented marking on the DOT-3AL cylinder # AR0118876

Figure 19: Indented marking on the DOT-3AL cylinder # AR0118876

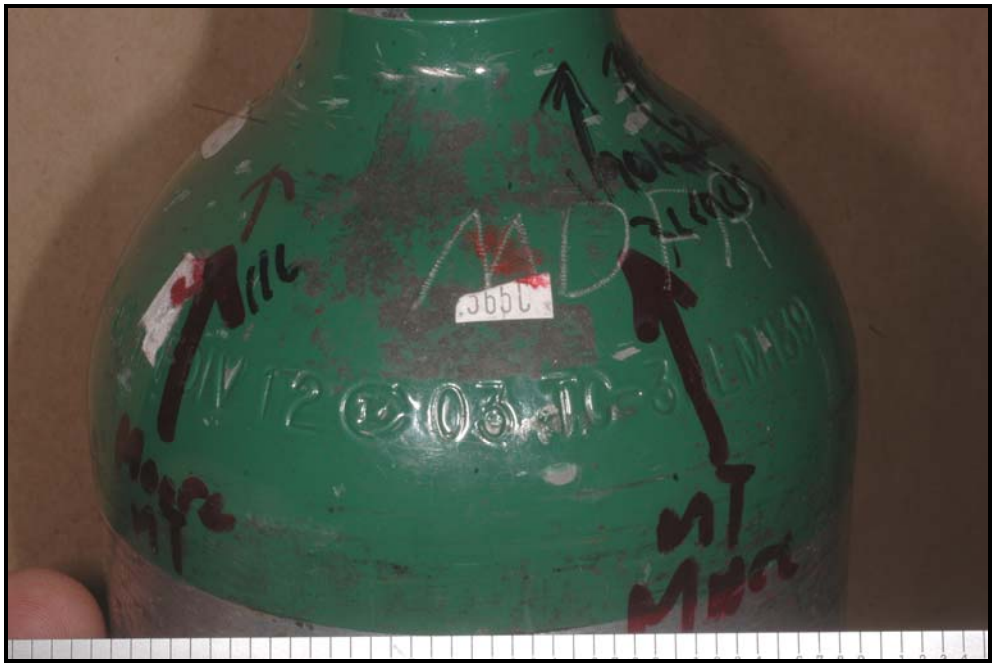

Figure 20: Indented marking on the DOT-3AL cylinder # AR0118876

Figure 21: Indented marking on the DOT-3AL cylinder # AR0118876

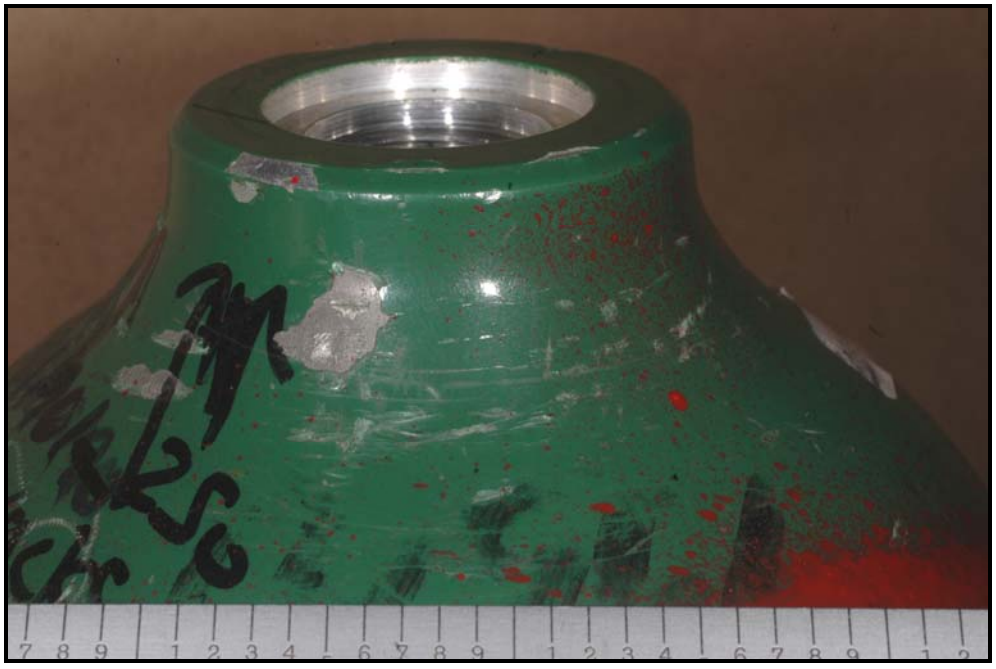

Figure 22: Shows the scratched paint on the cylinder # AR0118876.

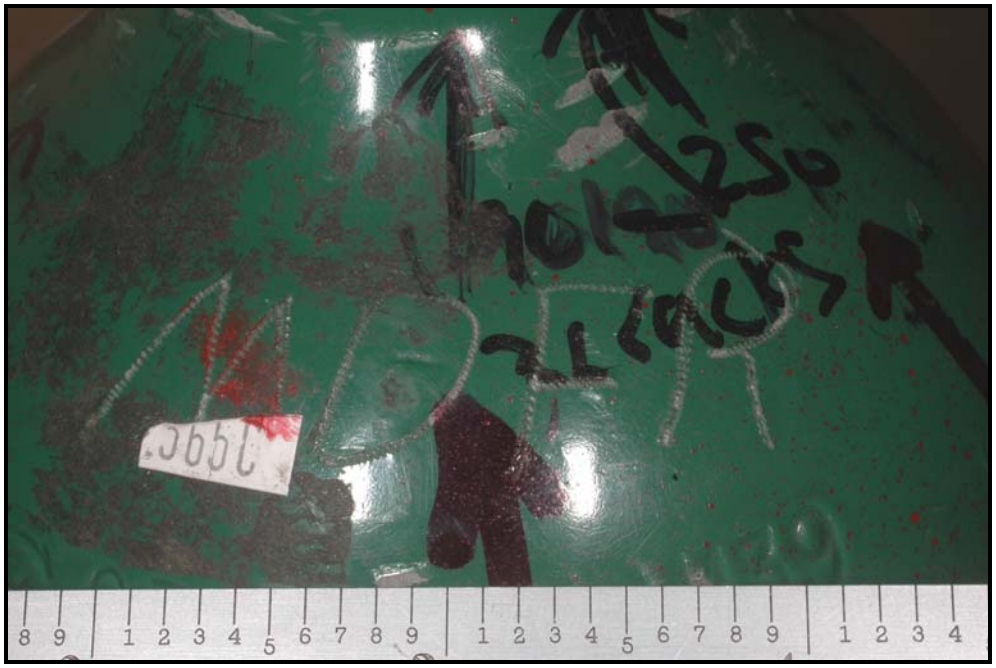

Figure 23: Shows the inscribed letter on the cylinder # AR0118876.

Figure 24: Shows the label on the cylinder # AR0118876.

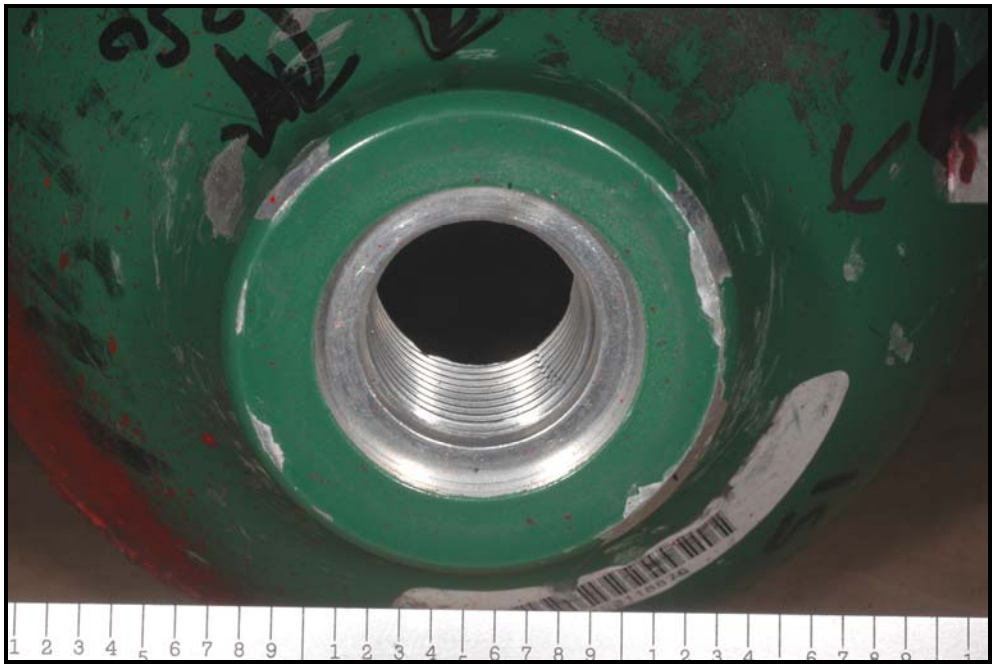

Figure 25: Shows the neck and the shoulder region of the cylinder # AR0118876

Figure 26: Shows the labels on the cylinder # AR0118876.

Figure 27: Shows the labels on the cylinder # AR0118876.

Figure 28: Shows the location of the indications pre-identified by DOT on the cylinder # AR0118876.

Figure 29: Shows the location of the indications pre-identified by DOT on the cylinder # AR0118876.

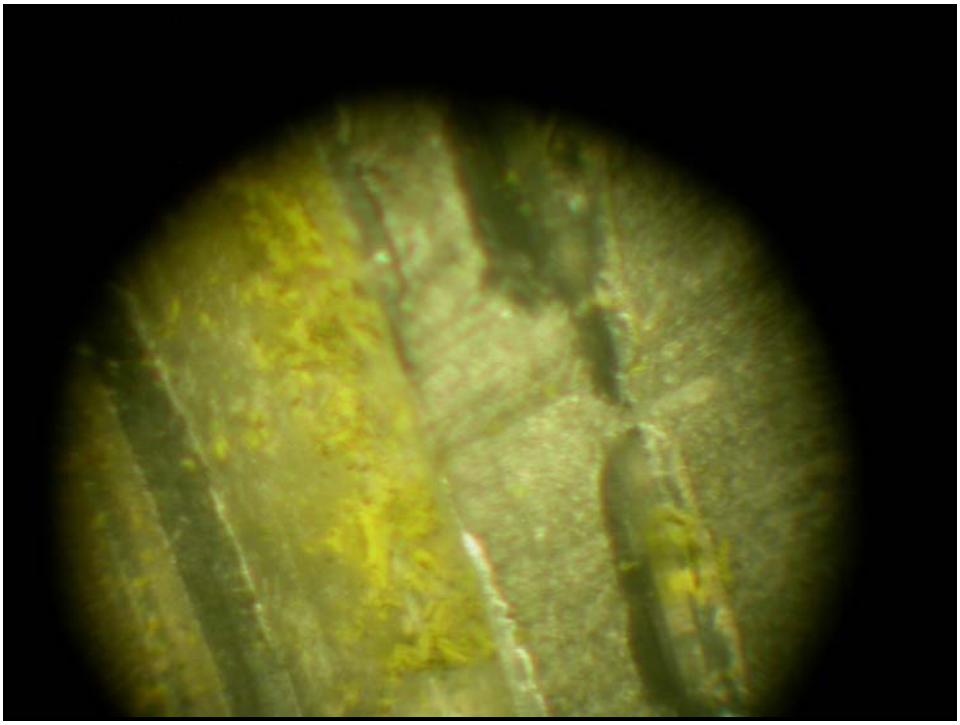

Figure 30: Shows borescope image of the indications in the shoulder area of DOT-3AL cylinder # AR0118876 at 116º location identified in Figure 29.

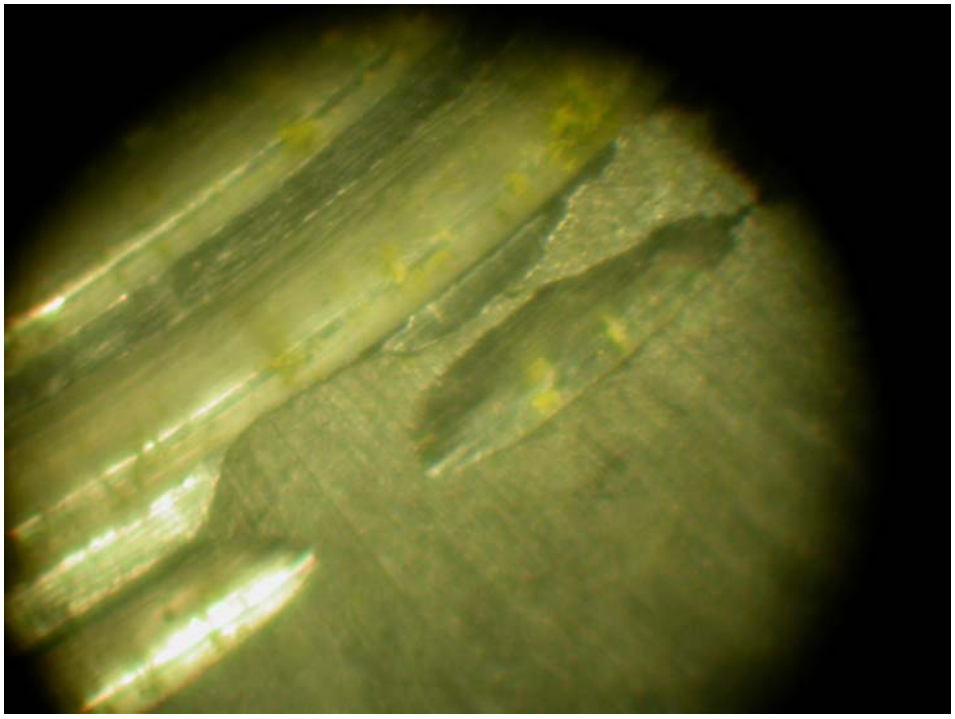

Figure 31: Shows borescope image of the indications in the shoulder area of DOT-3AL cylinder # AR0118876 at near 250º location identified in Figure 28.

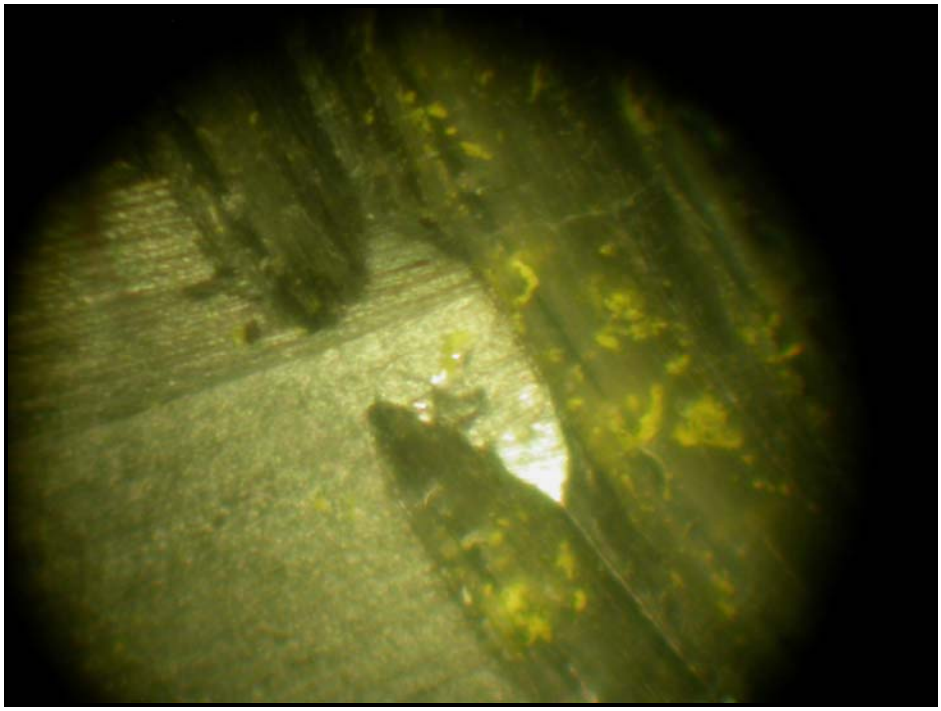

Figure 32: Shows borescope image of the indications in the shoulder area of DOT-3AL cylinder # AR0118876 at 250º location identified in Figure 28.

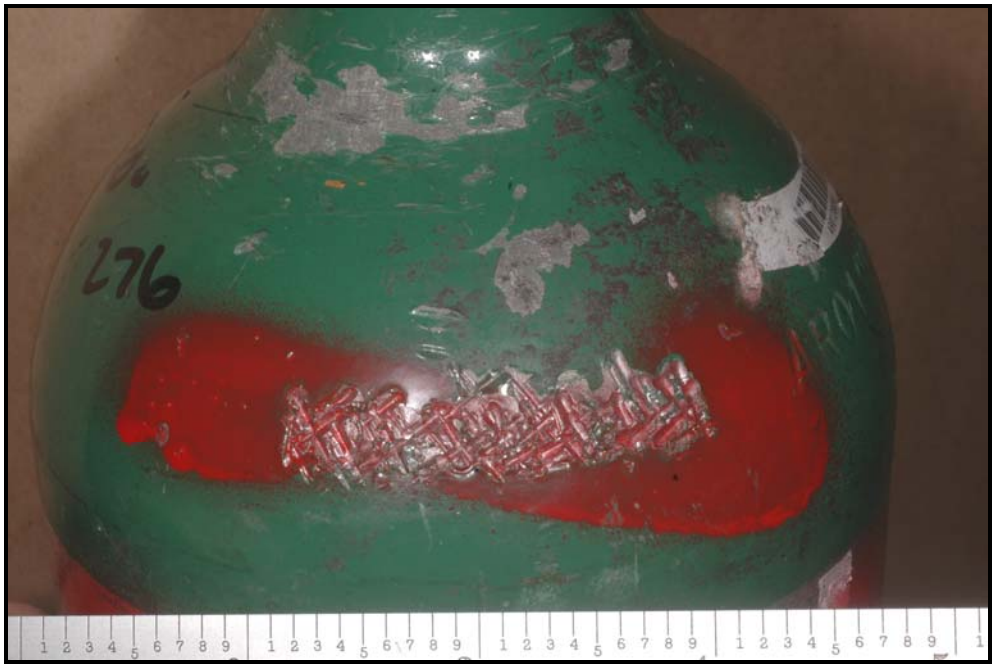

Figure 33: Indented marking on the DOT-3AL cylinder # AR0120056.

Figure 34: Indented marking on the DOT-3AL cylinder # AR0120056.

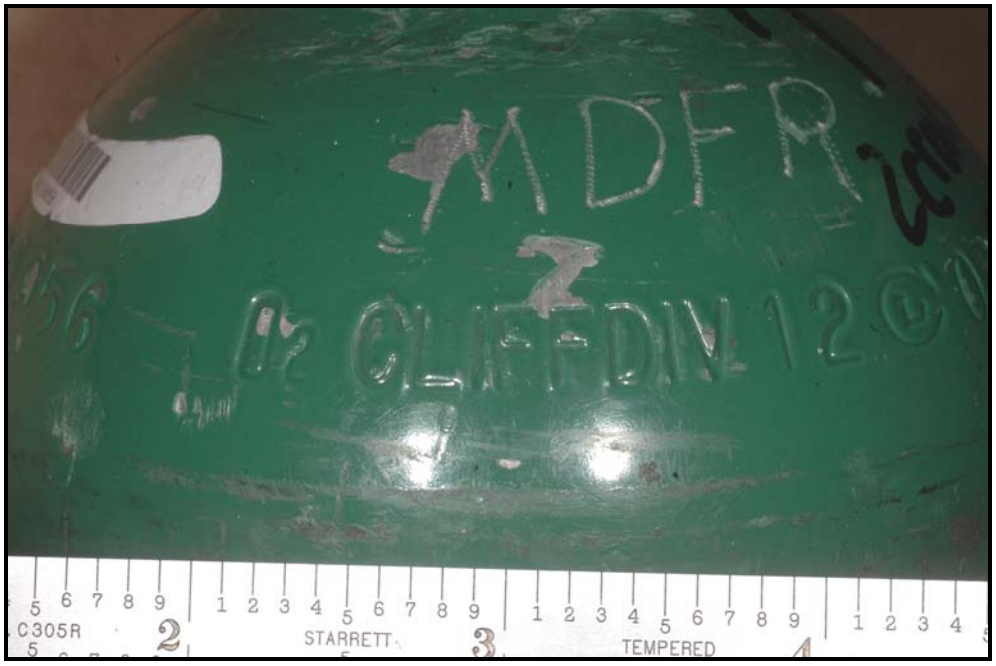

Figure 35: Indented marking on the DOT-3AL cylinder # AR0120056.

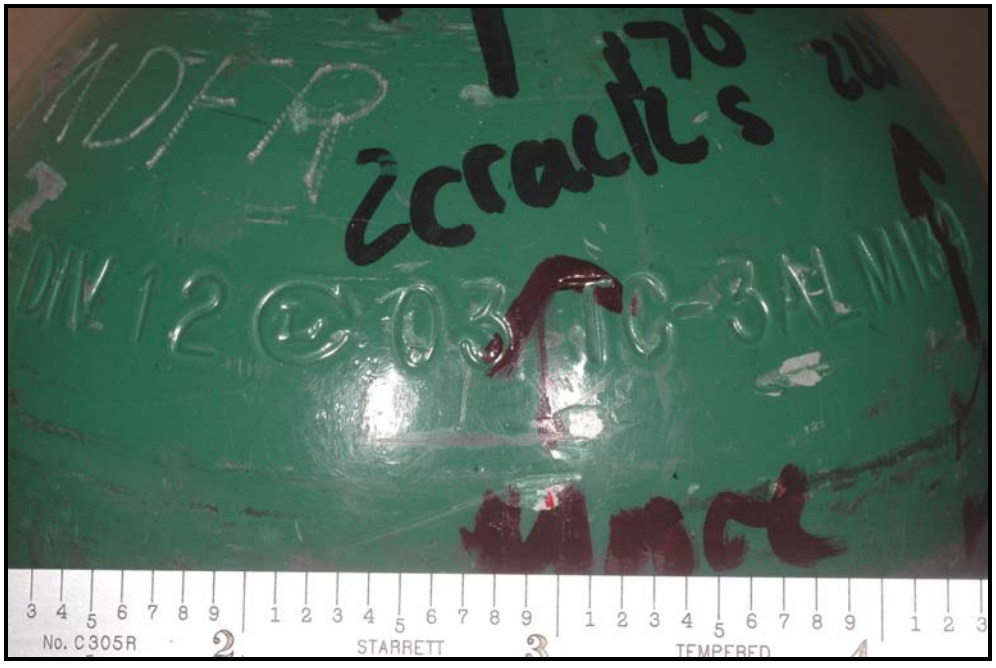

Figure 36: Indented marking on the DOT-3AL cylinder # AR0120056.

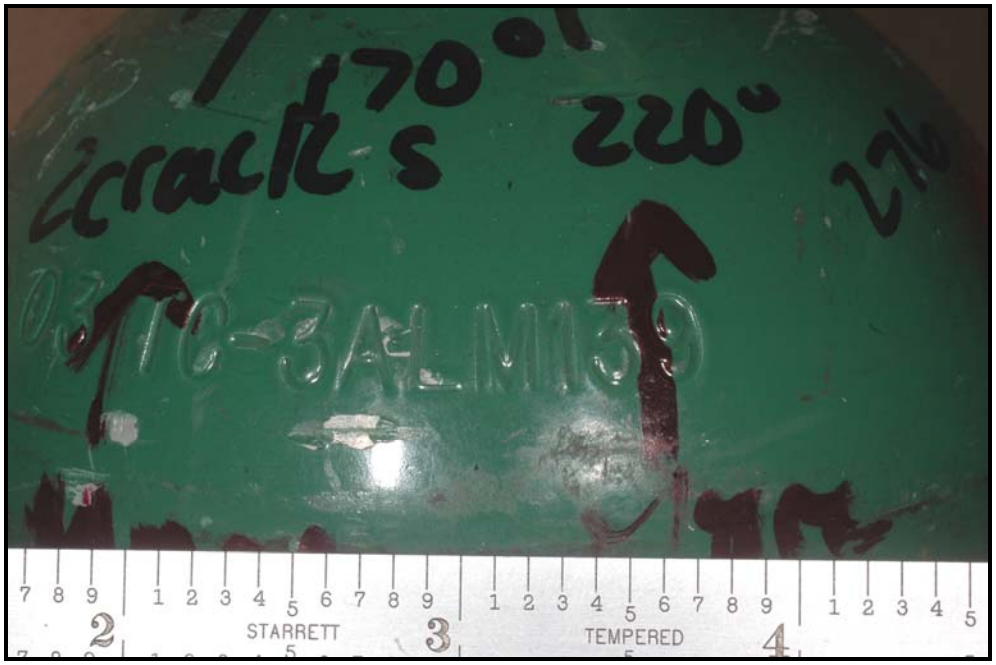

Figure 37: Indented marking on the DOT-3AL cylinder # AR0120056.

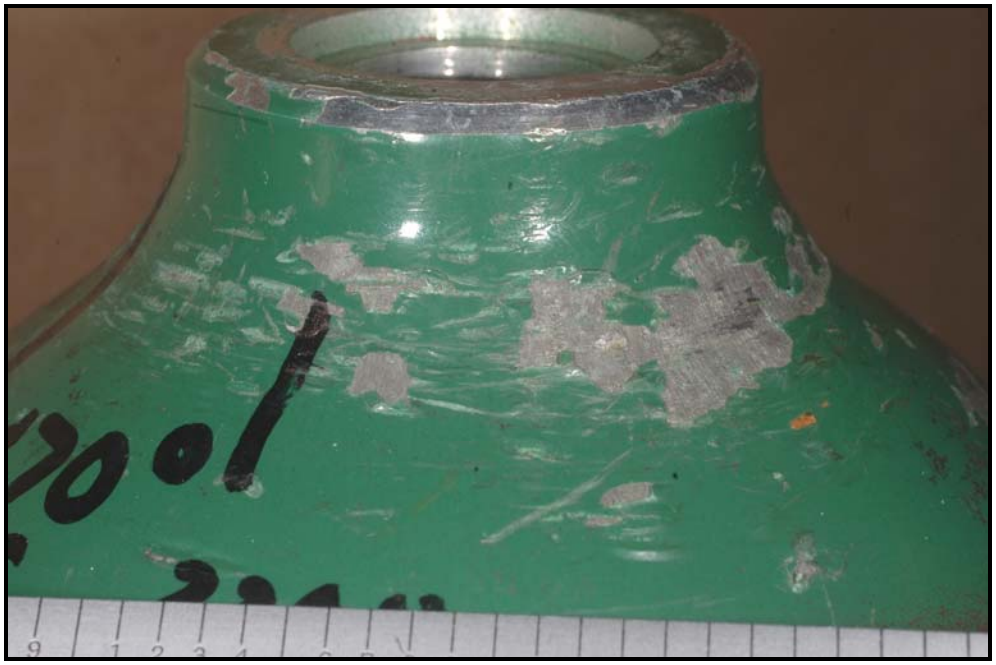

Figure 38: Shows the scratched paint on the cylinder # AR0120056.

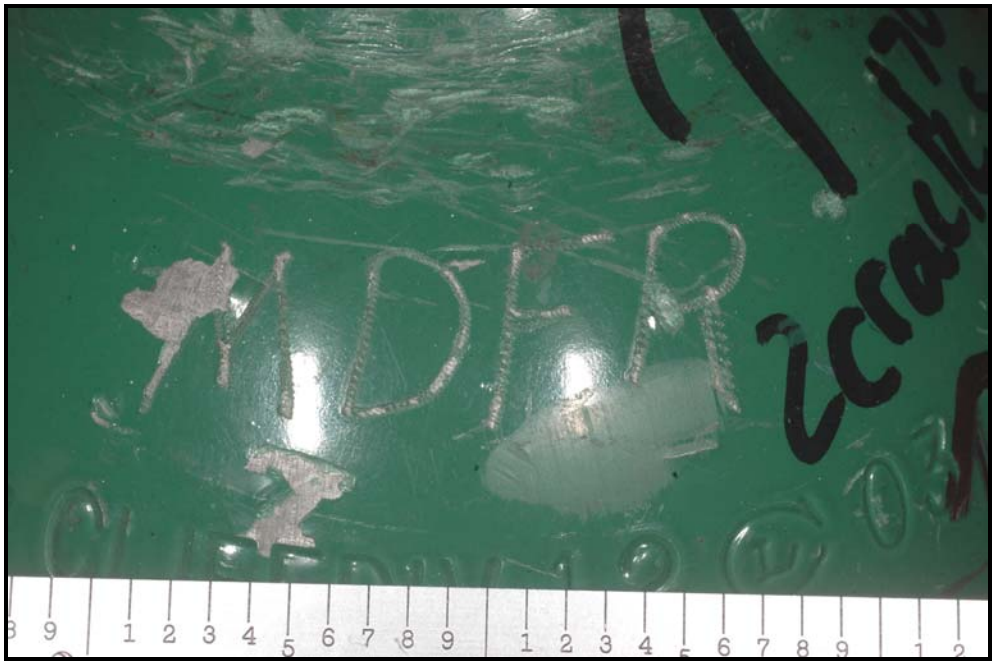

Figure 39: Shows the inscribed letter on the cylinder # AR0120056.

Figure 40: Shows the label on the cylinder # AR0120056.

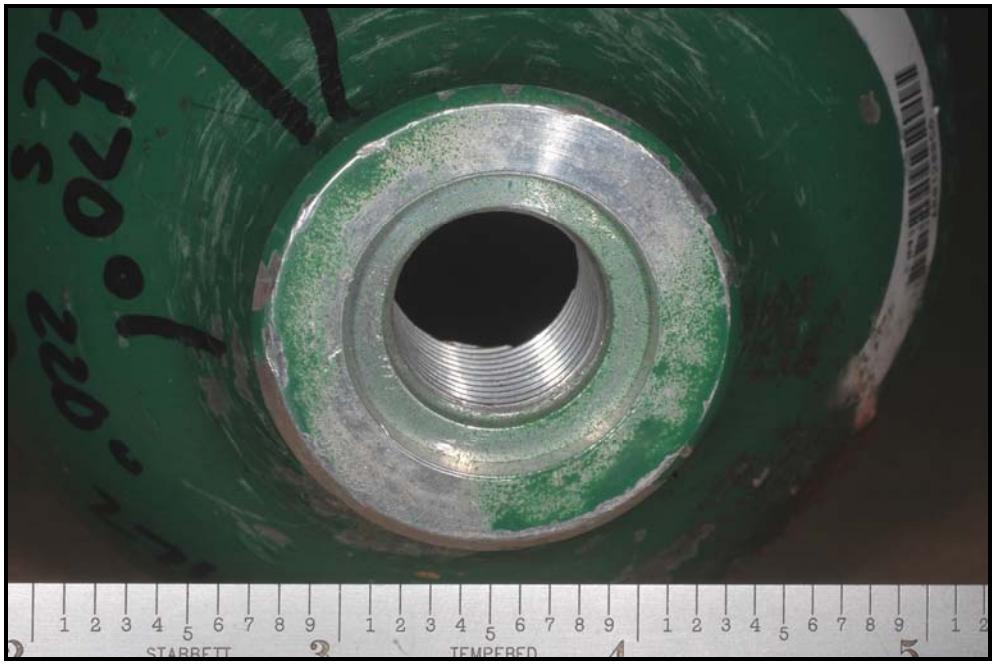

Figure 41: Shows the neck and the shoulder region of the cylinder # AR0120056.

Figure 42: Shows the labels on the cylinder # AR0120056.

Figure 43: Shows the labels on the cylinder # AR0120056.

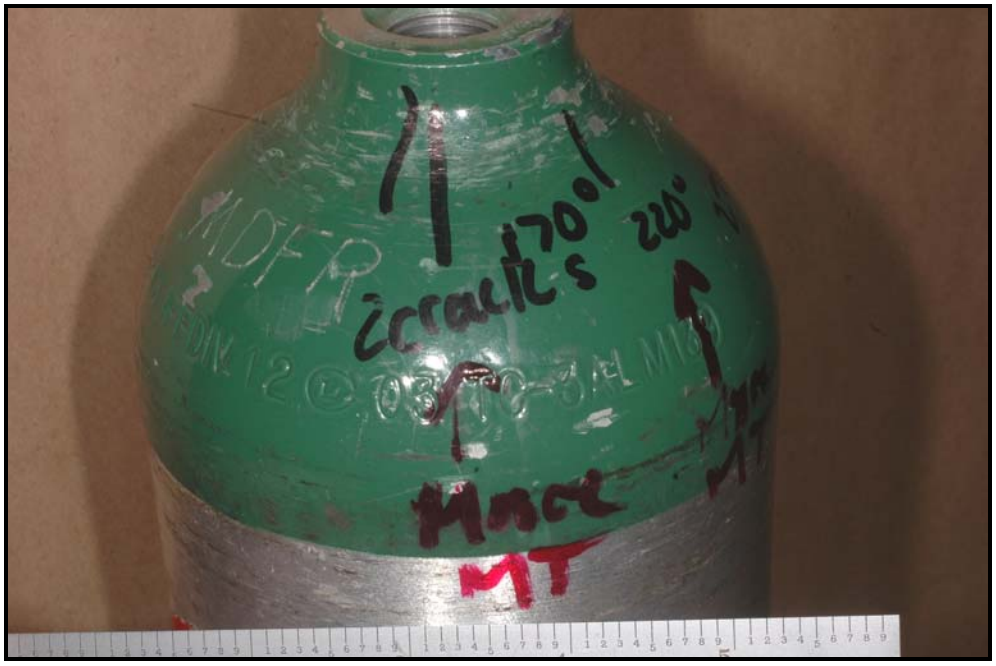

Figure 44: Shows the location of the indications pre-identified by DOT on the cylinder # AR0120056.

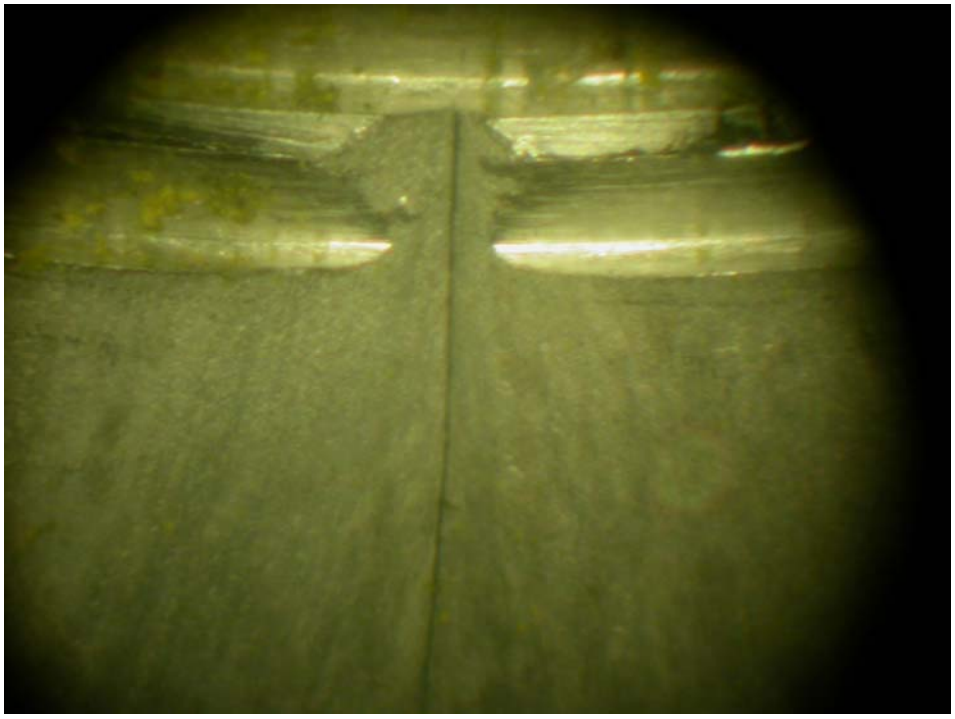

Figure 45: Shows borescope image of the indication in the shoulder area of DOT-3AL cylinder # AR0120056 at 170º location identified in Figure 44.

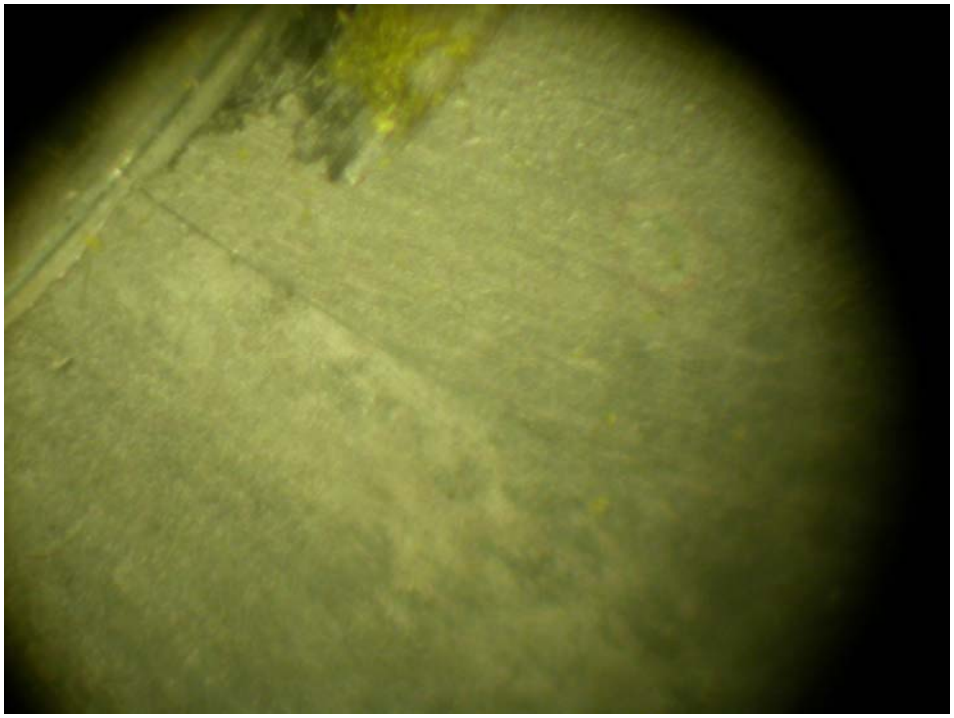

Figure 46: Shows borescope image of the indication in the shoulder area of DOT-3AL cylinder # AR0120056 at 220º location identified in Figure 44.

Figure 47: Shows the location at which the cylinders were cut to expose the indications in neck region.

Figure 48: Shows the inside surface of the cylinder # AR0119524 head.

Figure 49: Shows the indications in the folds of the neck area of the cylinder # AR0119524.

Figure 50: Shows the stereoscope image of the indications in the neck area of the cylinder # AR0119524

Figure 51: Shows stereoscope image of additional indications in the neck area of the cylinder # AR0119524

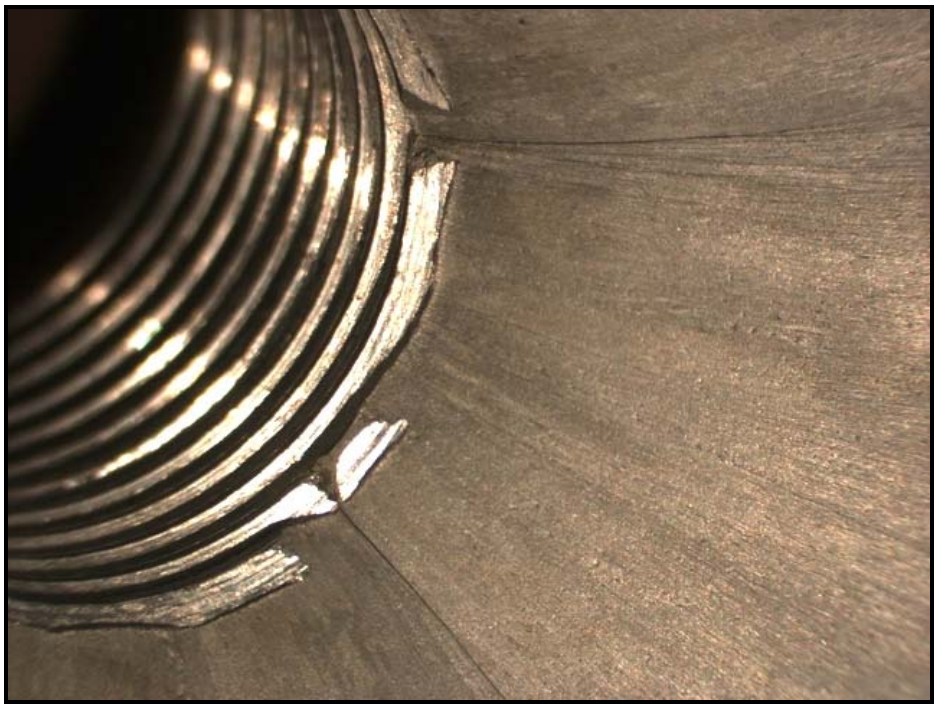

Figure 52: Shows stereoscope image of the indications shown in Figure 50 extending up to the threads of the neck of cylinder # AR0119524

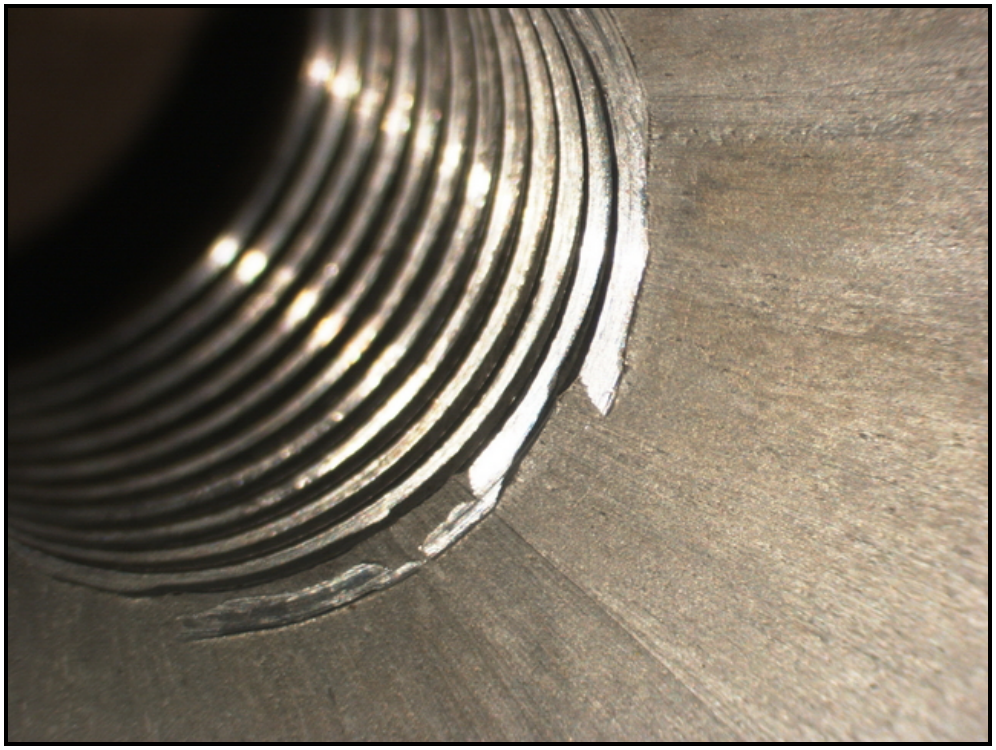

Figure 53: Shows stereoscope image of the indications shown in Figure 51 extending up to the threads of the neck of cylinder # AR0119524

Figure 54: Shows the inside surface of the cylinder # AR0118876 head.

Figure 55: Shows the indications in the folds of the neck area of the cylinder # AR0118876.

Figure 56: Shows the stereoscope image of the indications in the neck area of the cylinder # AR0118876

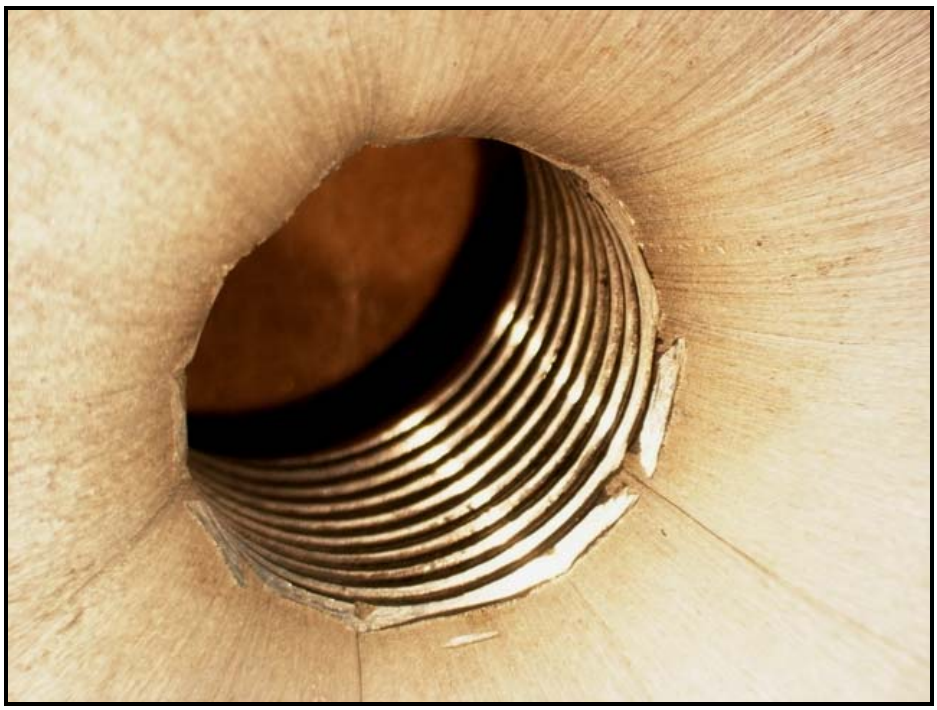

Figure 57: Shows stereoscope image of the indications shown in Figure 56 extending up to the threads of the neck of cylinder # AR0118876

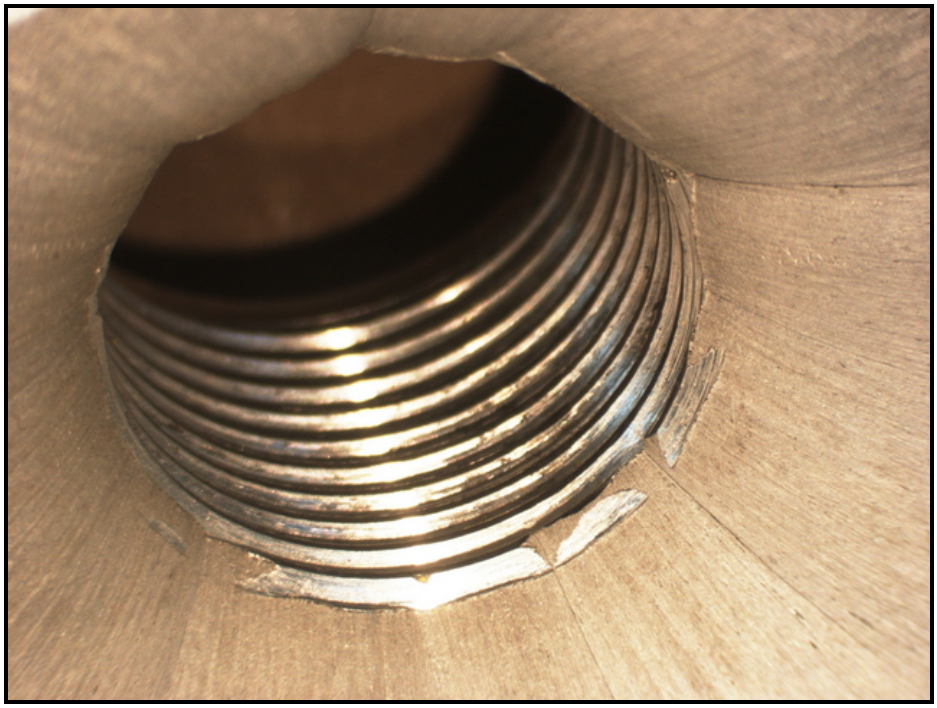

Figure 58: Shows stereoscope image of the indications shown in Figure 56 extending up to the threads of the neck of cylinder # AR0118876

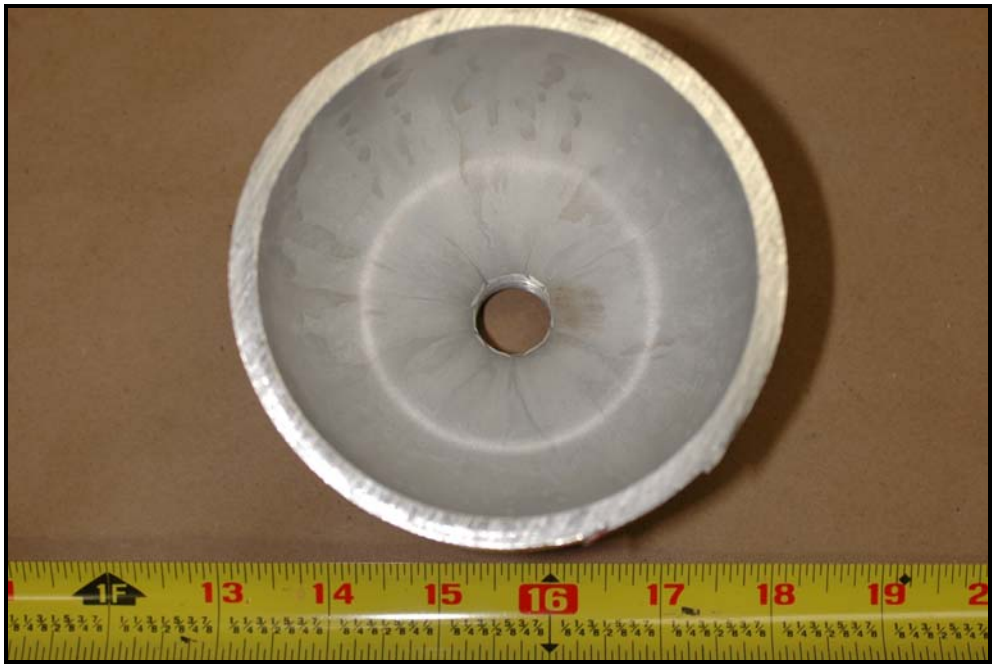

Figure 59: Shows the inside surface of the cylinder # AR0120056 head.

Figure60: Shows the indications in the folds of the neck area of the cylinder # AR0120056.

Figure 61: Shows the stereoscope image of the indications in the neck area of the cylinder # AR0120056

Figure 62: Shows the stereoscope image of additional indications in the neck area of the cylinder # AR0120056

Figure 63: Shows stereoscope image of the indications shown in Figure 61 extending up to the threads of the neck of cylinder # AR0120056

Figure 64: The three cylinder heads in the vacuum chamber for liquid dye penetration.

Figure 65: Shows the three cylinder head removed from the vacuum chamber after dye penetration.

Figure 66: Indications observed on the three cylinder heads after dye penetration test

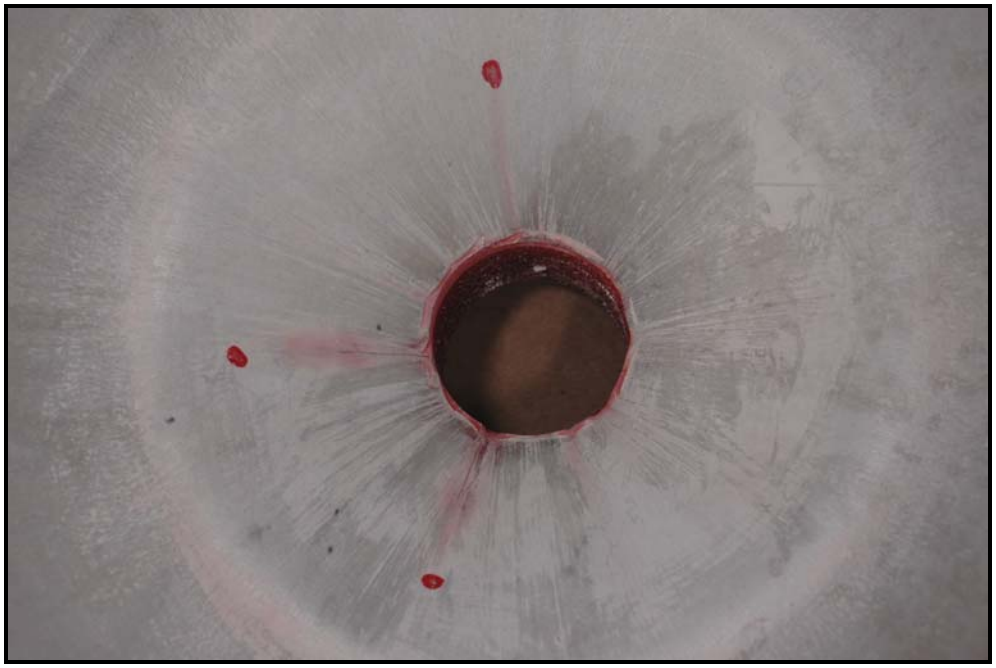

Figure 67: Shows the indications in neck area in the cylinder # AR0119524 exposed after dye penetration test

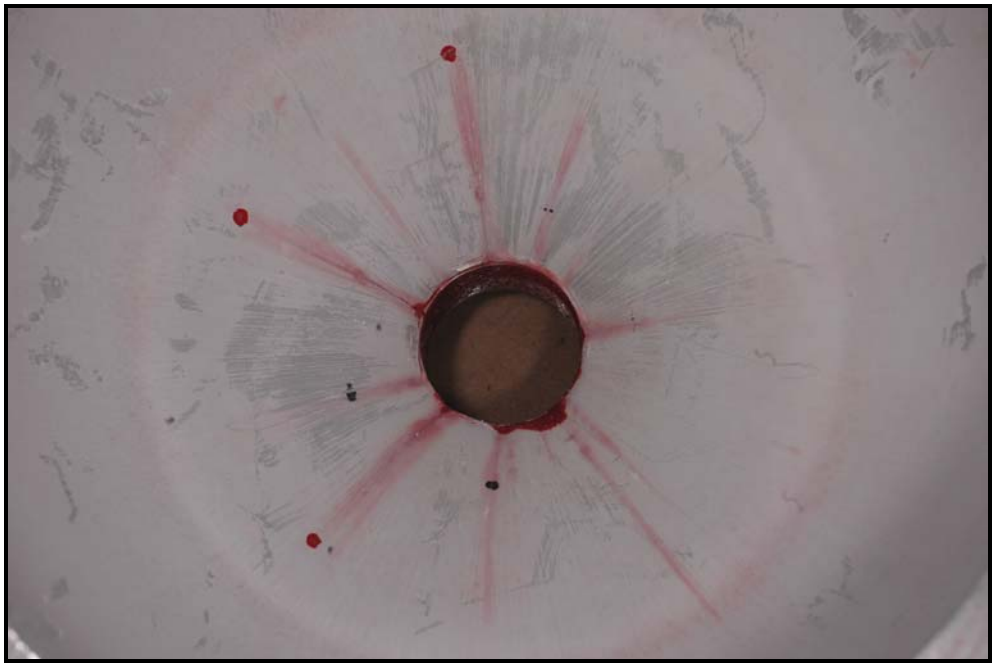

Figure 68: Shows the indications in neck area in the cylinder # AR0118876 exposed after dye penetration test

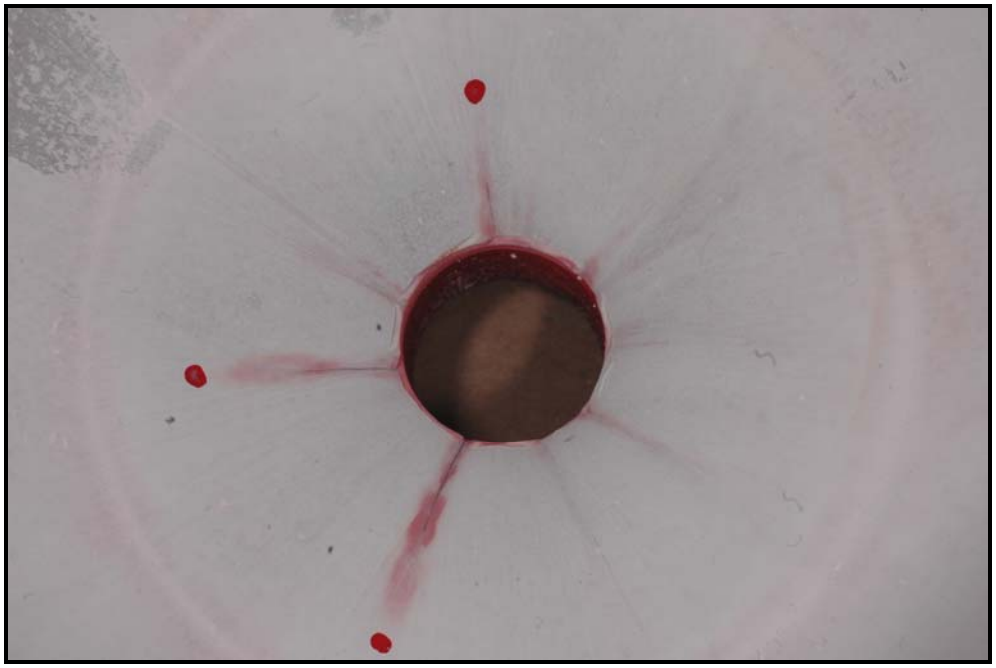

Figure 69: Shows the indications in neck area in the cylinder # AR0120056 exposed after dye penetration test

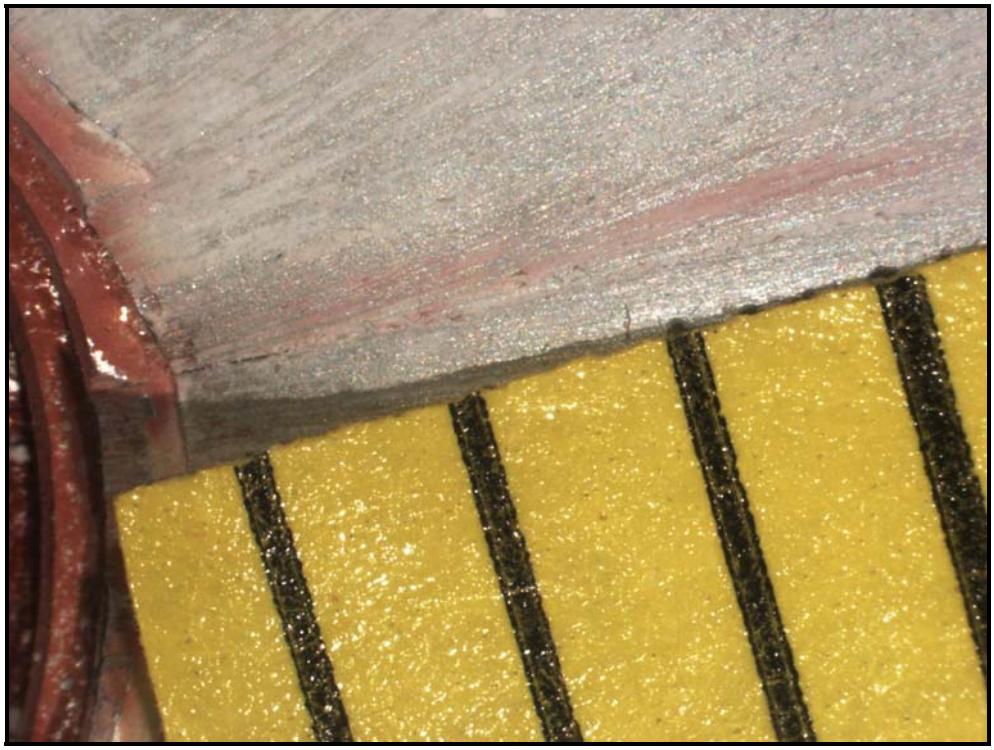

Figure 70: Stereoscope image of the indication in the neck area in the cylinder # AR0119524 exposed after dye penetration test

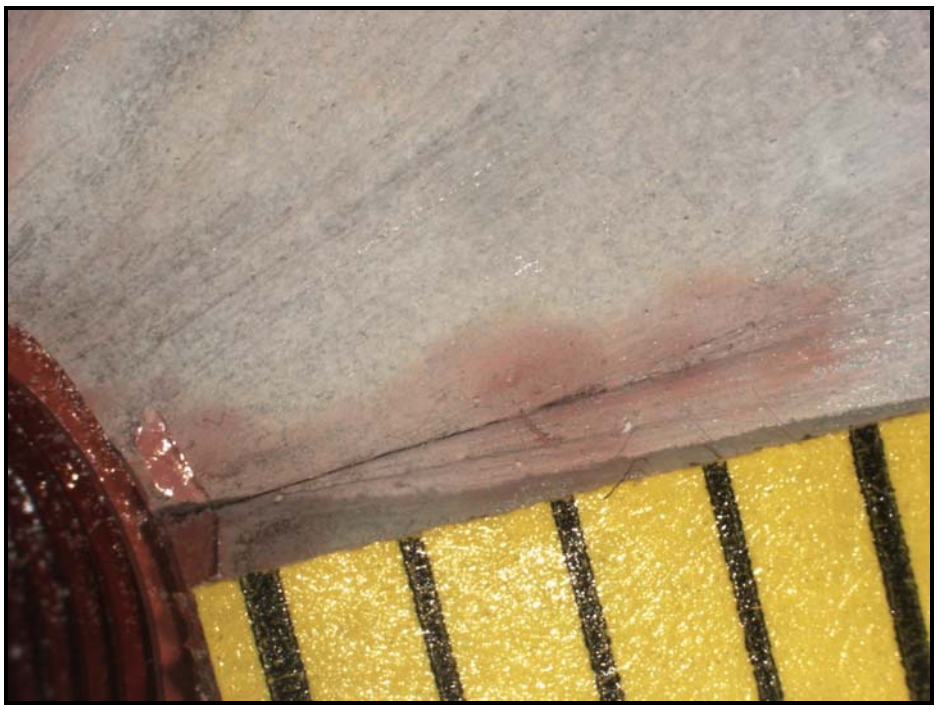

Figure 71: Stereoscope image of additional indication in the neck area in the cylinder # AR0119524 exposed after dye penetration test

Figure 72: Stereoscope image of additional indication in the neck area in the cylinder # AR0119524 exposed after dye penetration test

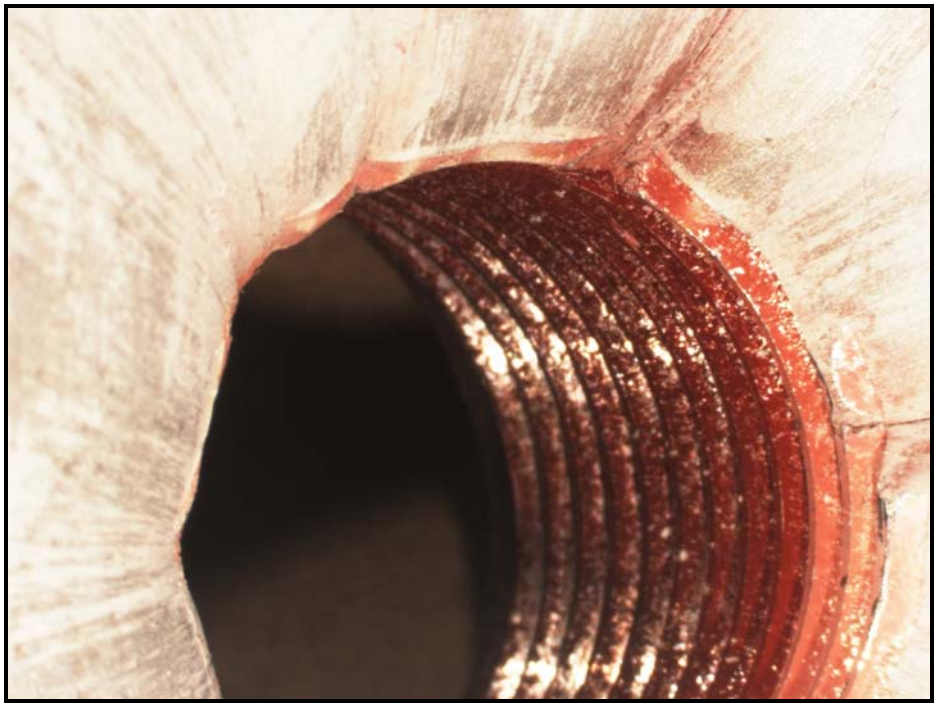

Figure 73: Stereoscope image of indication in the neck thread in the cylinder # AR0119524 exposed after dye penetration test

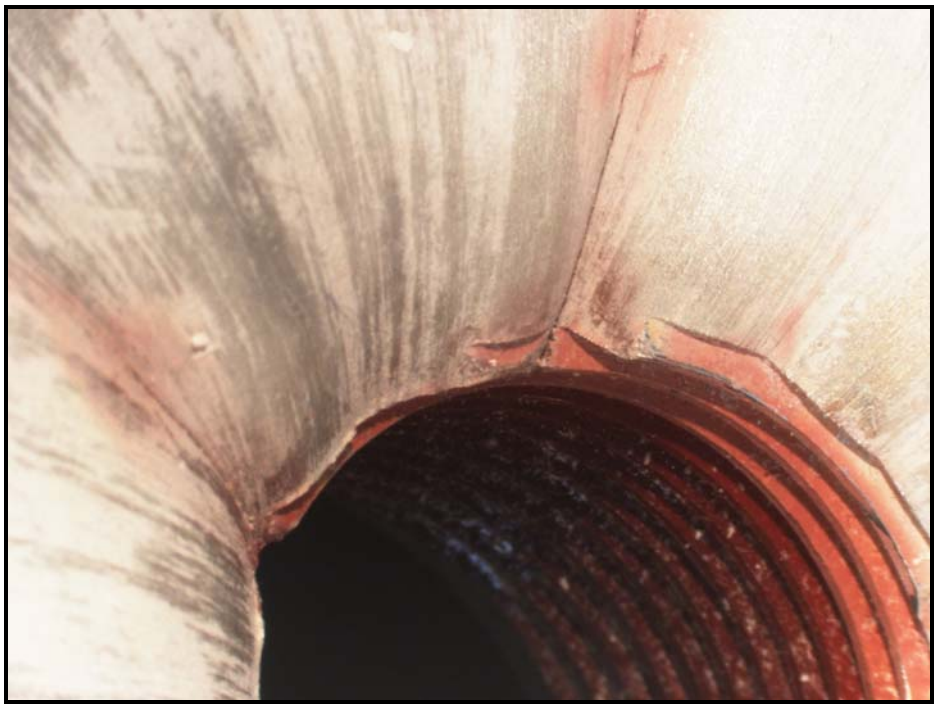

Figure 74: Stereoscope image of additional indications in the neck thread in the cylinder # AR0119524 exposed after dye penetration test

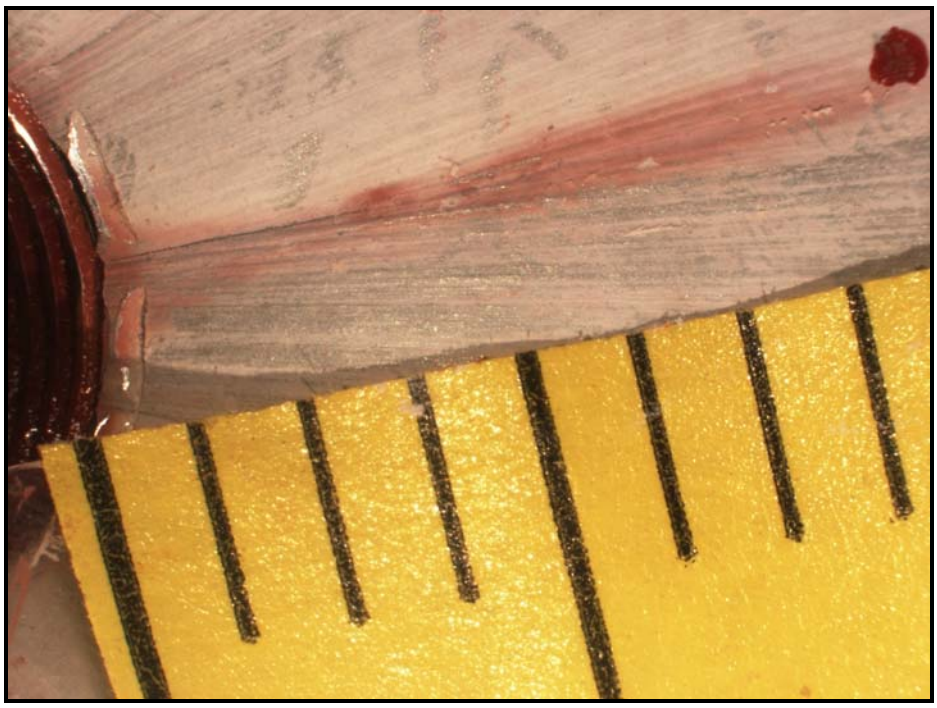

Figure 75: Stereoscope image of the indication in the neck area in the cylinder # AR0118876 exposed after dye penetration test

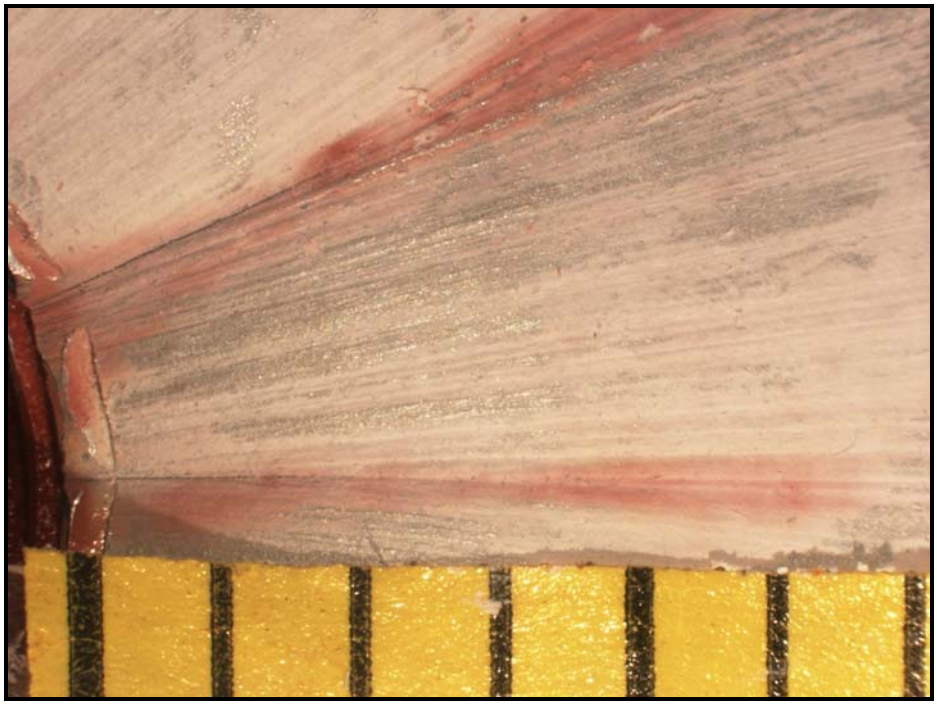

Figure 76: Stereoscope image of additional indication in the neck area in the cylinder # AR0118876 exposed after dye penetration test

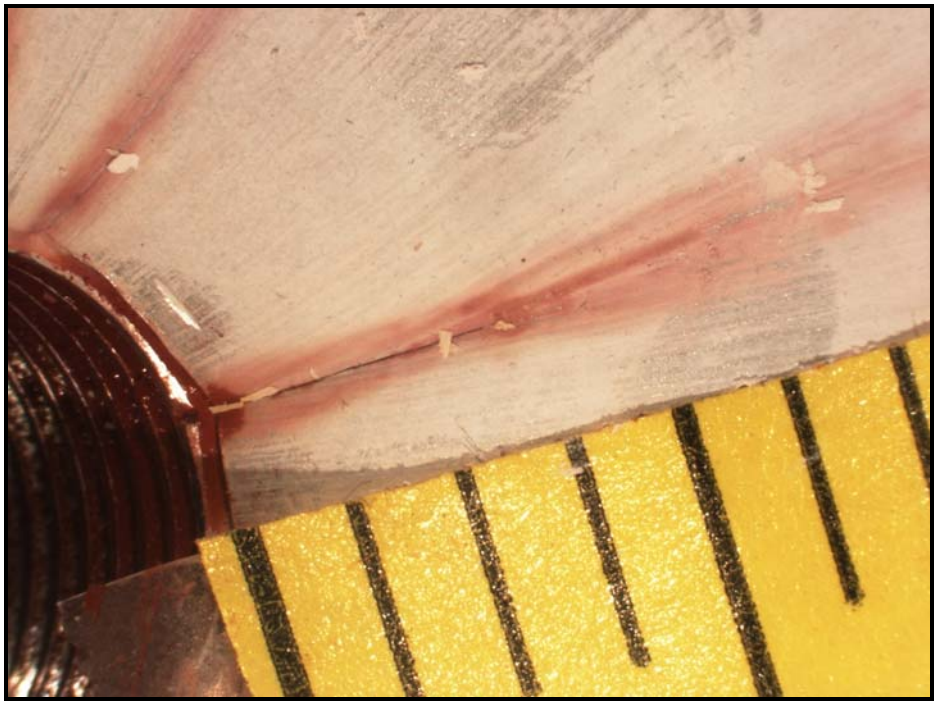

Figure 77: Stereoscope image of additional indication in the neck area in the cylinder # AR0118876 exposed after dye penetration test

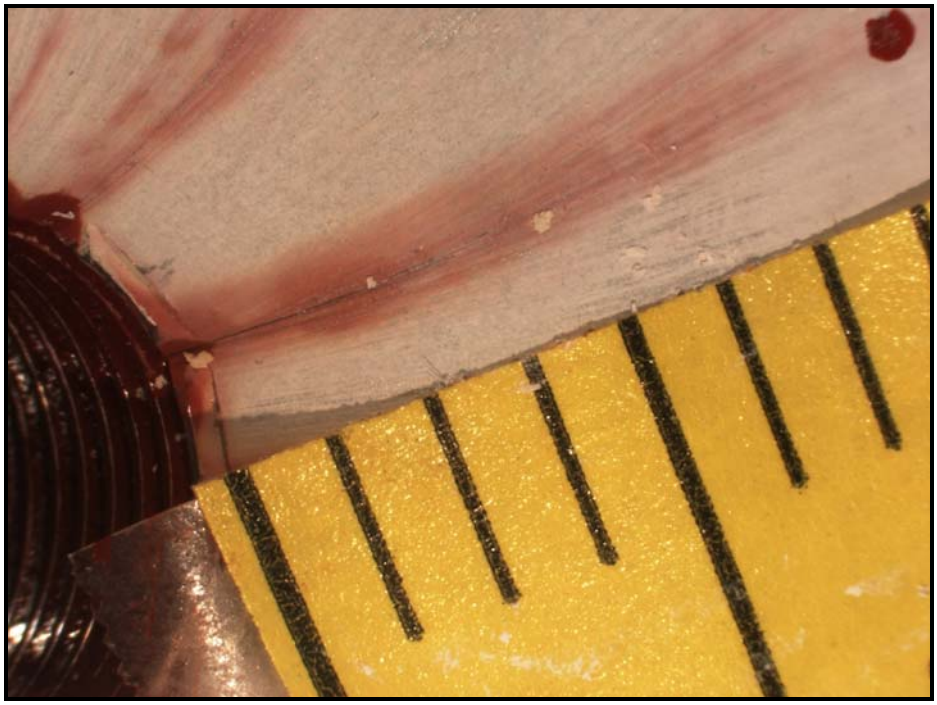

Figure 78: Stereoscope image of additional indication in the neck area in the cylinder # AR0118876 exposed after dye penetration test

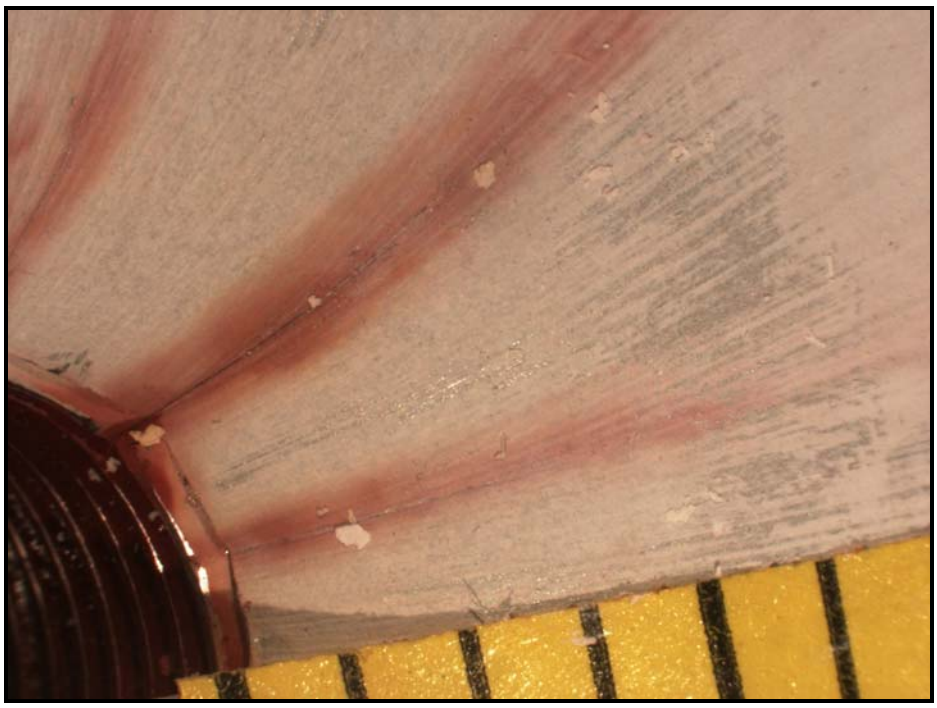

Figure 79: Stereoscope image of additional indication in the neck area in the cylinder # AR0118876 exposed after dye penetration test

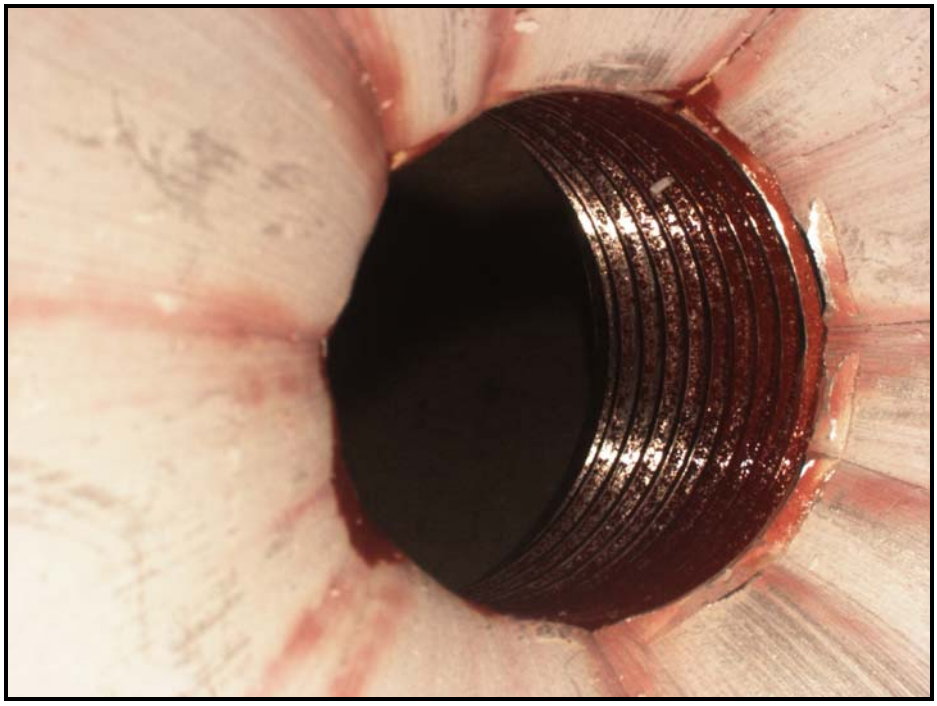

Figure 80: Stereoscope image of indication in the neck thread in the cylinder # AR0118876 exposed after dye penetration test

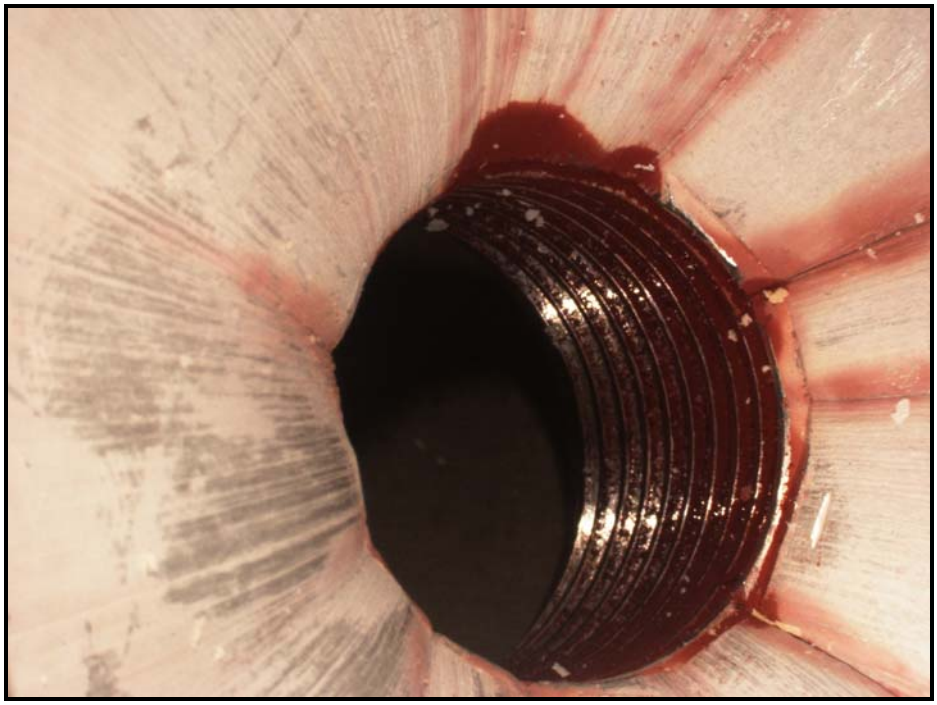

Figure 81: Stereoscope image of additional indication in the neck thread in the cylinder # AR0118876 exposed after dye penetration test

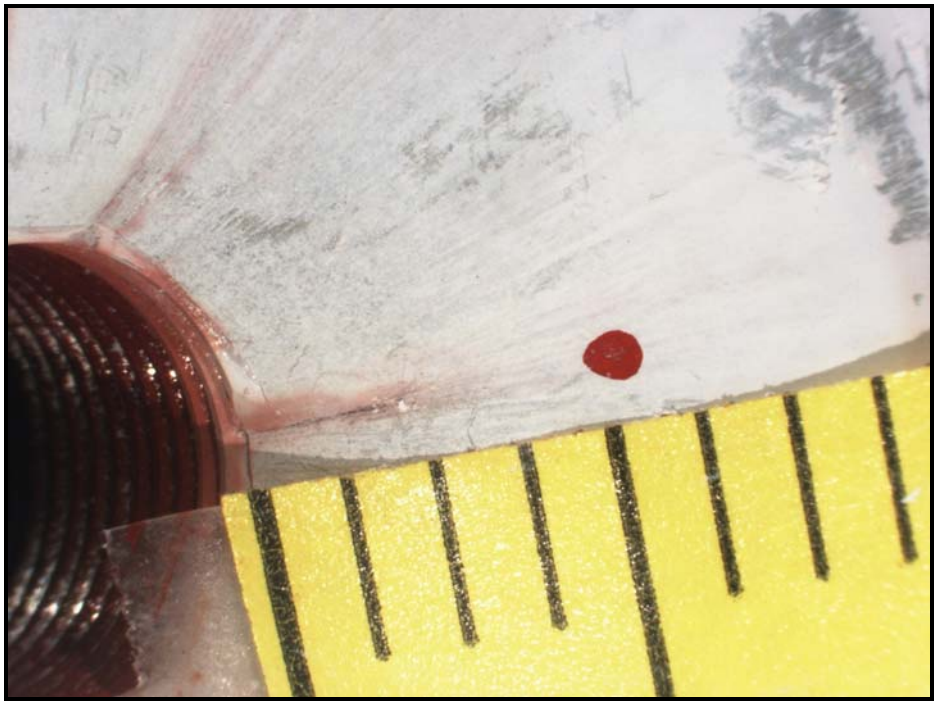

Figure 82: Stereoscope image of the indication in the neck area in the cylinder # AR0120056 exposed after dye penetration test

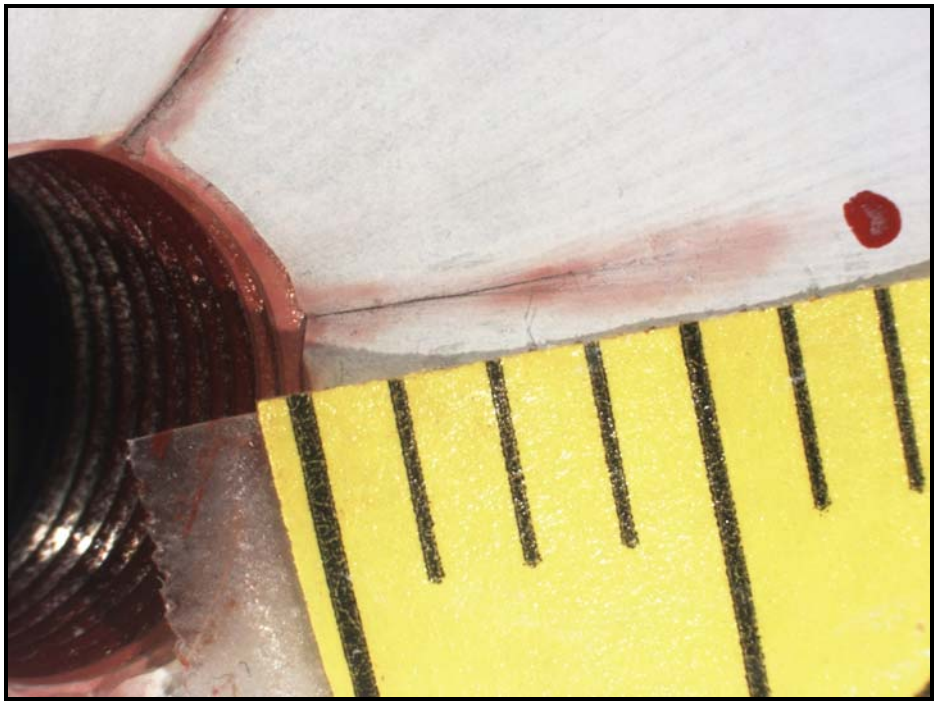

Figure 83: Stereoscope image of additional indication in the neck area in the cylinder # AR0120056 exposed after dye penetration test

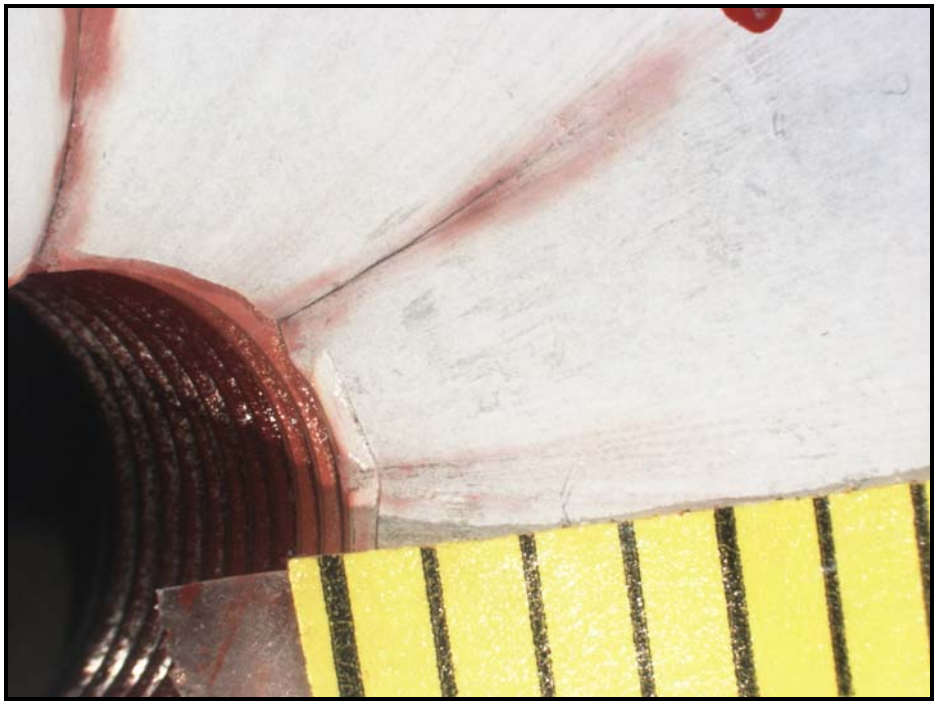

Figure 84: Stereoscope image of additional indication in the neck area in the cylinder # AR0120056 exposed after dye penetration test

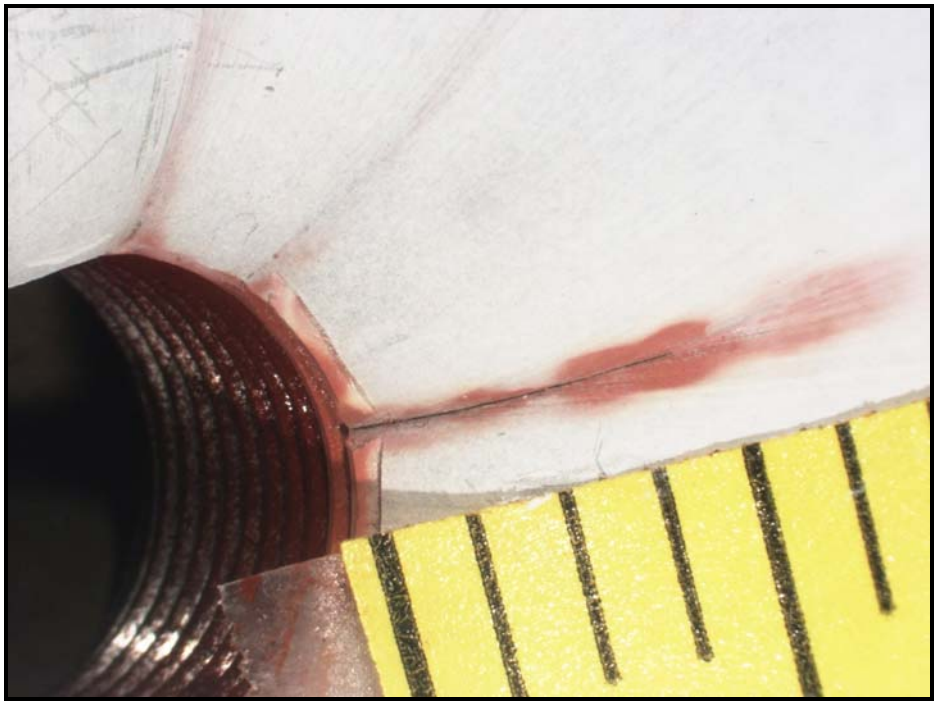

Figure 85: Stereoscope image of additional indication in the neck area in the cylinder # AR0120056 exposed after dye penetration test

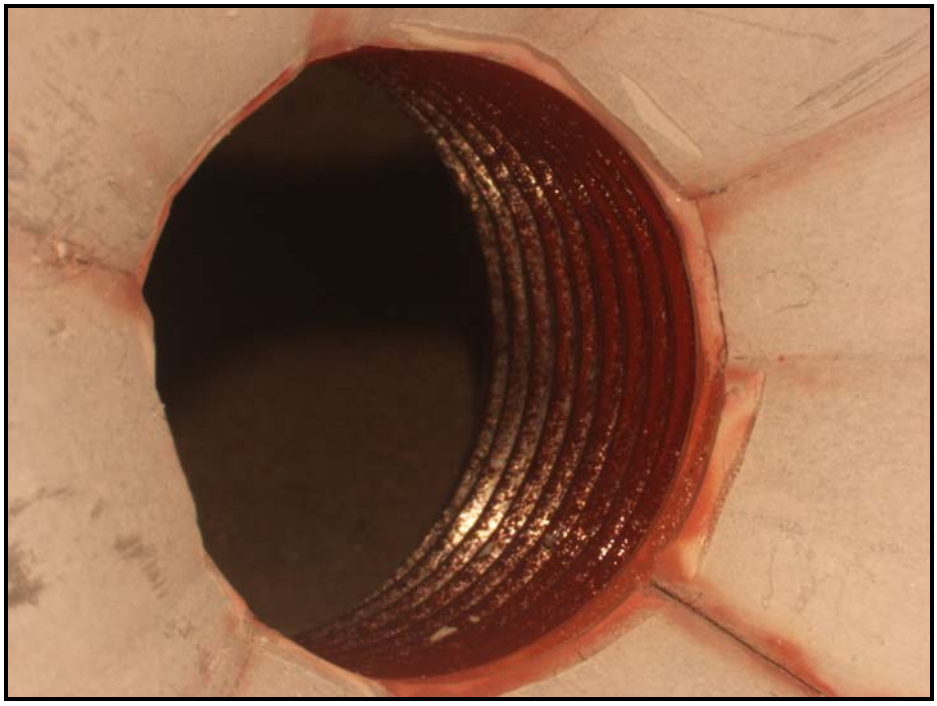

Figure 86: Stereoscope image of indications in the neck thread in the cylinder # AR0118876 exposed after dye penetration test

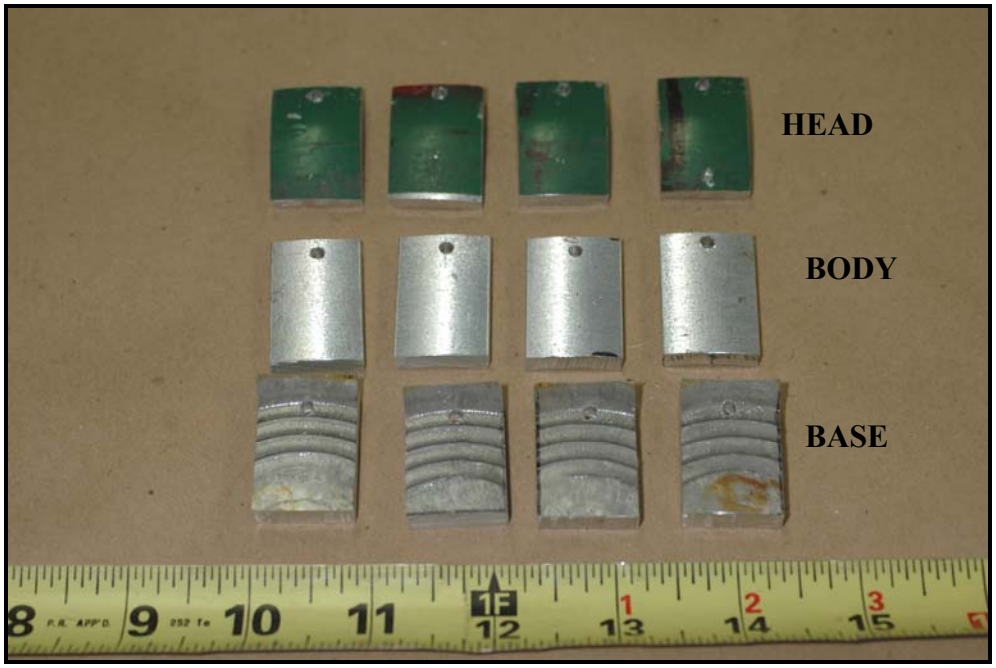

Figure 87: Shows the outer surface of the specimens from the head, body and base machined for assessing inter-crystalline corrosion

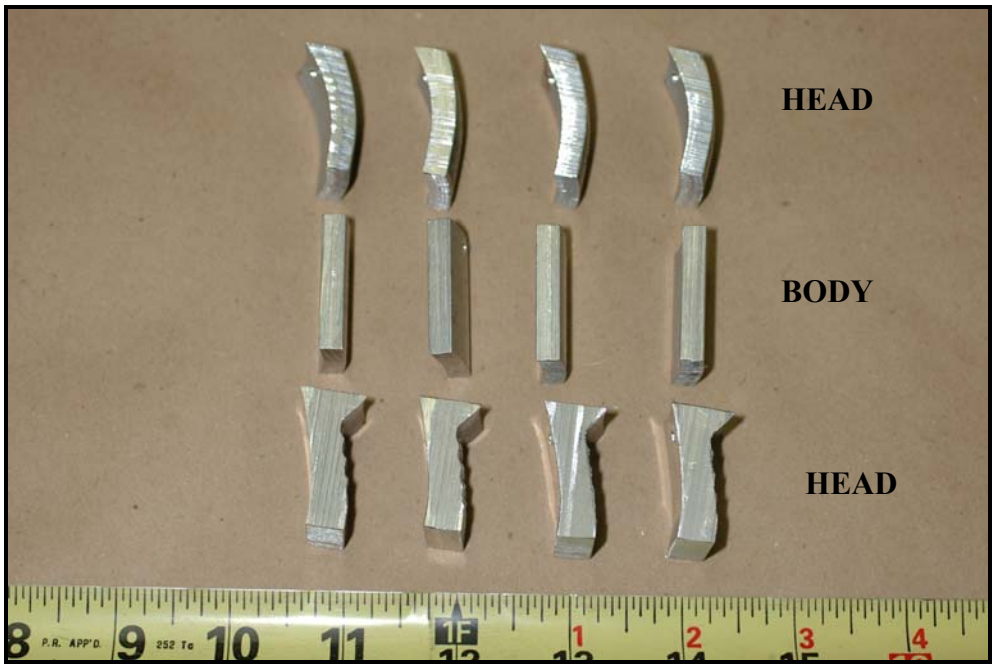

Figure 88: Shows the cross-section of the specimens from the head, body and base machined for assessing inter-crystalline corrosion

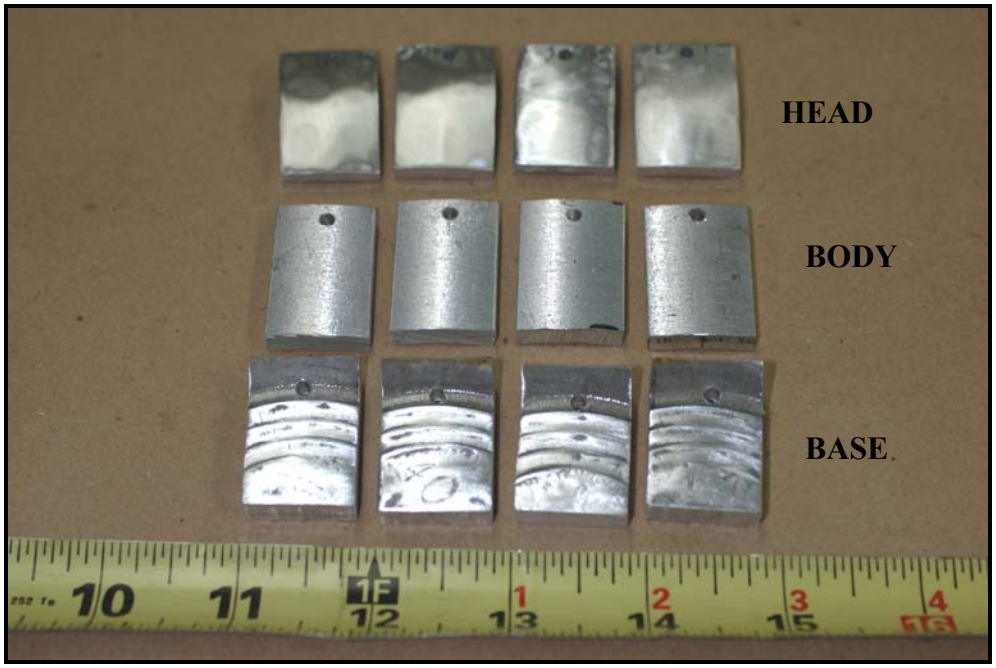

Figure 89: Shows the outer surface of the specimens after removing the paint from the head and coating from the base.

Figure 90: Shows the inside surface of the specimens from the head, body and base machined for assessing inter-crystalline corrosion

Figure 91: Set up for cleaning the samples before corrosion test.

Figure 92: Shows set up for etching the specimens for 6 hours to assess the susceptibility to inter-crystalline corrosion.

Figure 93: Shows the temperature at which the test was performed.

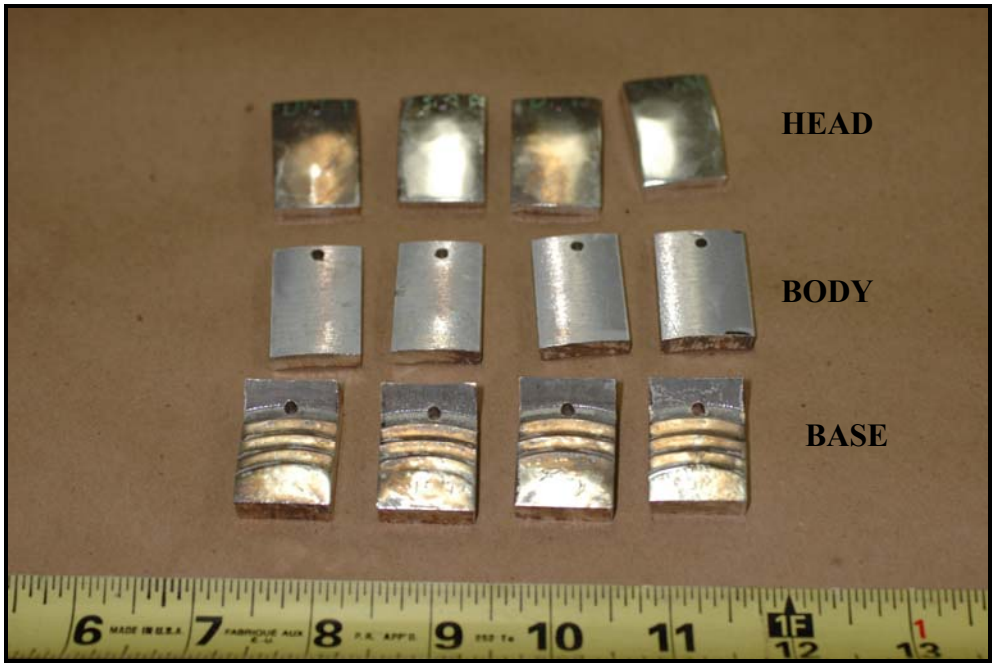

Figure 94: Shows the outer surface of the specimens after the corrosion test.

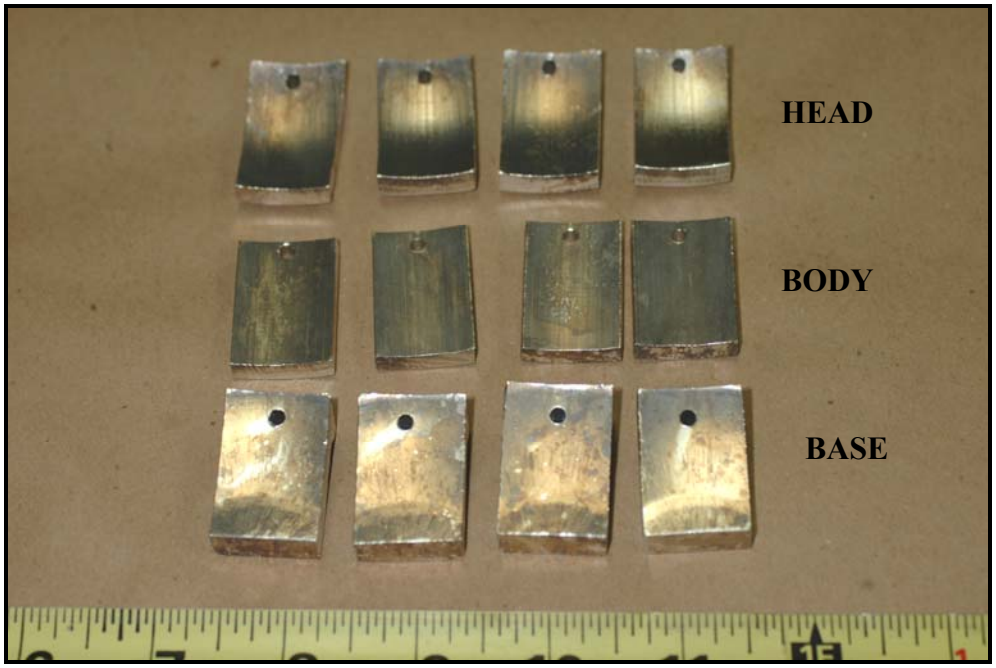

Figure 95: Shows the inner surface of the specimens after the corrosion test.

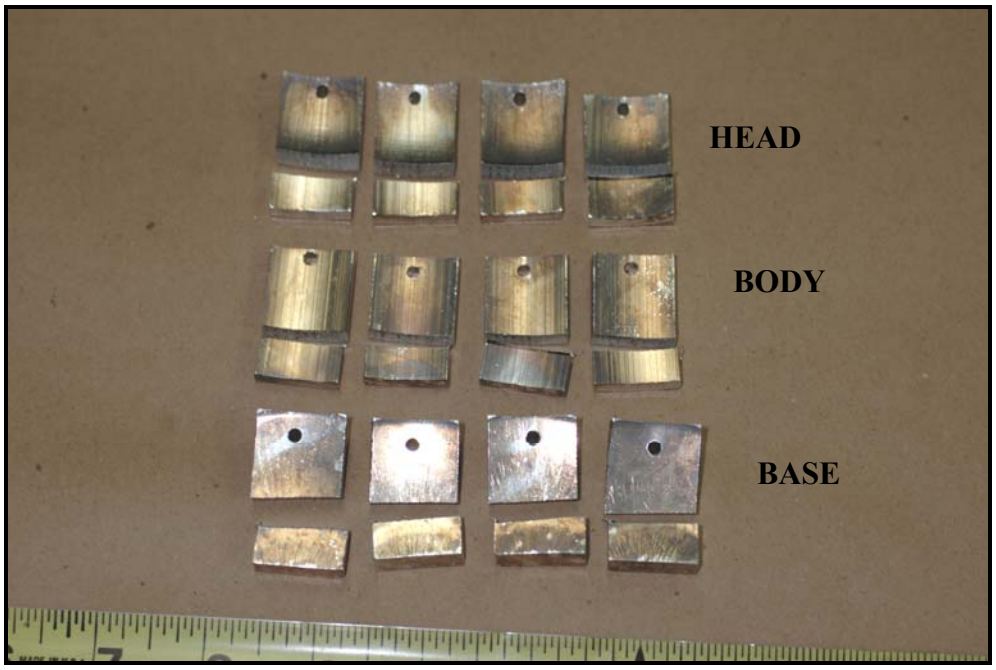

Figure 96: Shows the samples sectioned for microscopic examination. The smaller sections from each sample was mounted in epoxy and mechanically polished.

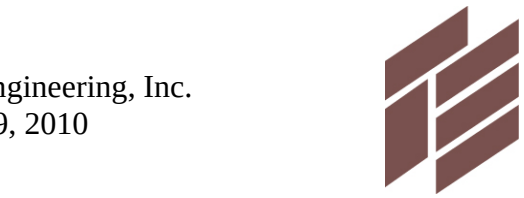

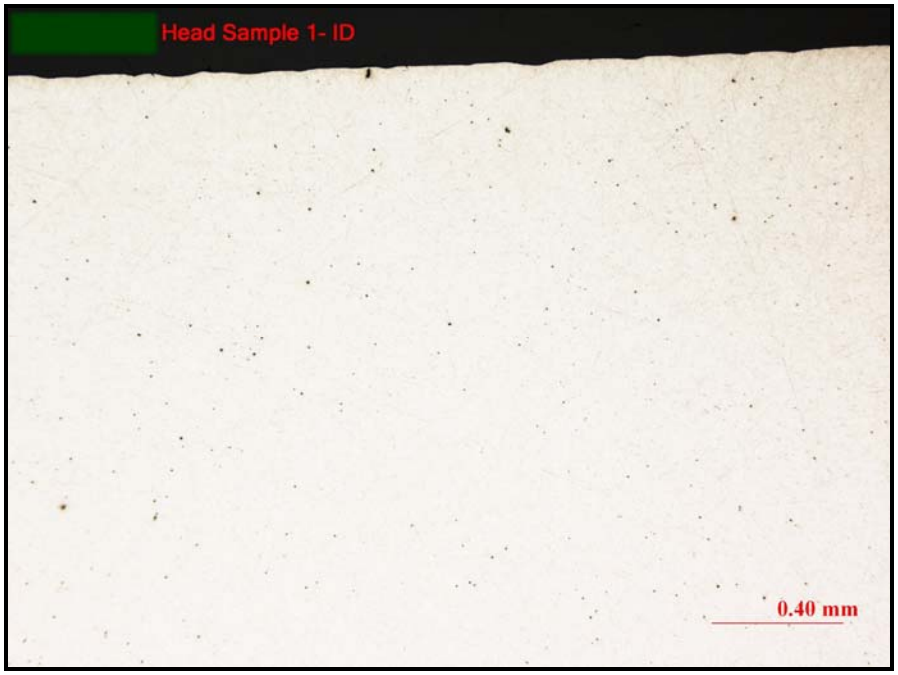

Figure 97: Microscope image shows the unetched ID of the sample 1 from the head of the cylinder # AR0118876. Magnification: 50X.

Figure 98: Microscope image shows the unetched ID of the sample 1 from the head of the cylinder # AR0118876. Magnification: 200X.

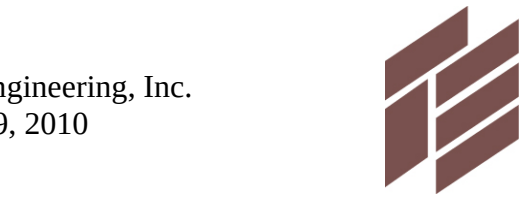

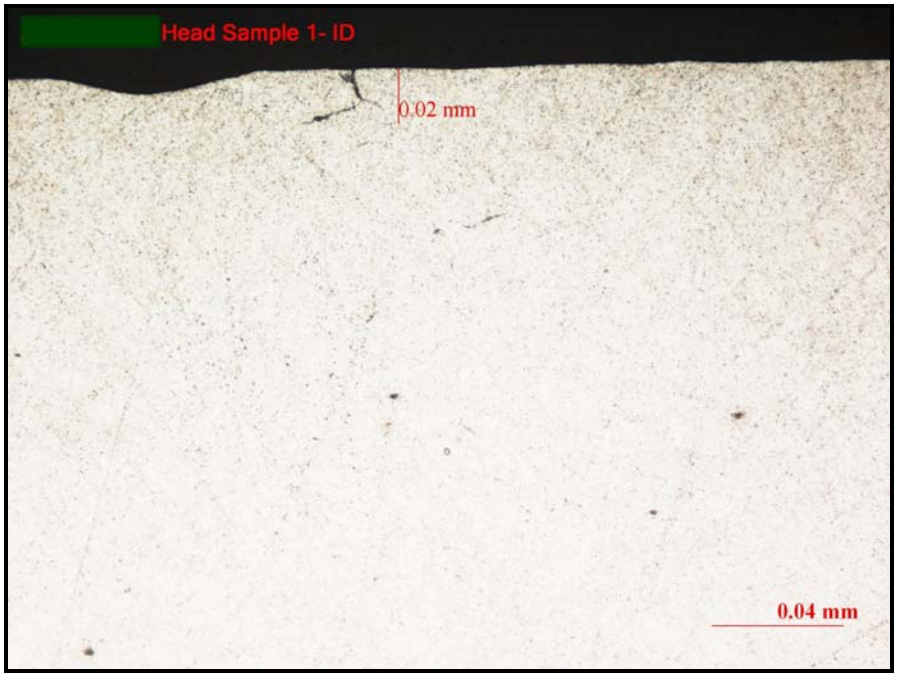

Figure 99: Microscope image shows the unetched ID of the sample 1 from the head of the cylinder # AR0118876. Inter-crystalline attack < 0.1 mm. Magnification: 500X.

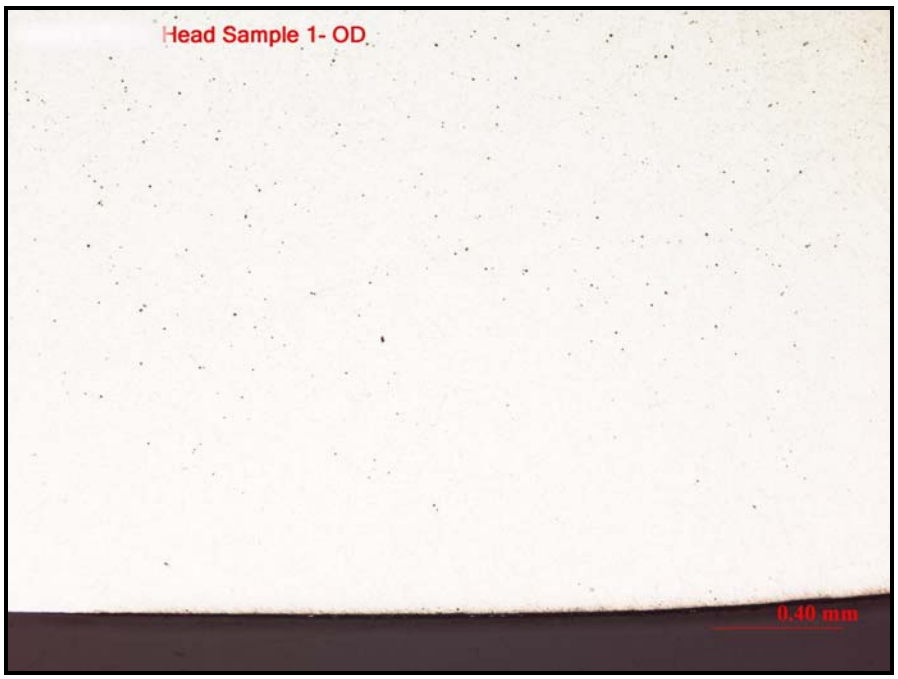

Figure 100: Microscope image shows the unetched OD of the sample 1 from the head of the cylinder # AR0118876. No inter-crystalline attack observed. Magnification: 50X.

Figure 101: Microscope image shows the unetched OD of the sample 1 from the head of the cylinder # AR0118876. No inter-crystalline attack observed. Magnification: 200X.

Figure 102: Microscope image shows the unetched ID of the sample 2 from the head of the cylinder # AR0118876. No inter-crystalline attack observed. Magnification 50X.

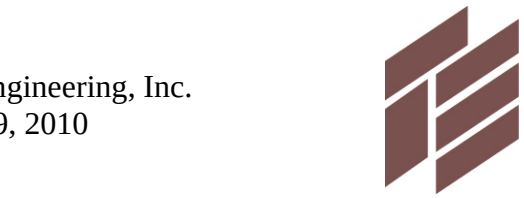

Figure 103: Microscope image shows the unetched ID of the sample 2 from the head of the cylinder # AR0118876. No inter-crystalline attack observed. Magnification: 200X.

Figure 104: Microscope image shows the unetched OD of the sample 2 from the head of the cylinder # AR0118876. Magnification: 50X.

Figure 105: Microscope image shows the unetched OD of the sample 2 from the head of the cylinder # AR0118876. Magnification: 200X.

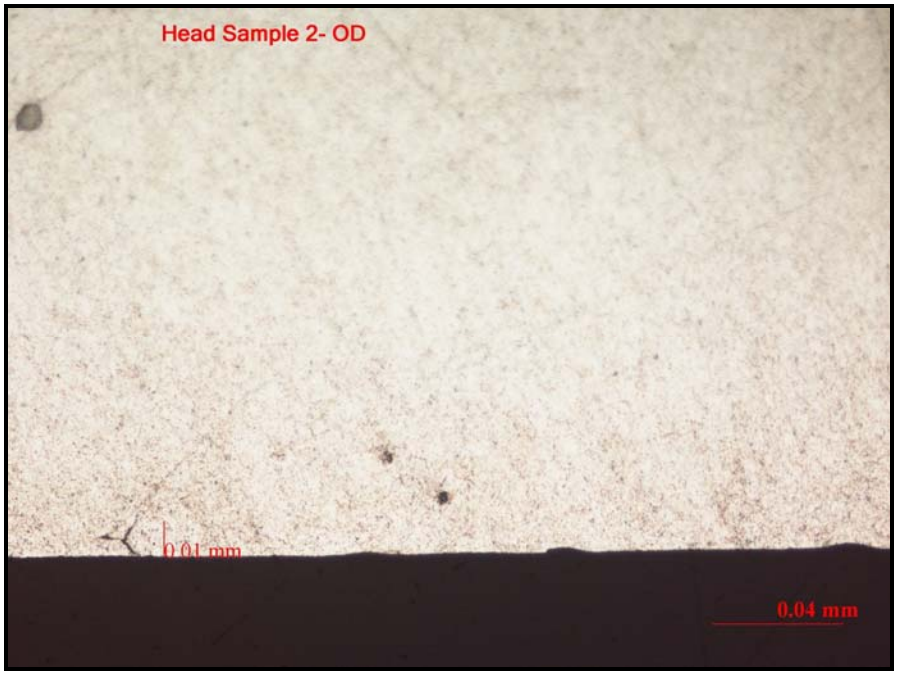

Figure 106: Microscope image shows the unetched OD of the sample 2 from Head of the cylinder # AR0118876. Inter-crystalline attack < 0.1 mm. Magnification: 500X.

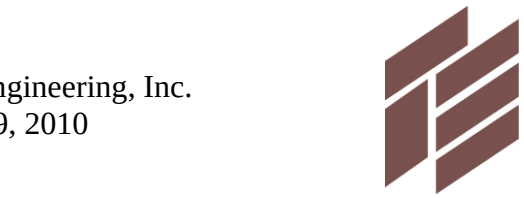

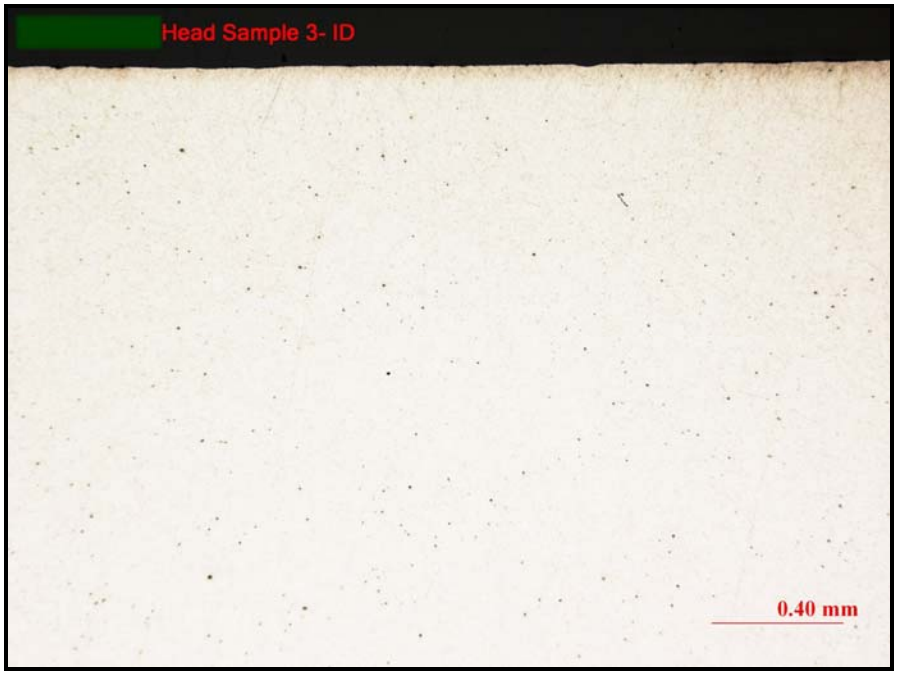

Figure 107: Microscope image shows the unetched ID of the sample 3 from the head of the cylinder # AR0118876. No inter-crystalline attack observed. Magnification: 50X.

Figure 108: Microscope image shows the unetched ID of the sample 3 from the head of the cylinder # AR0118876. No inter-crystalline attack observed. Magnification: 200X.

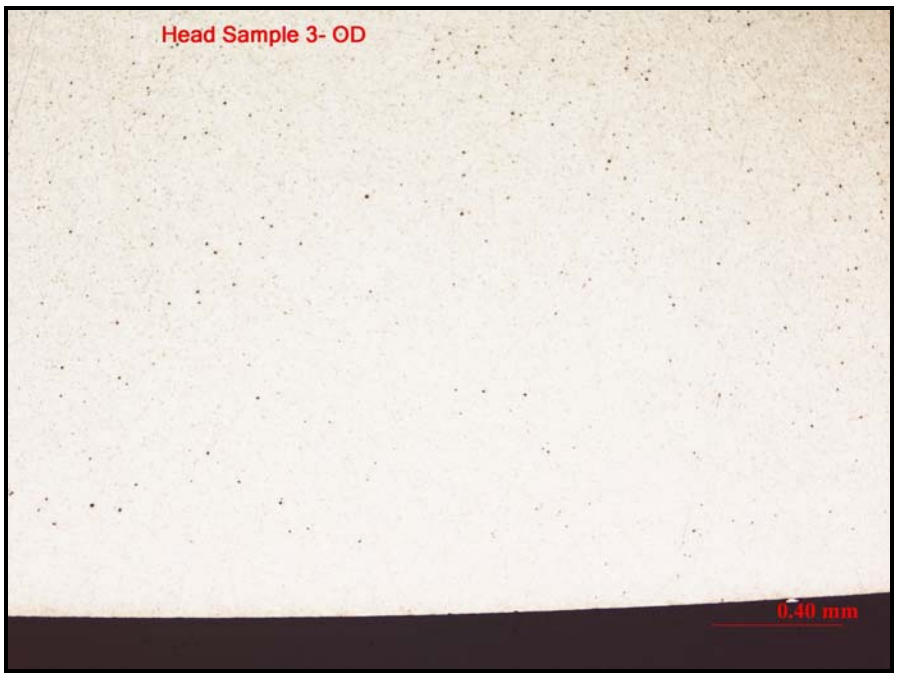

Figure 109: Microscope image shows the unetched OD of the sample 3 from the head of the cylinder # AR0118876. No inter-crystalline attack observed. Magnification: 50X.

Figure 110: Microscope image shows the unetched OD of the sample 3 from the head of the cylinder # AR0118876. No inter-crystalline attack observed. Magnification: 200X.

Figure 111: Microscope image shows the unetched ID of the sample 4 from the head of the cylinder # AR0118876. No inter-crystalline attack observed. Magnification: 50X.

Figure 112: Microscope image shows the unetched ID of the sample 4 from the head of the cylinder # AR0118876. No inter-crystalline attack observed. Magnification: 200X.

Figure 113: Microscope image shows the unetched OD of the sample 4 from the head of the cylinder # AR0118876. No inter-crystalline attack observed. Magnification: 50X.

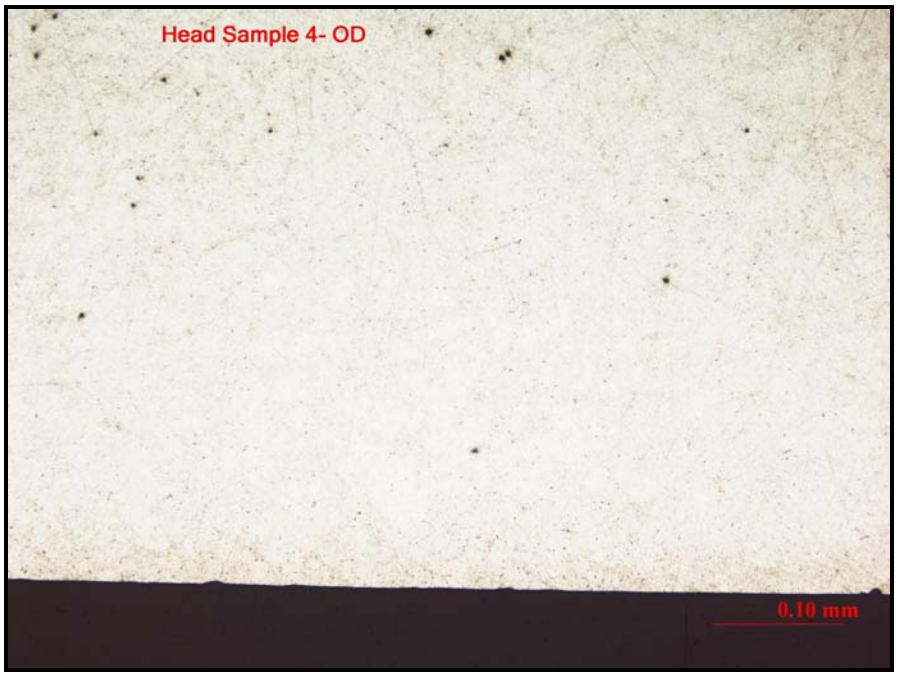

Figure 114: Microscope image shows the unetched OD of the sample4 from the head of the cylinder # AR0118876. No inter-crystalline attack observed. Magnification: 200X.

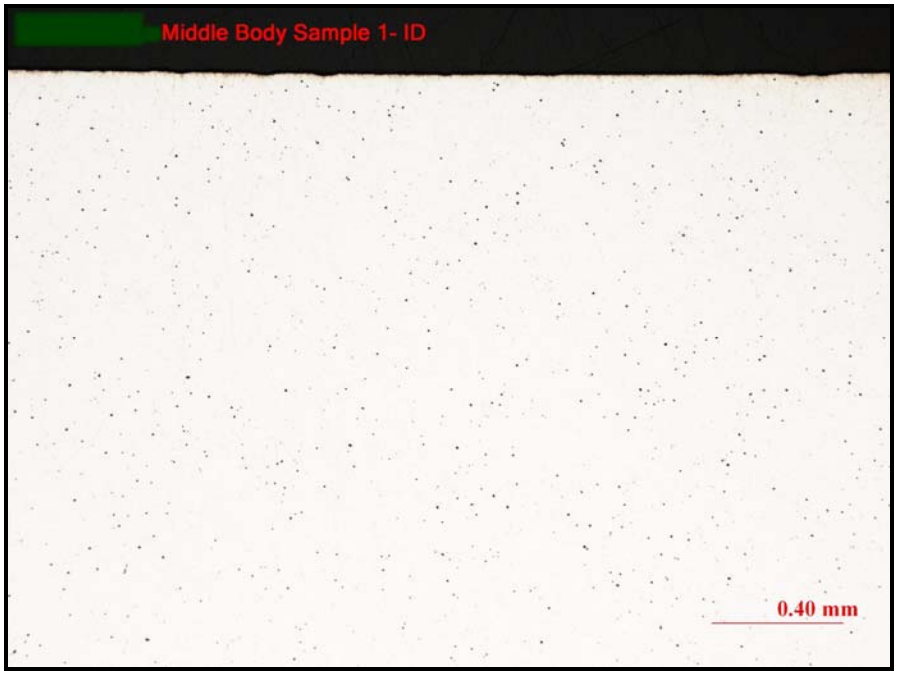

Figure 115: Microscope image shows the unetched ID of the sample 1 from the middle body of the cylinder # AR0118876. No inter-crystalline attack observed. Magnification: 50X.

Figure116: Microscope image shows the unetched ID of the sample 1 from the middle body of the cylinder # AR0118876. No inter-crystalline attack observed. Magnification: 200X.

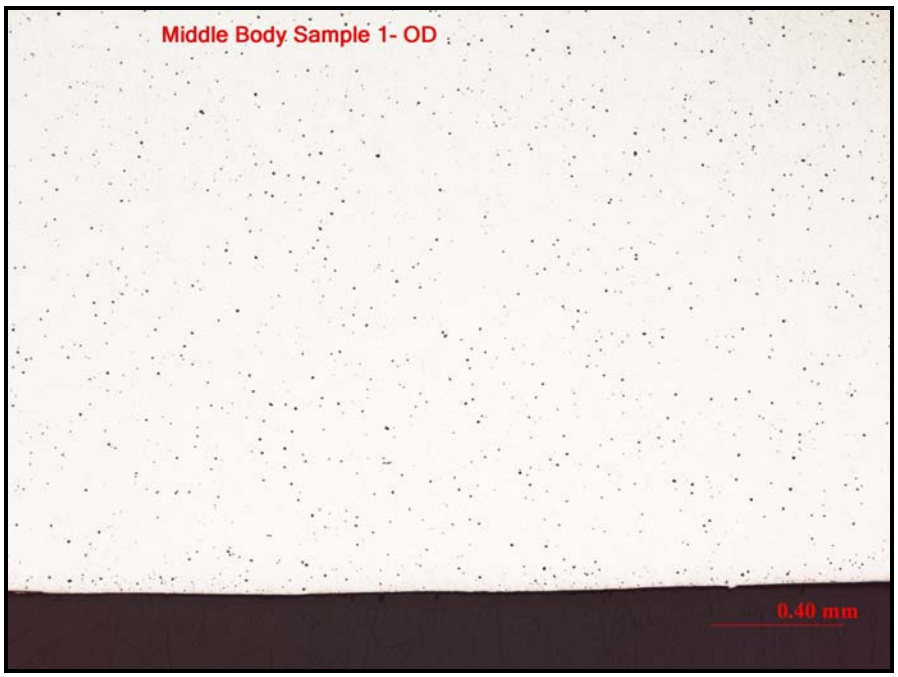

Figure 117: Microscope image shows the unetched OD of the sample 1 from the middle body of the cylinder # AR0118876. No inter-crystalline attack observed. Magnification: 50X.

Figure 118: Microscope image shows the unetched OD of the sample 1 from the middle body of the cylinder # AR0118876. No inter-crystalline attack observed. Magnification: 200X.

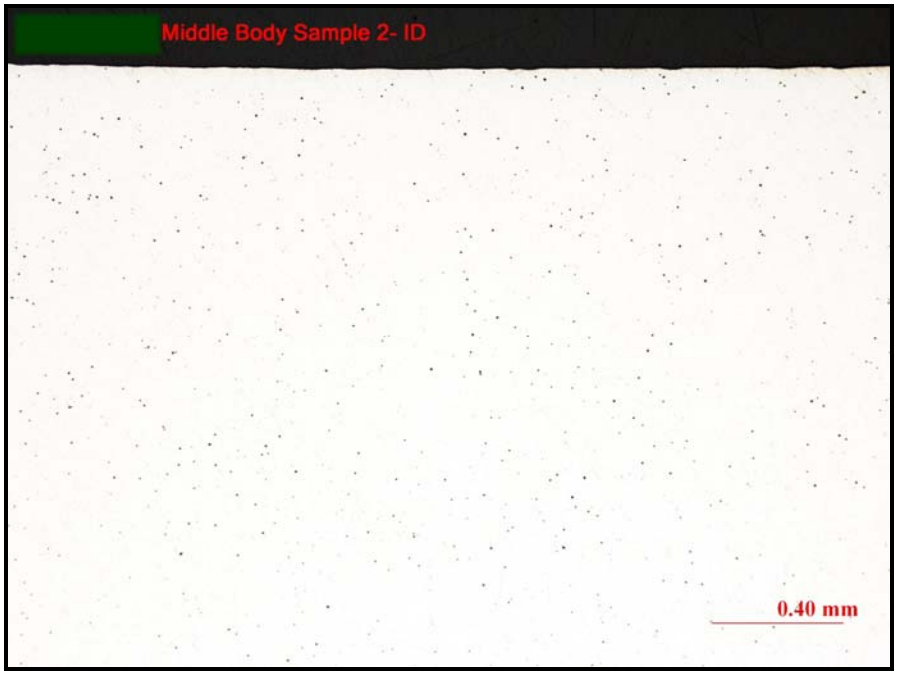

Figure 119: Microscope image shows the unetched ID of the sample 2 from the middle body of the cylinder # AR0118876. No inter-crystalline attack observed. Magnification: 50X.

Figure 120: Microscope image shows the unetched ID of the sample 2 from the middle body of the cylinder # AR0118876. No inter-crystalline attack observed. Magnification: 200X.

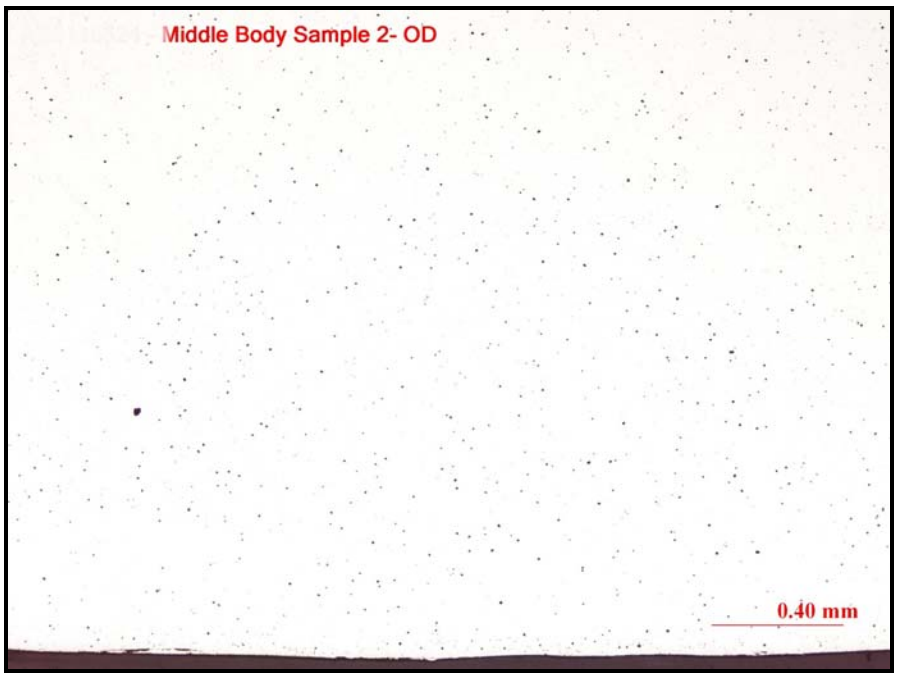

Figure 121: Microscope image shows the unetched OD of the sample 2 from the middle body of the cylinder # AR0118876. No inter-crystalline attack observed. Magnification: 50X.

Figure 122: Microscope image shows the unetched OD of the sample 2 from the middle body of the cylinder # AR0118876. No inter-crystalline attack observed. Magnification: 200X.

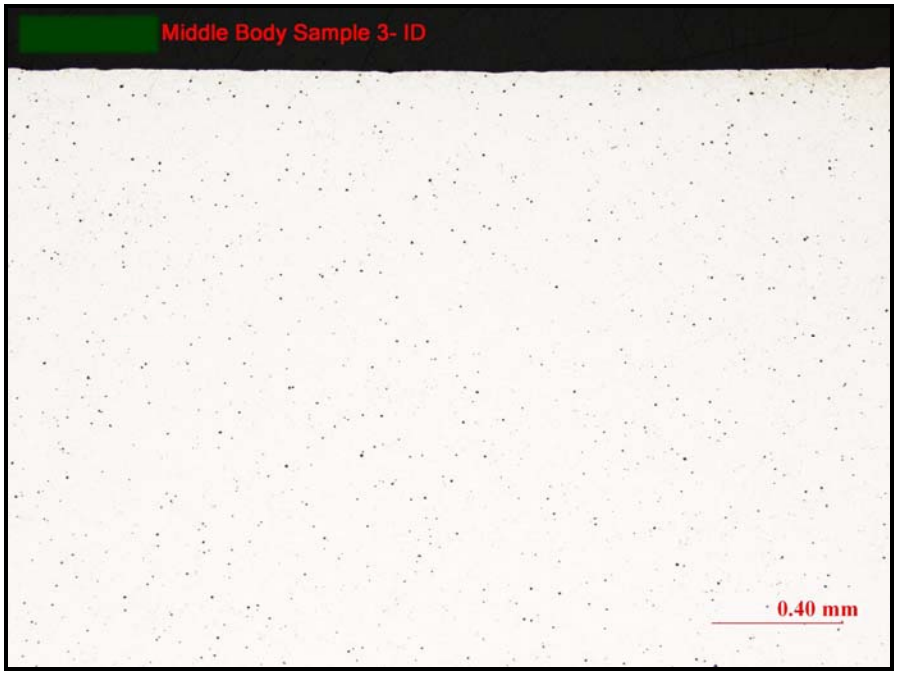

Figure 123: Microscope image shows the unetched ID of the sample 3 from the middle body of the cylinder # AR0118876. No inter-crystalline attack observed. Magnification: 50X.

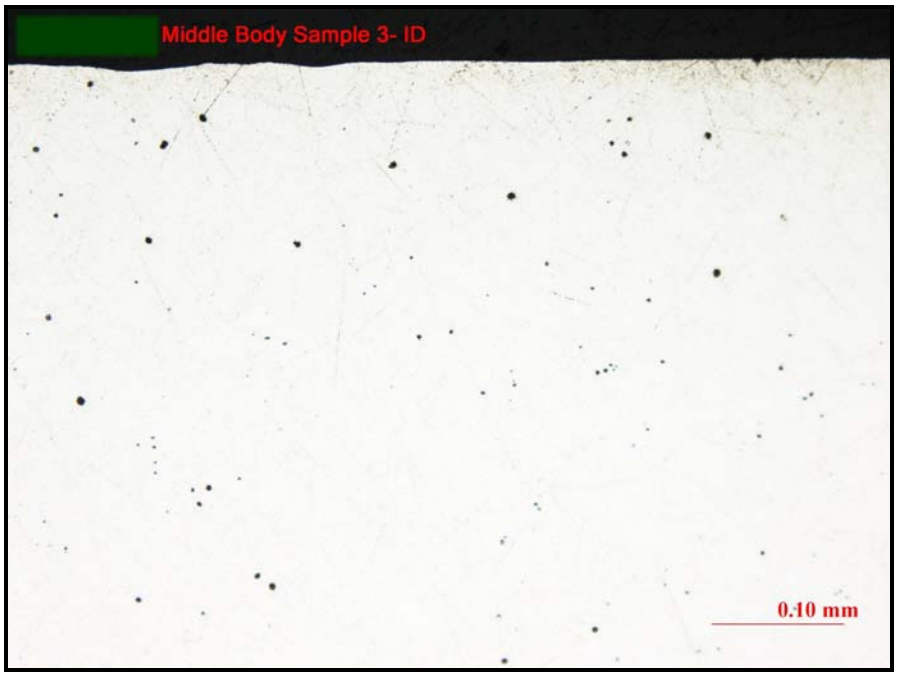

Figure 124: Microscope image shows the unetched ID of the sample 3 from the middle body of the cylinder # AR0118876. No inter-crystalline attack observed. Magnification: 200X.

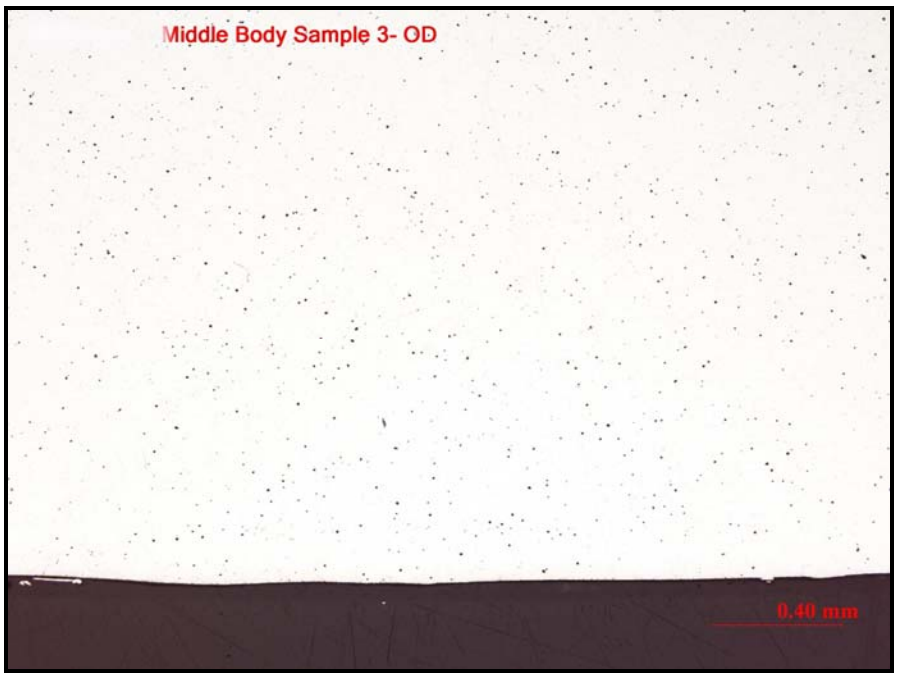

Figure 125: Microscope image shows the unetched OD of the sample 3 from the middle body of the cylinder # AR0118876. No inter-crystalline attack observed. Magnification: 50X.

Figure 126: Microscope image shows the unetched OD of the sample 3 from the middle body of the cylinder # AR0118876. No inter-crystalline attack observed. Magnification: 200X.

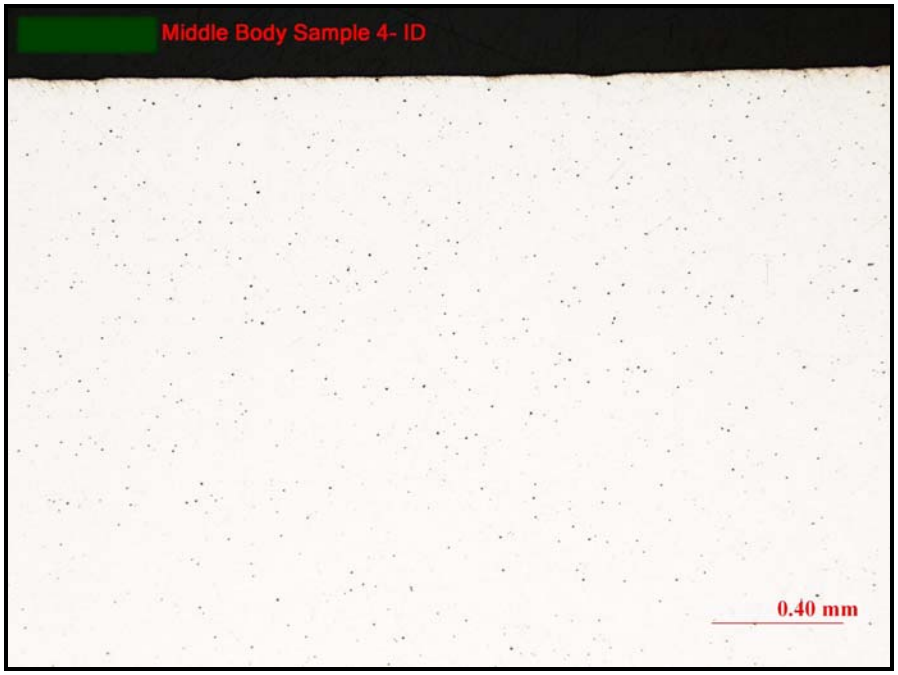

Figure 127: Microscope image shows the unetched ID of the sample 4 from the middle body of the cylinder # AR0118876. No inter-crystalline attack observed. Magnification: 50X.

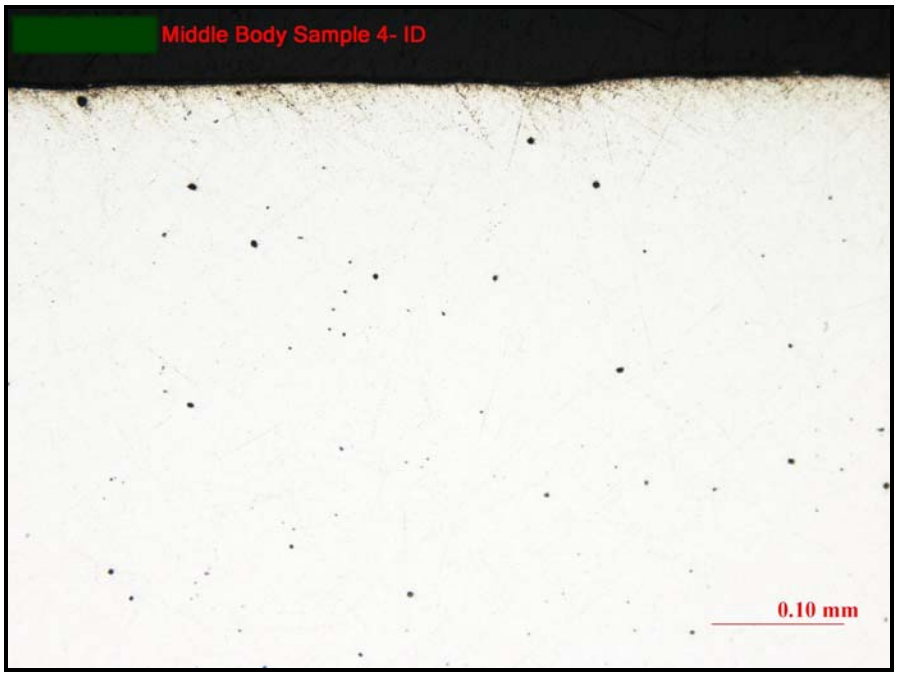

Figure 128: Microscope image shows the unetched ID of the sample 4 from the middle body of the cylinder # AR0118876. No inter-crystalline attack observed. Magnification: 200X.

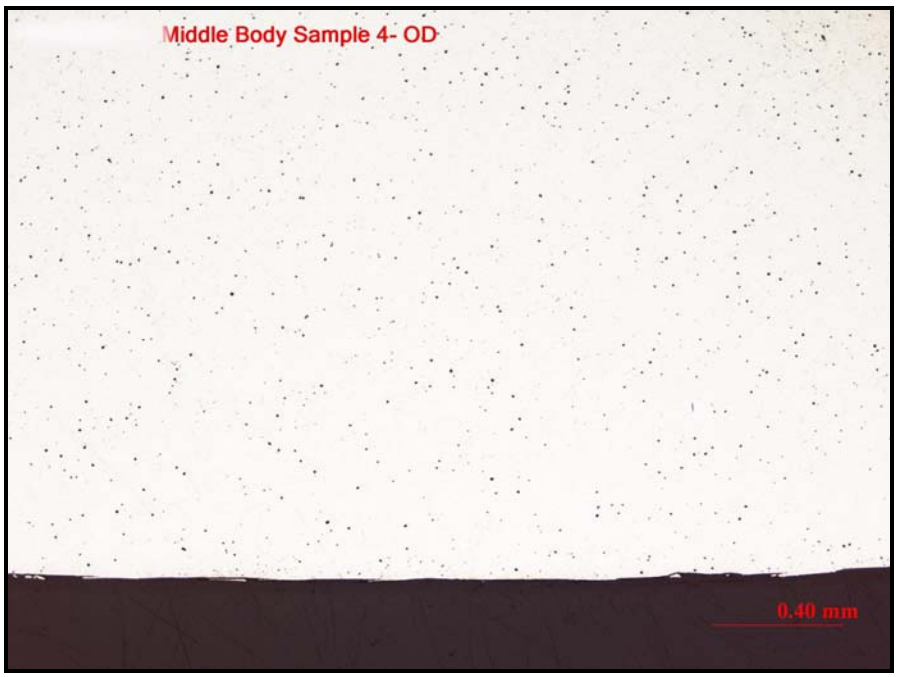

Figure 129: Microscope image shows the unetched OD of the sample 4 from the middle body of the cylinder # AR0118876. No inter-crystalline attack observed. Magnification: 50X.

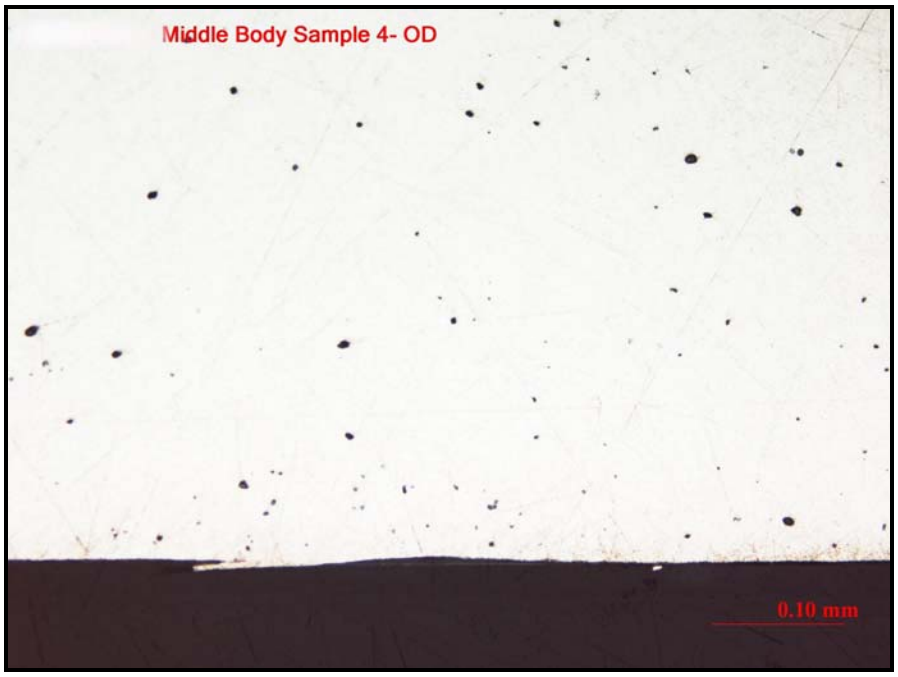

Figure 130: Microscope image shows the unetched OD of the sample 4 from the middle body of the cylinder # AR0118876. No inter-crystalline attack observed. Magnification: 200X.

Figure 131: Microscope image shows the unetched ID of the sample 1 from base of the cylinder # AR0118876. No inter-crystalline attack observed. Magnification: 50X.

Figure 132: Microscope image shows the unetched ID of the sample 1 from base of the cylinder # AR0118876. No inter-crystalline attack observed. Magnification: 200X.

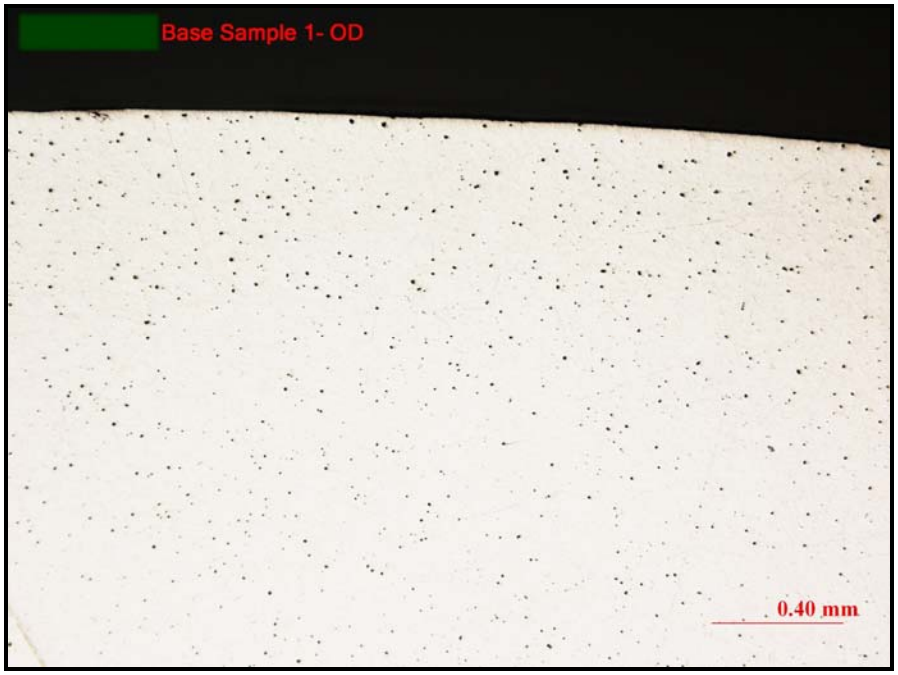

Figure 133: Microscope image shows the unetched OD of the sample 1 from base of the cylinder # AR0118876. Magnification: 50X.

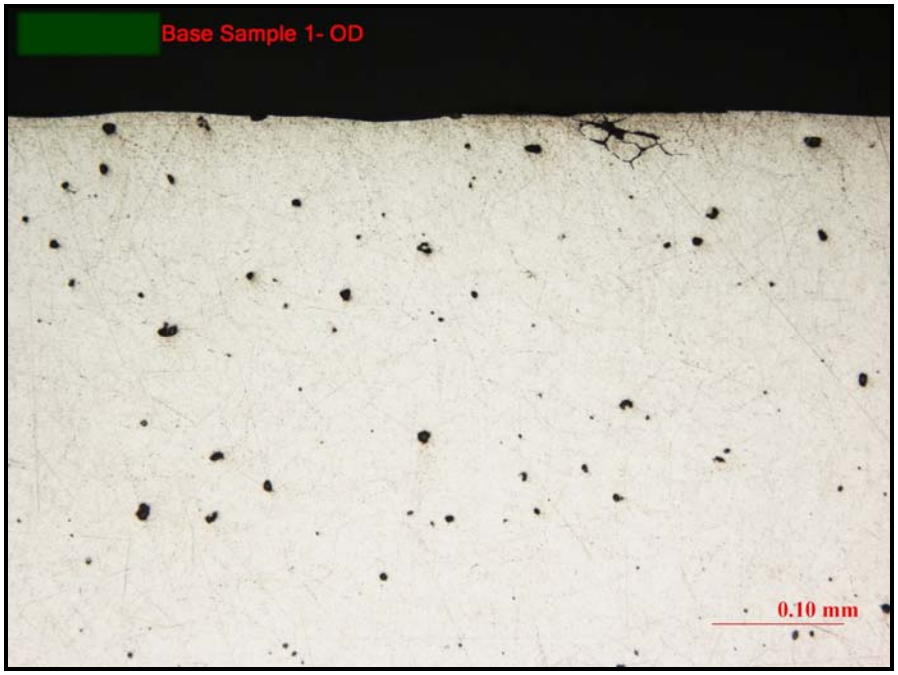

Figure 134: Microscope image shows the unetched OD of the sample 1 from base of the cylinder # AR0118876. Magnification: 200X.

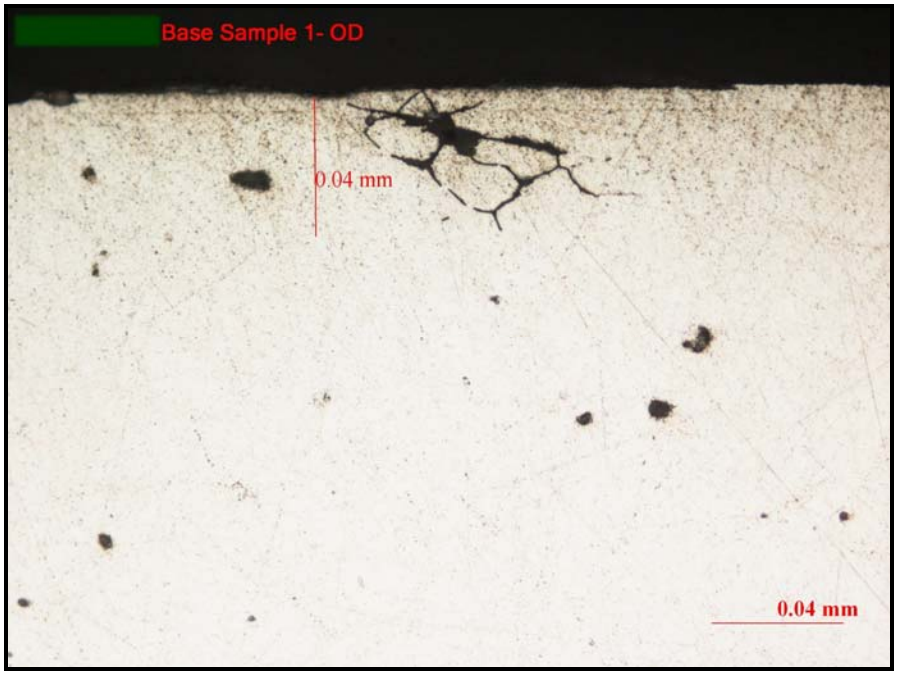

Figure 135: Microscope image shows the unetched OD of the sample 1 from base of the cylinder # AR0118876. Inter-crystalline attack < 0.1 mm. Magnification: 500X.

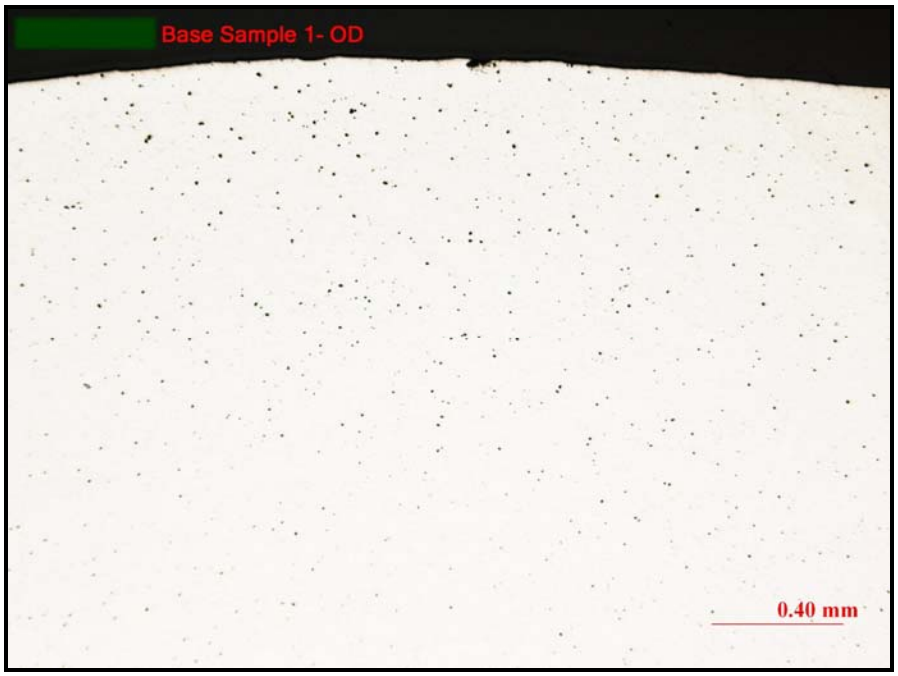

Figure 136: Microscope image shows the unetched OD of the sample 1 from base of the cylinder # AR0118876. Magnification: 50X.

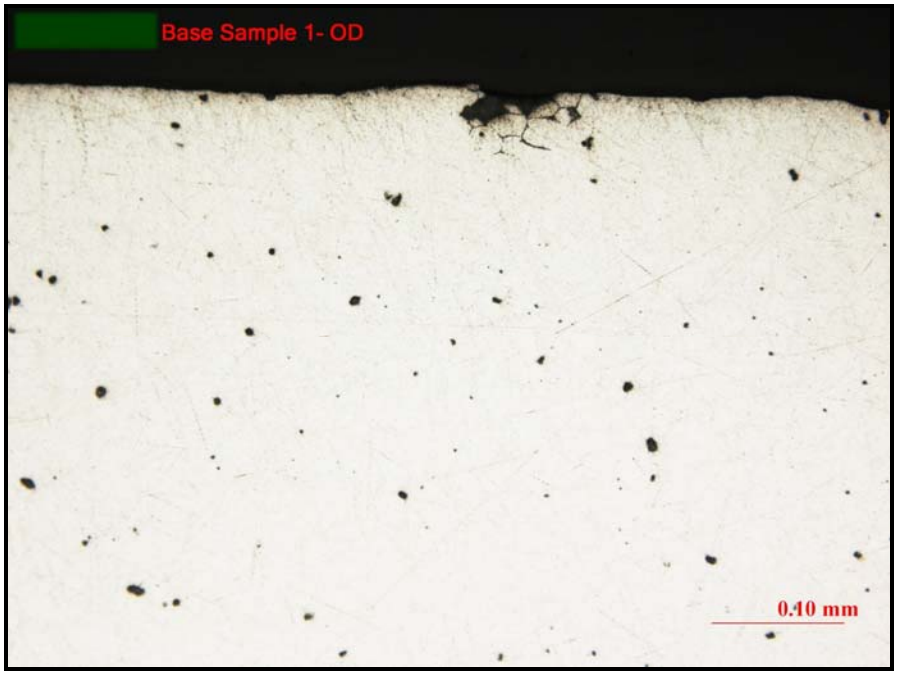

Figure 137: Microscope image shows the unetched OD of the sample 1 from base of the cylinder # AR0118876. Magnification: 200X.

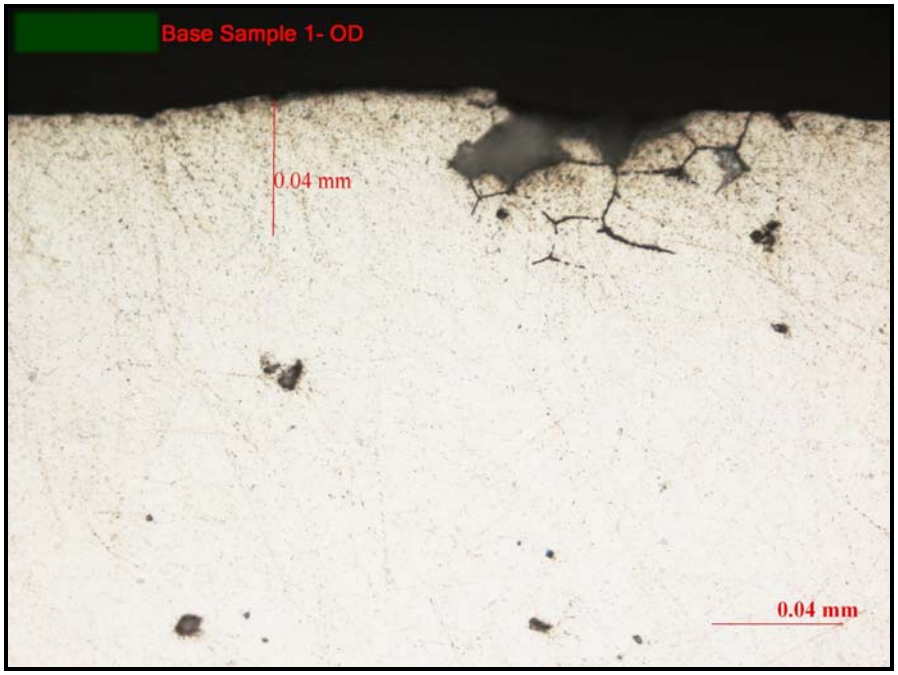

Figure 138: Microscope image shows the unetched OD of the sample 1 from base of the cylinder # AR0118876. Inter-crystalline attack< 0.1 mm. Magnification: 500X.

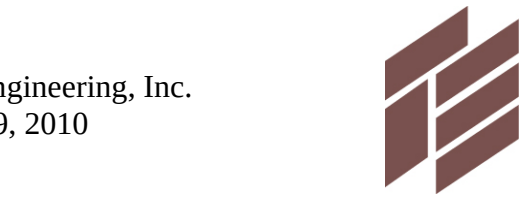

Figure 139: Microscope image shows the unetched ID of the sample 2 from base of the cylinder # AR0118876. No inter-crystalline attack observed. Magnification: 50X.

Figure 140: Microscope image shows the unetched ID of the sample 2 from base of the cylinder # AR0118876. No inter-crystalline attack observed. Magnification: 200X.

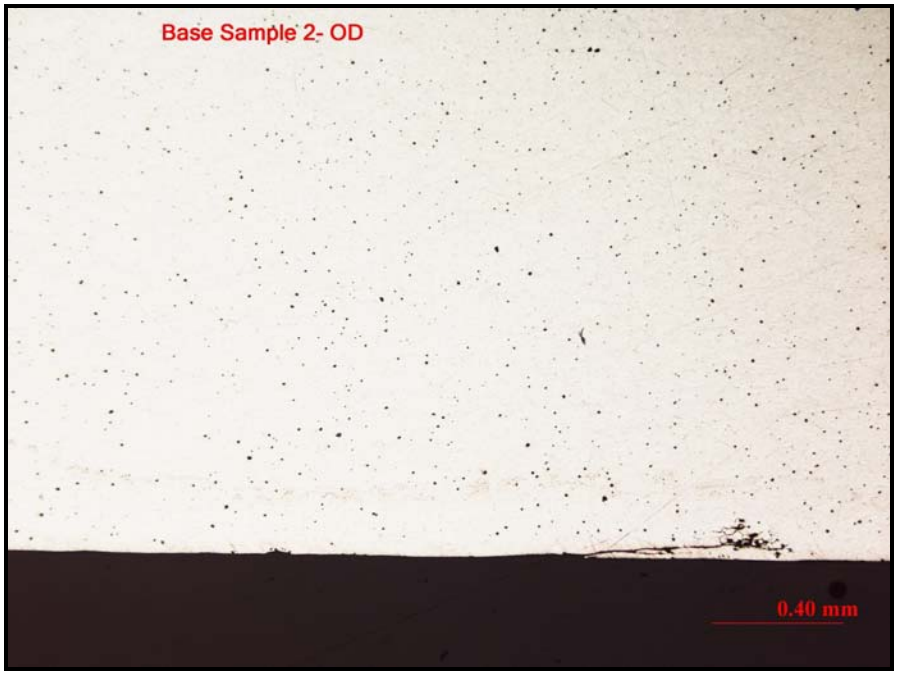

Figure 141: Microscope image shows the unetched OD of the sample 2 from base of the cylinder # AR0118876. No inter-crystalline attack observed. Magnification: 50X.

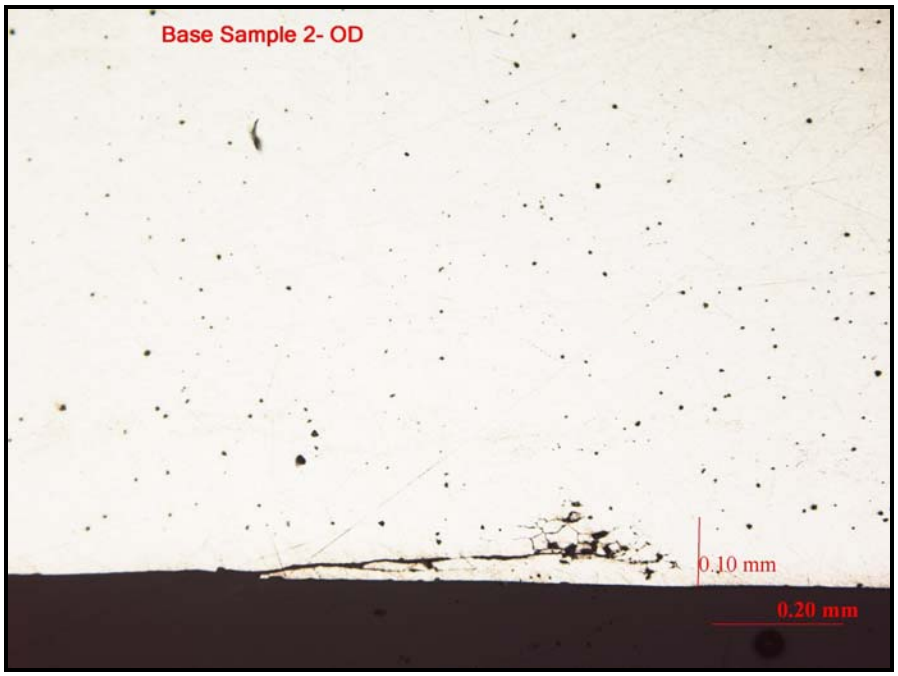

Figure 142: Microscope image shows the unetched OD of the sample 2 from base of the cylinder # AR0118876. Inter-crystalline attack = 0.1 mm. Magnification: 100X.

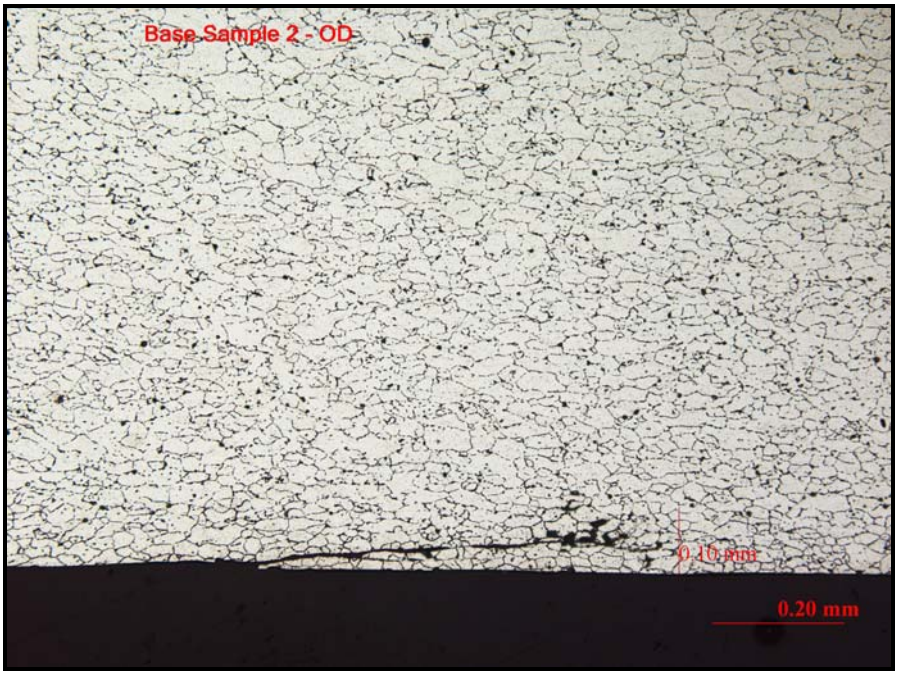

Figure 143: Microscope image shows the etched OD of the sample 2 from base of the cylinder # AR0118876. Inter-crystalline attack = 0.1 mm. Magnification: 100X. Etchant: Keller's etch

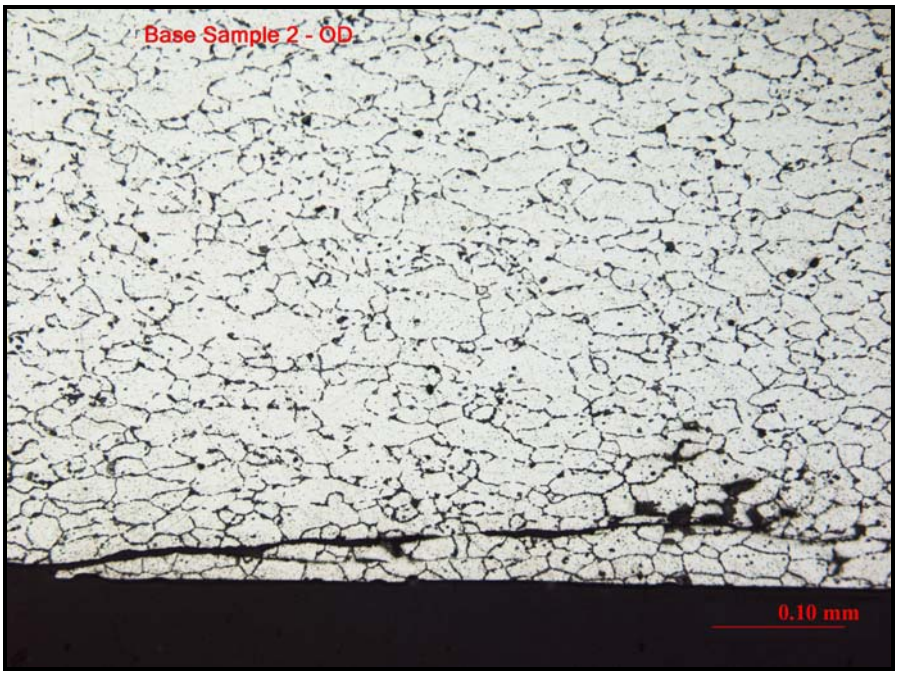

Figure 144: Microscope image shows the etched OD of the sample 2 from base of the cylinder # AR0118876. Magnification: 200X. Etchant: Keller's etch

Figure 145: Microscope image shows the unetched ID of the sample 3 from the base of the cylinder # AR0118876. No inter-crystalline attack observed. Magnification: 50X.

Figure 146: Microscope image shows the unetched ID of the sample 3 from the base of the cylinder # AR0118876. No inter-crystalline attack observed. Magnification: 200X.

Figure 147: Microscope image shows the unetched OD of the sample 3 from the base of the cylinder # AR0118876. Magnification: 50X.

Figure 148: Microscope image shows the unetched OD of the sample 3 from the base of the cylinder # AR0118876. Magnification: 200X.

Figure 149: Microscope image shows the unetched OD of the sample 3 from the base of the cylinder # AR0118876. Inter-crystalline attack < 0.1 mm. Magnification: 500X.

Figure 150: Microscope image shows the unetched ID of the sample 4 from the base of the cylinder # AR0118876. No inter-crystalline attack observed. Magnification: 50X.

Figure 151: Microscope image shows the unetched ID of the sample 4 from the base of the cylinder # AR0118876. No inter-crystalline attack observed. Magnification: 200X.

Figure 152: Microscope image shows the unetched OD of the sample 4 from the base of the cylinder # AR0118876. Magnification: 50X.

Figure 153: Microscope image shows the unetched OD of the sample 4 from the base of the cylinder # AR0118876. Inter-crystalline attack observed. Magnification: 200X.

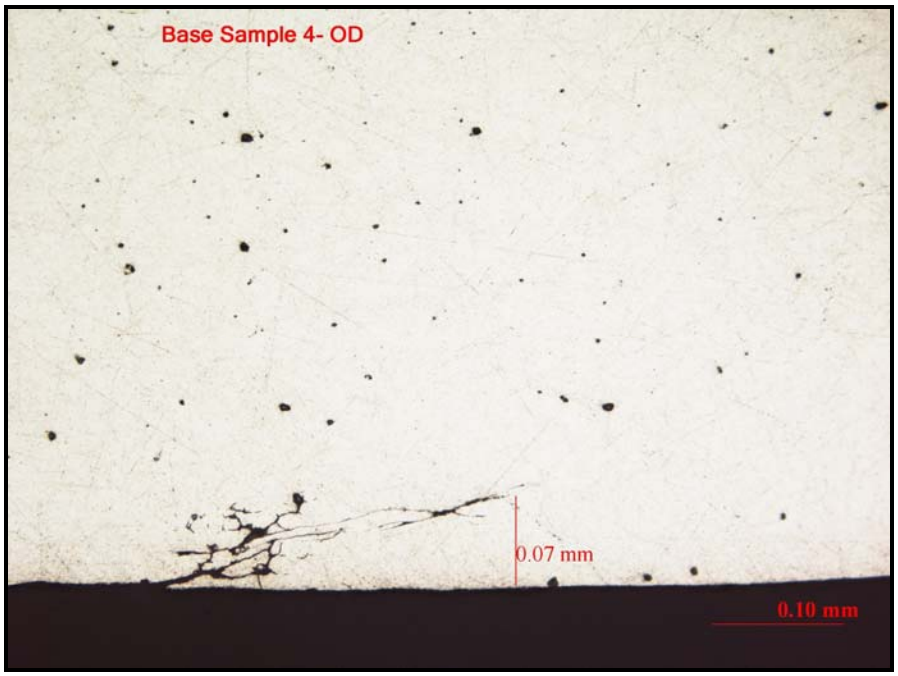

Figure 154: Microscope image shows the unetched OD of the sample 4 from the base of the cylinder # AR0118876. Inter-crystalline attack < 0.1 mm. Magnification: 200X.

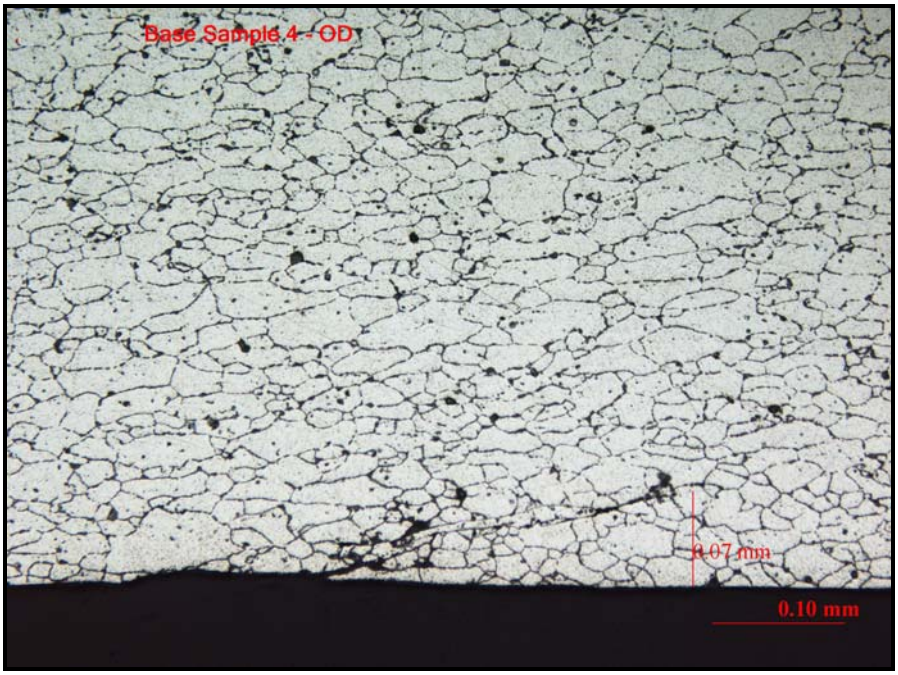

Figure 155: Microscope image shows the unetched OD of the sample 4 from the base of the cylinder # AR0118876. Inter-crystalline attack < 0.1 mm. Magnification: 200X. Etchant: Keller's etch

Figure 156: Microscope image shows the unetched OD of the sample 4 from the base of the cylinder # AR0118876. Magnification: 50X.

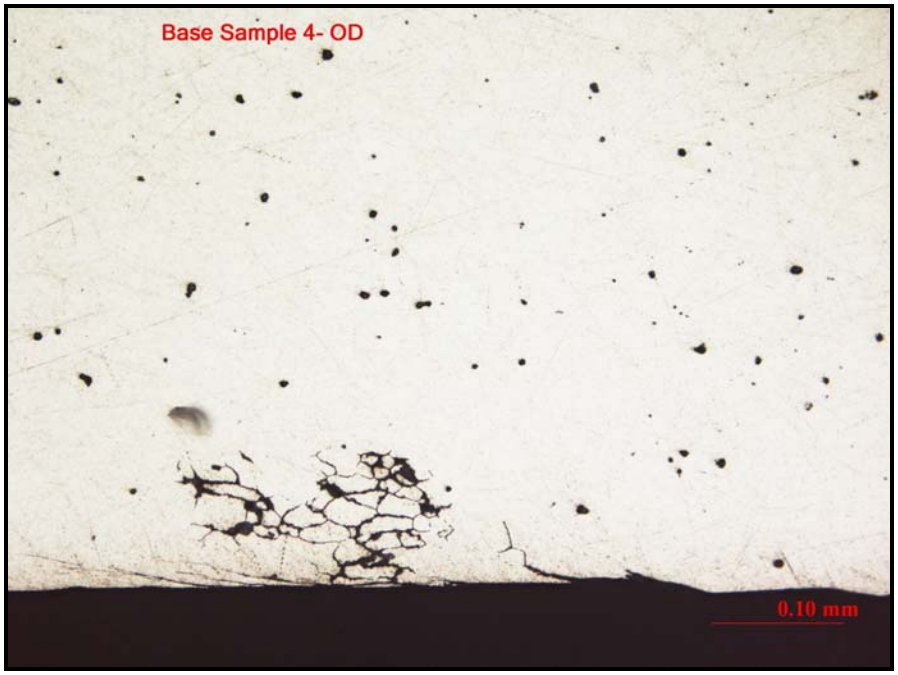

Figure 157: Microscope image shows the unetched OD of the sample 4 from the base of the cylinder # AR0118876. Inter-crystalline attack observed. Magnification: 200X.

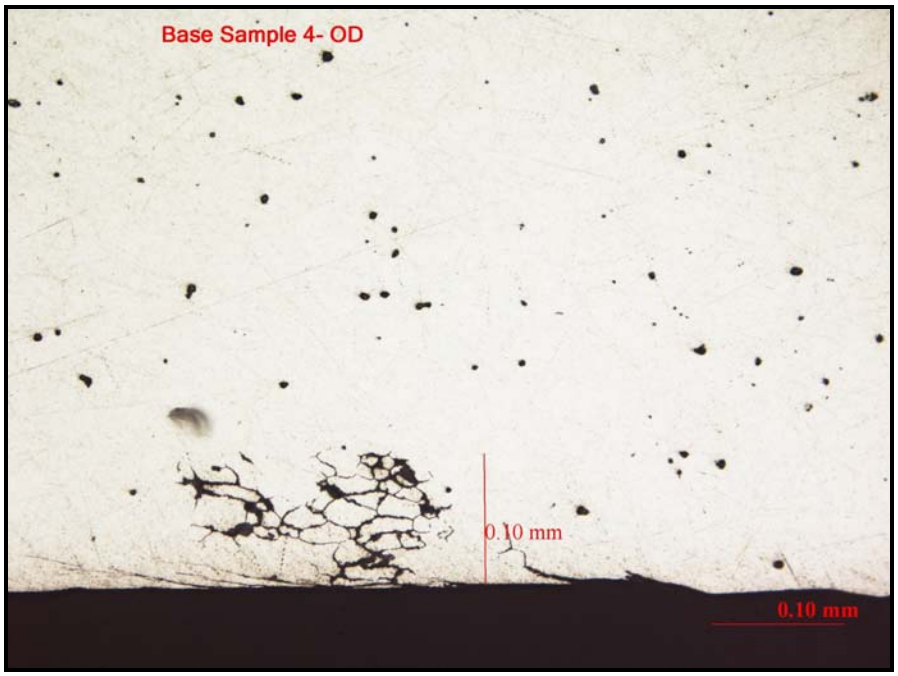

Figure 158: Microscope image shows the unetched ID of the sample 1 from Head of the cylinder # AR0118876. Inter-crystalline attack = 0.1 mm. Magnification: 200X.

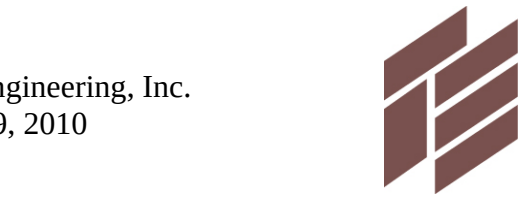

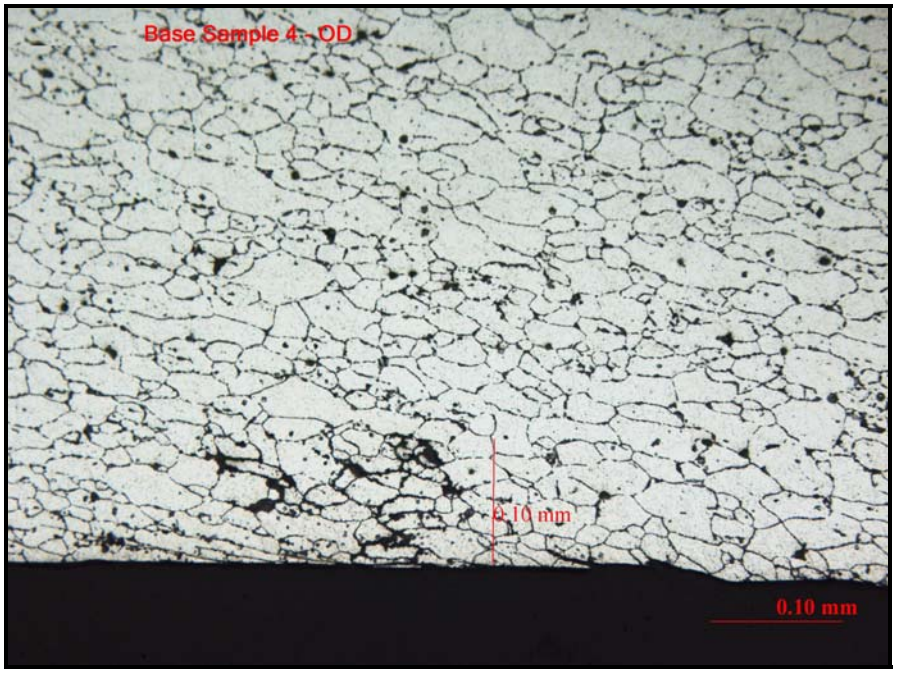

Figure 159: Microscope image shows the etched OD of the sample 4 from the base of the cylinder # AR0118876. Inter-crystalline attack = 0.1 mm. Magnification: 200X. Etchant: Keller's etch

Figure 160: Shows the machined compact tension samples 1 and 2.

Figure 161: Shows the machined compact tension samples 3 to 8.

Figure 162: Shows the set up at the beginning of the 90 day sustained load cracking test.

Figure 163: Shows the test set up at the end of the 90 day sustained load cracking test.

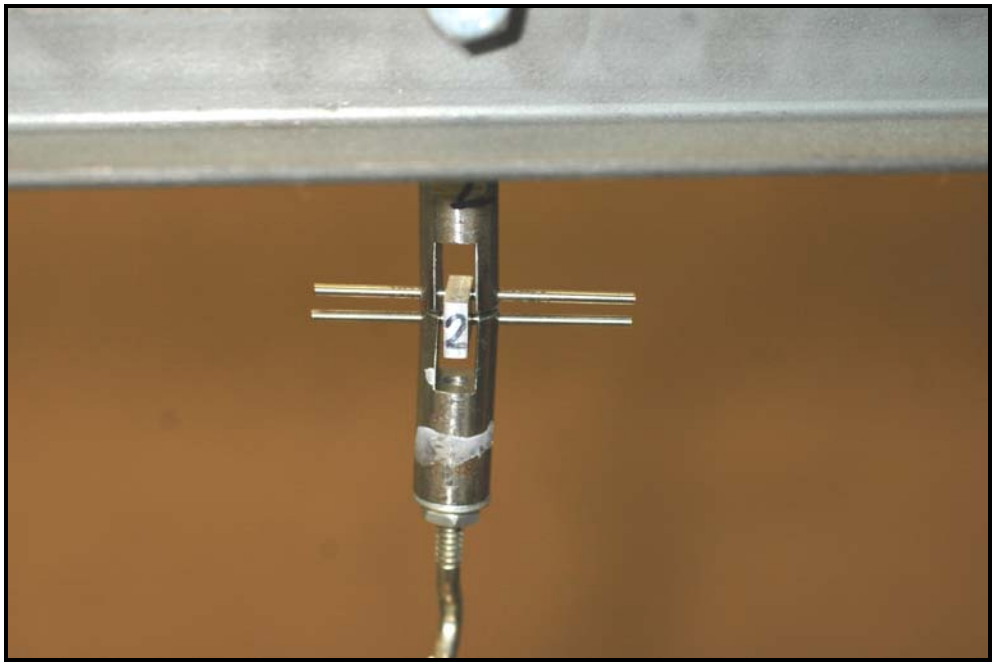

Figure 164: Shows the unloaded compact tension sample 2 at the end of the 90 day test. Note the sample didn't break after the 90 day test.

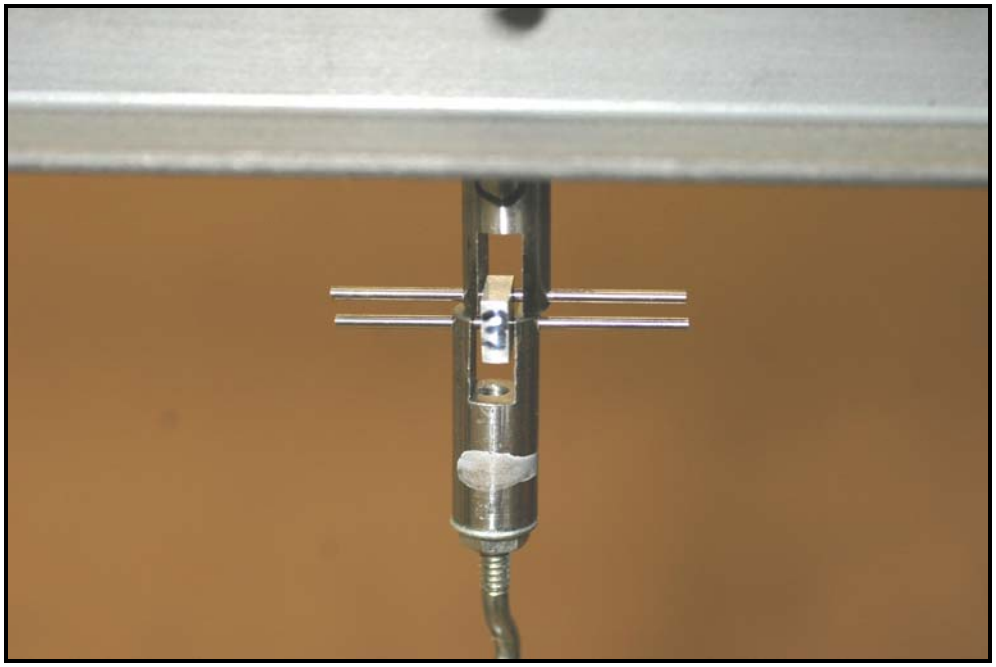

Figure 165: Shows the unloaded compact tension sample 3 at the end of the 90 day test. Note the sample didn't break after the 90 day test.

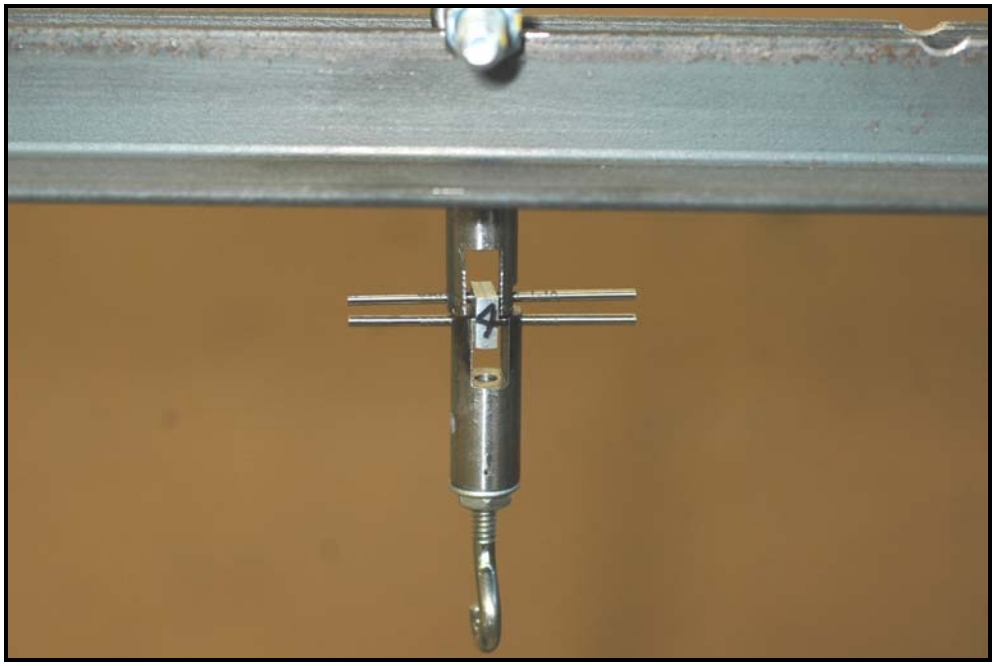

Figure 166: Shows the unloaded compact tension sample 4 at the end of the 90 day test. Note the sample didn't break after the 90 day test.

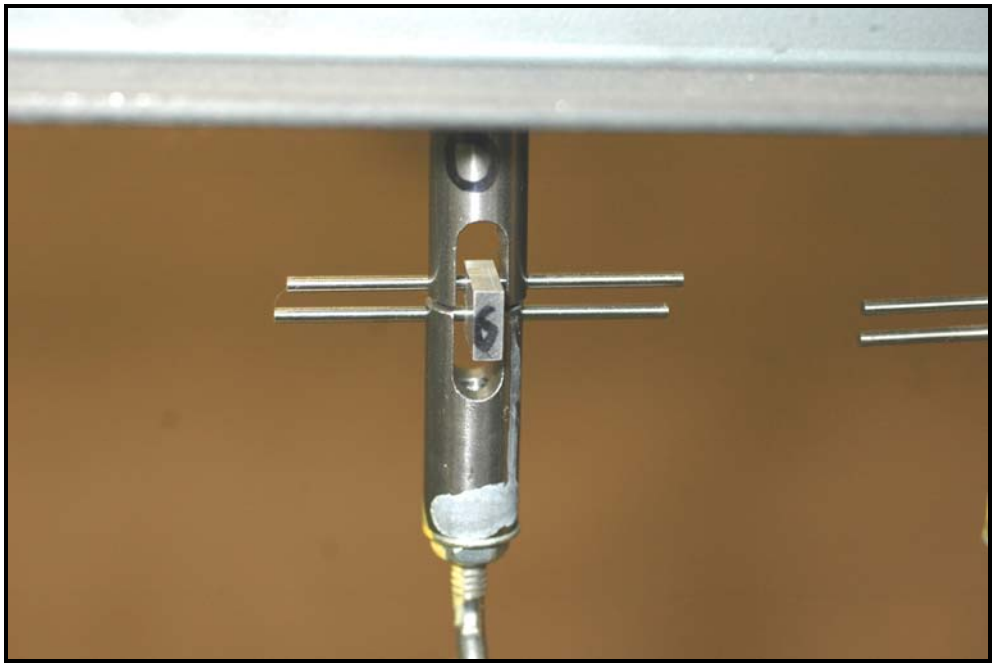

Figure 167: Shows the unloaded compact tension sample 6 at the end of the 90 day test. Note the sample didn't break after the 90 day test.

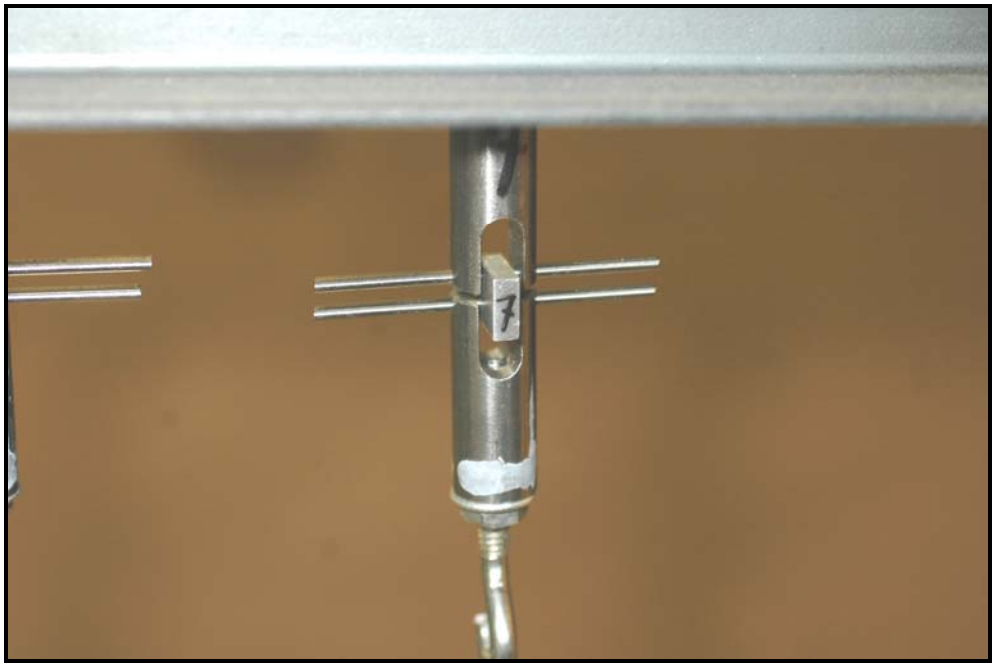

Figure 168: Shows the unloaded compact tension sample 7 at the end of the 90 day test. Note the sample didn't break after the 90 day test.

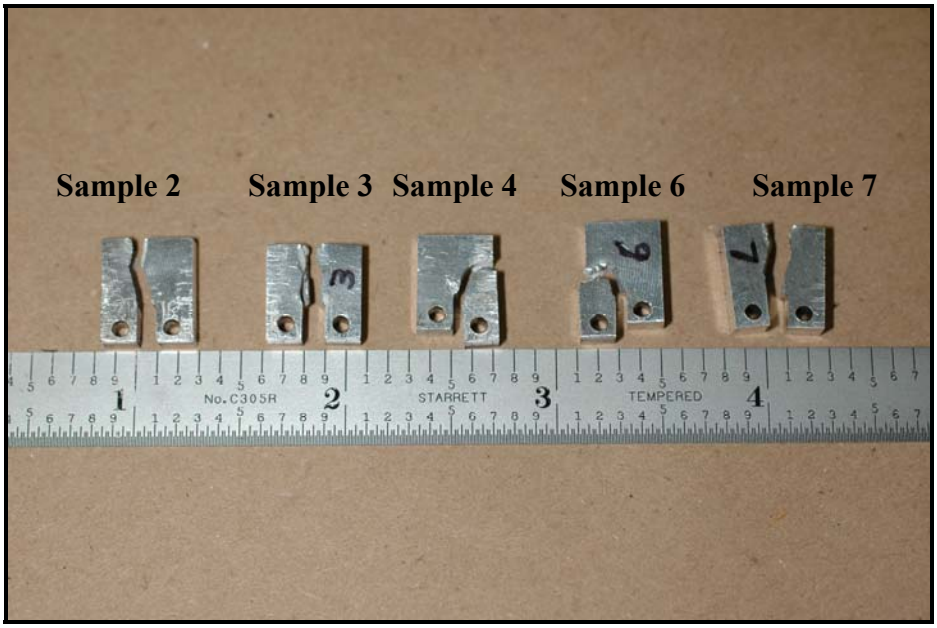

Figure 169: Shows the failed samples after being subjected to post-fatigue and final overload fracture. The fracture surface of each of these specimens was observed using the SEM.

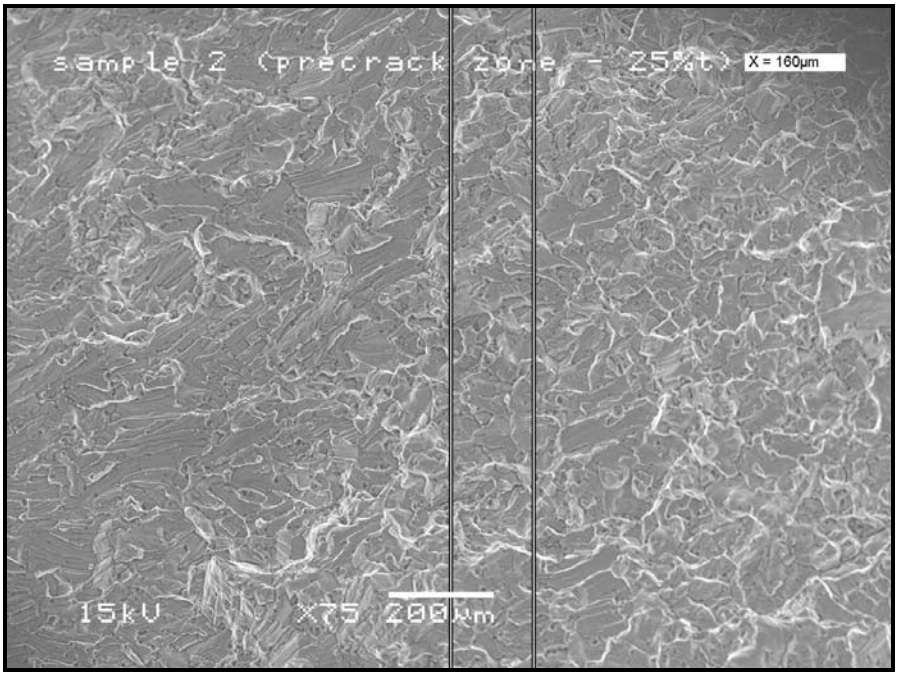

Figure 170: SEM image of sample 2 shows the fracture surface along the 0.16 mm distance from the pre-fatigue crack zone at 25% thickness, 75X. Fatigue was observed throughout the 0.16 mm distance from pre-fatigue crack zone.

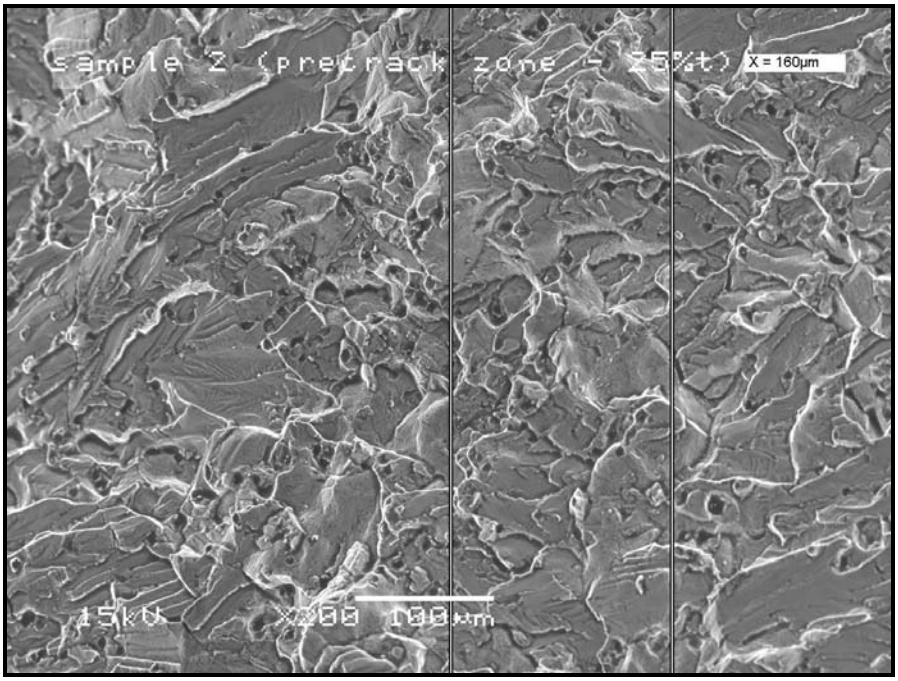

Figure 171: SEM image of sample 2 shows the fracture surface along the 0.16 mm distance from the pre-fatigue crack zone at 25% thickness, 200X. Fatigue was observed throughout the 0.16 mm distance from pre-fatigue crack zone.

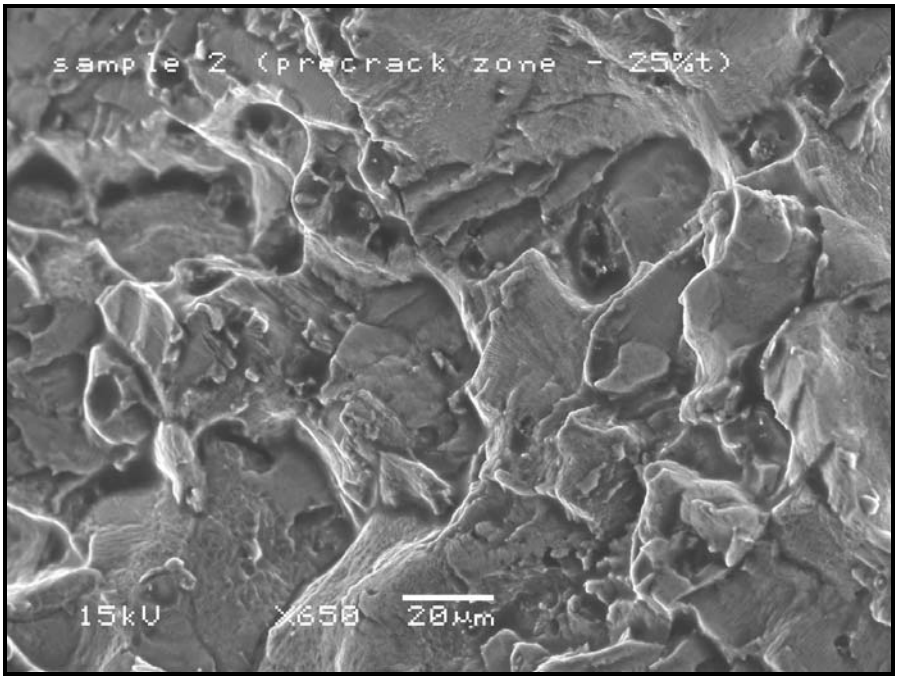

Figure 172: SEM image of sample 2 shows the fracture surface at the pre-fatigue crack zone at 25% thickness, 650X. Fatigue striations were observed throughout the pre-fatigue crack zone.

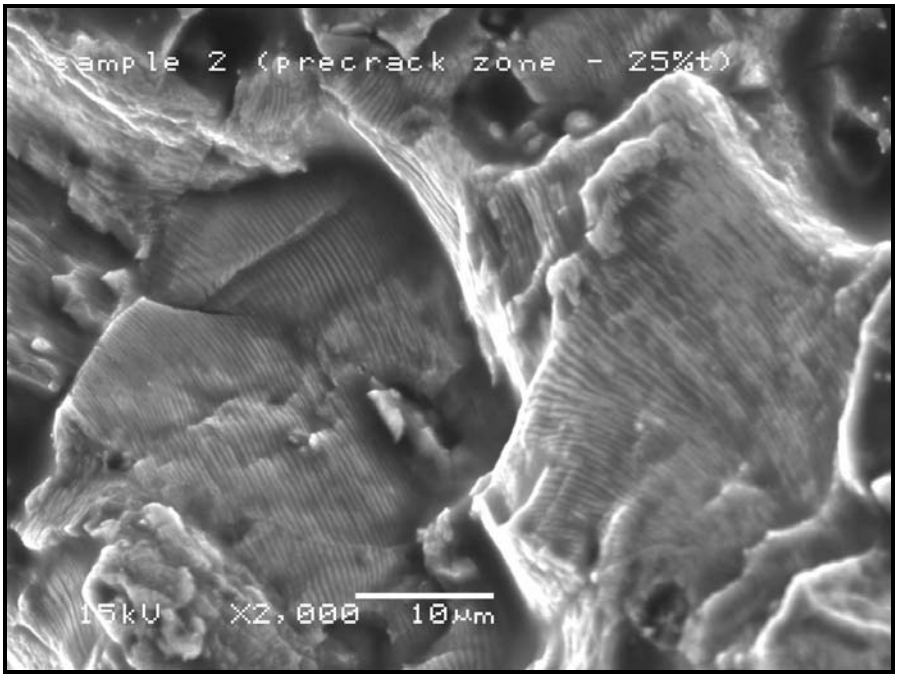

Figure 173: SEM image of sample 2 shows the fracture surface at the pre-fatigue crack zone at 25% thickness, 2000X. Fatigue striations were observed throughout the pre-fatigue crack zone.

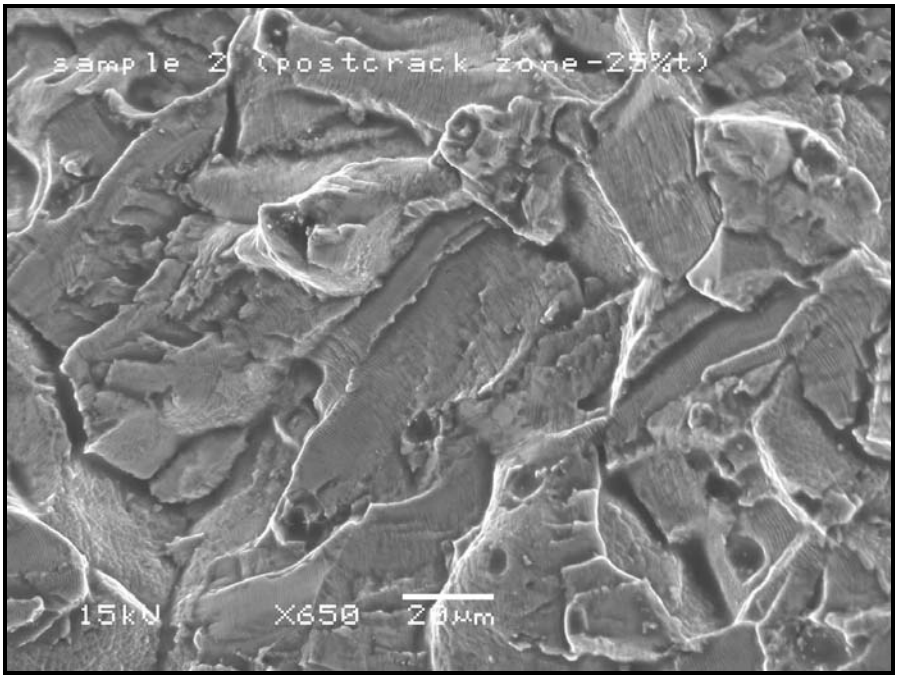

Figure 174: SEM image of sample 2 shows the fracture surface at the post-fatigue crack zone at 25% thickness, 650X. Fatigue striations were observed throughout the post-fatigue crack zone along the 0.16 mm from the pre-fatigue crack zone.

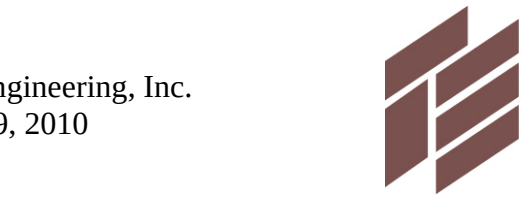

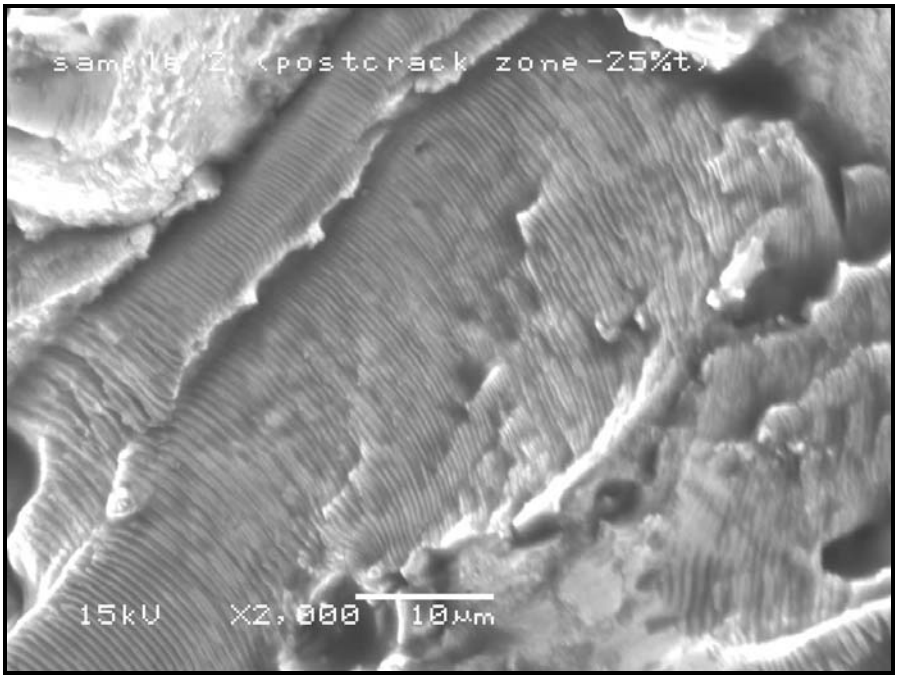

Figure 175: SEM image of sample 2 shows the fracture surface at the post-fatigue crack zone at 25% thickness, 650X. Fatigue striations were observed throughout the post-fatigue crack zone along the 0.16 mm from the pre-fatigue crack zone.

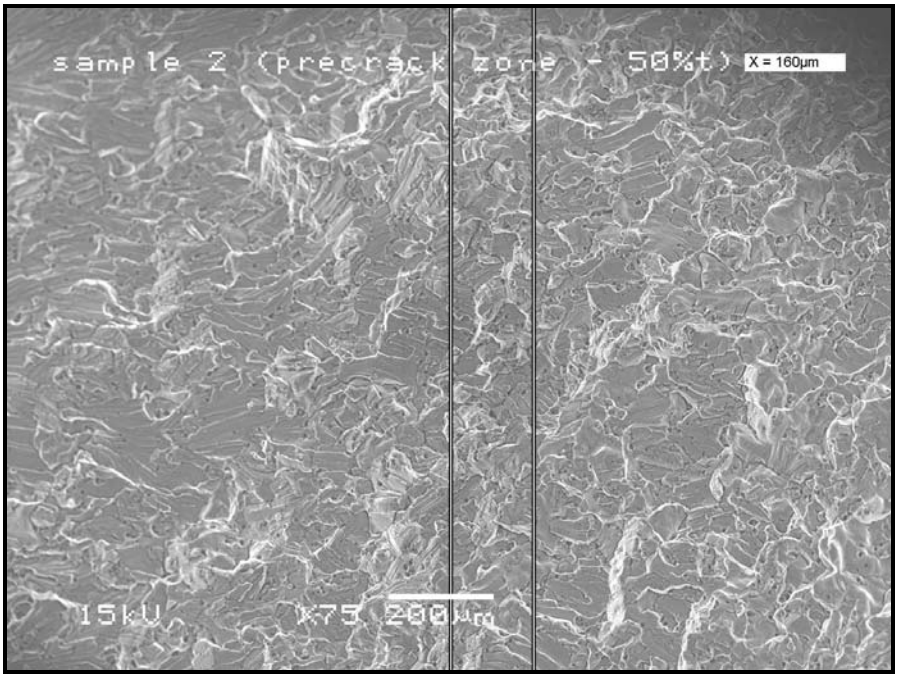

Figure 176: SEM image of sample 2 shows the fracture surface along the 0.16 mm distance from the pre-fatigue crack zone at 50% thickness, 75X. Fatigue was observed throughout the 0.16 mm distance from pre-fatigue crack zone.

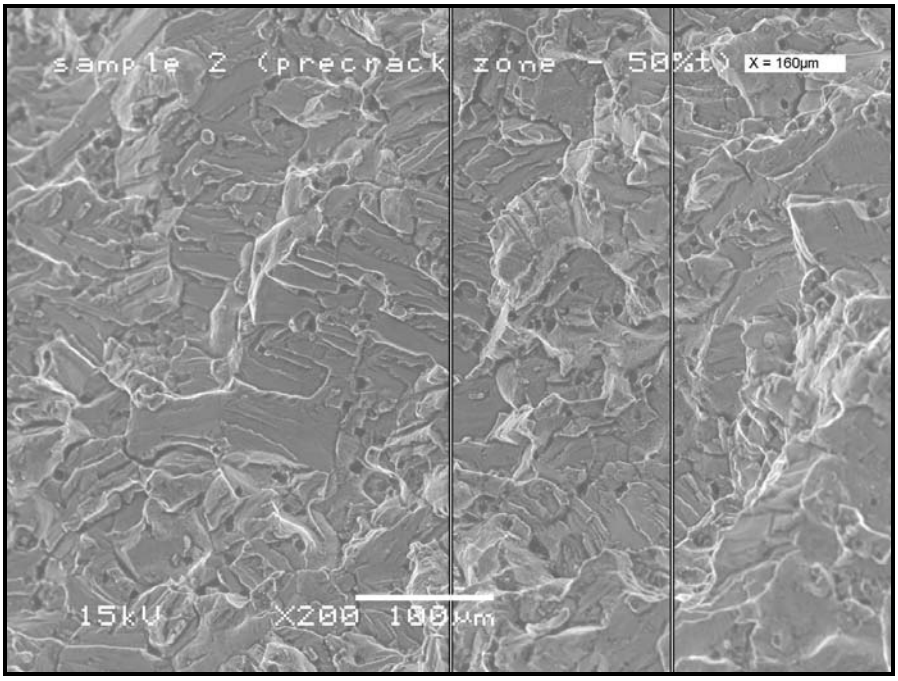

Figure 177: SEM image of sample 2 shows the fracture surface along the 0.16 mm distance from the pre-fatigue crack zone at 50% thickness, 200X. Fatigue was observed throughout the 0.16 mm distance from pre-fatigue crack zone.

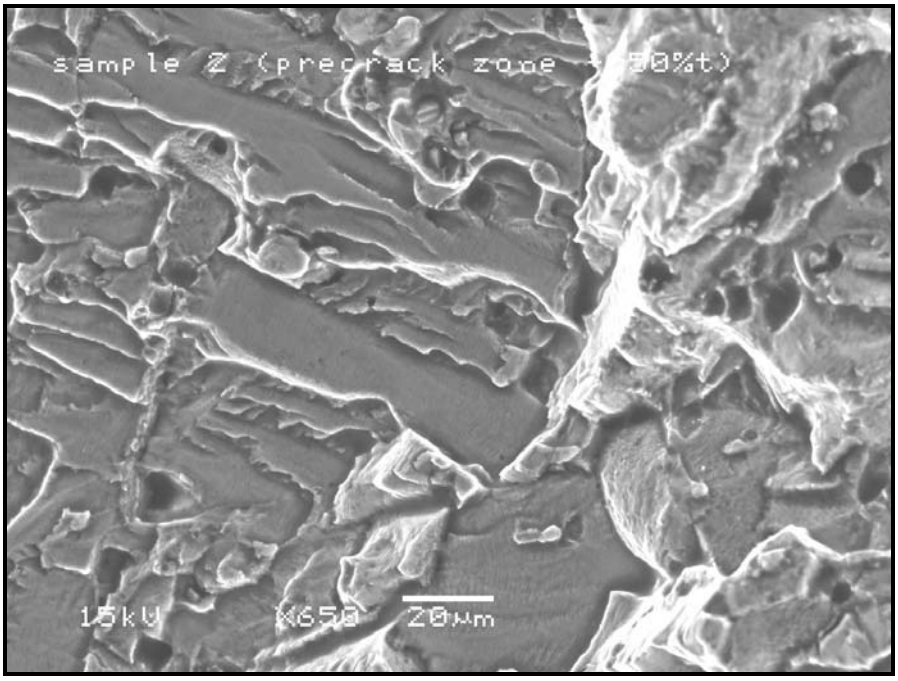

Figure 178: SEM image of sample 2 shows the fracture surface at the pre-fatigue crack zone at 50% thickness, 650X. Fatigue striations were observed throughout the pre-fatigue crack zone.

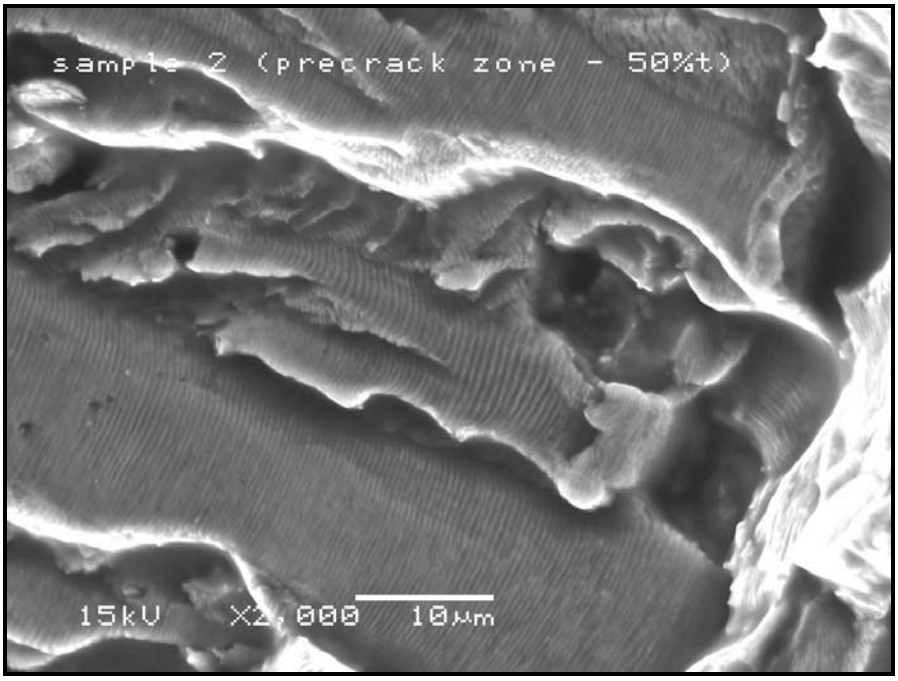

Figure 179: SEM image of sample 2 shows the fracture surface at the pre-fatigue crack zone at 50% thickness, 2000X. Fatigue striations were observed throughout the pre-fatigue crack zone.

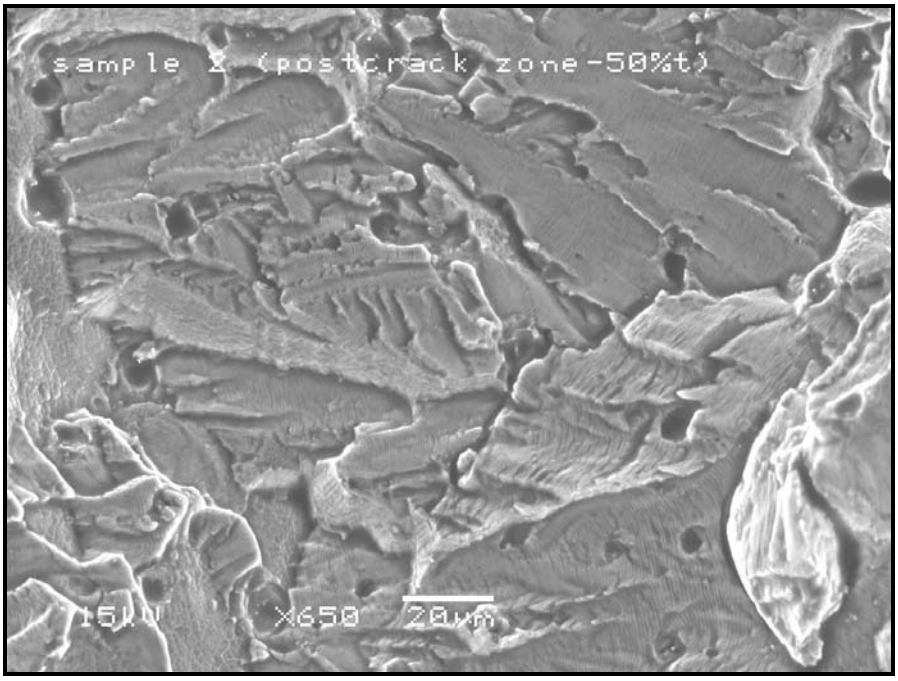

Figure 180: SEM image of sample 2 shows the fracture surface at the post-fatigue crack zone at 50% thickness, 650X. Fatigue striations were observed throughout the post-fatigue crack zone along the 0.16 mm from the pre-fatigue crack zone.

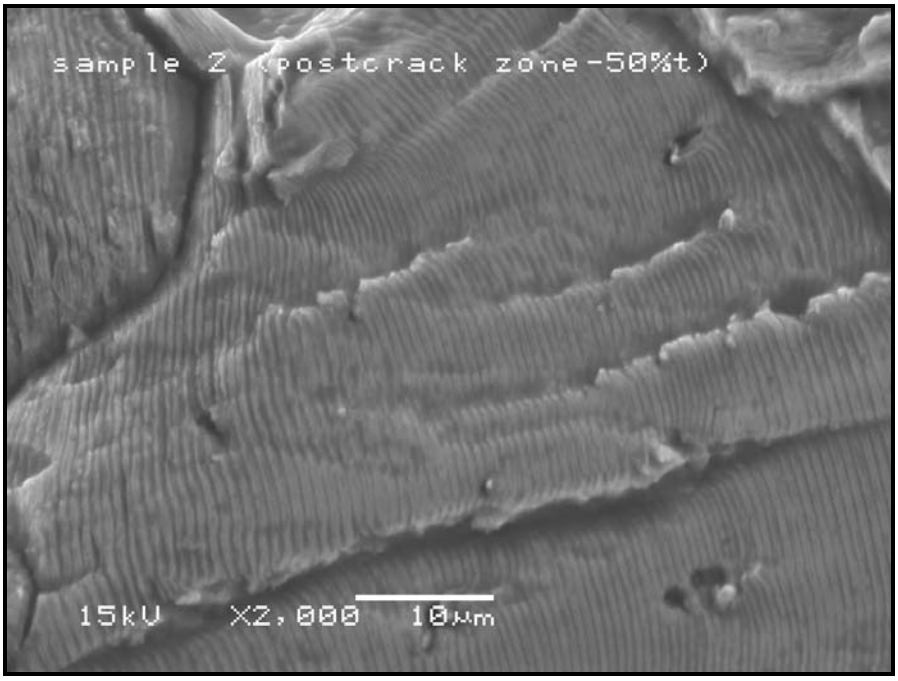

Figure 181: SEM image of sample 2 shows the fracture surface at the post-fatigue crack zone at 50% thickness, 650X. Fatigue striations were observed throughout the post-fatigue crack zone along the 0.16 mm from the pre-fatigue crack zone.

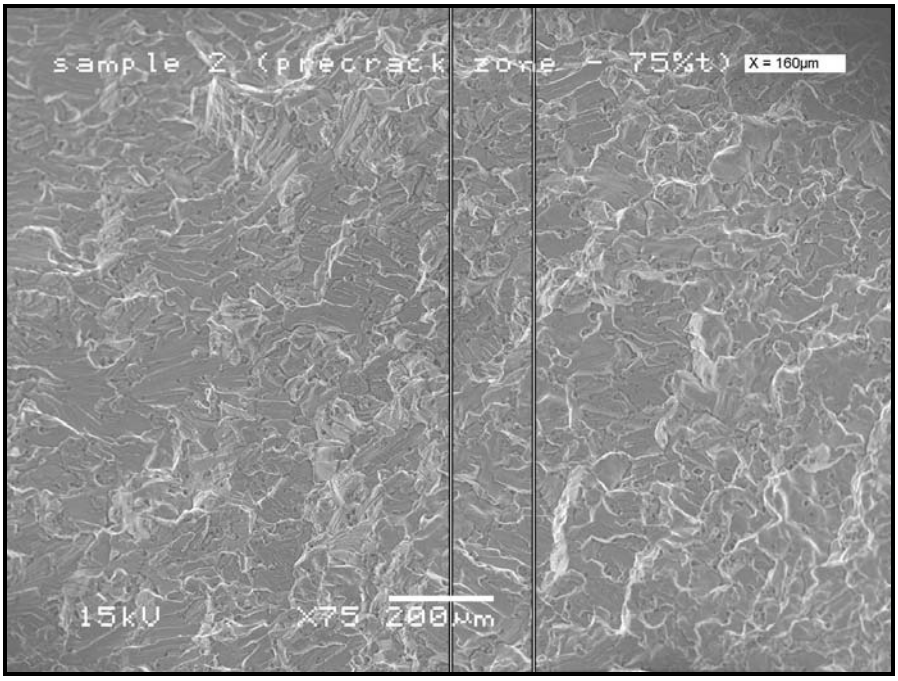

Figure 182: SEM image of sample 2 shows the fracture surface along the 0.16 mm distance from the pre-fatigue crack zone at 75% thickness, 75X. Fatigue was observed throughout the 0.16 mm distance from pre-fatigue crack zone.

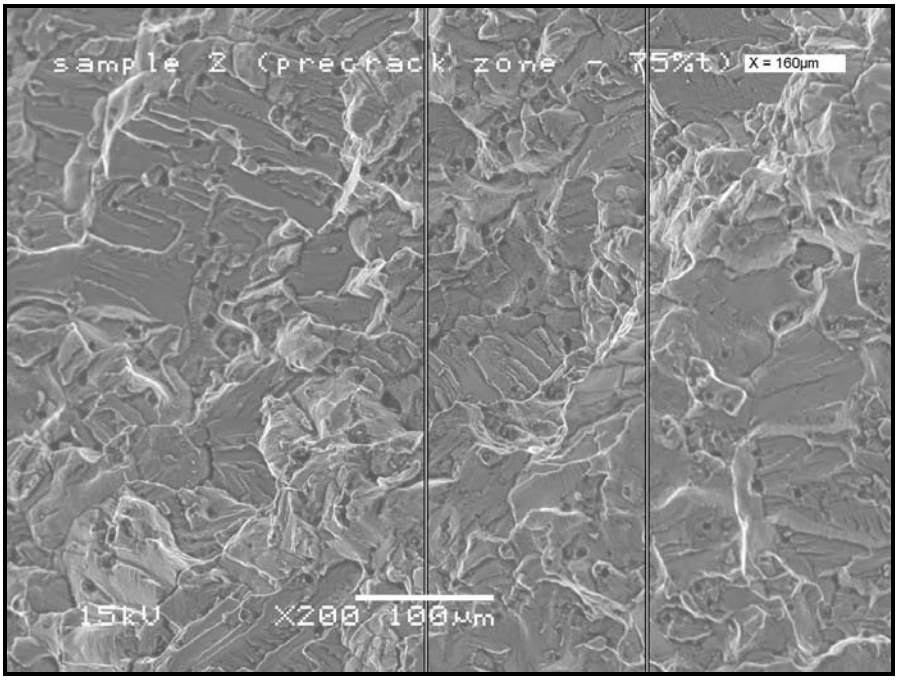

Figure 183: SEM image of sample 2 shows the fracture surface along the 0.16 mm distance from the pre-fatigue crack zone at 75% thickness, 200X. Fatigue was observed throughout the 0.16 mm distance from pre-fatigue crack zone.

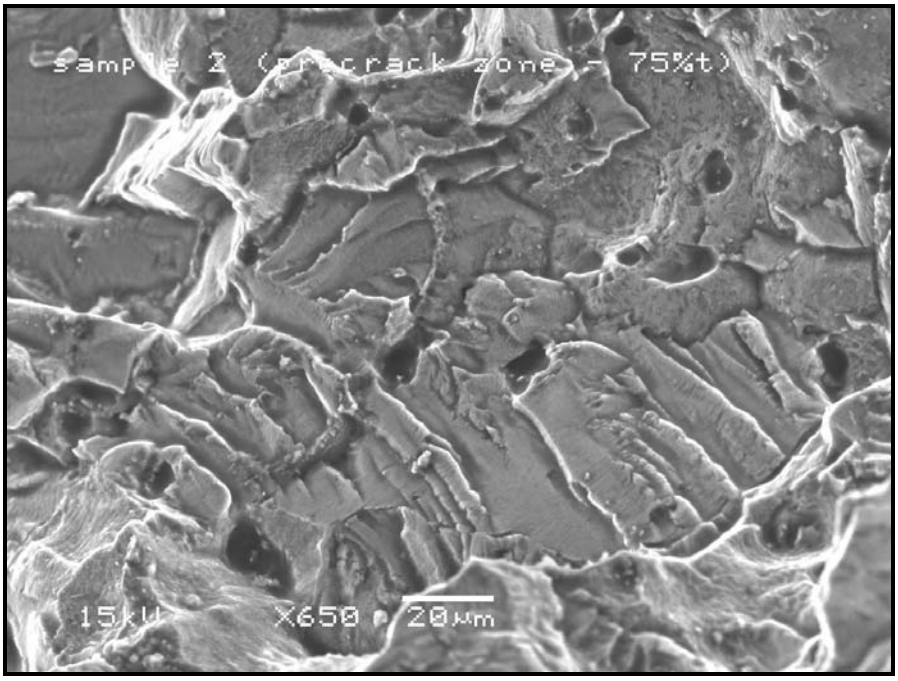

Figure 184: SEM image of sample 2 shows the fracture surface at the pre-fatigue crack zone at 75% thickness, 650X. Fatigue striations were observed throughout the pre-fatigue crack zone.

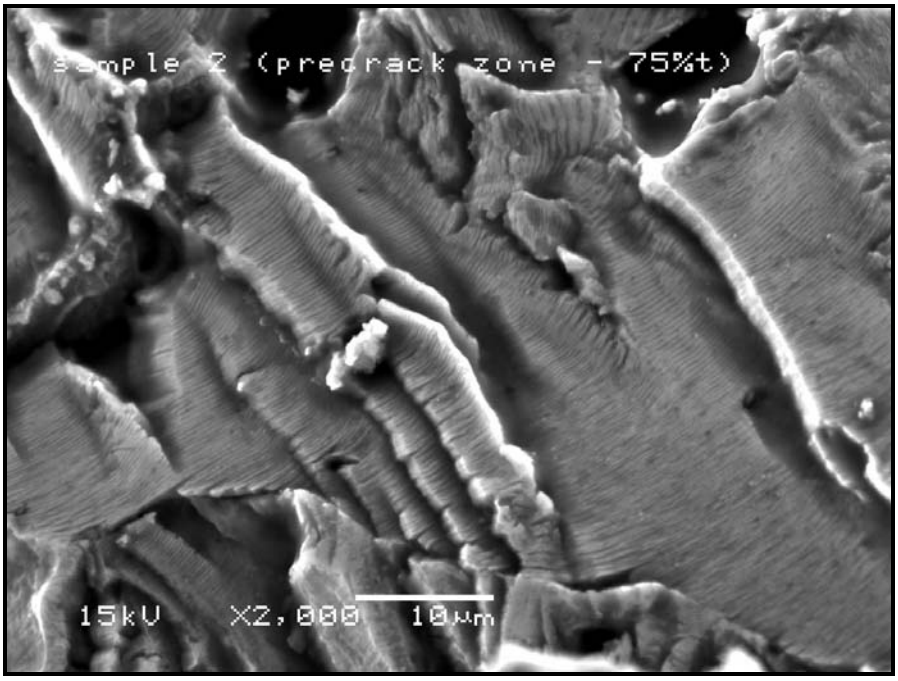

Figure 185: SEM image of sample 2 shows the fracture surface at the pre-fatigue crack zone at 75% thickness, 2000X. Fatigue striations were observed throughout the pre-fatigue crack zone.

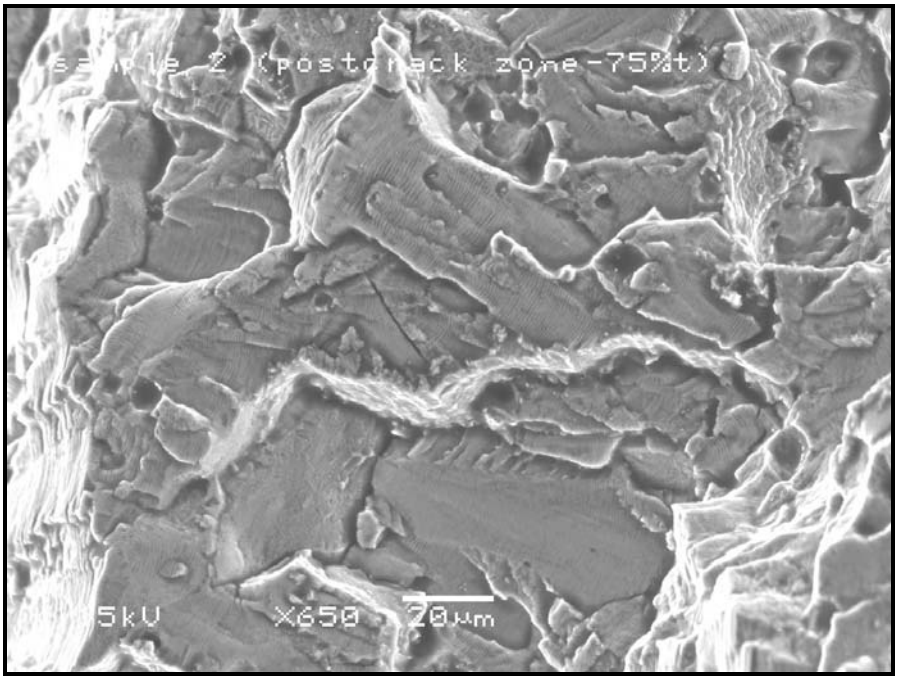

Figure 186: SEM image of sample 2 shows the fracture surface at the post-fatigue crack zone at 75% thickness, 650X. Fatigue striations were observed throughout the post-fatigue crack zone along the 0.16 mm from the pre-fatigue crack zone.

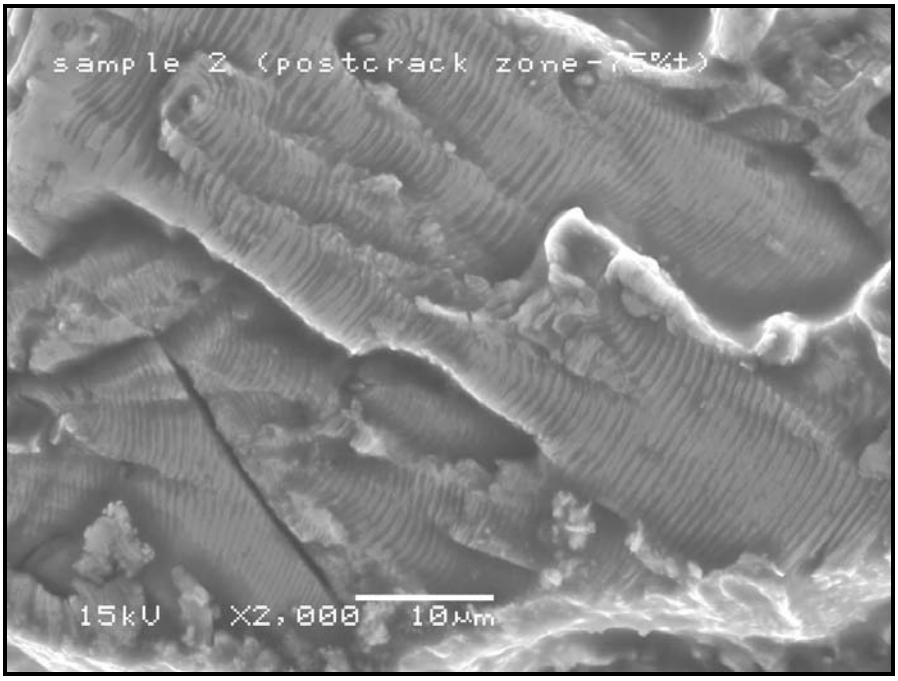

Figure 187: SEM image of sample 2 shows the fracture surface at the post-fatigue crack zone at 75% thickness, 2000X. Fatigue striations were observed throughout the post-fatigue crack zone along the 0.16 mm from the pre-fatigue crack zone.

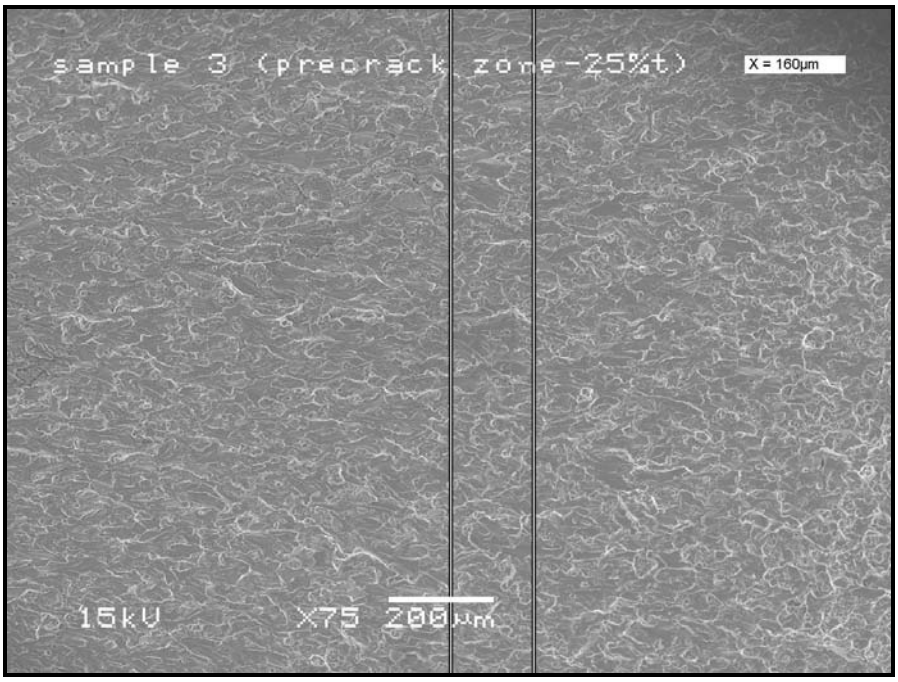

Figure 188: SEM image of sample 3 shows the fracture surface along the 0.16 mm distance from the pre-fatigue crack zone at 25% thickness, 75X. Fatigue was observed throughout the 0.16 mm distance from pre-fatigue crack zone.

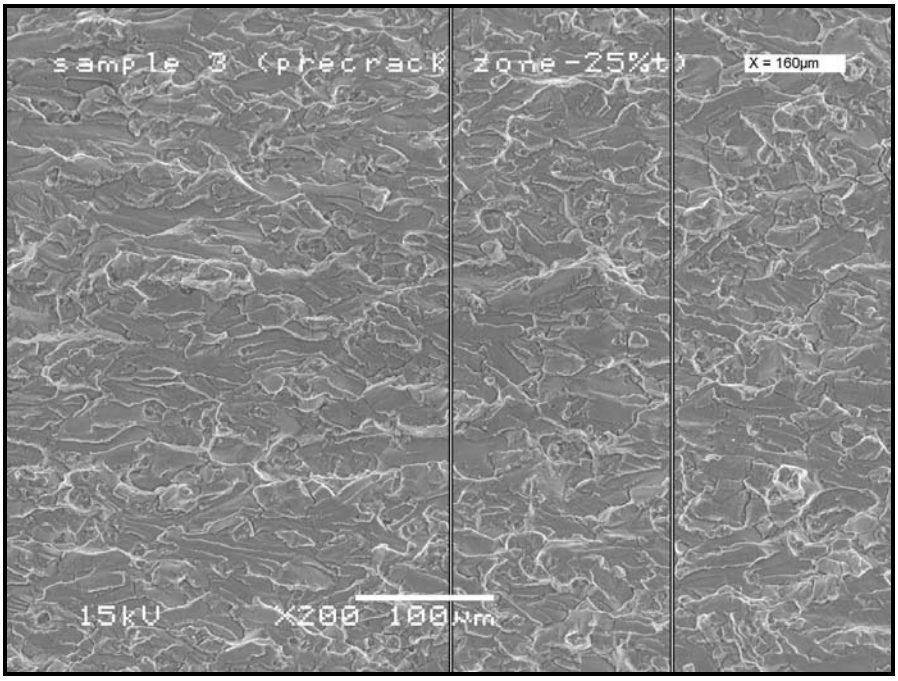

Figure 189: SEM image of sample 3 shows the fracture surface along the 0.16 mm distance from the pre-fatigue crack zone at 25% thickness, 200X. Fatigue was observed throughout the 0.16 mm distance from pre-fatigue crack zone.

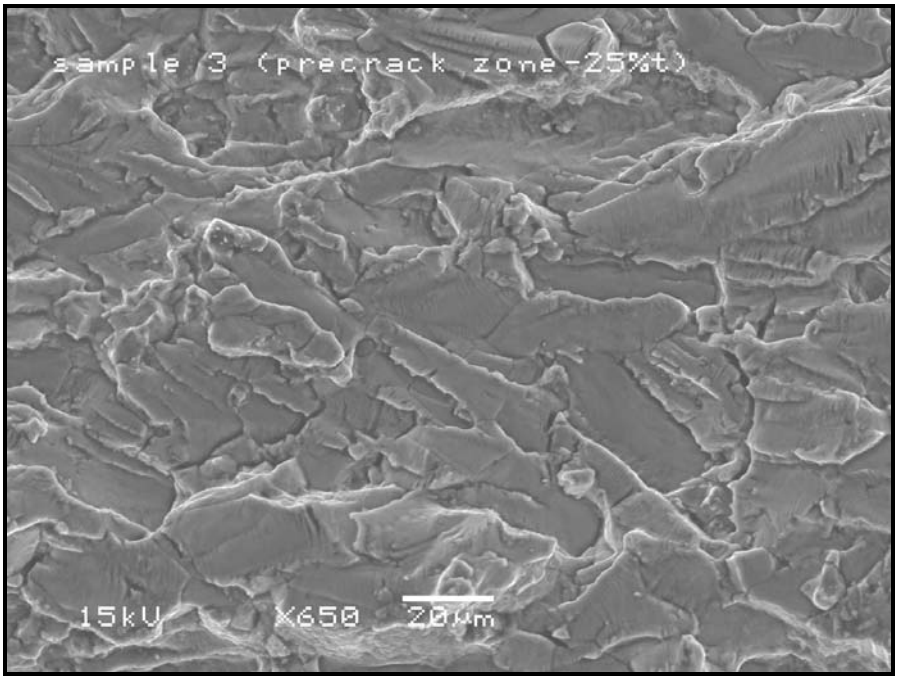

Figure 190: SEM image of sample 3 shows the fracture surface at the pre-fatigue crack zone at 25% thickness, 650X. Fatigue striations were observed throughout the pre-fatigue crack zone.

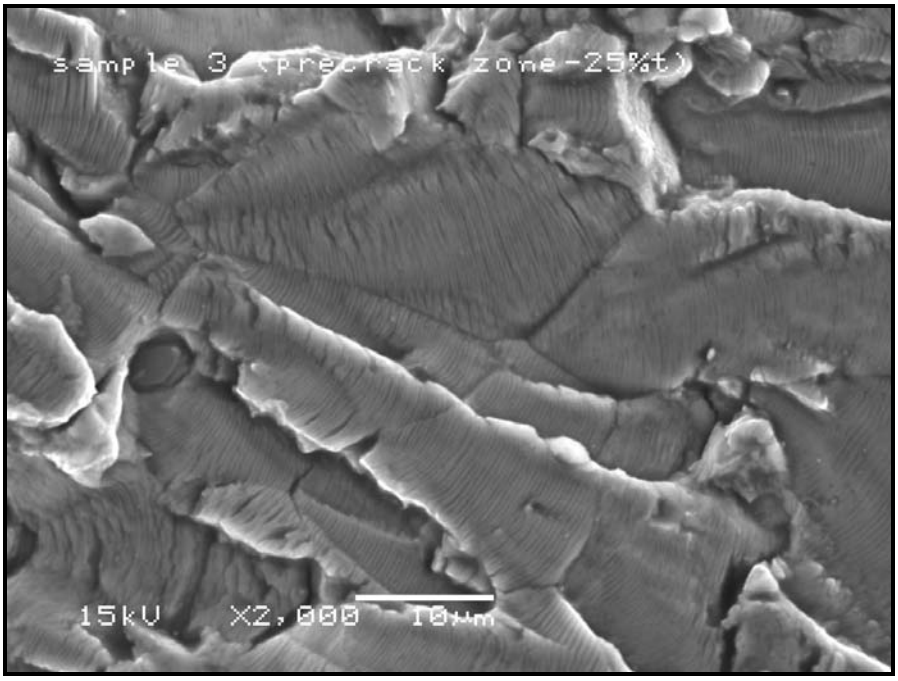

Figure 191: SEM image of sample 3 shows the fracture surface at the pre-fatigue crack zone at 25% thickness, 2000X. Fatigue striations were observed throughout the pre-fatigue crack zone.

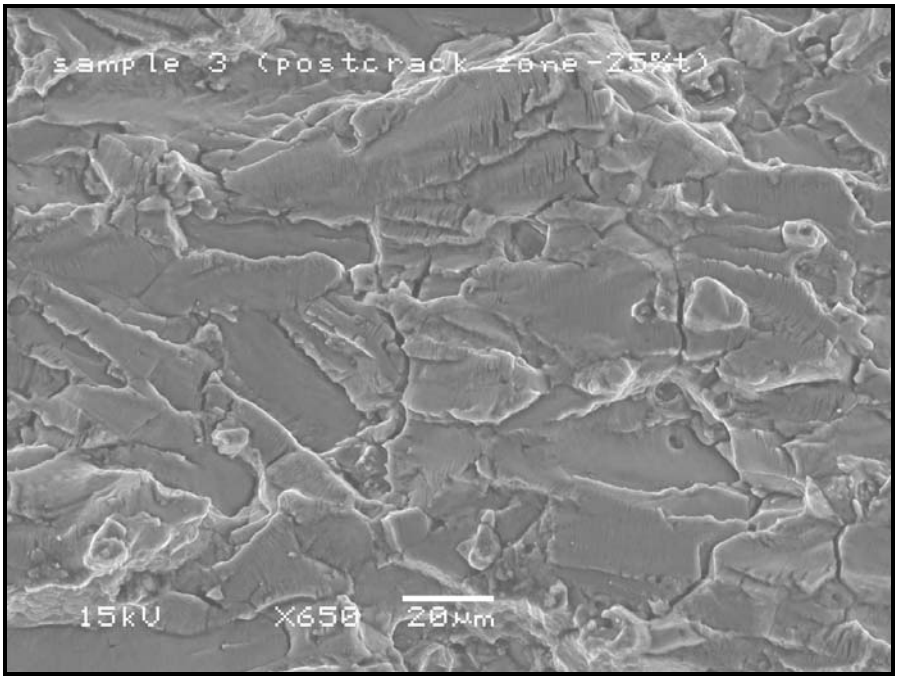

Figure 192: SEM image of sample 3 shows the fracture surface at the post-fatigue crack zone at 25% thickness, 650X. Fatigue striations were observed throughout the post-fatigue crack zone along the 0.16 mm from the pre-fatigue crack zone.

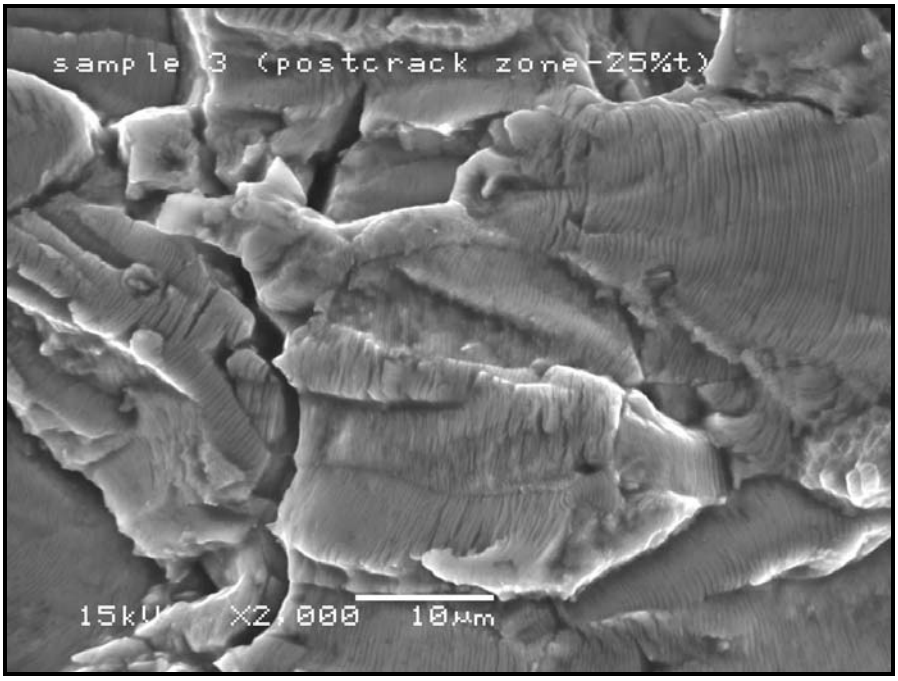

Figure 193: SEM image of sample 3 shows the fracture surface at the post-fatigue crack zone at 25% thickness, 2000X. Fatigue striations were observed throughout the post-fatigue crack zone along the 0.16 mm from the pre-fatigue crack zone.

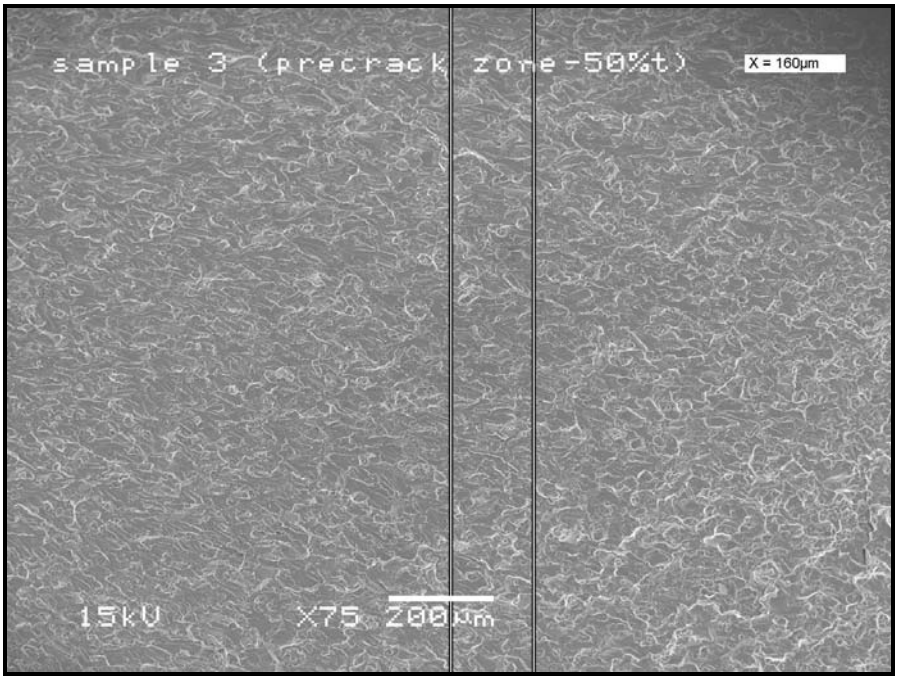

Figure 194: SEM image of sample 3 shows the fracture surface along the 0.16 mm distance from the pre-fatigue crack zone at 50% thickness, 75X. Fatigue was observed throughout the 0.16 mm distance from pre-fatigue crack zone.

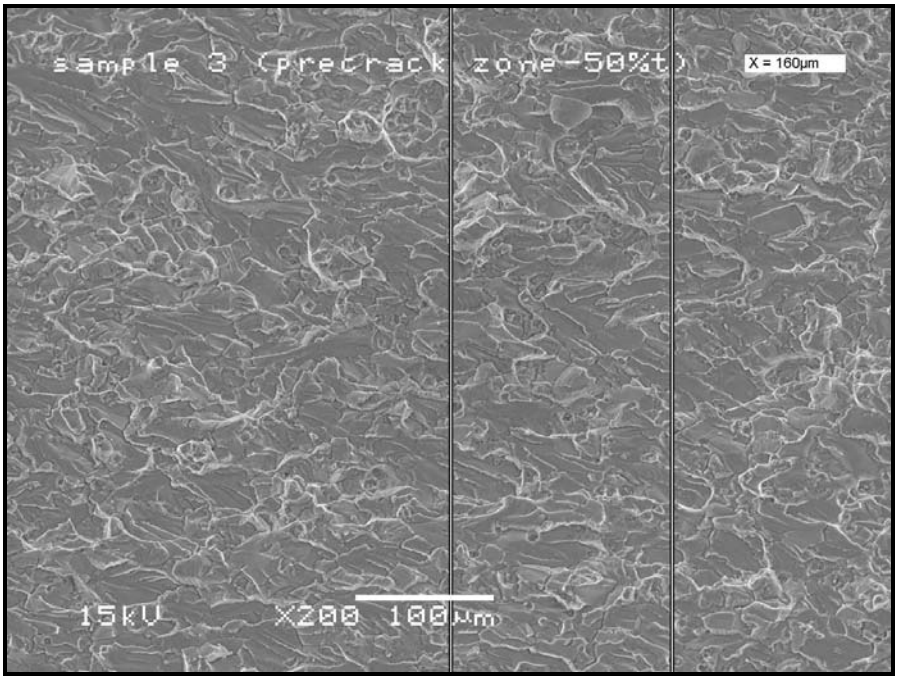

Figure 195: SEM image of sample 3 shows the fracture surface along the 0.16 mm distance from the pre-fatigue crack zone at 50% thickness, 200X. Fatigue was observed throughout the 0.16 mm distance from pre-fatigue crack zone.

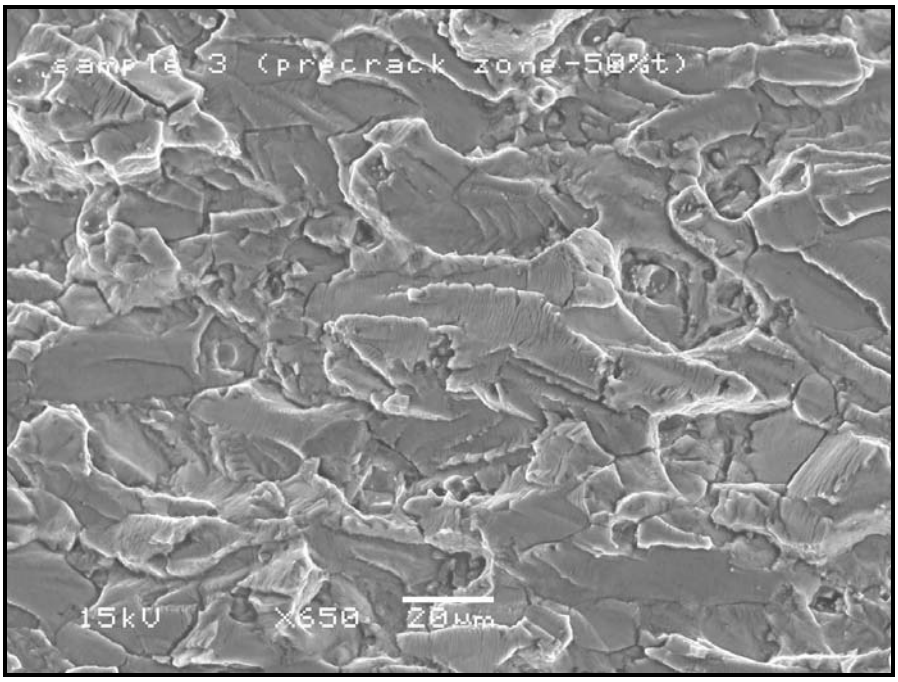

Figure 196: SEM image of sample 3 shows the fracture surface at the pre-fatigue crack zone at 50% thickness, 650X. Fatigue striations were observed throughout the pre-fatigue crack zone.

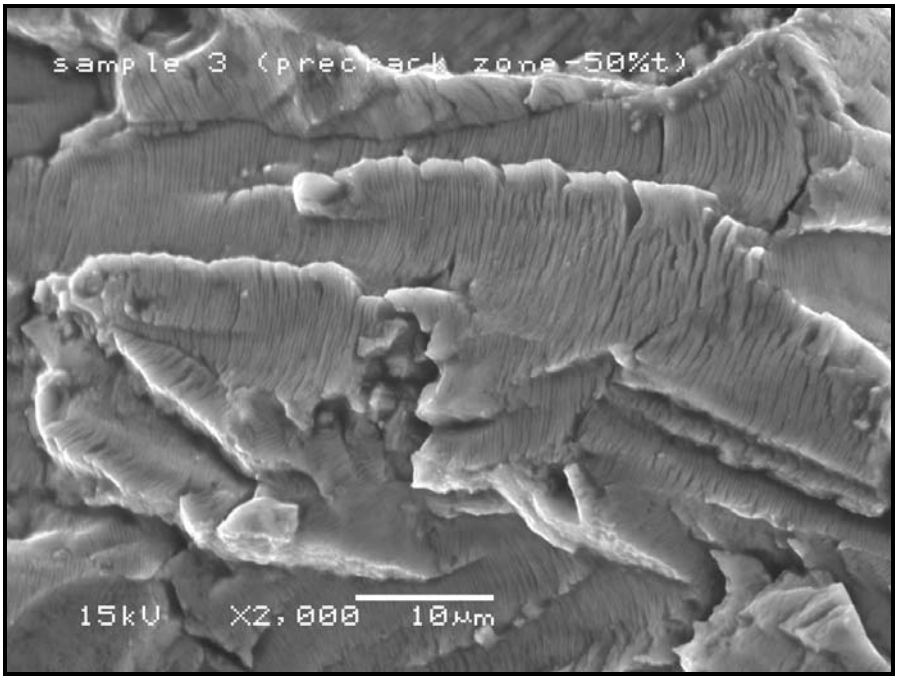

Figure 197: SEM image of sample 3 shows the fracture surface at the pre-fatigue crack zone at 50% thickness, 2000X. Fatigue striations were observed throughout the pre-fatigue crack zone.

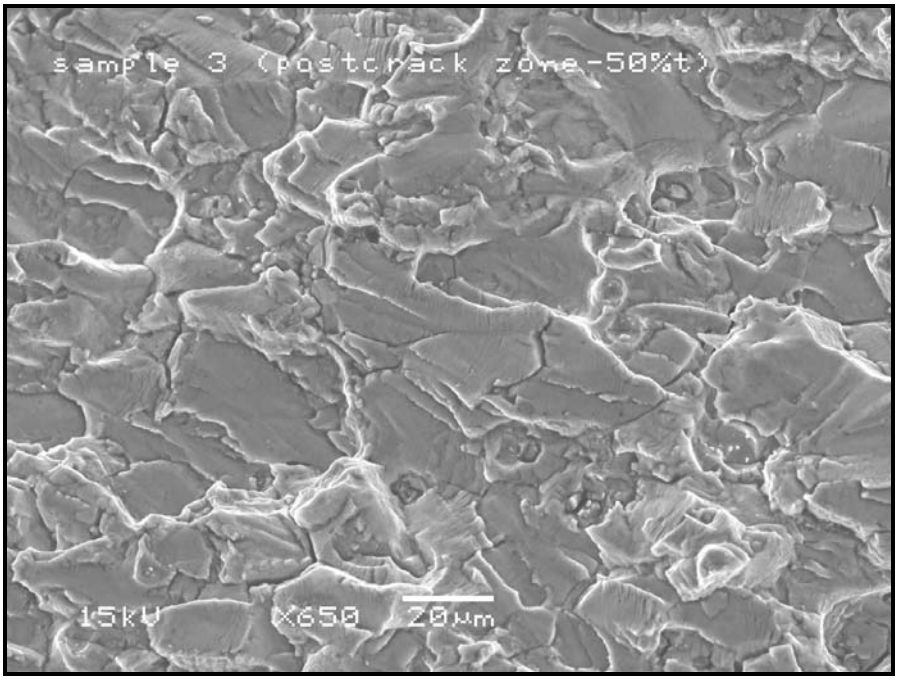

Figure 198: SEM image of sample 3 shows the fracture surface at the post-fatigue crack zone at 50% thickness, 650X. Fatigue striations were observed throughout the post-fatigue crack zone along the 0.16 mm from the pre-fatigue crack zone.

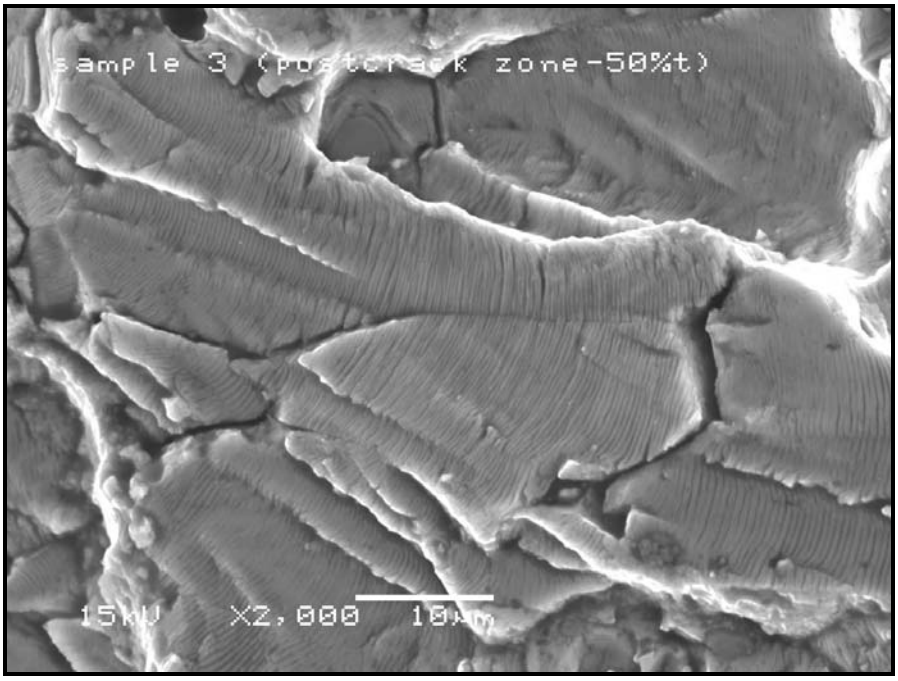

Figure 199: SEM image of sample 3 shows the fracture surface at the post-fatigue crack zone at 50% thickness, 2000X. Fatigue striations were observed throughout the post-fatigue crack zone along the 0.16 mm from the pre-fatigue crack zone.

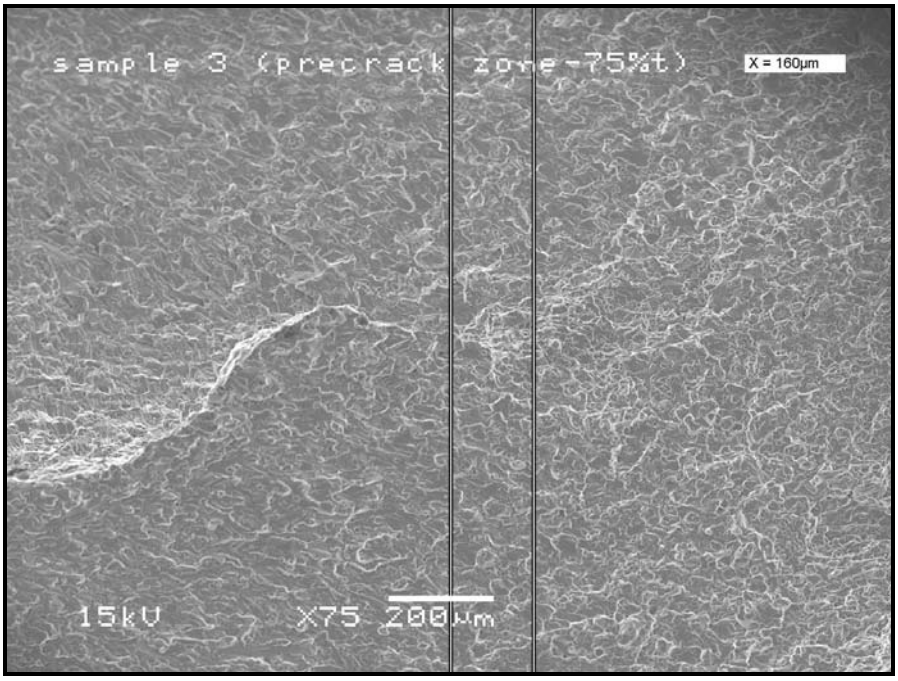

Figure 200: SEM image of sample 3 shows the fracture surface along the 0.16 mm distance from the pre-fatigue crack zone at 75% thickness, 75X. Fatigue was observed throughout the 0.16 mm distance from pre-fatigue crack zone.

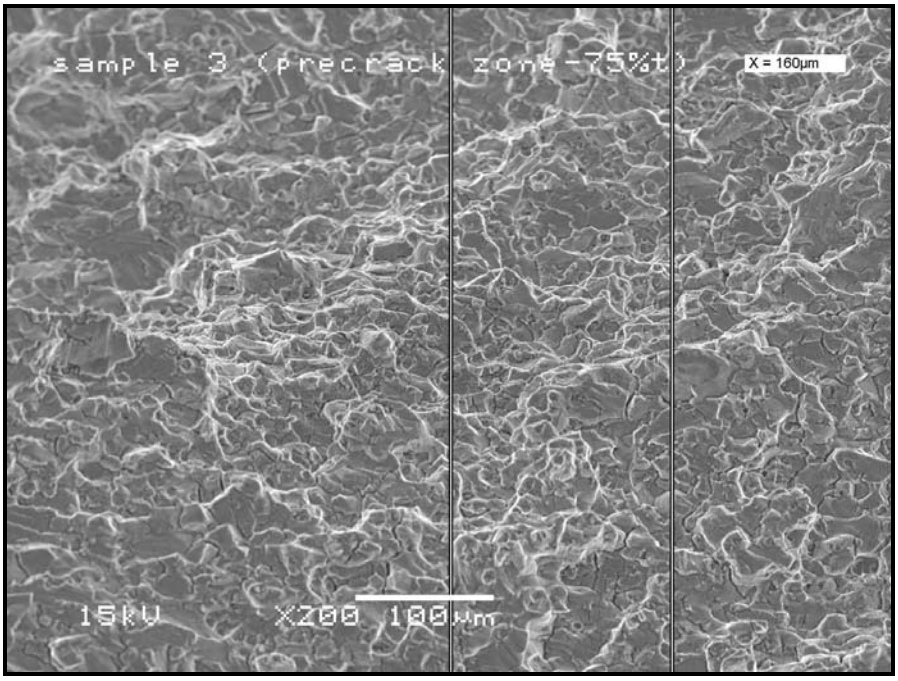

Figure 201: SEM image of sample 3 shows the fracture surface along the 0.16 mm distance from the pre-fatigue crack zone at 75% thickness, 200X. Fatigue was observed throughout the 0.16 mm distance from pre-fatigue crack zone.

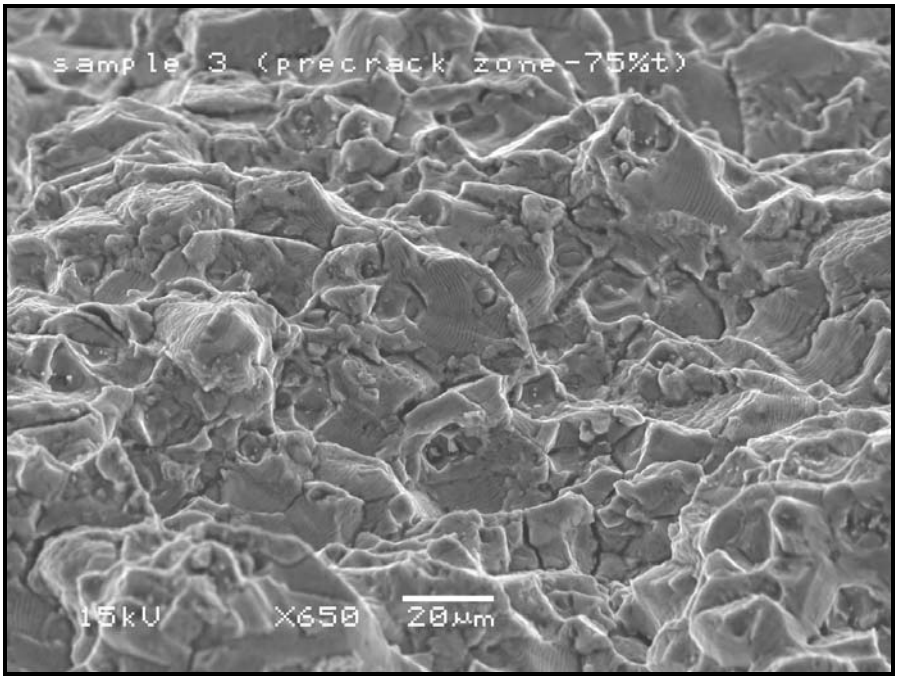

Figure 202: SEM image of sample 3 shows the fracture surface at the pre-fatigue crack zone at 75% thickness, 650X. Fatigue striations were observed throughout the pre-fatigue crack zone.

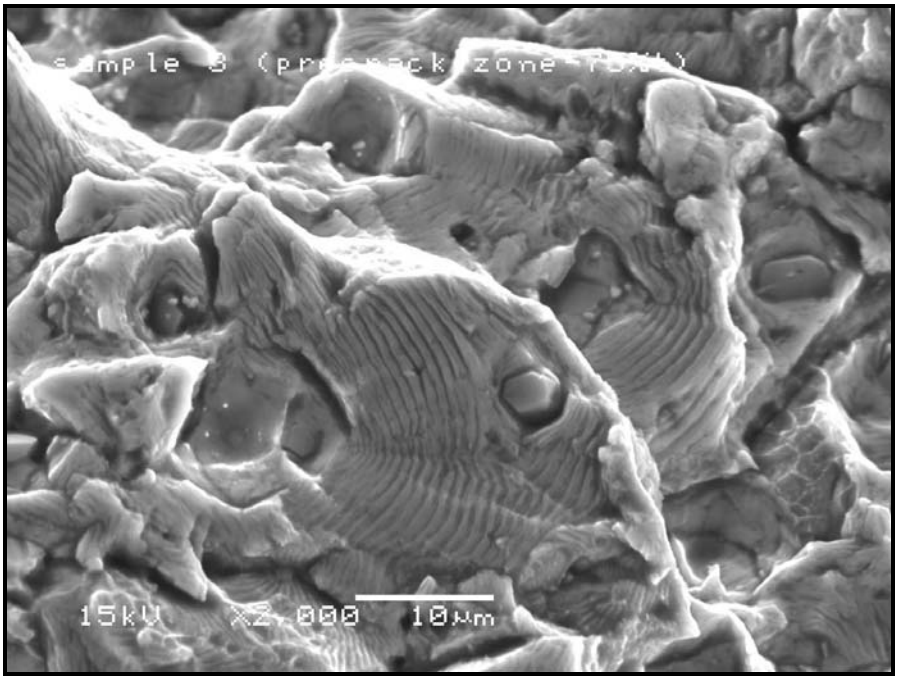

Figure 203: SEM image of sample 3 shows the fracture surface at the pre-fatigue crack zone at 75% thickness, 2000X. Fatigue striations were observed throughout the pre-fatigue crack zone.

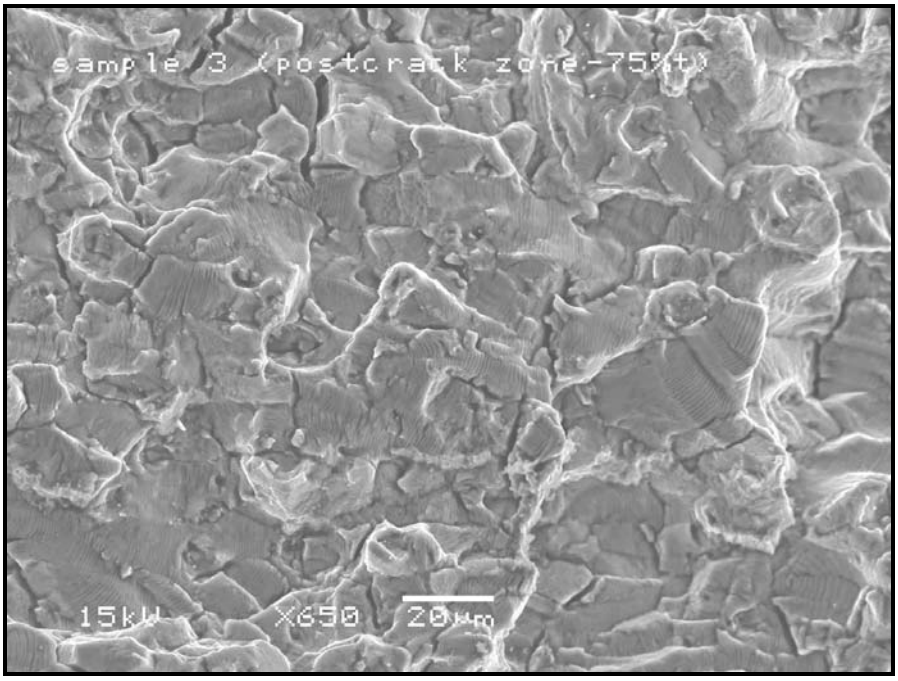

Figure 204: SEM image of sample 3 shows the fracture surface at the post-fatigue crack zone at 75% thickness, 650X. Fatigue striations were observed throughout the post-fatigue crack zone along the 0.16 mm from the pre-fatigue crack zone.

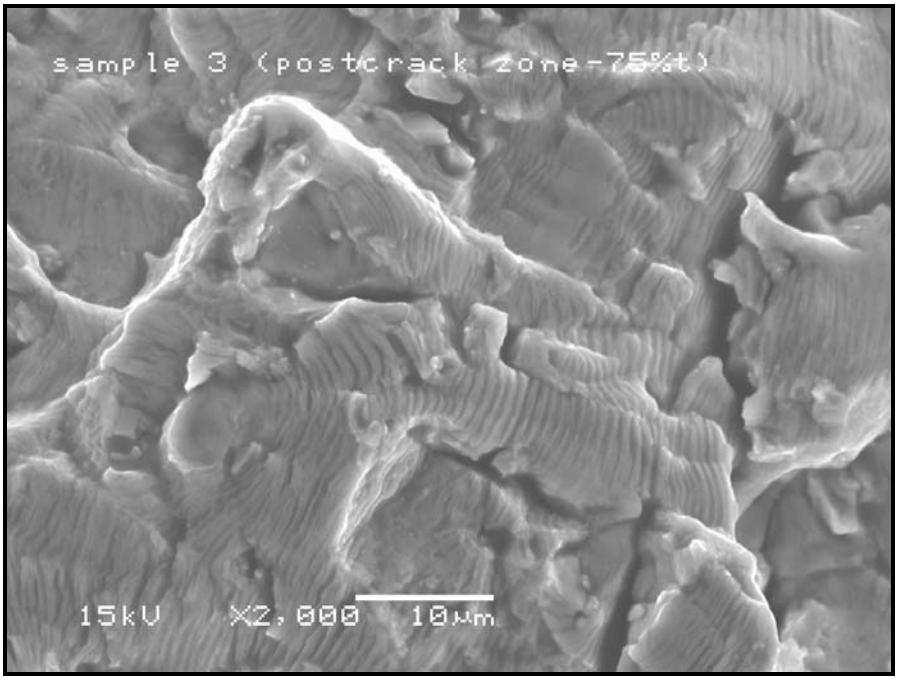

Figure 205: SEM image of sample 3 shows the fracture surface at the post-fatigue crack zone at 75% thickness, 2000X. Fatigue striations were observed throughout the post-fatigue crack zone along the 0.16 mm from the pre-fatigue crack zone.

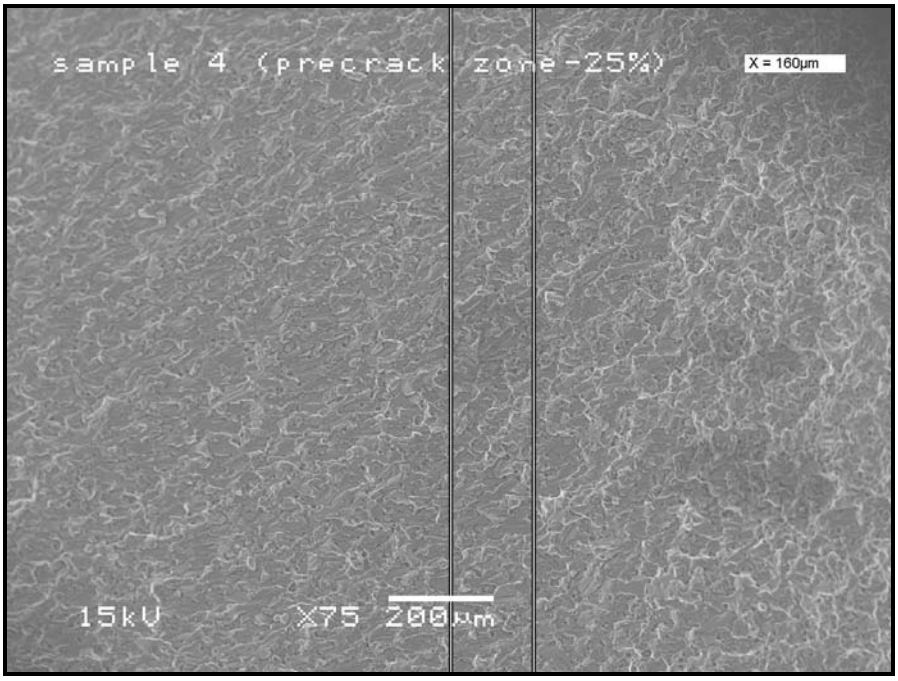

Figure 206: SEM image of sample 4 shows the fracture surface along the 0.16 mm distance from the pre-fatigue crack zone at 25% thickness, 75X. Fatigue was observed throughout the 0.16 mm distance from pre-fatigue crack zone.

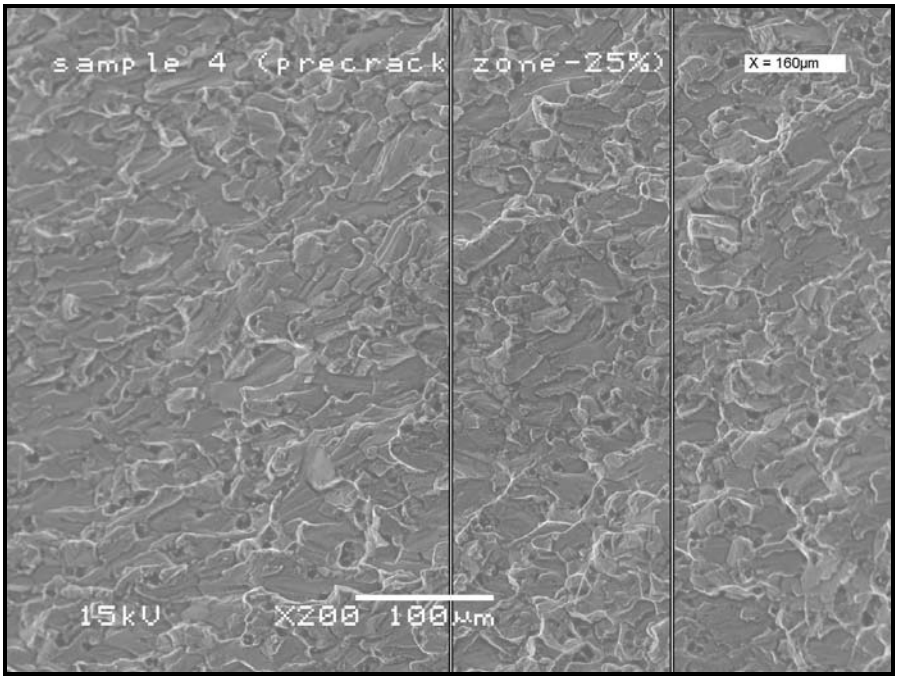

Figure 207: SEM image of sample 4 shows the fracture surface along the 0.16 mm distance from the pre-fatigue crack zone at 25% thickness, 200X. Fatigue was observed throughout the 0.16 mm distance from pre-fatigue crack zone.

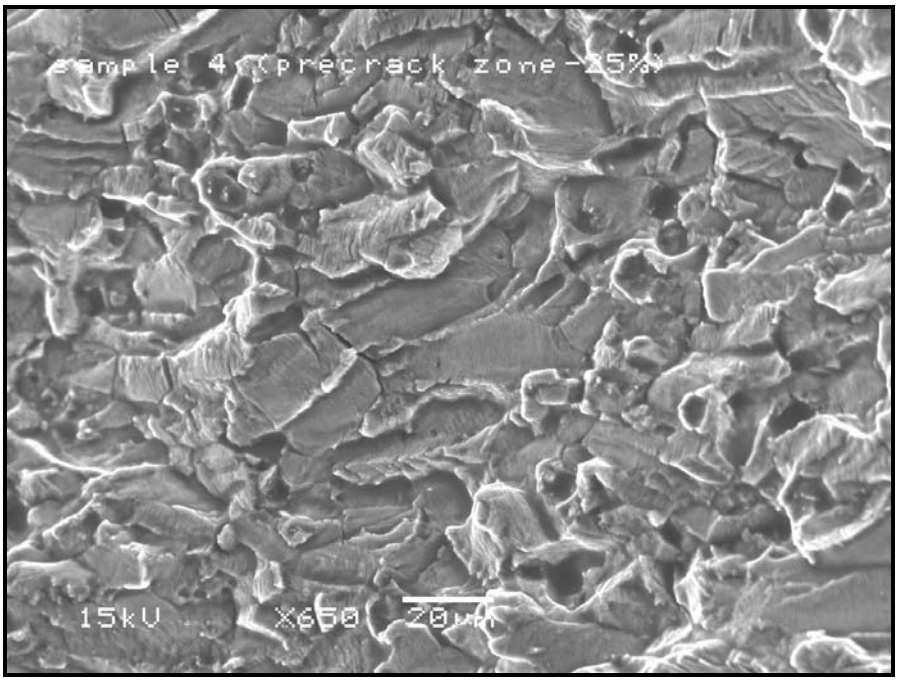

Figure 208: SEM image of sample 4 shows the fracture surface at the pre-fatigue crack zone at 25% thickness, 650X. Fatigue striations were observed throughout the pre-fatigue crack zone.

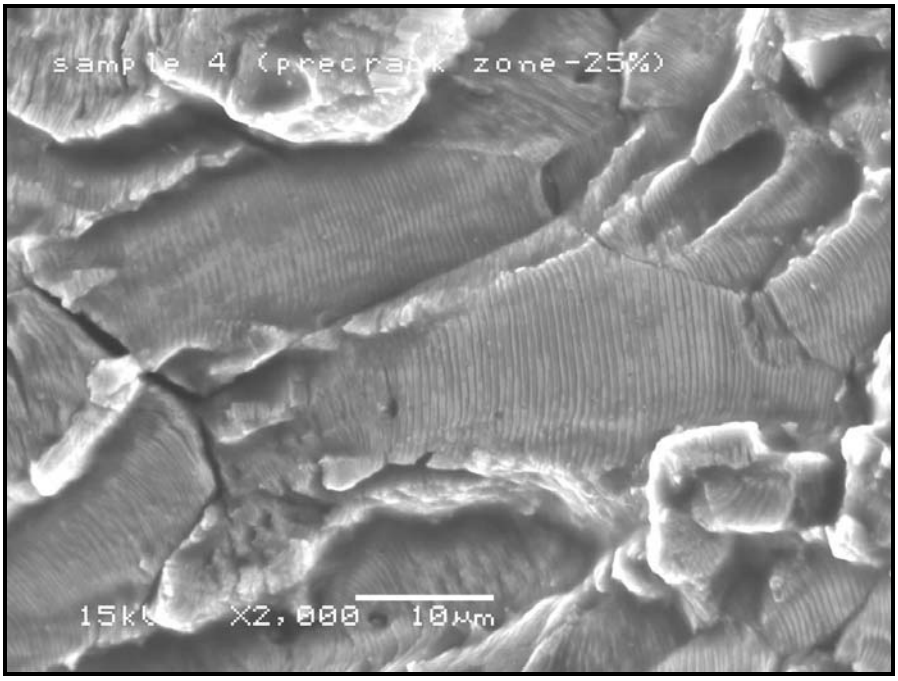

Figure 209: SEM image of sample 4 shows the fracture surface at the pre-fatigue crack zone at 25% thickness, 2000X. Fatigue striations were observed throughout the pre-fatigue crack zone.

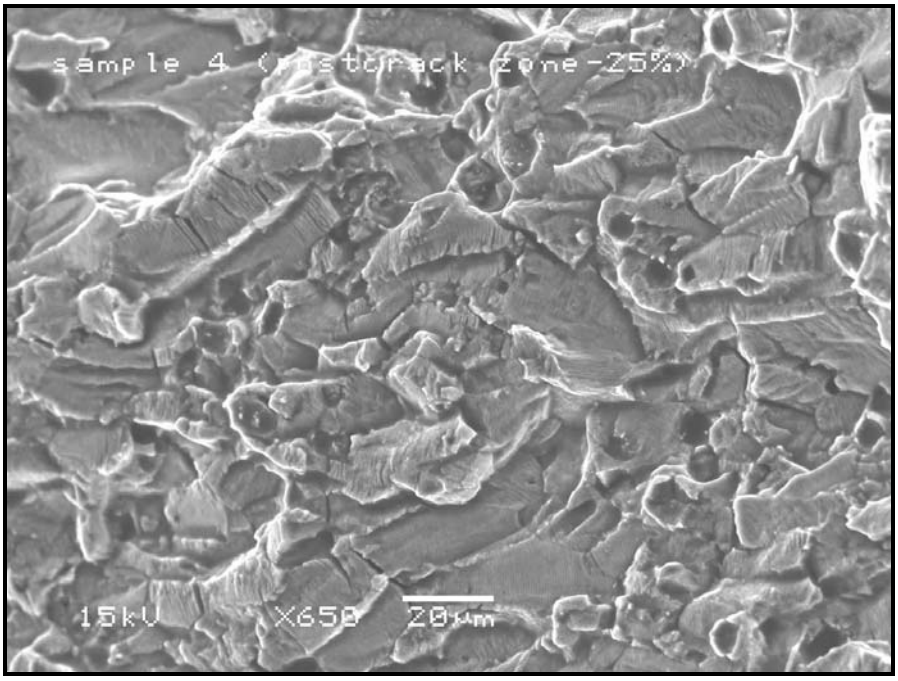

Figure 210: SEM image of sample 4 shows the fracture surface at the post-fatigue crack zone at 25% thickness, 650X. Fatigue striations were observed throughout the post-fatigue crack zone along the 0.16 mm from the pre-fatigue crack zone.

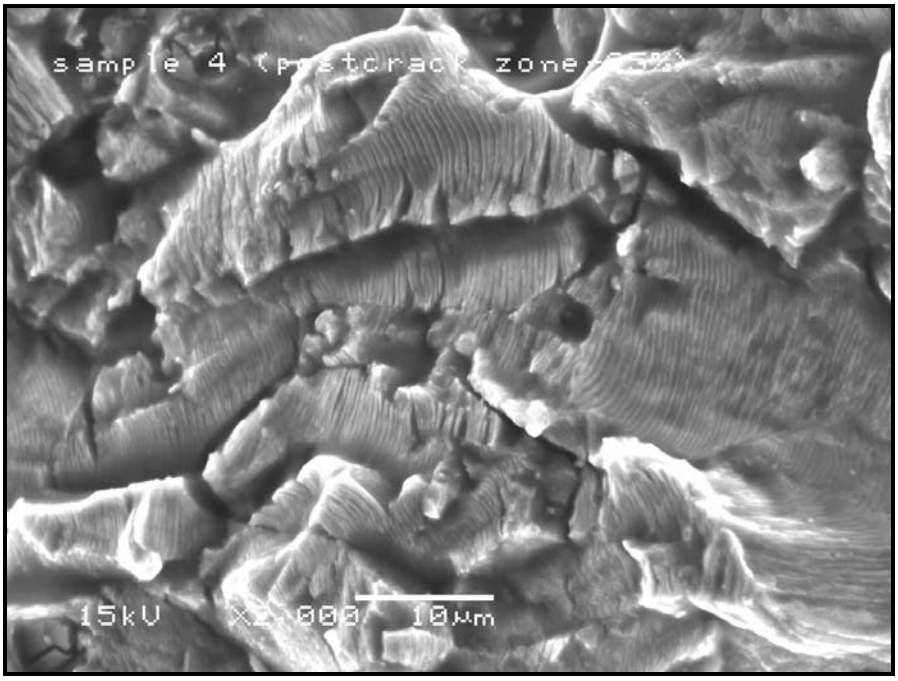

Figure 211: SEM image of sample 4 shows the fracture surface at the post-fatigue crack zone at 25% thickness, 2000X. Fatigue striations were observed throughout the post-fatigue crack zone along the 0.16 mm from the pre-fatigue crack zone.

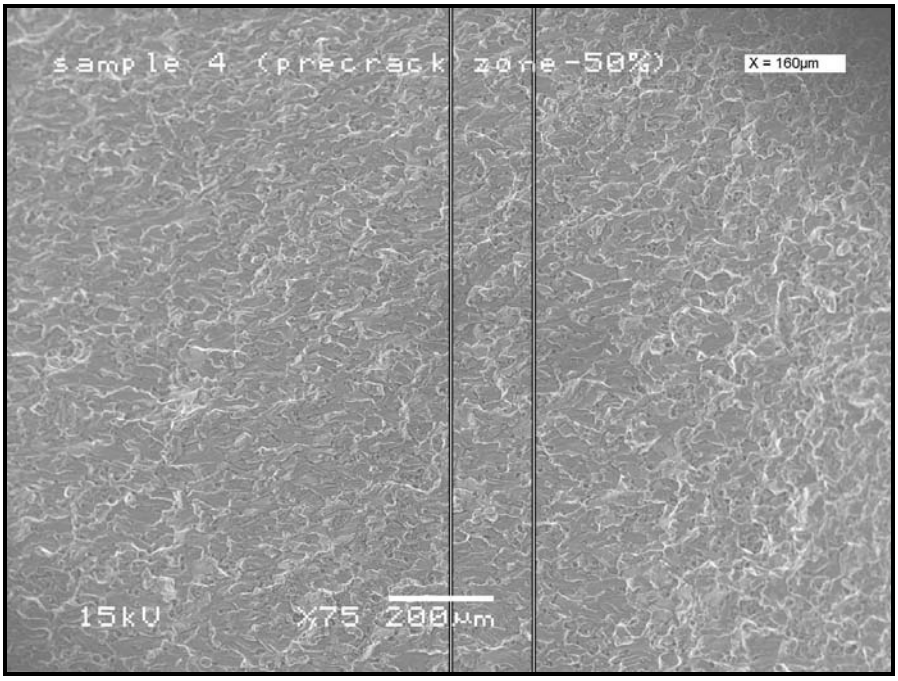

Figure 212: SEM image of sample 4 shows the fracture surface along the 0.16 mm distance from the pre-fatigue crack zone at 50% thickness, 75X. Fatigue was observed throughout the 0.16 mm distance from pre-fatigue crack zone.

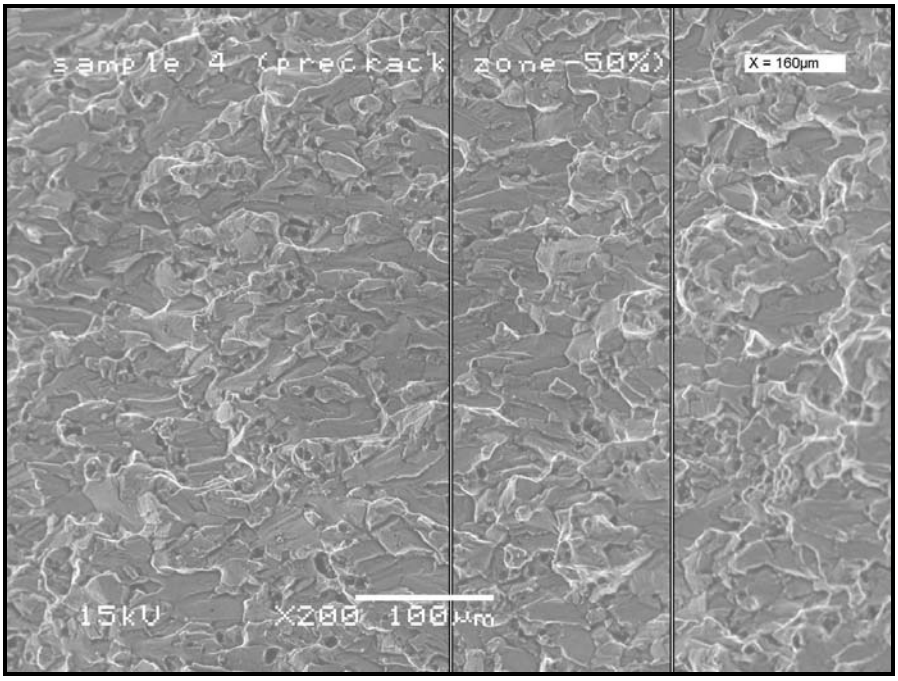

Figure 213: SEM image of sample 4 shows the fracture surface along the 0.16 mm distance from the pre-fatigue crack zone at 50% thickness, 200X. Fatigue was observed throughout the 0.16 mm distance from pre-fatigue crack zone.

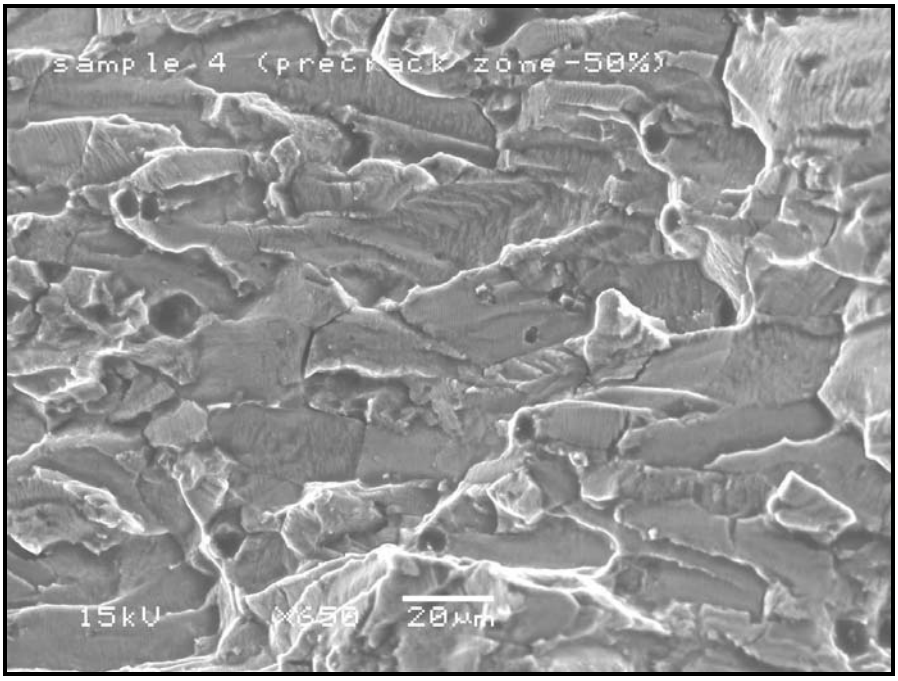

Figure 214: SEM image of sample 4 shows the fracture surface at the pre-fatigue crack zone at 50% thickness, 650X. Fatigue striations were observed throughout the pre-fatigue crack zone.

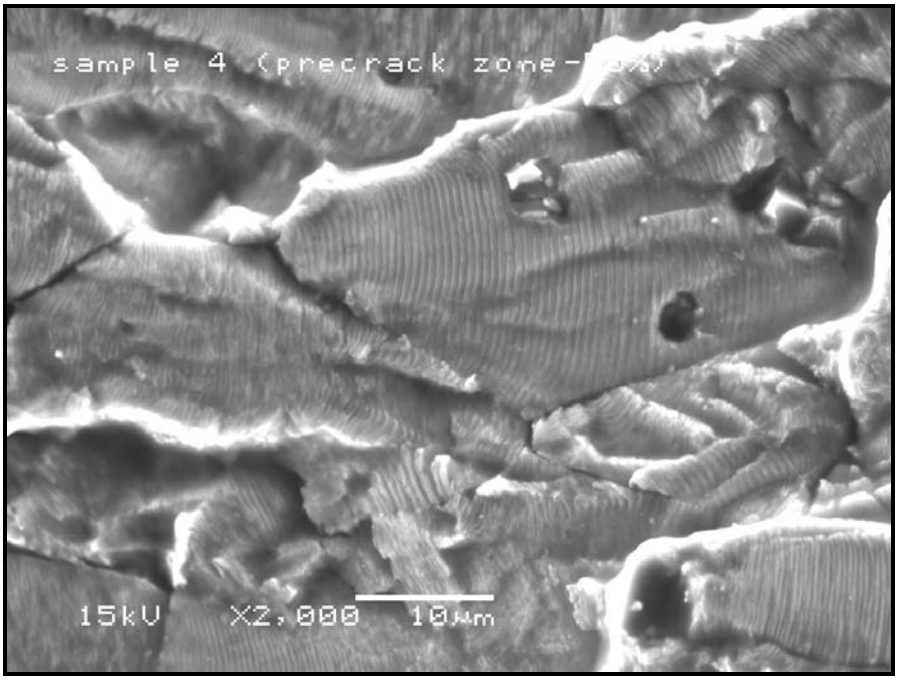

Figure 215: SEM image of sample 4 shows the fracture surface at the pre-fatigue crack zone at 50% thickness, 2000X. Fatigue striations were observed throughout the pre-fatigue crack zone.

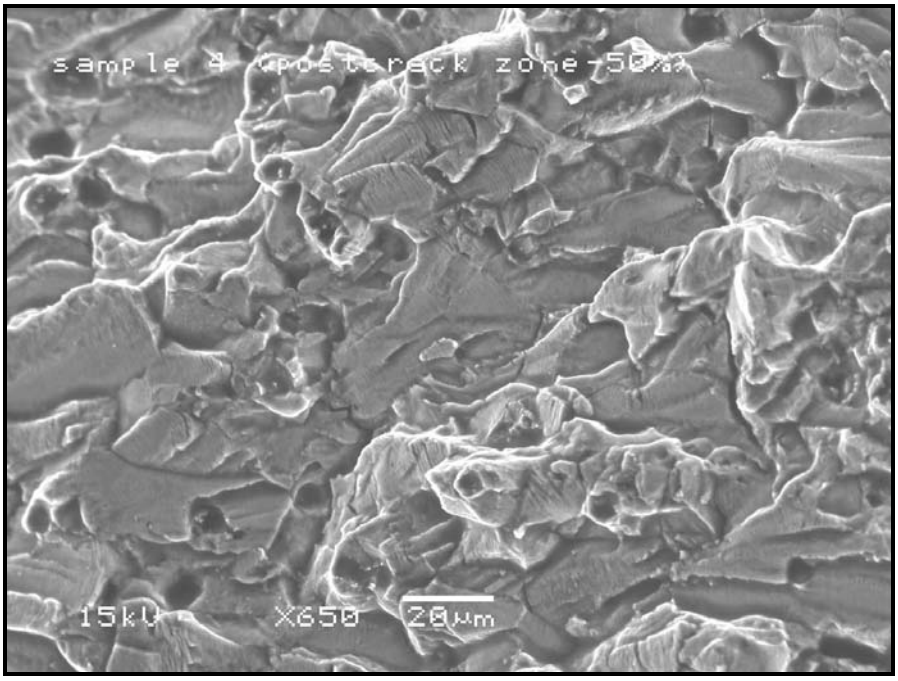

Figure 216: SEM image of sample 4 shows the fracture surface at the post-fatigue crack zone at 50% thickness, 650X. Fatigue striations were observed throughout the post-fatigue crack zone along the 0.16 mm from the pre-fatigue crack zone.

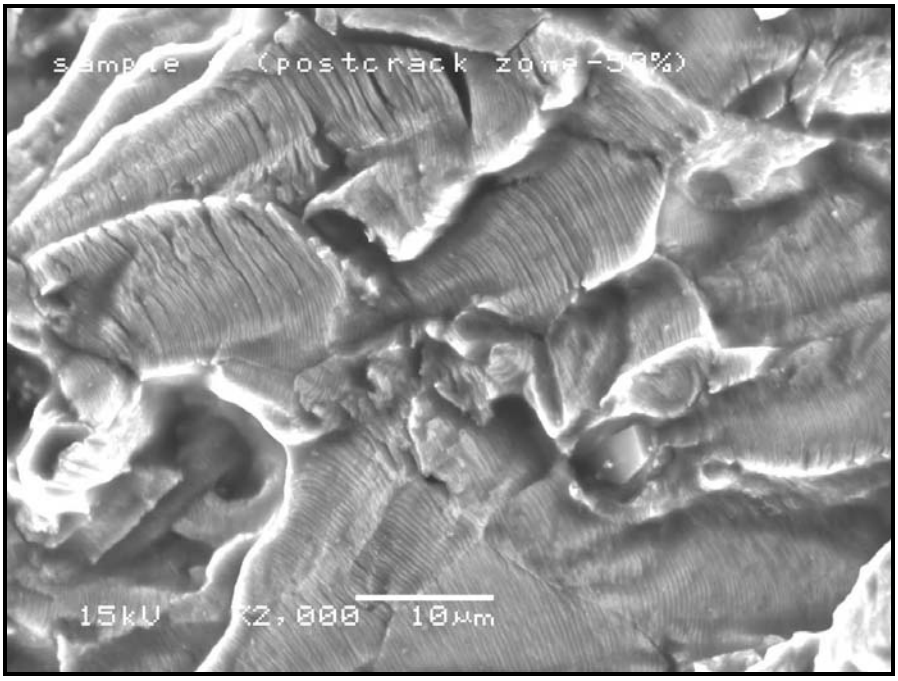

Figure 217: SEM image of sample 4 shows the fracture surface at the post-fatigue crack zone at 50% thickness, 2000X. Fatigue striations were observed throughout the post-fatigue crack zone along the 0.16 mm from the pre-fatigue crack zone.

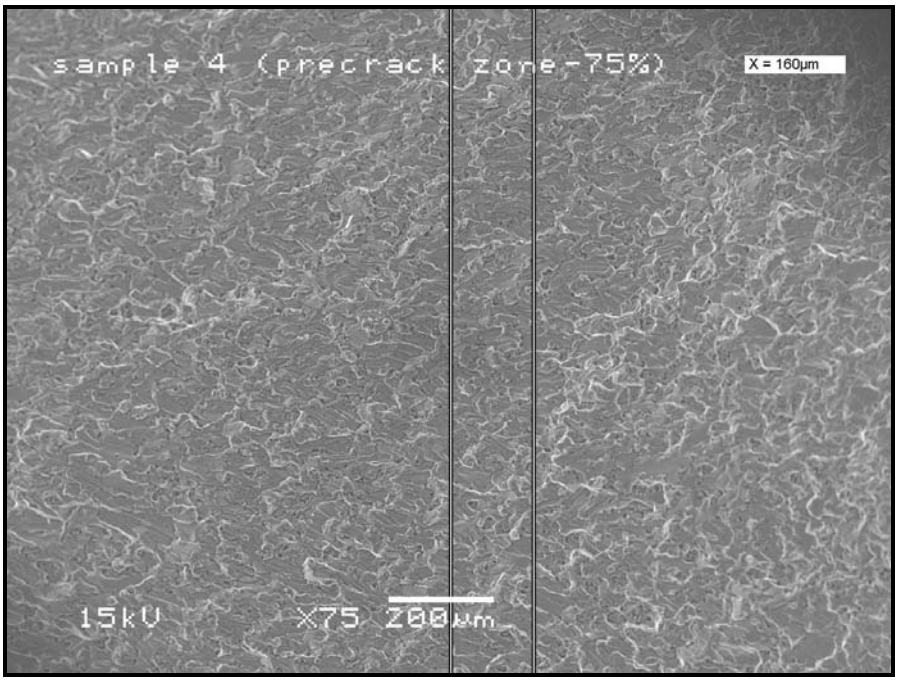

Figure 218: SEM image of sample 4 shows the fracture surface along the 0.16 mm distance from the pre-fatigue crack zone at 75% thickness, 75X. Fatigue was observed throughout the 0.16 mm distance from pre-fatigue crack zone.

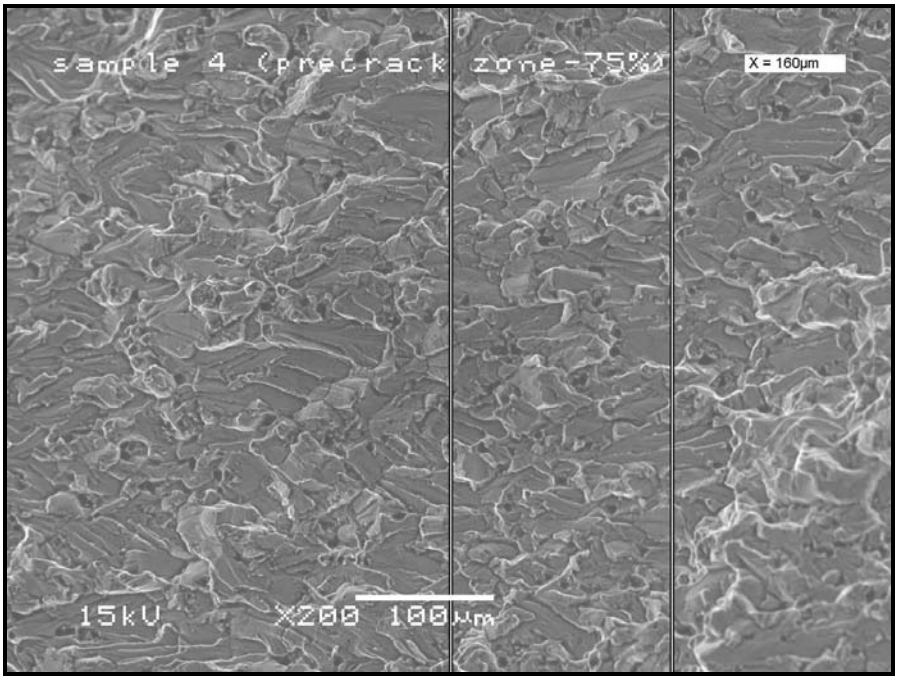

Figure 219: SEM image of sample 4 shows the fracture surface along the 0.16 mm distance from the pre-fatigue crack zone at 75% thickness, 200X. Fatigue was observed throughout the 0.16 mm distance from pre-fatigue crack zone.

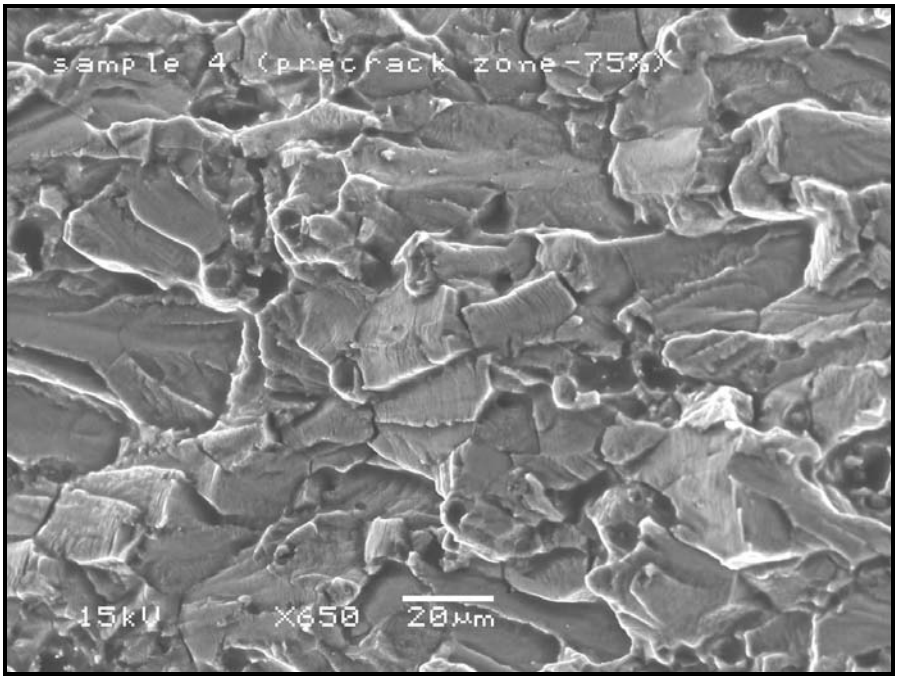

Figure 220: SEM image of sample 4 shows the fracture surface at the pre-fatigue crack zone at 75% thickness, 650X. Fatigue striations were observed throughout the pre-fatigue crack zone.

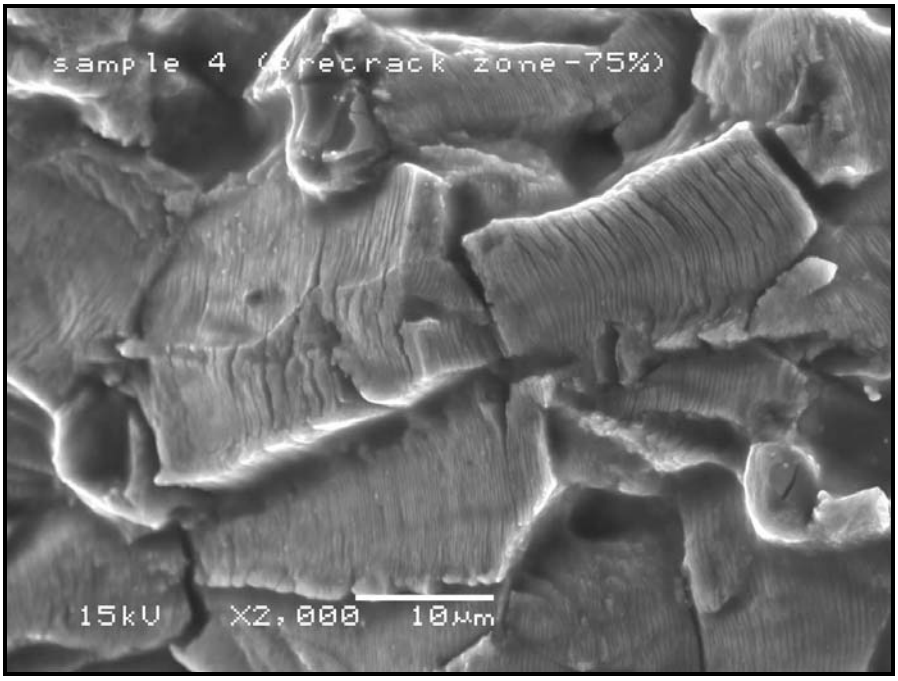

Figure 221: SEM image of sample 4 shows the fracture surface at the pre-fatigue crack zone at 75% thickness, 2000X. Fatigue striations were observed throughout the pre-fatigue crack zone.

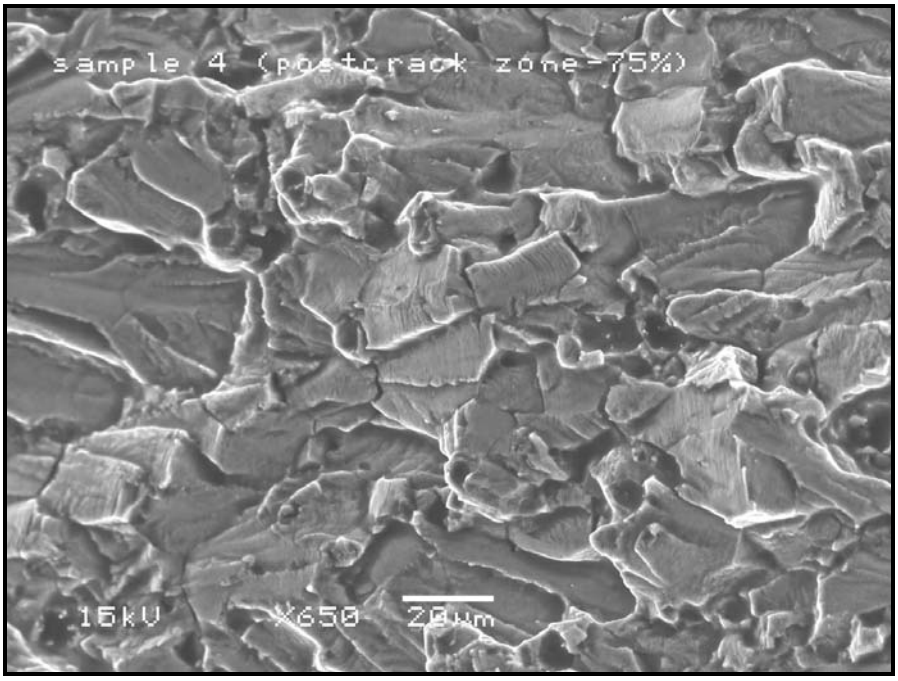

Figure 222: SEM image of sample 4 shows the fracture surface at the post-fatigue crack zone at 75% thickness, 650X. Fatigue striations were observed throughout the post-fatigue crack zone along the 0.16 mm from the pre-fatigue crack zone.

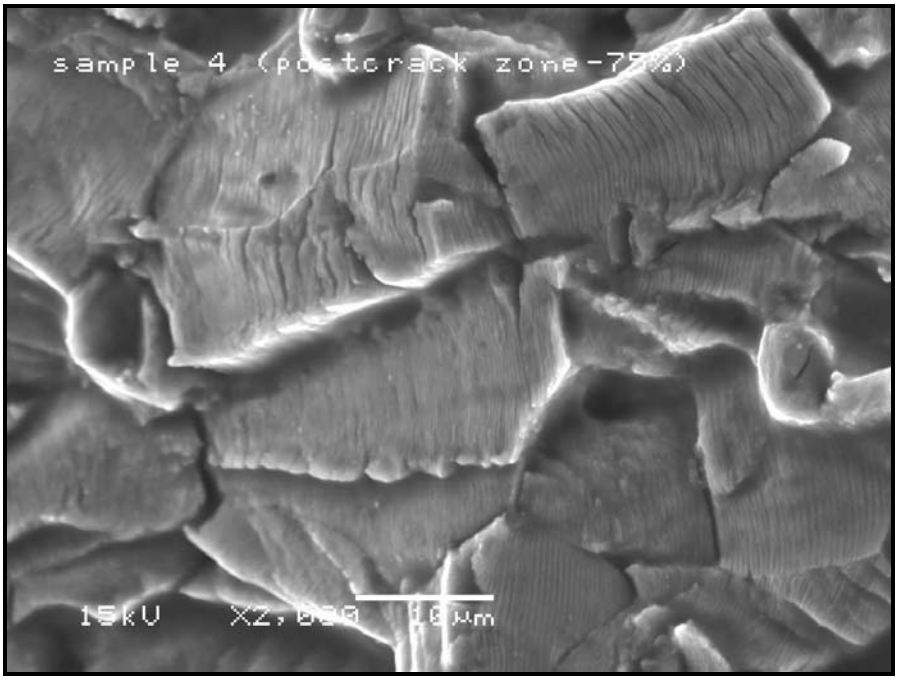

Figure 223: SEM image of sample 4 shows the fracture surface at the post-fatigue crack zone at 75% thickness, 2000X. Fatigue striations were observed throughout the post-fatigue crack zone along the 0.16 mm from the pre-fatigue crack zone.

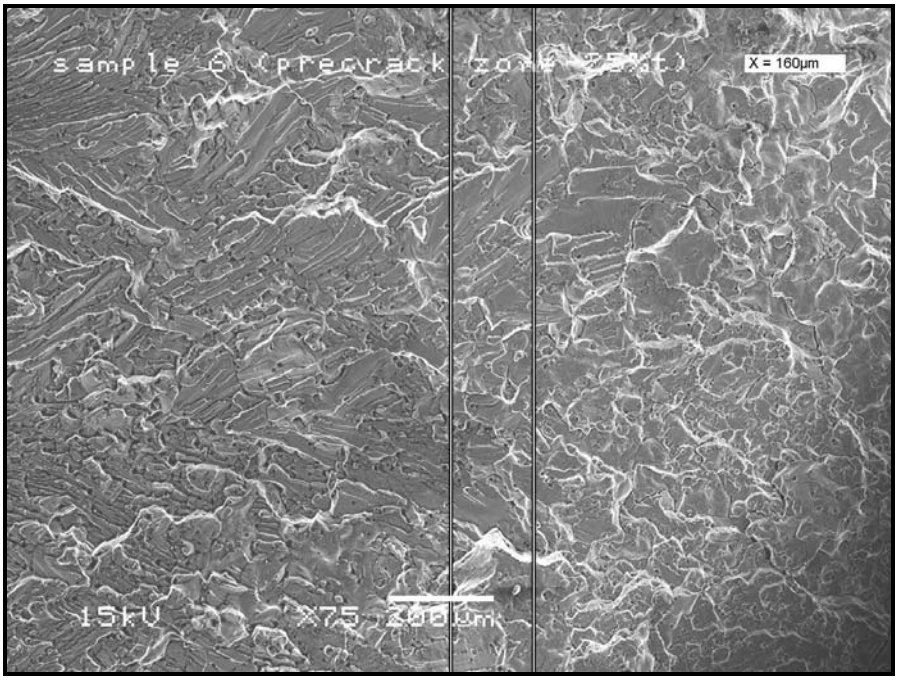

Figure 224: SEM image of sample 6 shows the fracture surface along the 0.16 mm distance from the pre-fatigue crack zone at 25% thickness, 75X. Fatigue was observed throughout the 0.16 mm distance from pre-fatigue crack zone.

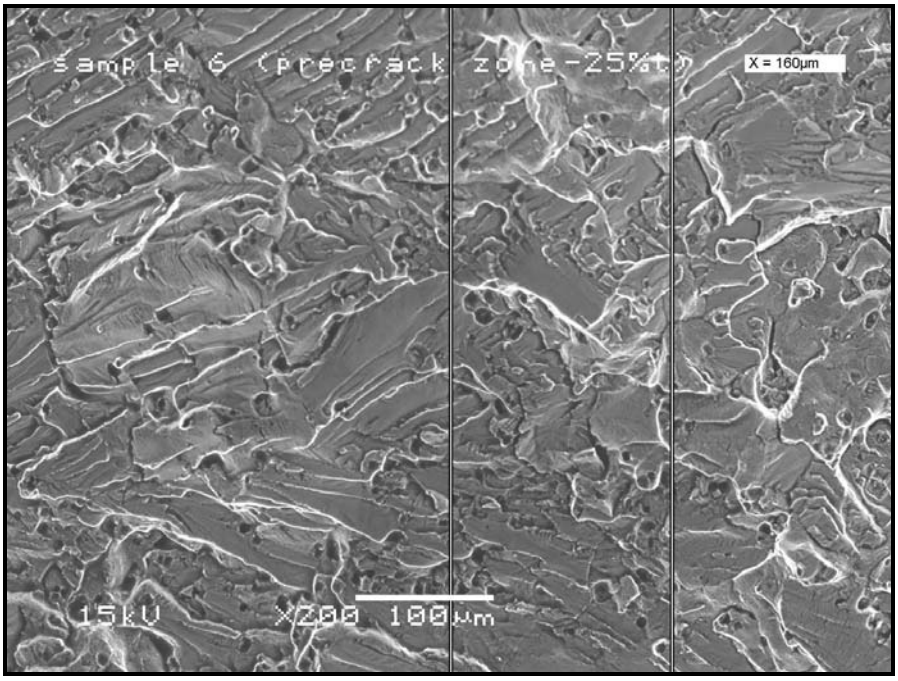

Figure 225: SEM image of sample 6 shows the fracture surface along the 0.16 mm distance from the pre-fatigue crack zone at 25% thickness, 200X. Fatigue was observed throughout the 0.16 mm distance from pre-fatigue crack zone.

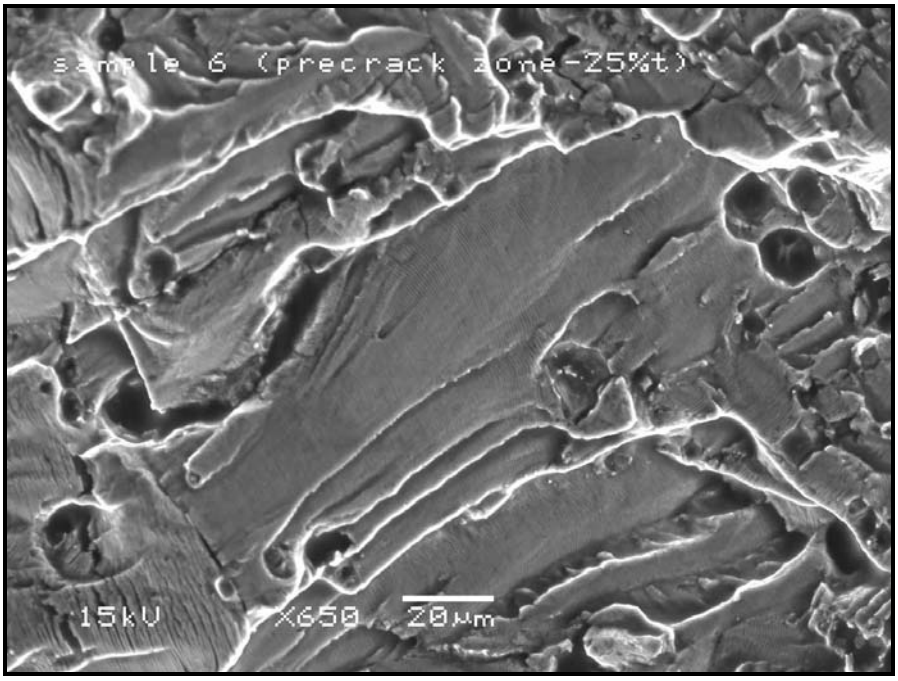

Figure 226: SEM image of sample 6 shows the fracture surface at the pre-fatigue crack zone at 25% thickness, 650X. Fatigue striations were observed throughout the pre-fatigue crack zone.

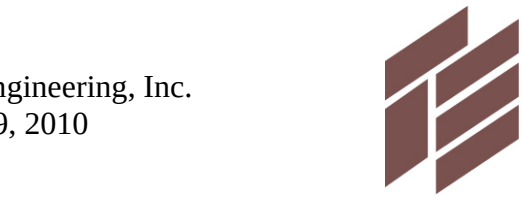

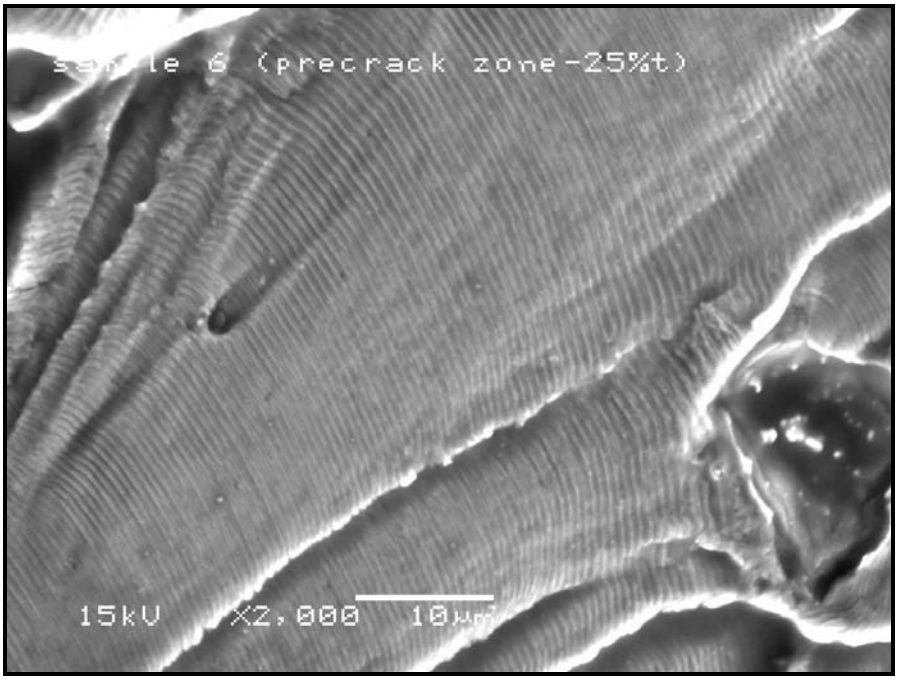

Figure 227: SEM image of sample 6 shows the fracture surface at the pre-fatigue crack zone at 25% thickness, 2000X. Fatigue striations were observed throughout the pre-fatigue crack zone.

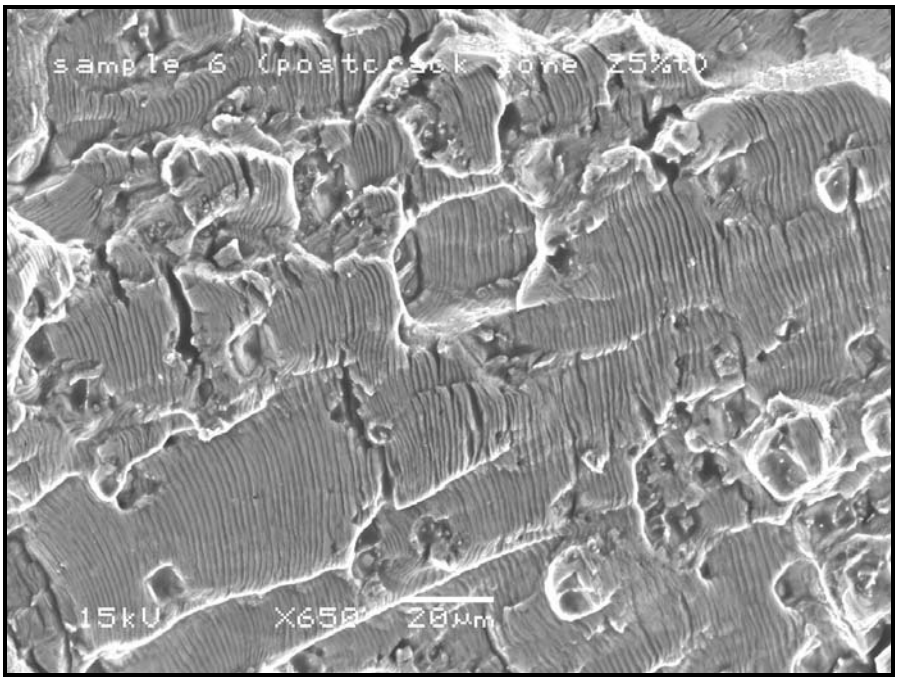

Figure 228: SEM image of sample 6 shows the fracture surface at the post-fatigue crack zone at 25% thickness, 650X. Fatigue striations were observed throughout the post-fatigue crack zone along the 0.16 mm from the pre-fatigue crack zone.

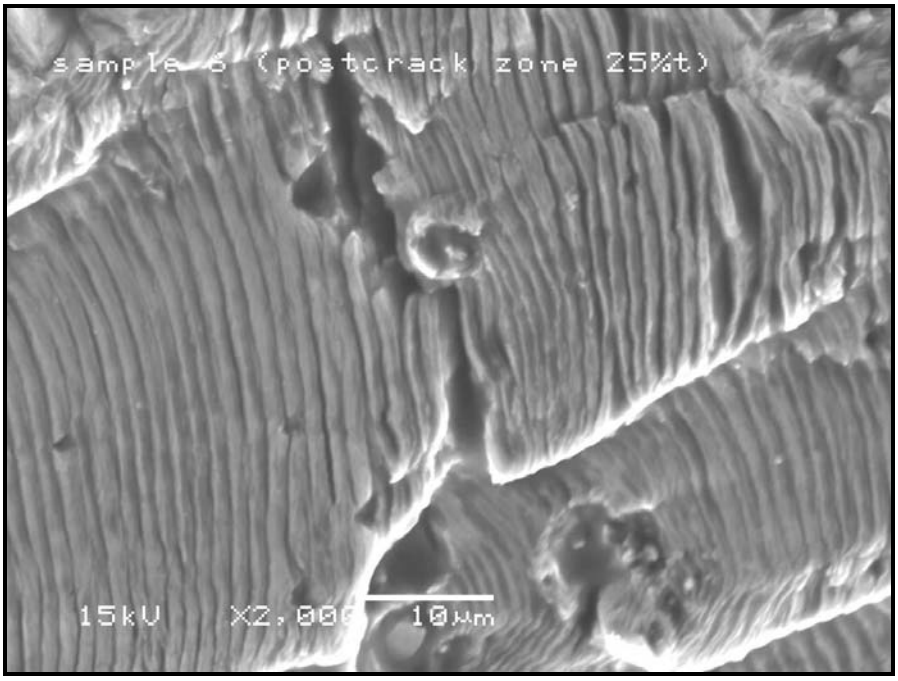

Figure 229: SEM image of sample 6 shows the fracture surface at the post-fatigue crack zone at 25% thickness, 650X. Fatigue striations were observed throughout the post-fatigue crack zone along the 0.16 mm from the pre-fatigue crack zone.

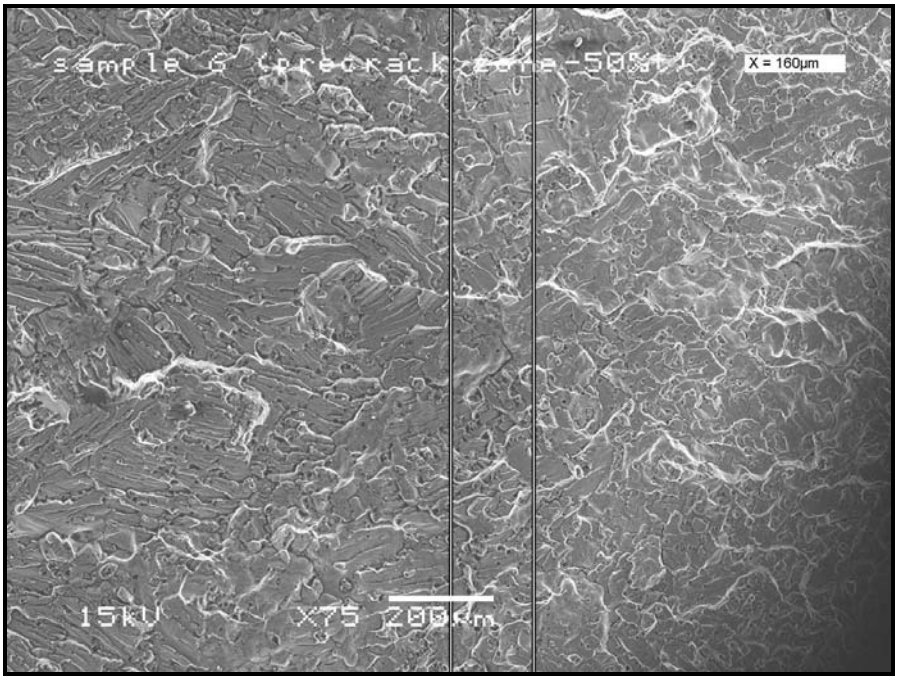

Figure 230: SEM image of sample 6 shows the fracture surface along the 0.16 mm distance from the pre-fatigue crack zone at 50% thickness, 75X. Fatigue was observed throughout the 0.16 mm distance from pre-fatigue crack zone.

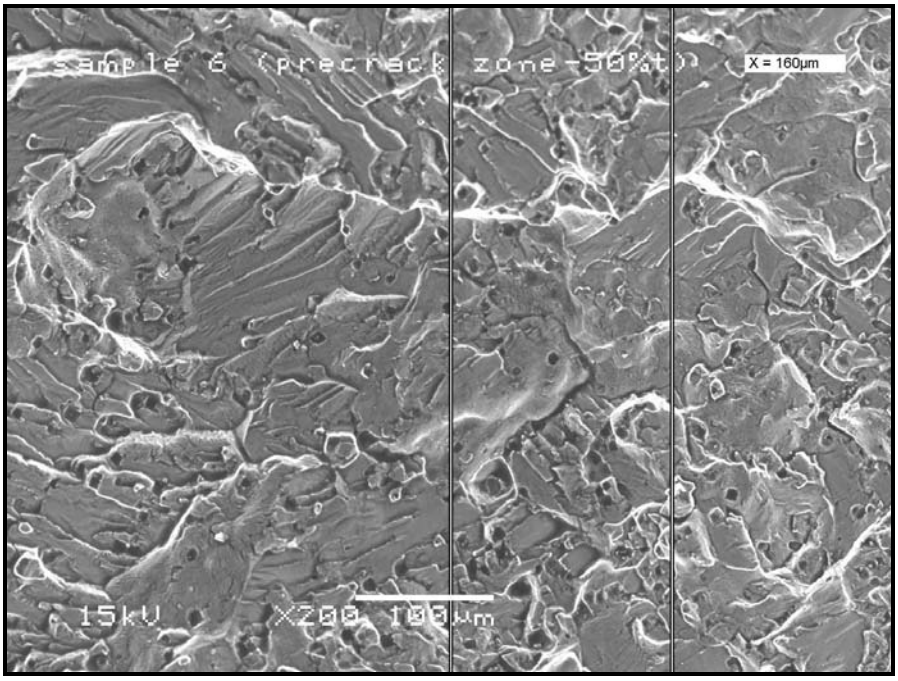

Figure 231: SEM image of sample 6 shows the fracture surface along the 0.16 mm distance from the pre-fatigue crack zone at 50% thickness, 200X. Fatigue was observed throughout the 0.16 mm distance from pre-fatigue crack zone.

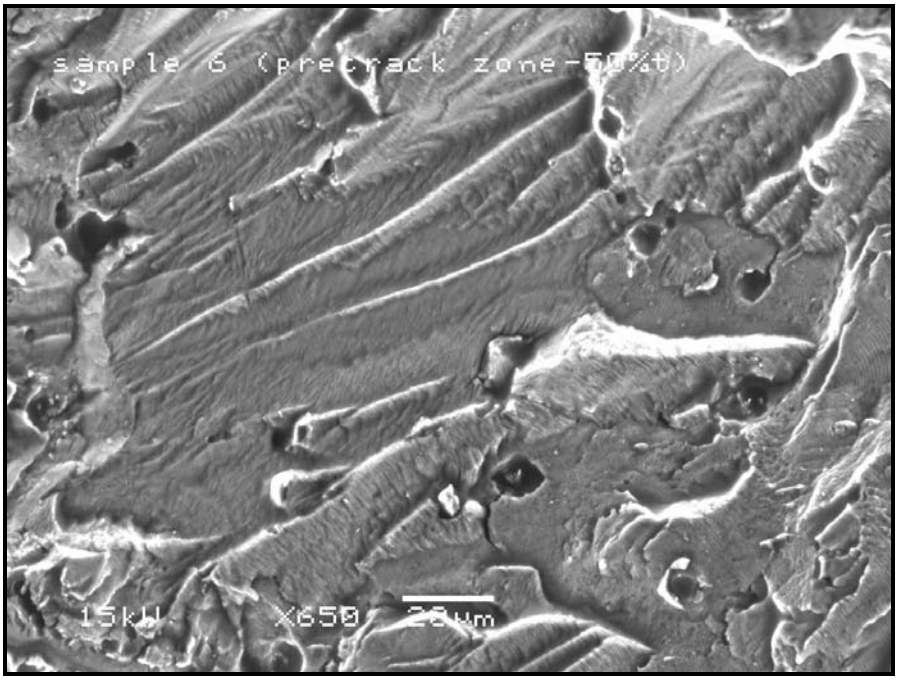

Figure 232: SEM image of sample 6 shows the fracture surface at the pre-fatigue crack zone at 50% thickness, 650X. Fatigue striations were observed throughout the pre-fatigue crack zone.

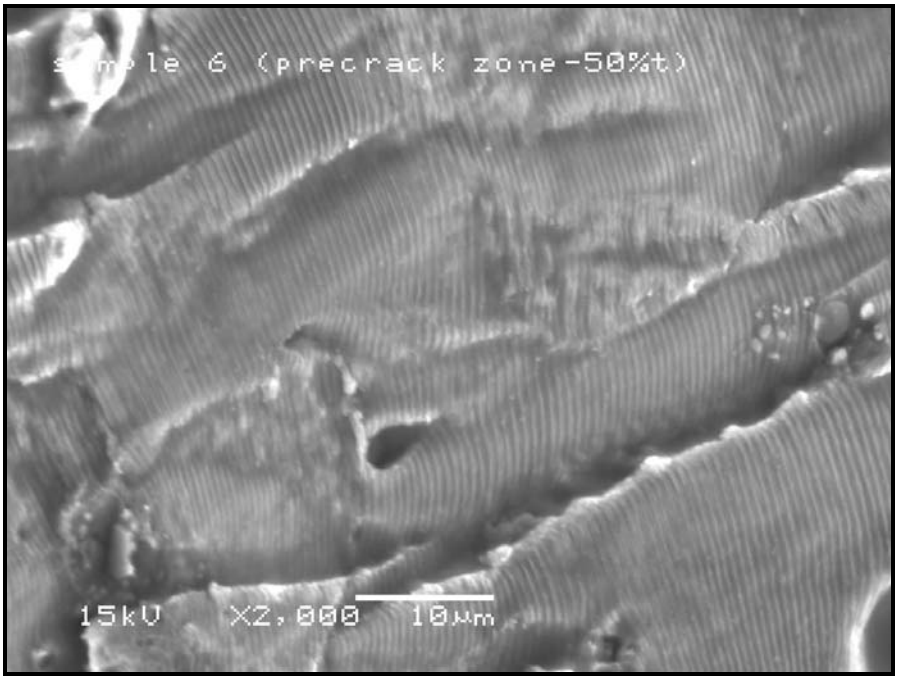

Figure 233: SEM image of sample 6 shows the fracture surface at the pre-fatigue crack zone at 50% thickness, 2000X. Fatigue striations were observed throughout the pre-fatigue crack zone.

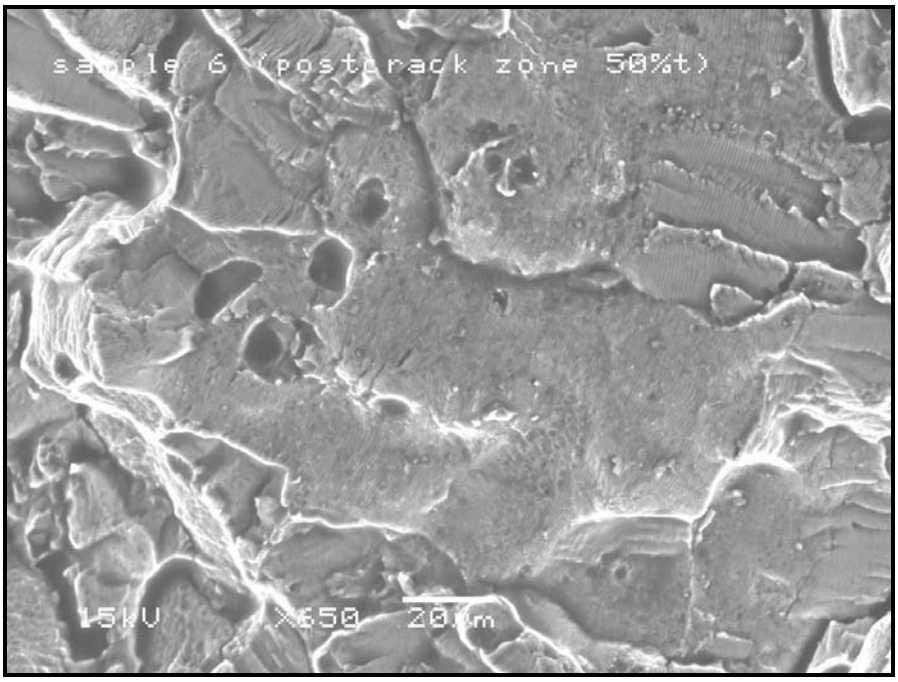

Figure 234: SEM image of sample 6 shows the fracture surface at the post-fatigue crack zone at 50% thickness, 650X. Fatigue striations were observed throughout the post-fatigue crack zone along the 0.16 mm from the pre-fatigue crack zone.

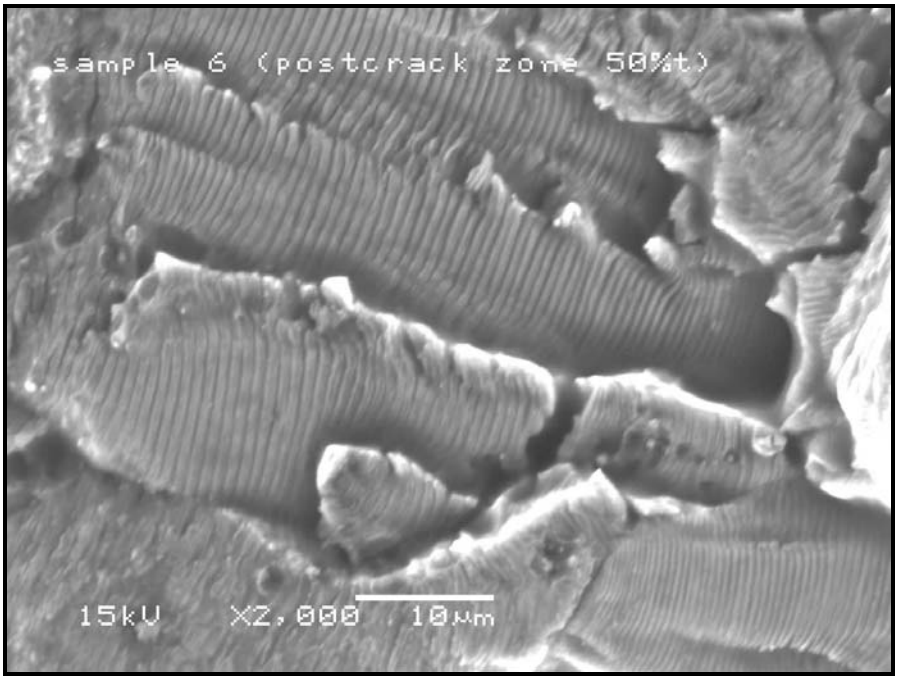

Figure 235: SEM image of sample 6 shows the fracture surface at the post-fatigue crack zone at 50% thickness, 650X. Fatigue striations were observed throughout the post-fatigue crack zone along the 0.16 mm from the pre-fatigue crack zone.

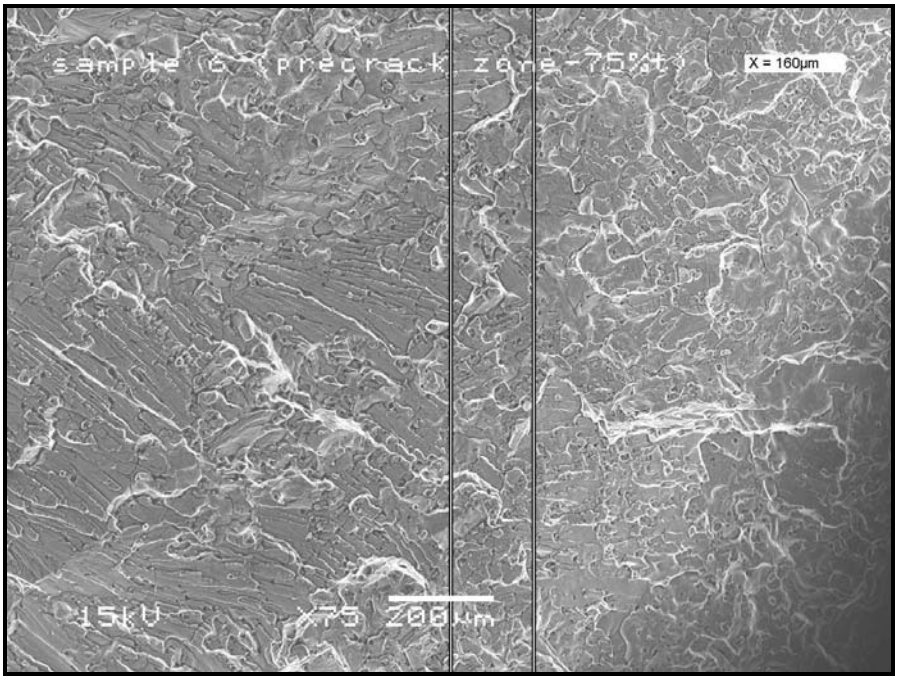

Figure 236: SEM image of sample 6 shows the fracture surface along the 0.16 mm distance from the pre-fatigue crack zone at 75% thickness, 75X. Fatigue was observed throughout the 0.16 mm distance from pre-fatigue crack zone.

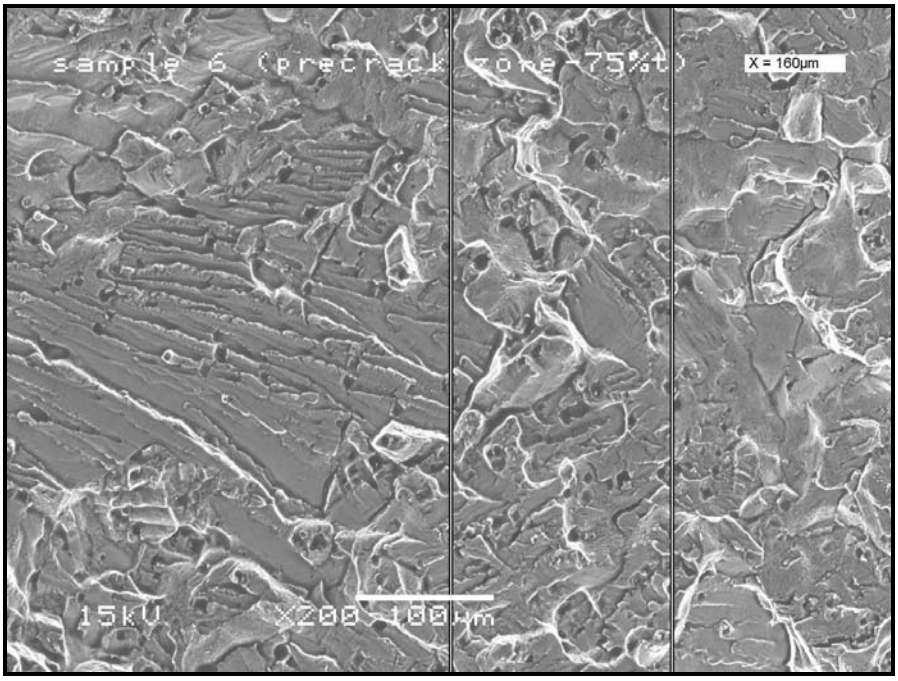

Figure 237: SEM image of sample 6 shows the fracture surface along the 0.16 mm distance from the pre-fatigue crack zone at 75% thickness, 200X. Fatigue was observed throughout the 0.16 mm distance from pre-fatigue crack zone.

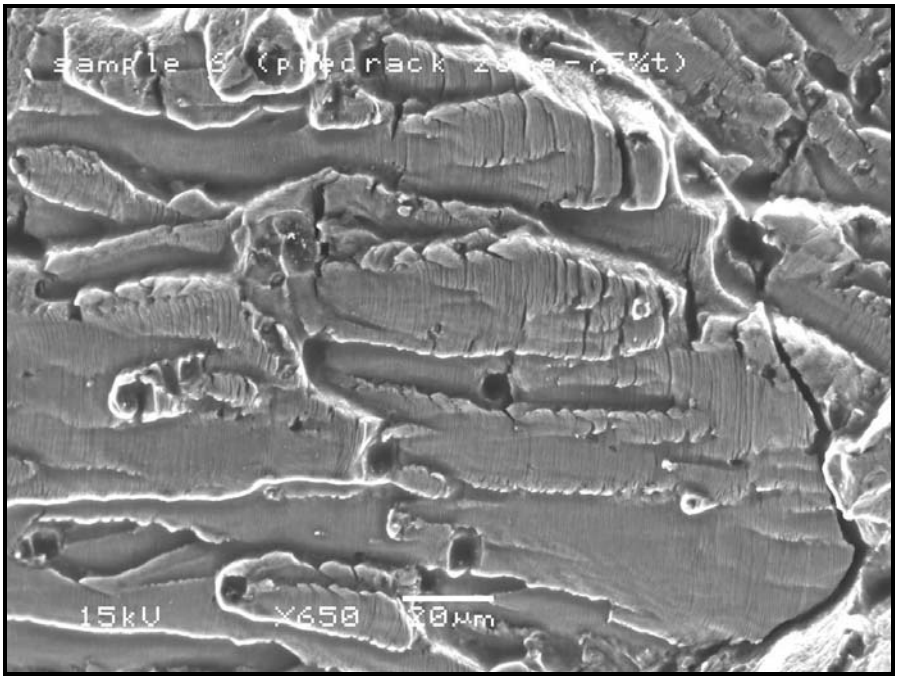

Figure 238: SEM image of sample 6 shows the fracture surface at the pre-fatigue crack zone at 75% thickness, 650X. Fatigue striations were observed throughout the pre-fatigue crack zone.

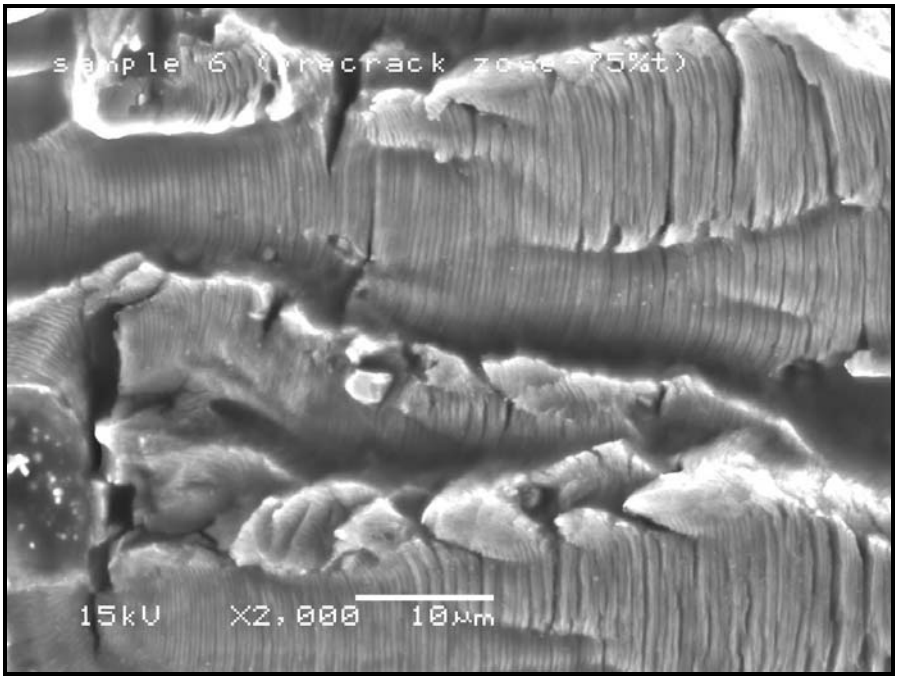

Figure 239: SEM image of sample 6 shows the fracture surface at the pre-fatigue crack zone at 75% thickness, 2000X. Fatigue striations were observed throughout the pre-fatigue crack zone.

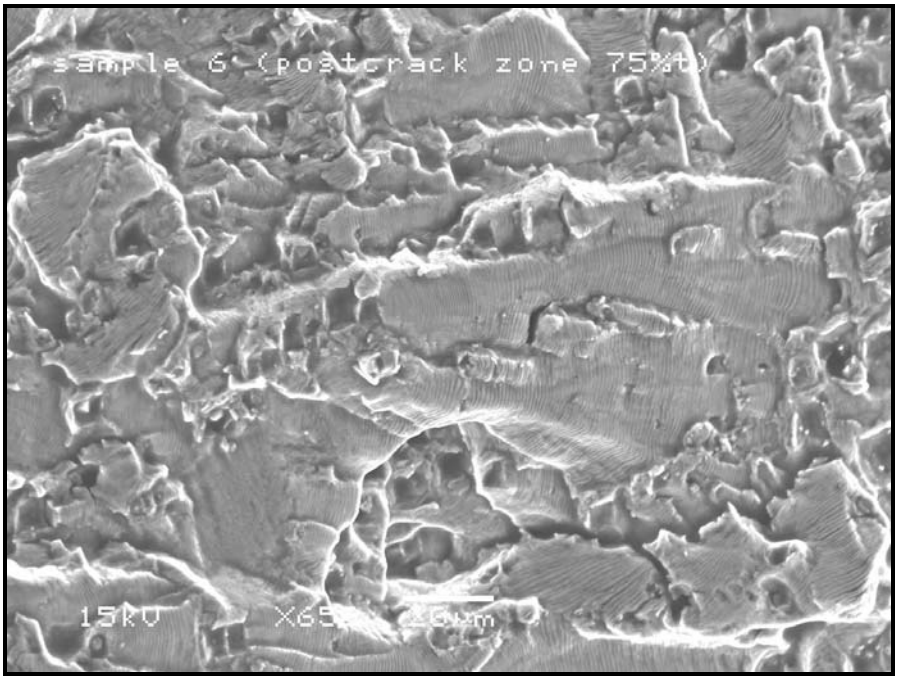

Figure 240: SEM image of sample 6 shows the fracture surface at the post-fatigue crack zone at 75% thickness, 650X. Fatigue striations were observed throughout the post-fatigue crack zone along the 0.16 mm from the pre-fatigue crack zone.

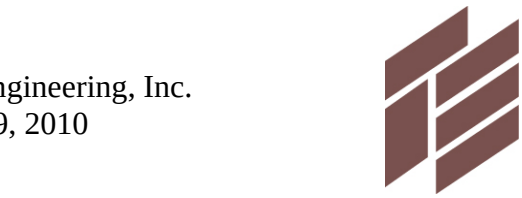

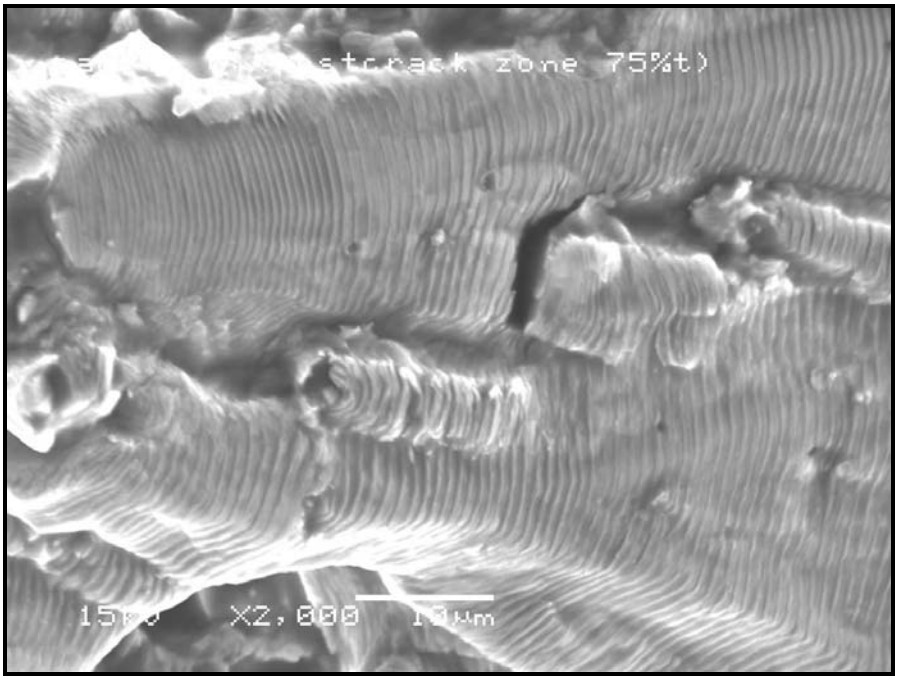

Figure 241: SEM image of sample 6 shows the fracture surface at the post-fatigue crack zone at 75% thickness, 2000X. Fatigue striations were observed throughout the post-fatigue crack zone along the 0.16 mm from the pre-fatigue crack zone.

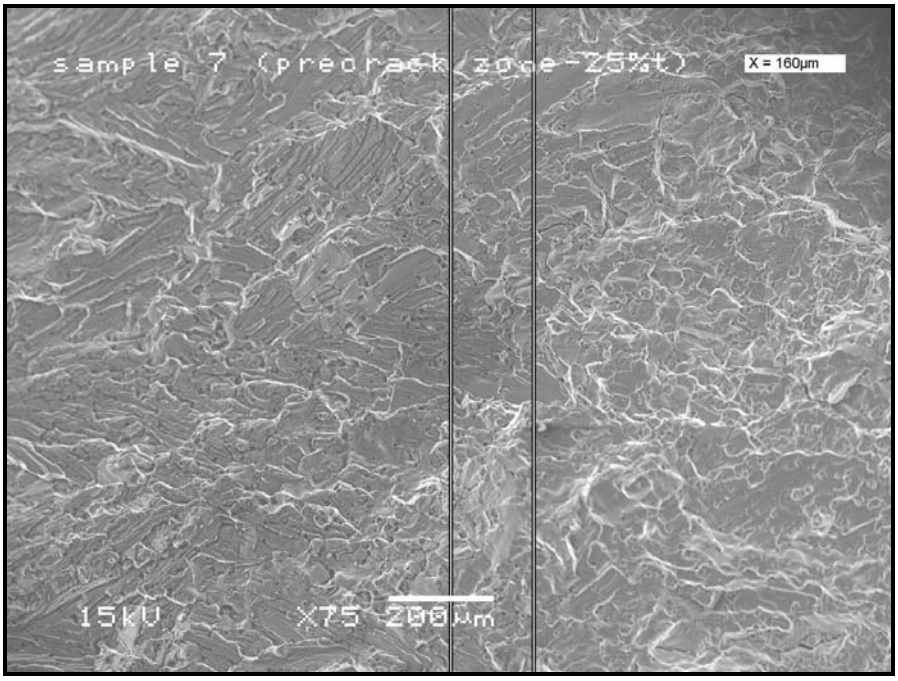

Figure 242: SEM image of sample 7 shows the fracture surface along the 0.16 mm distance from the pre-fatigue crack zone at 25% thickness, 75X. Fatigue was observed throughout the 0.16 mm distance from pre-fatigue crack zone.

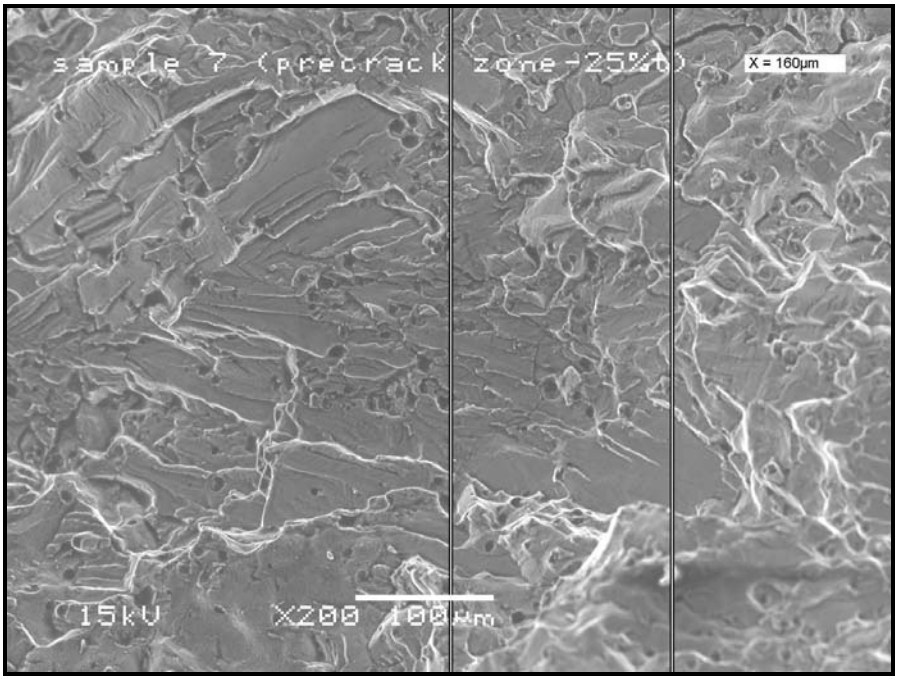

Figure 243: SEM image of sample 7 shows the fracture surface along the 0.16 mm distance from the pre-fatigue crack zone at 25% thickness, 200X. Fatigue was observed throughout the 0.16 mm distance from pre-fatigue crack zone.

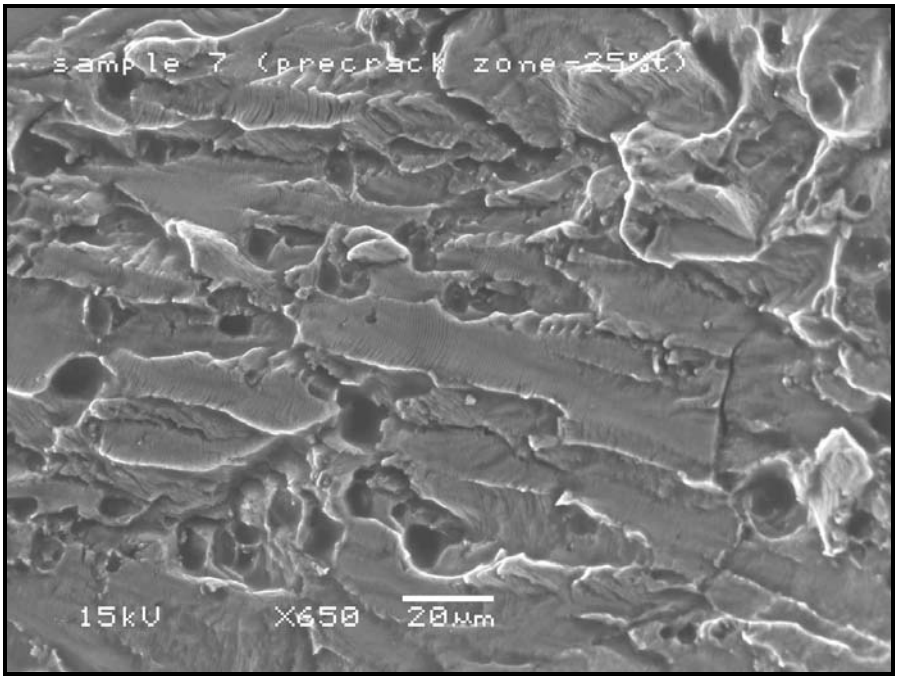

Figure 244: SEM image of sample 7 shows the fracture surface at the pre-fatigue crack zone at 25% thickness, 650X. Fatigue striations were observed throughout the pre-fatigue crack zone.

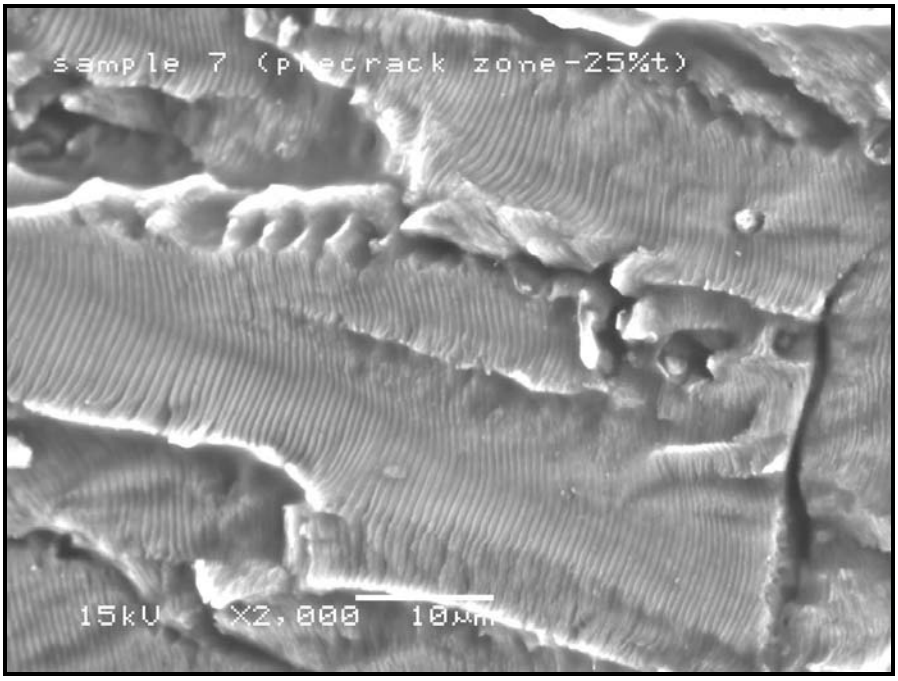

Figure 245: SEM image of sample 7 shows the fracture surface at the pre-fatigue crack zone at 25% thickness, 2000X. Fatigue striations were observed throughout the pre-fatigue crack zone.

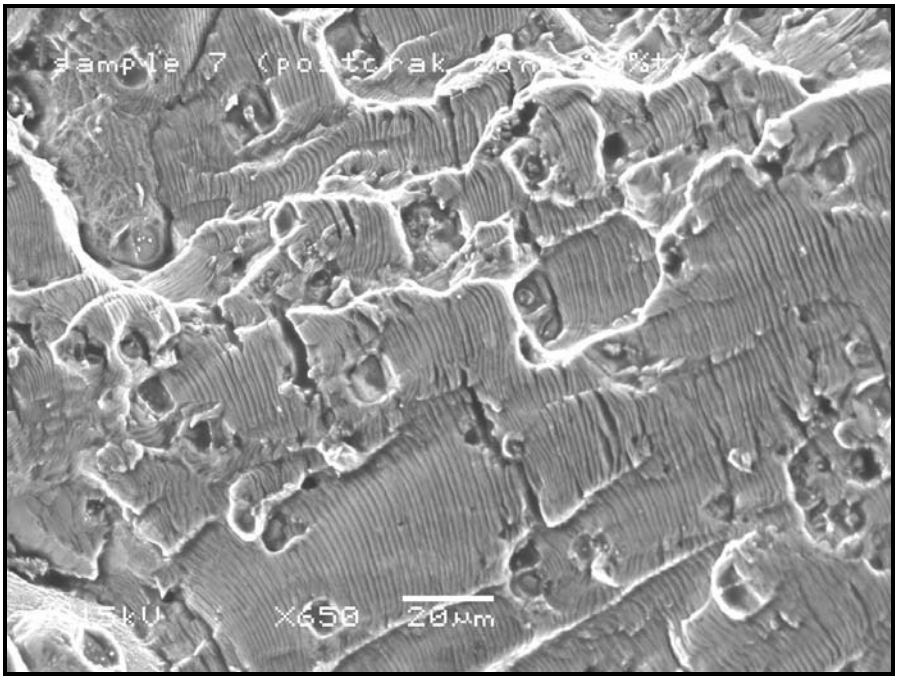

Figure 246: SEM image of sample 7 shows the fracture surface at the post-fatigue crack zone at 25% thickness, 650X. Fatigue striations were observed throughout the post-fatigue crack zone along the 0.16 mm from the pre-fatigue crack zone.

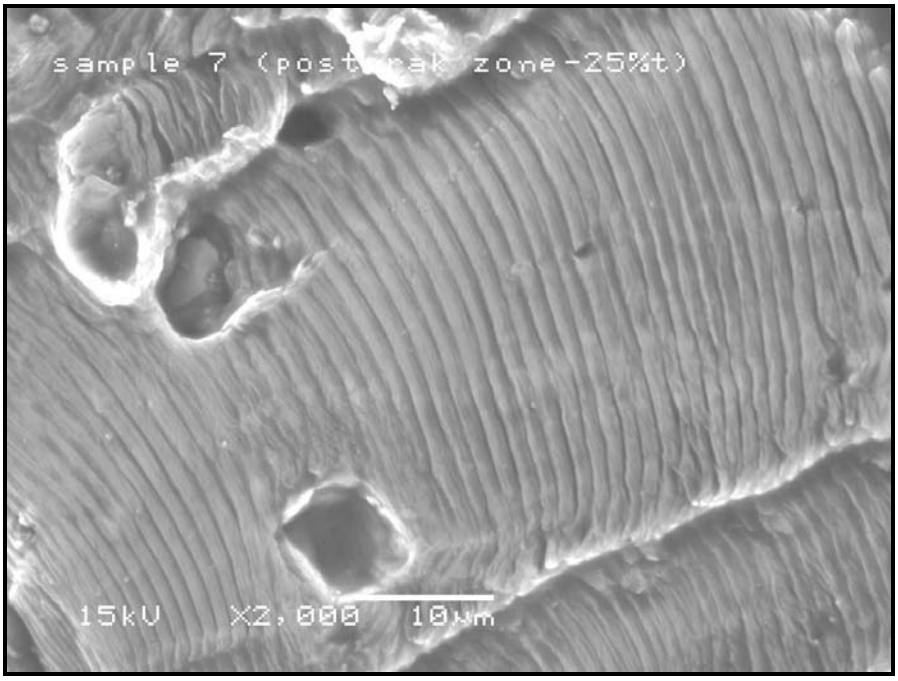

Figure 247: SEM image of sample 7 shows the fracture surface at the post-fatigue crack zone at 25% thickness, 2000X. Fatigue striations were observed throughout the post-fatigue crack zone along the 0.16 mm from the pre-fatigue crack zone.

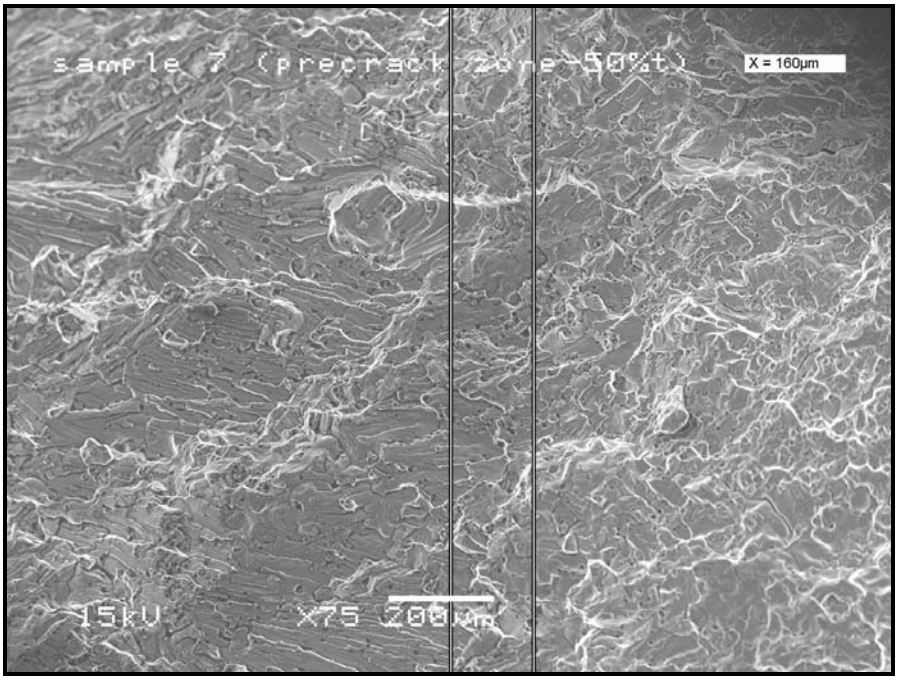

Figure 248: SEM image of sample 7 shows the fracture surface along the 0.16 mm distance from the pre-fatigue crack zone at 50% thickness, 75X. Fatigue was observed throughout the 0.16 mm distance from pre-fatigue crack zone.

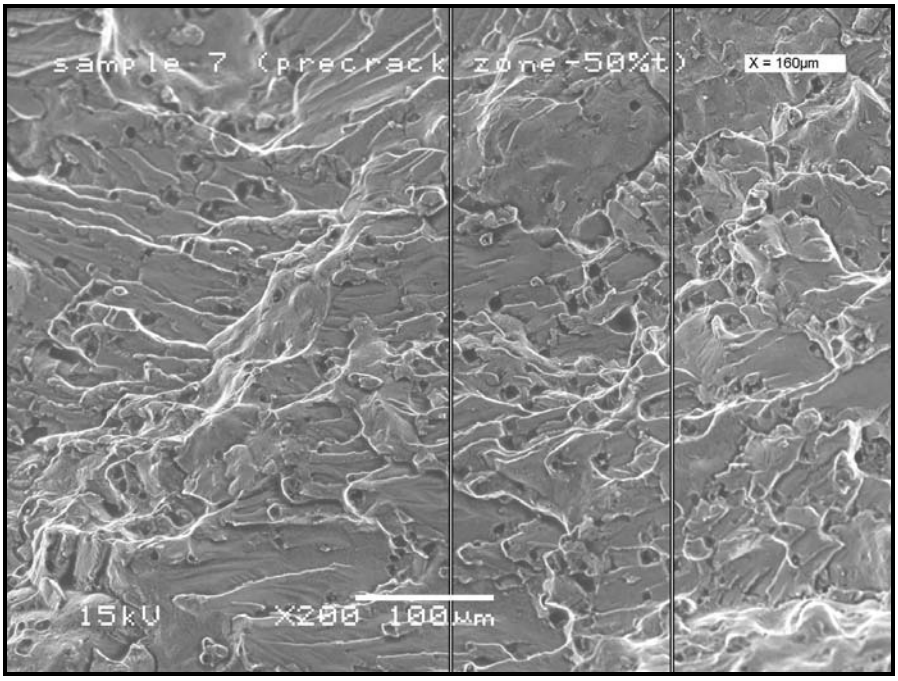

Figure 249: SEM image of sample 7 shows the fracture surface along the 0.16 mm distance from the pre-fatigue crack zone at 50% thickness, 200X. Fatigue was observed throughout the 0.16 mm distance from pre-fatigue crack zone.

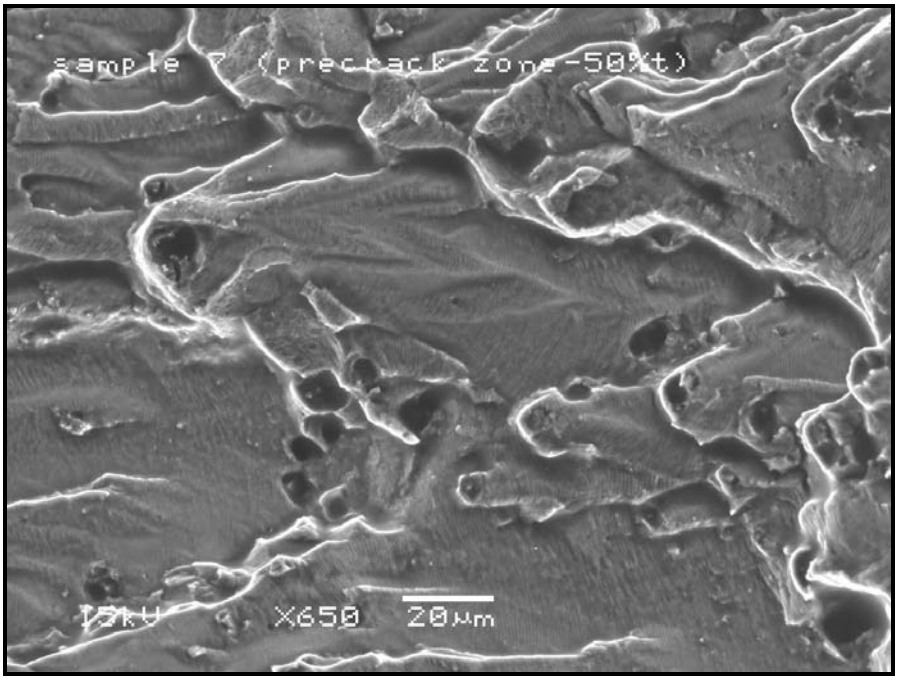

Figure 250: SEM image of sample 7 shows the fracture surface at the pre-fatigue crack zone at 50% thickness, 650X. Fatigue striations were observed throughout the pre-fatigue crack zone.

Figure 251: SEM image of sample 7 shows the fracture surface at the pre-fatigue crack zone at 50% thickness, 2000X. Fatigue striations were observed throughout the pre-fatigue crack zone.

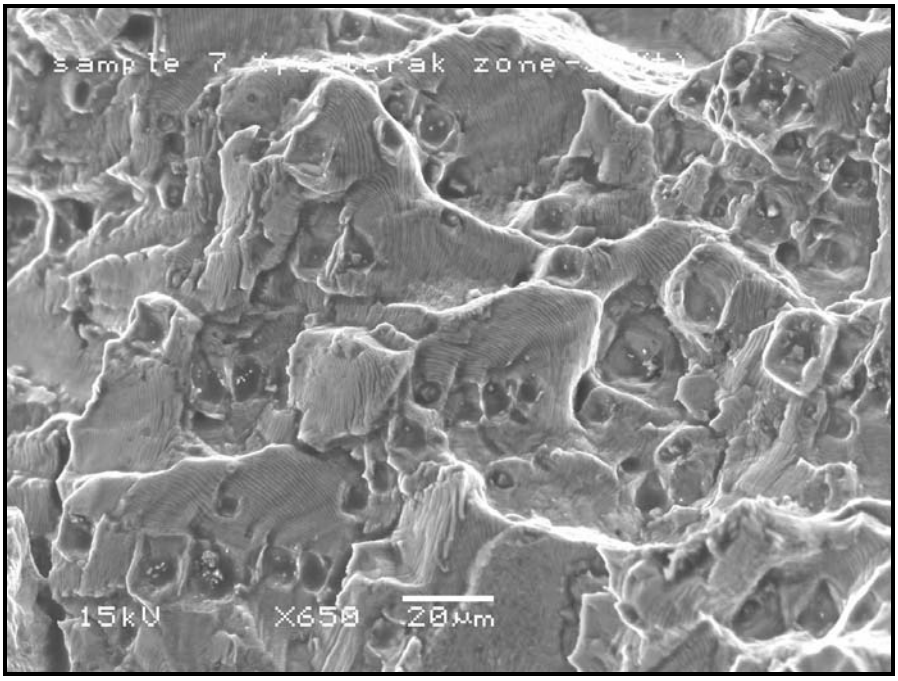

Figure 252: SEM image of sample 7 shows the fracture surface at the post-fatigue crack zone at 50% thickness, 650X. Fatigue striations were observed throughout the post-fatigue crack zone along the 0.16 mm from the pre-fatigue crack zone.

Figure 253: SEM image of sample 7 shows the fracture surface at the post-fatigue crack zone at 50% thickness, 2000X. Fatigue striations were observed throughout the post-fatigue crack zone along the 0.16 mm from the pre-fatigue crack zone.

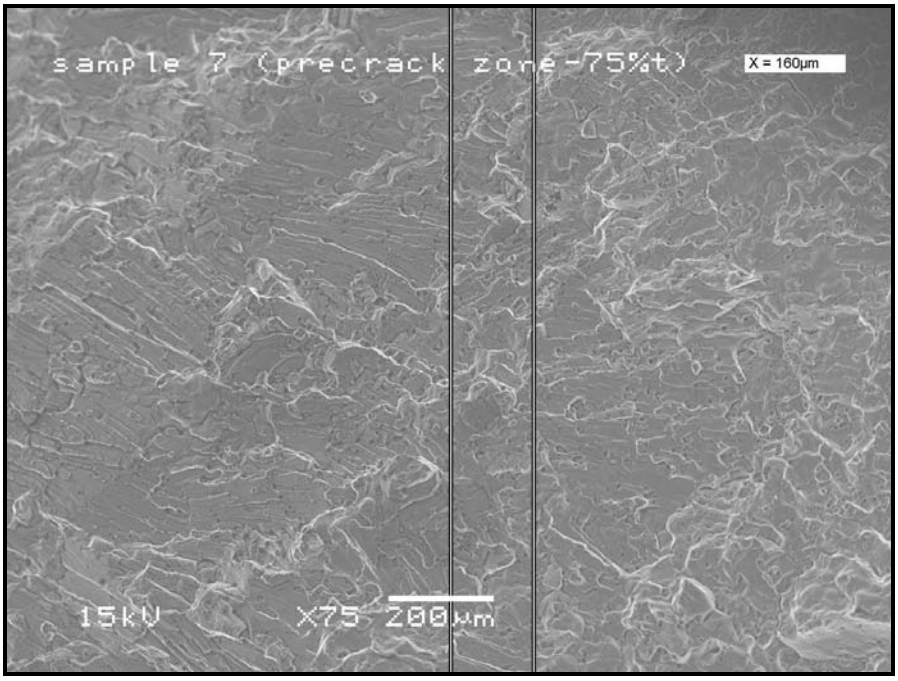

Figure 254: SEM image of sample 7 shows the fracture surface along the 0.16 mm distance from the pre-fatigue crack zone at 75% thickness, 75X. Fatigue was observed throughout the 0.16 mm distance from pre-fatigue crack zone.

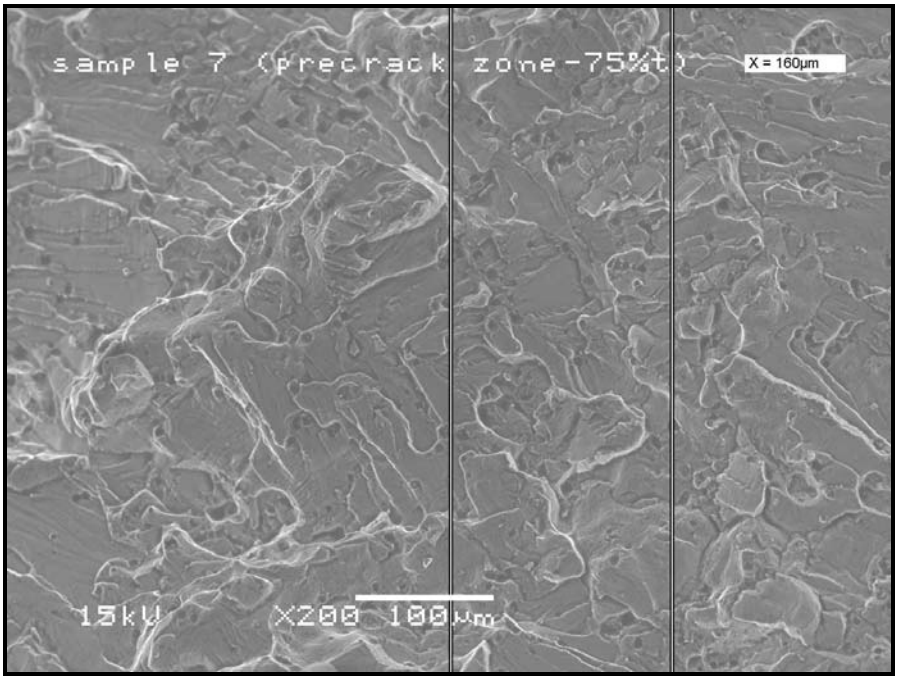

Figure 255: SEM image of sample 7 shows the fracture surface along the 0.16 mm distance from the pre-fatigue crack zone at 75% thickness, 200X. Fatigue was observed throughout the 0.16 mm distance from pre-fatigue crack zone.

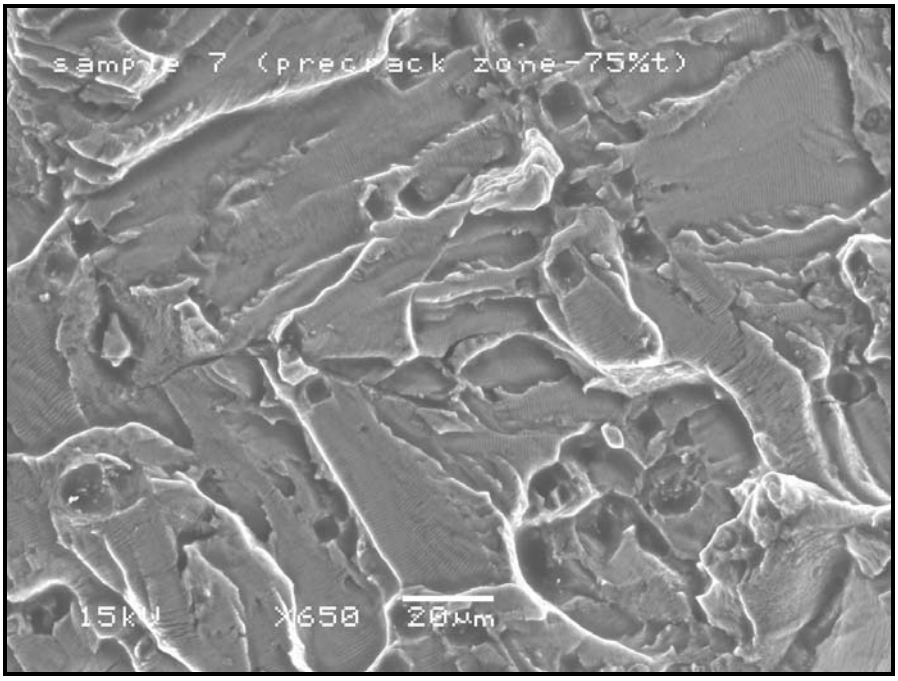

Figure 256: SEM image of sample 7 shows the fracture surface at the pre-fatigue crack zone at 75% thickness, 650X. Fatigue striations were observed throughout the pre-fatigue crack zone.

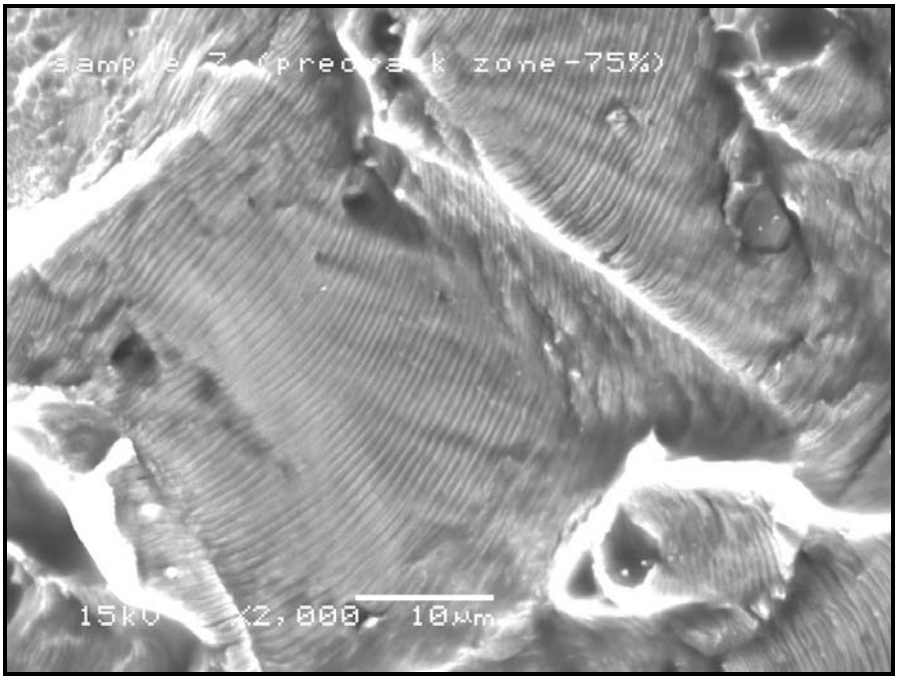

Figure 257: SEM image of sample 7 shows the fracture surface at the pre-fatigue crack zone at 75% thickness, 2000X. Fatigue striations were observed throughout the pre-fatigue crack zone.

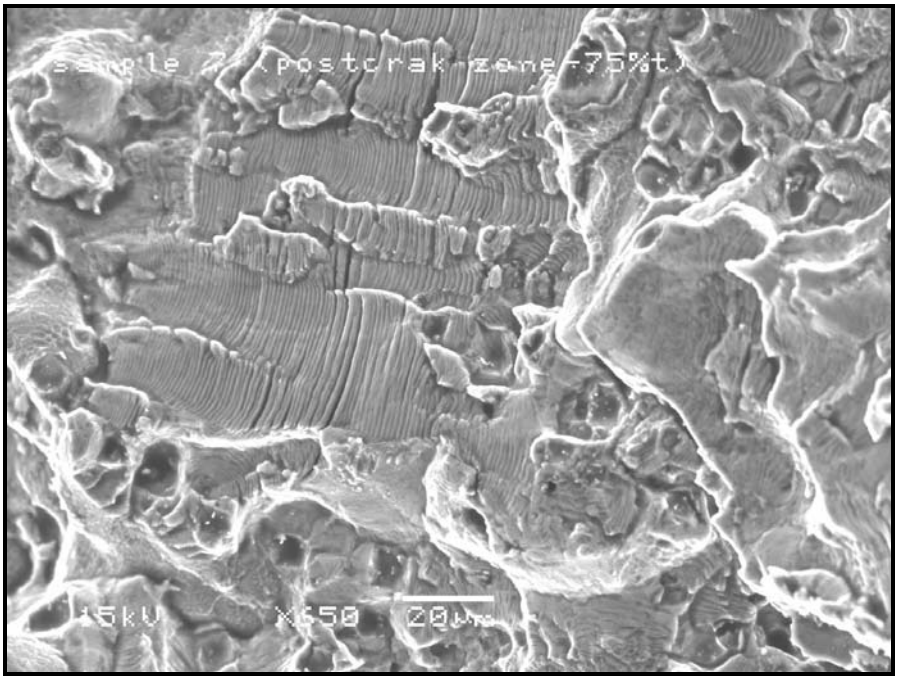

Figure 258: SEM image of sample 7 shows the fracture surface at the post-fatigue crack zone at 75% thickness, 650X. Fatigue striations were observed throughout the post-fatigue crack zone along the 0.16 mm from the pre-fatigue crack zone.

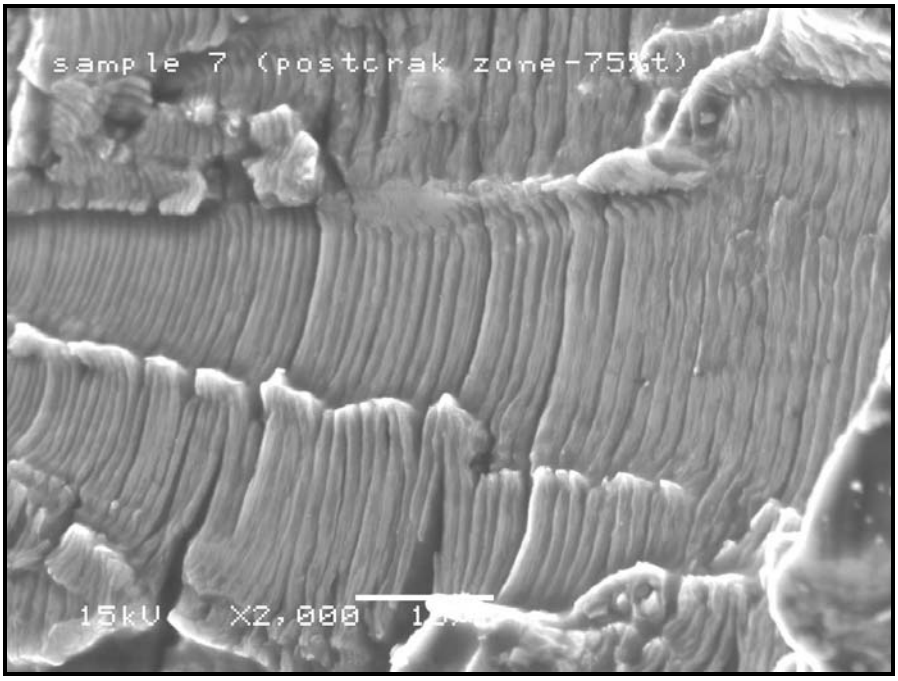

Figure 259: SEM image of sample 7 shows the fracture surface at the post-fatigue crack zone at 75% thickness, 2000X. Fatigue striations were observed throughout the post-fatigue crack zone along the 0.16 mm from the pre-fatigue crack zone.

Figure 260: Shows the section of the neck region of cylinder # AR0119524 cut for fractographic analysis.

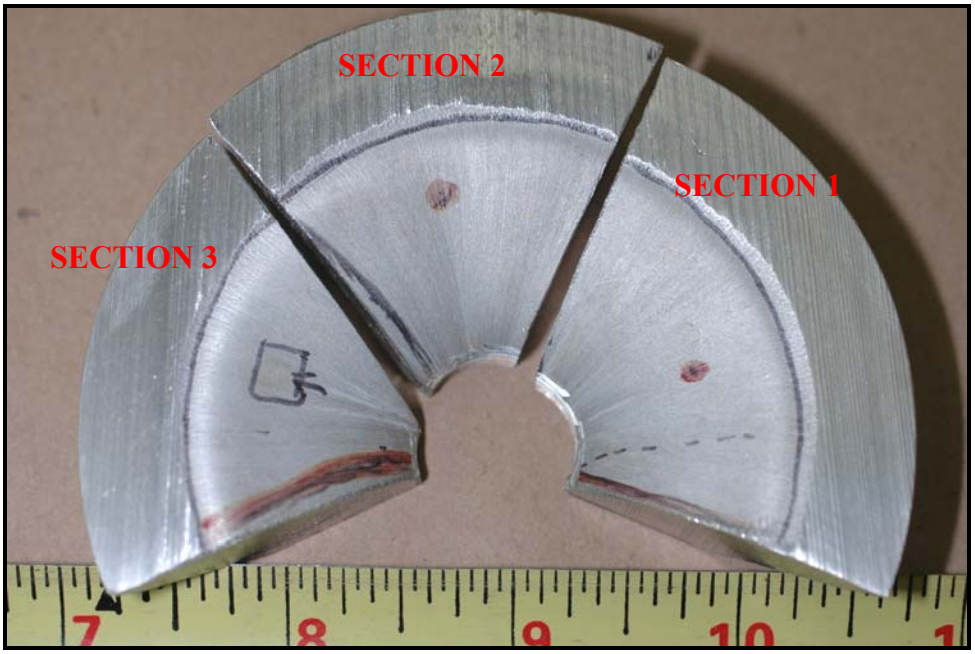

Figure 261: Shows the section of the neck region of cylinder # AR0119524 cut for fractographic analysis. Section 1 was used for SEM observation of fracture surface. Sections 2 and 3 were used for metallographic analysis.

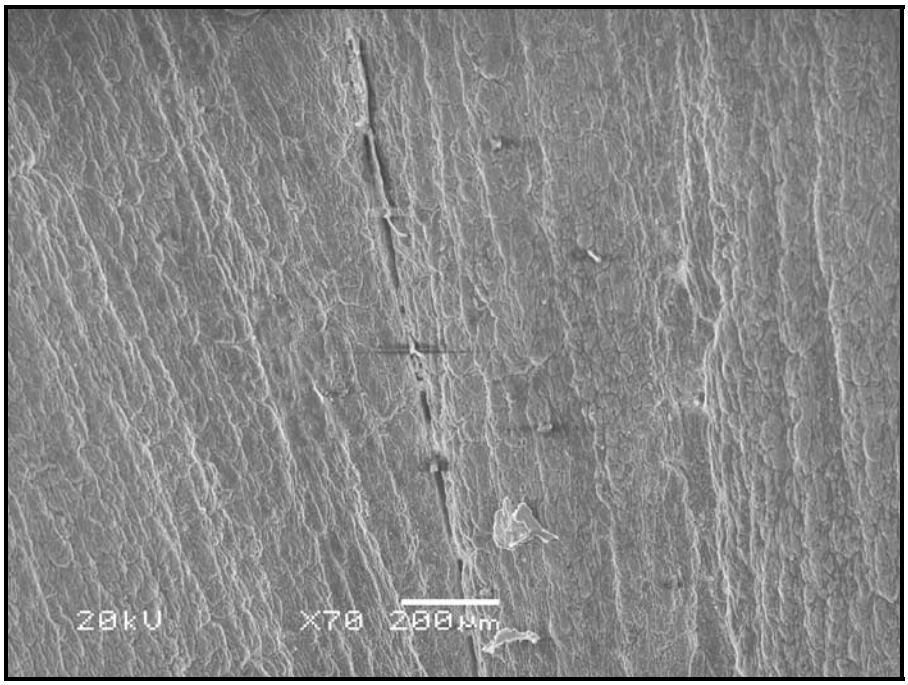

Figure 262: Shows the crack in the neck forming folds of section 1 from cylinder # AR0119524 identified in Figure 261. Magnification: 70X

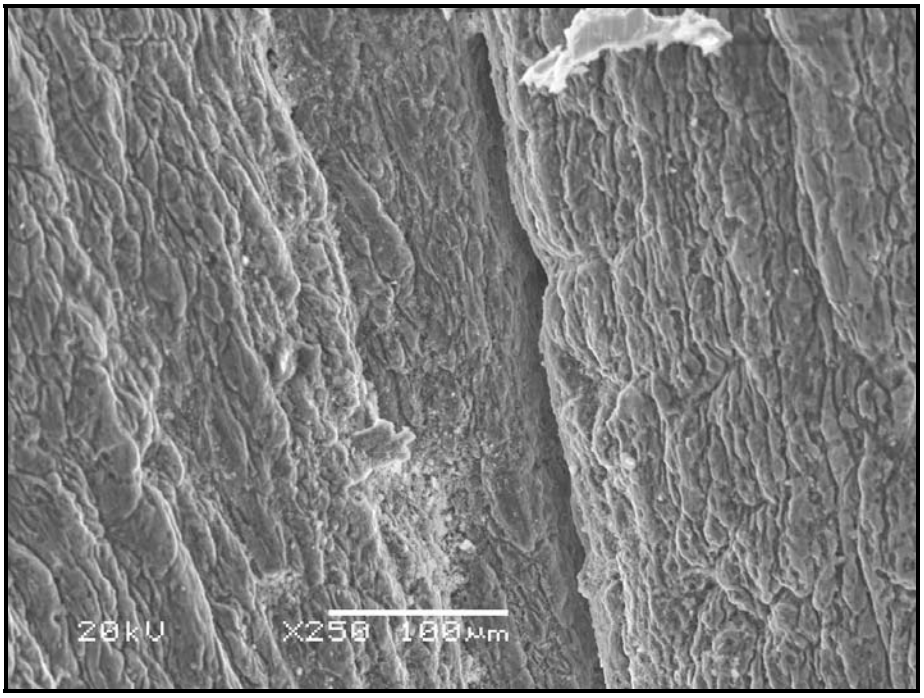

Figure 263: Shows the crack in the neck forming folds of section 1 from cylinder # AR0119524 identified in Figure 261. Magnification: 250X

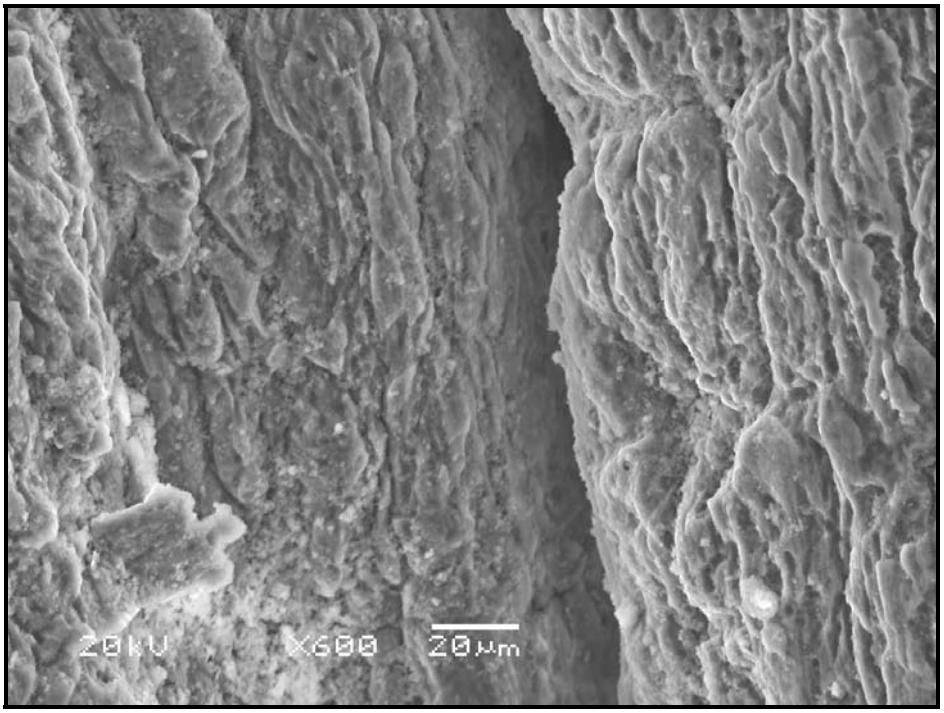

Figure 264: Shows the crack in the neck forming folds of section 1 from cylinder # AR0119524 identified in Figure 261. Magnification: 600X

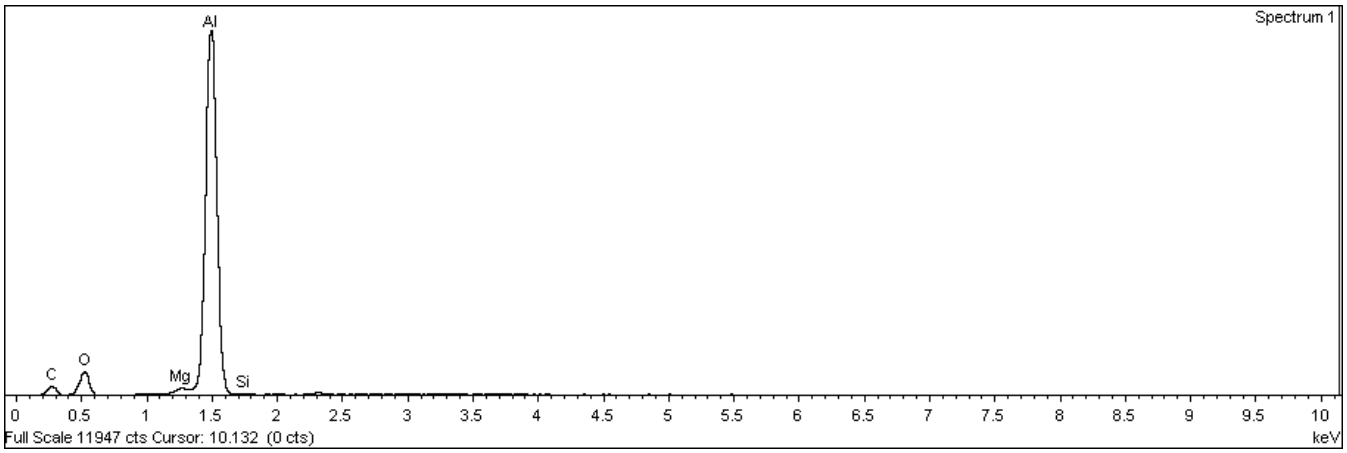

Figure 265: Shows the EDS spectra of the deposit observed on the fracture surface.

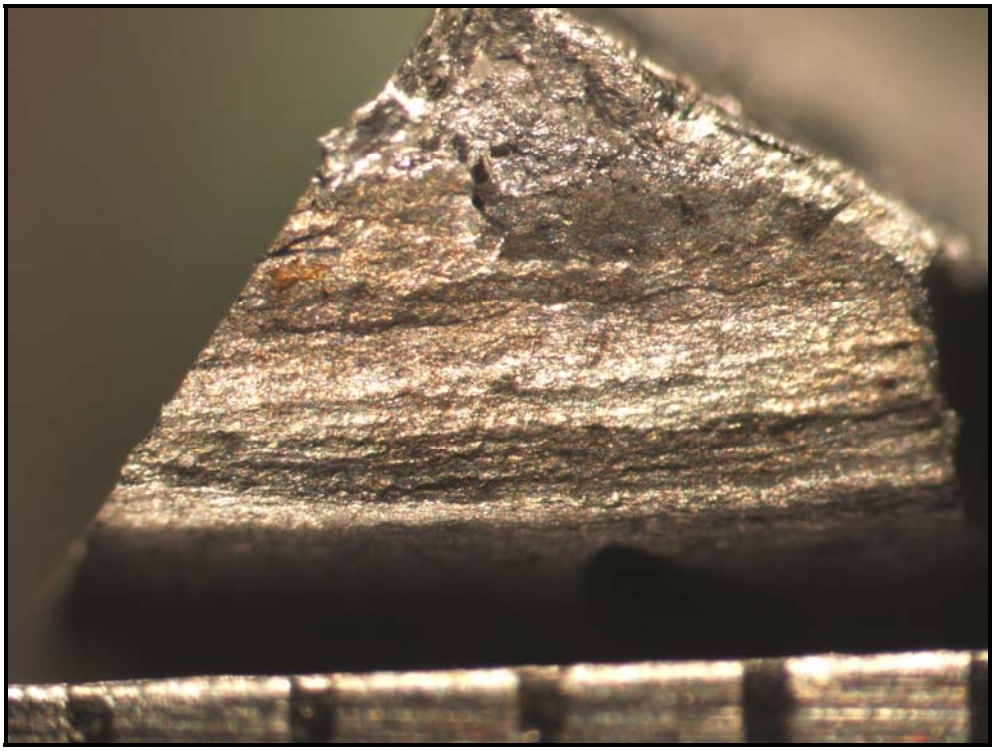

Figure: 266: Stereoscope image of the fracture surface of the after cleaning. Shows the surface is damaged and has rubbing marks.

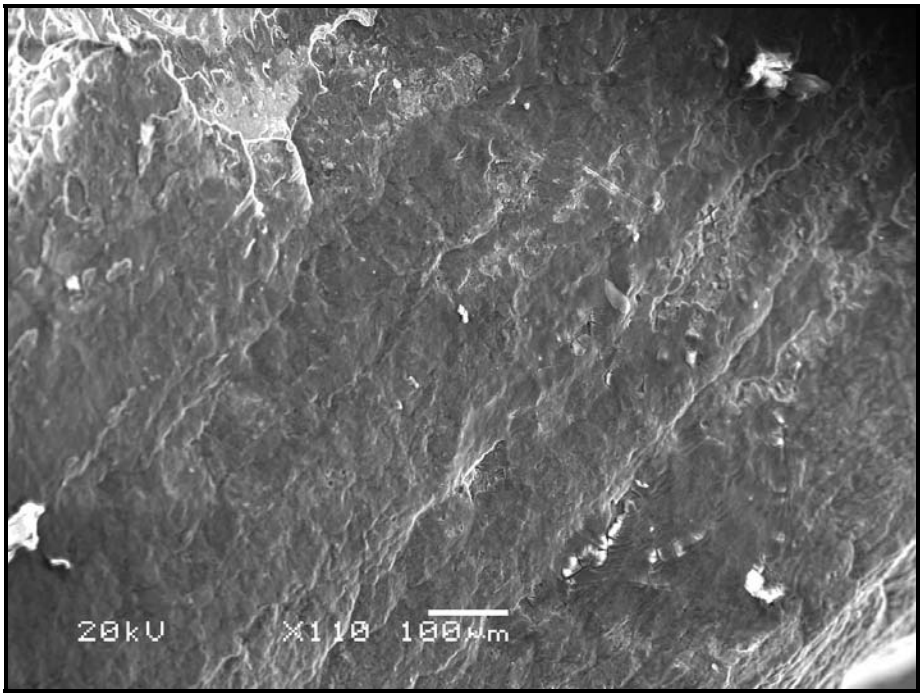

Figure 267: SEM image of the fracture surface after cleaning shows the fracture surface is damaged has rubbing marks and an oxide layer. Magnification: 110X

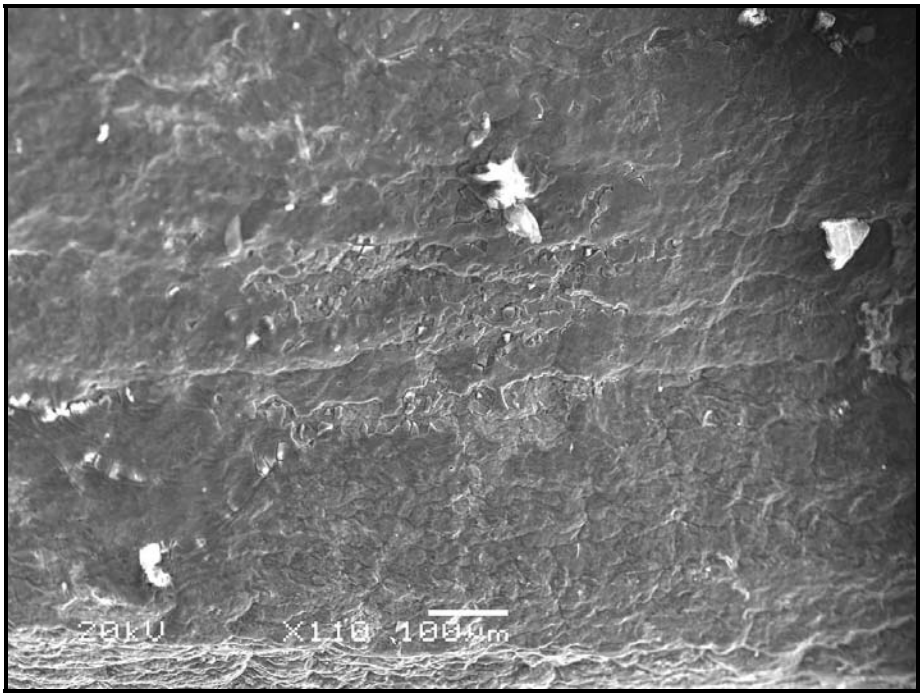

Figure 268: SEM image of the fracture surface after cleaning shows the fracture surface is damaged has rubbing marks and an oxide layer. Magnification: 110X

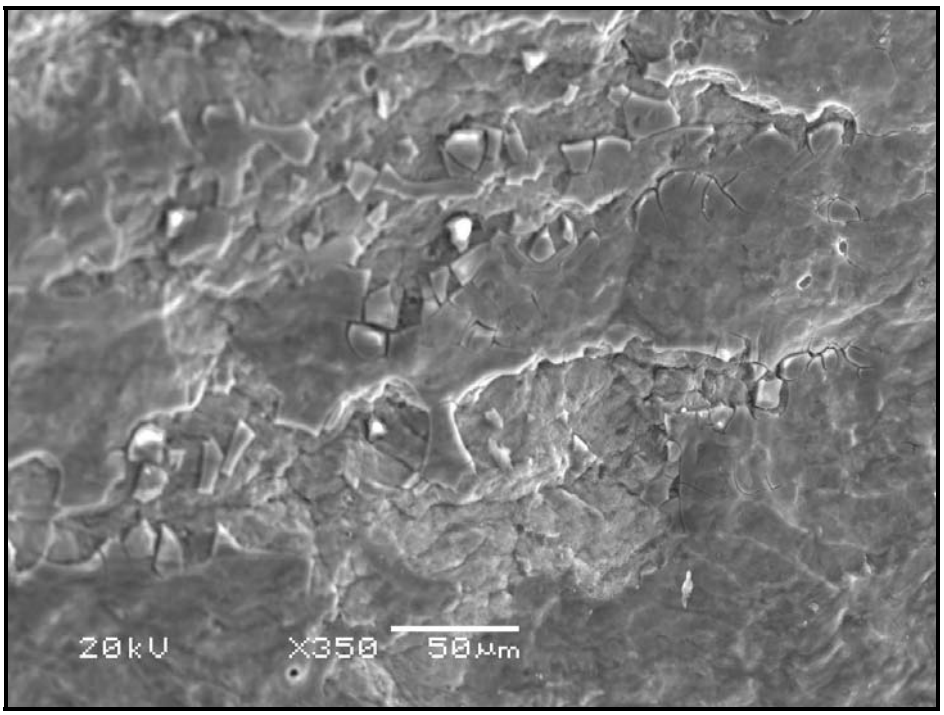

Figure 269: SEM image of the fracture surface after cleaning shows the fracture surface is damaged has rubbing marks and an oxide layer. Magnification: 350X

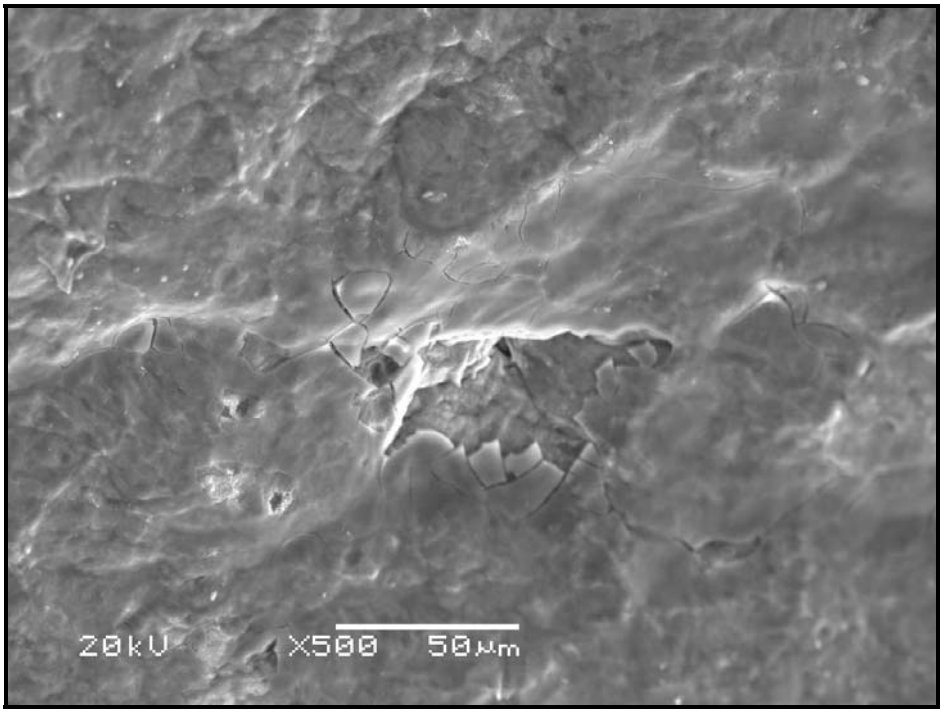

Figure 270: SEM image of the fracture surface after cleaning shows the fracture surface is damaged has rubbing marks and an oxide layer. Magnification: 500X

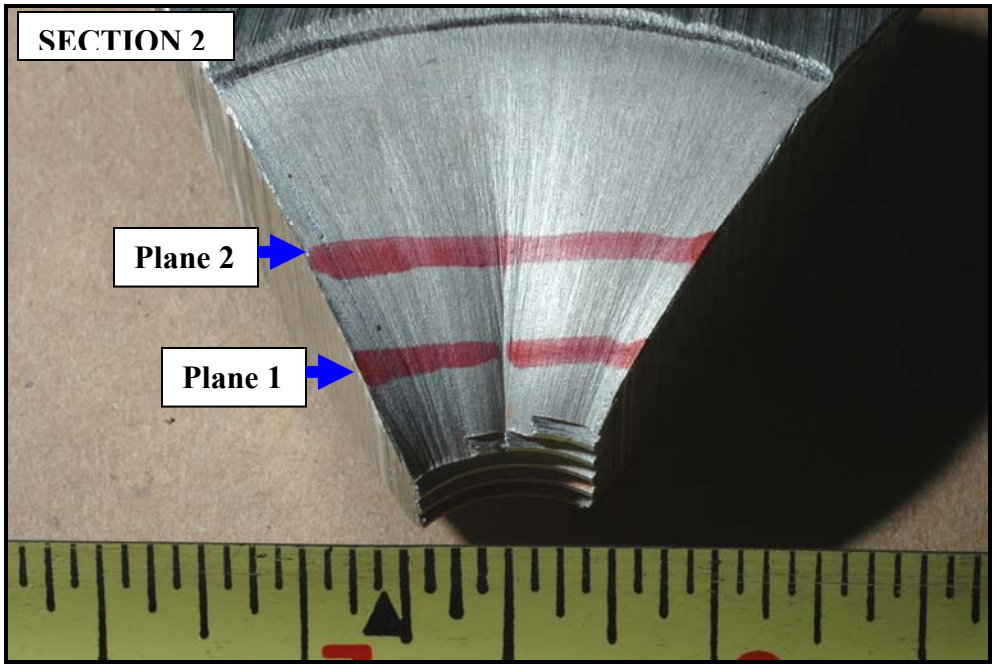

Figure 271: Shows the section 2 from cylinder # AR0119524. This section was cut on plane 1 and plane 2 and mounted for microstructural observation.

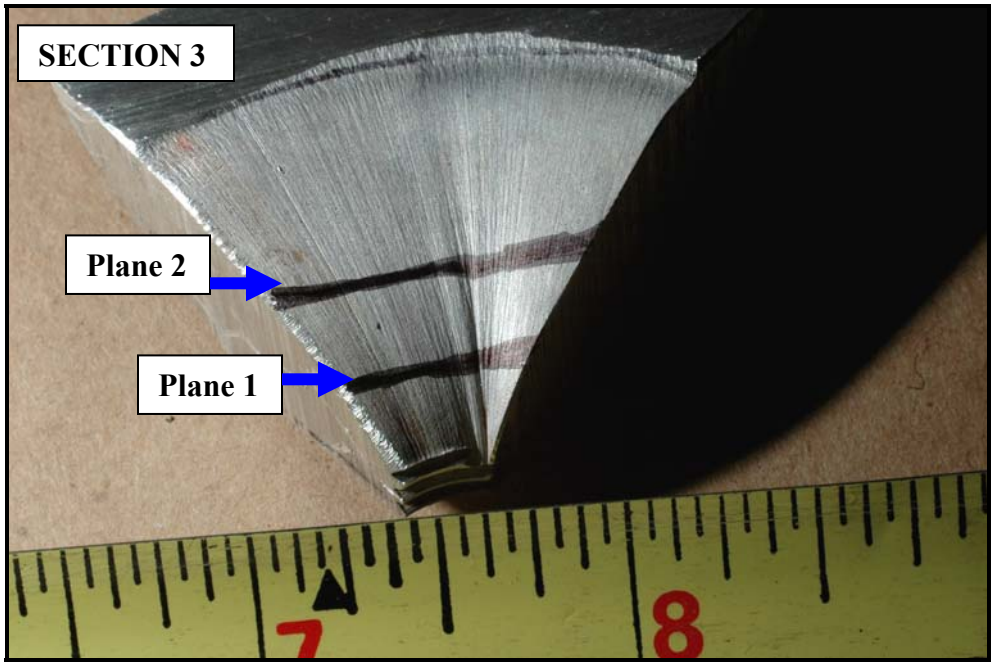

Figure 272: Shows the section 2 from cylinder # AR0119524. This section was cut on plane 1 and plane 2 and mounted for microstructural observation.

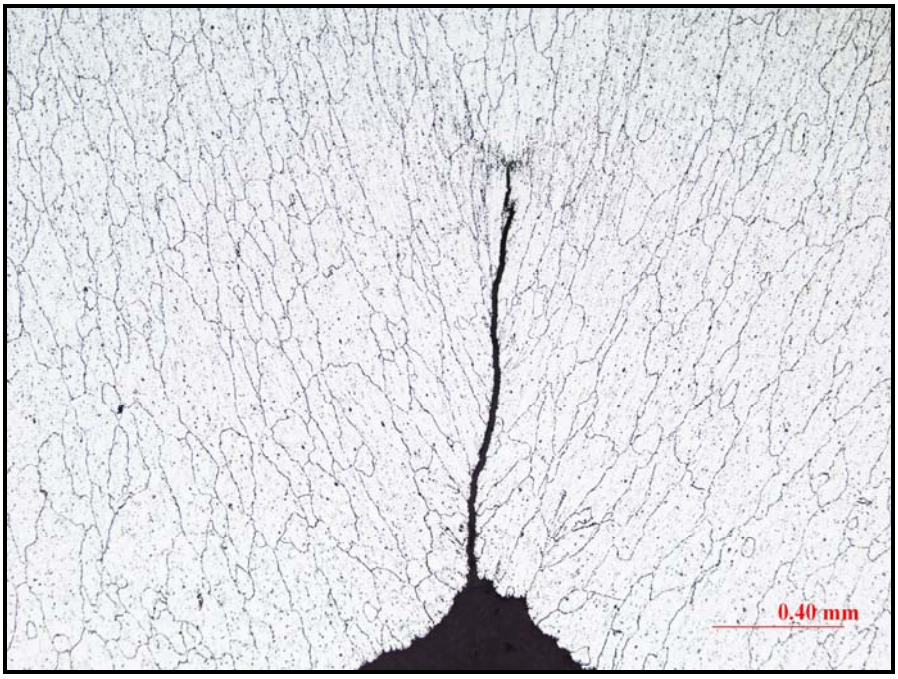

Figure 273: Shows the crack in the neck forming fold propagating from the ID to the OD in plane 1 of section 1. Magnification: 50X Etchant: Keller's Etch

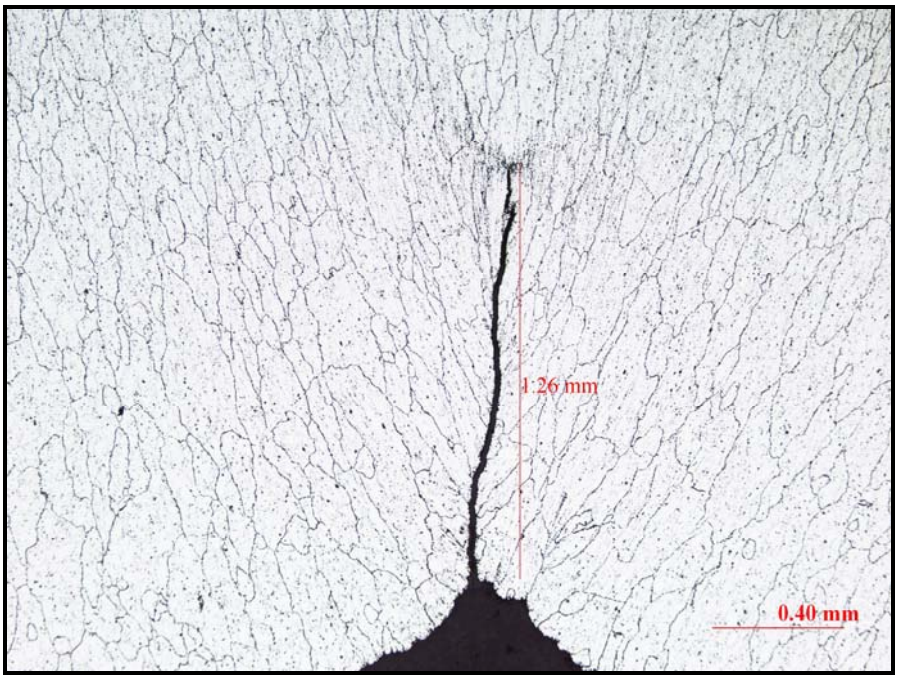

Figure 274: Shows the crack in the neck forming fold propagating from the ID to the OD in plane 1 of section 1. The crack is 1.26 mm deep. Magnification: 50X Etchant: Keller's Etch

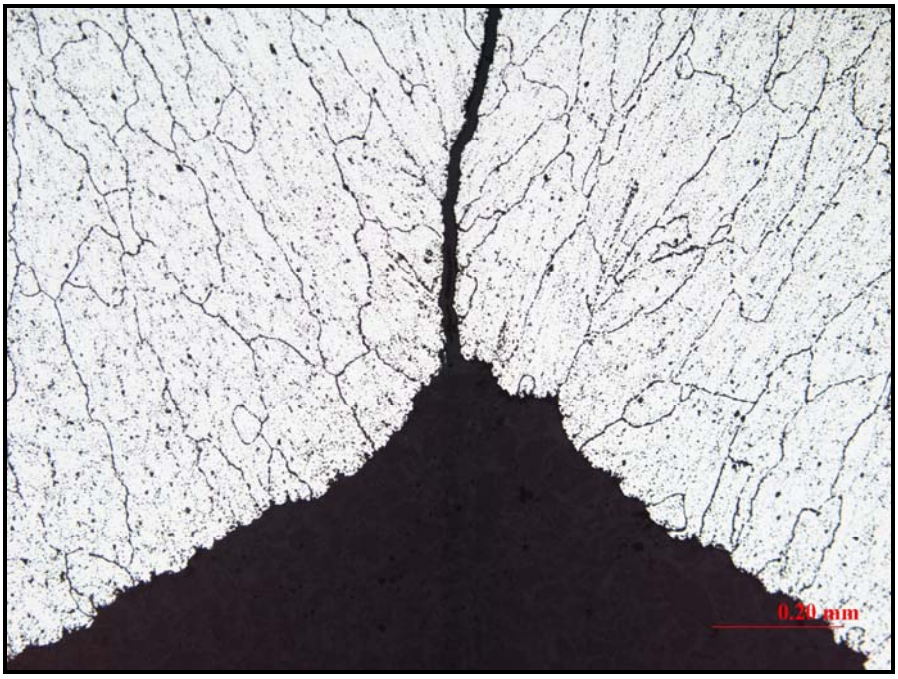

Figure 275: Shows the crack in the neck forming fold propagating from the ID to the OD in plane 1 of section 1. Magnification: 100X Etchant: Keller's Etch

Figure 276: Shows the crack in the neck forming fold propagating from the ID to the OD in plane 1 of section 1. Magnification: 100X Etchant: Keller's Etch

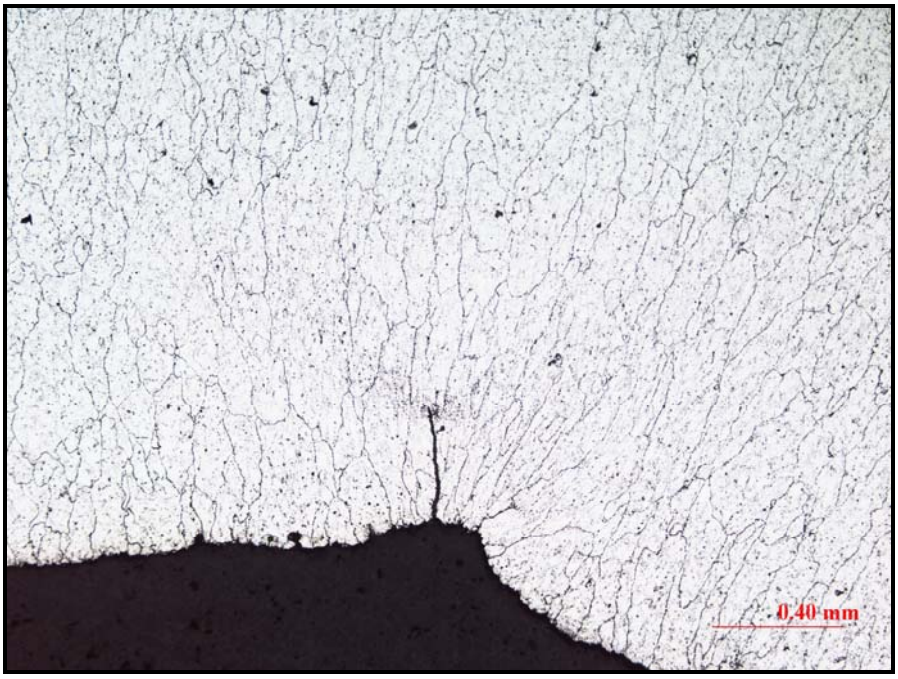

Figure 277: Shows the crack in the neck forming fold propagating from the ID to the OD in plane 2 of section 1. Magnification: 50X Etchant: Keller's Etch

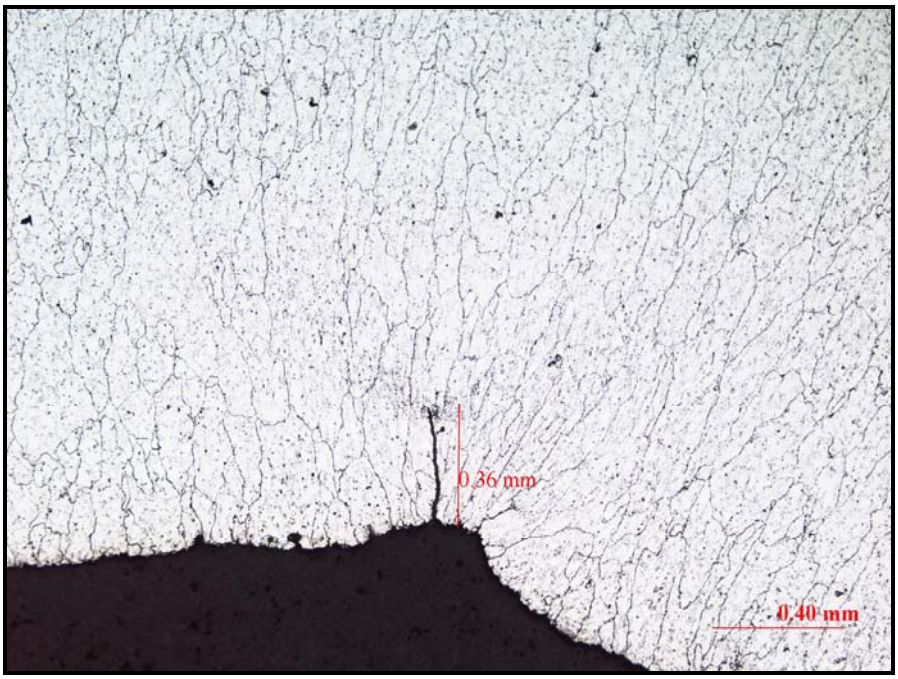

Figure 278: Shows the crack in the neck forming fold propagating from the ID to the OD in plane 2 of section 1. The crack is 0.36 mm deep. Magnification: 50X Etchant: Keller's Etch

Figure 279: Shows the crack in the neck forming fold propagating from the ID to the OD in plane 2 of section 1. Magnification: 100X Etchant: Keller's Etch

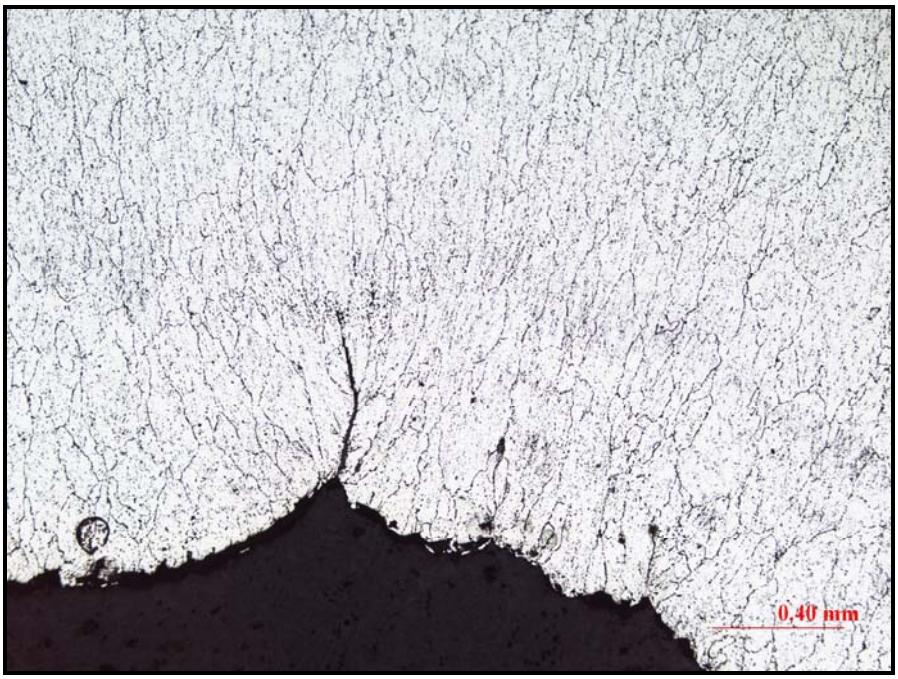

Figure 280: Shows the crack in the neck forming fold propagating from the ID to the OD in plane 1 of section 2. Magnification: 50X Etchant: Keller's Etch

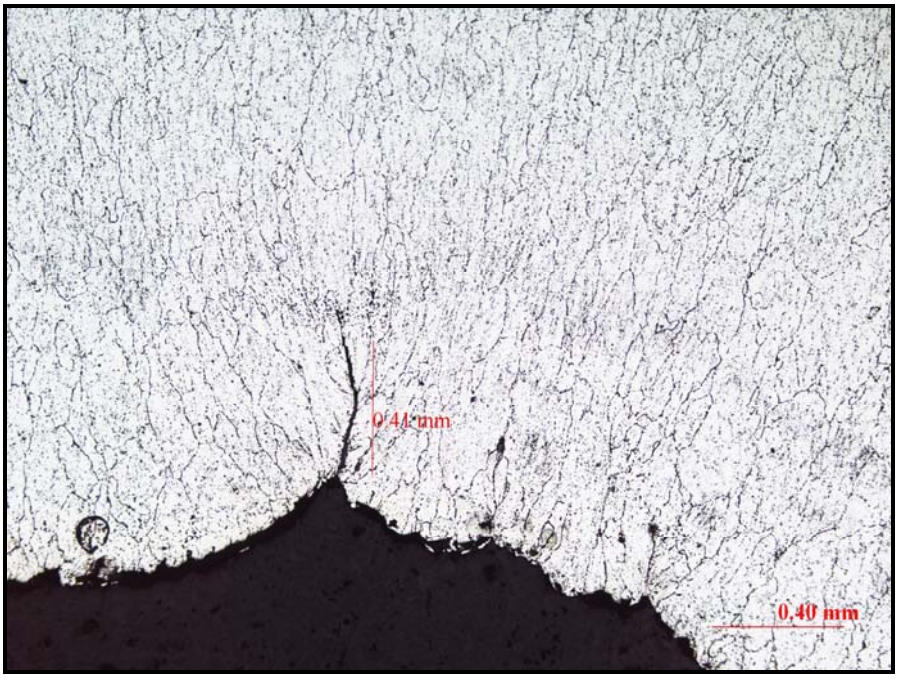

Figure 281: Shows the crack in the neck forming fold propagating from the ID to the OD in plane 1 of section 2. The crack is 0.41 mm deep. Magnification: 50X Etchant: Keller's Etch

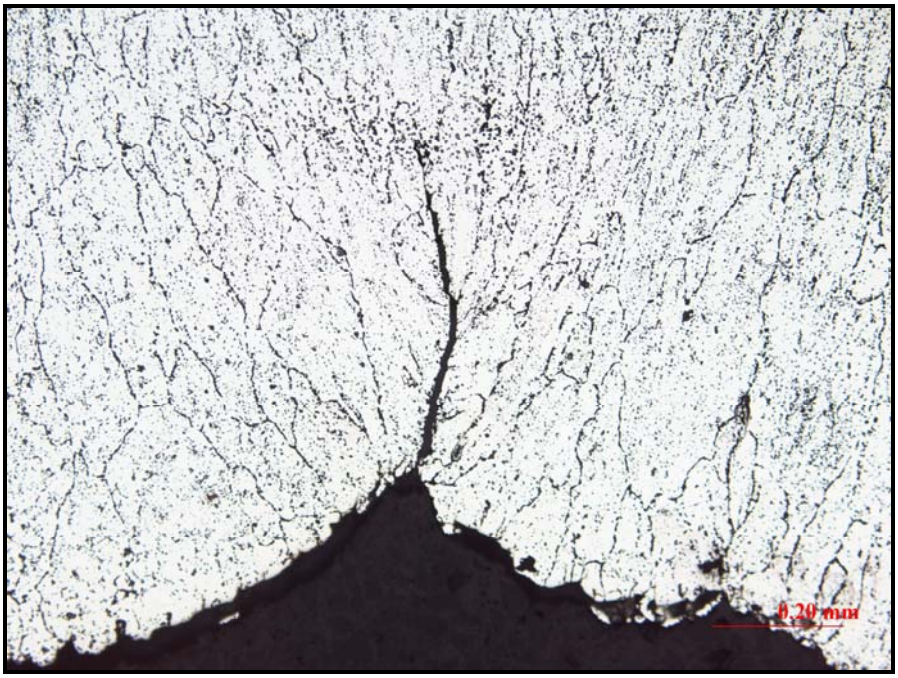

Figure 282: Shows the crack in the neck forming fold propagating from the ID to the OD in plane 1 of section 2. Magnification: 100X Etchant: Keller's Etch

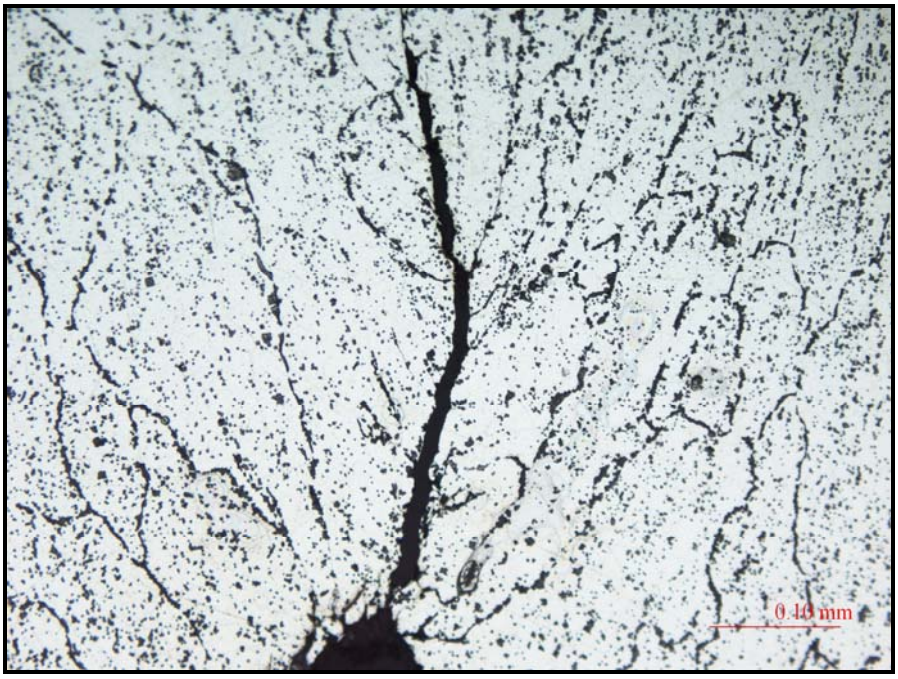

Figure 283: Shows the crack in the neck forming fold propagating from the ID to the OD in plane 1 of section 2. Magnification: 200X Etchant: Keller's Etch

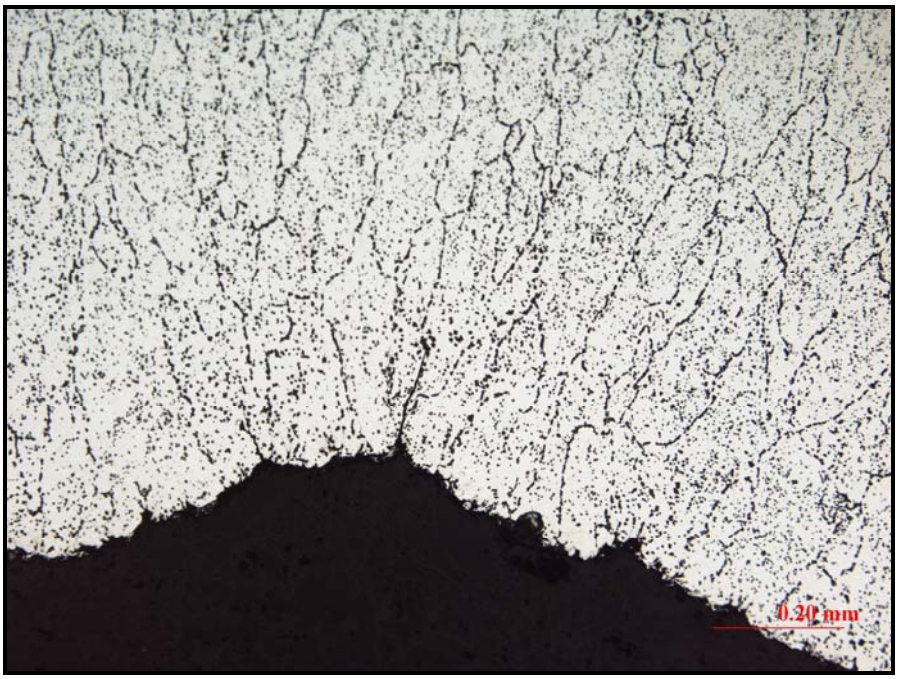

Figure 284: Shows the crack in the neck forming fold propagating from the ID to the OD in plane 2 of section 2. Magnification: 50X Etchant: Keller's Etch

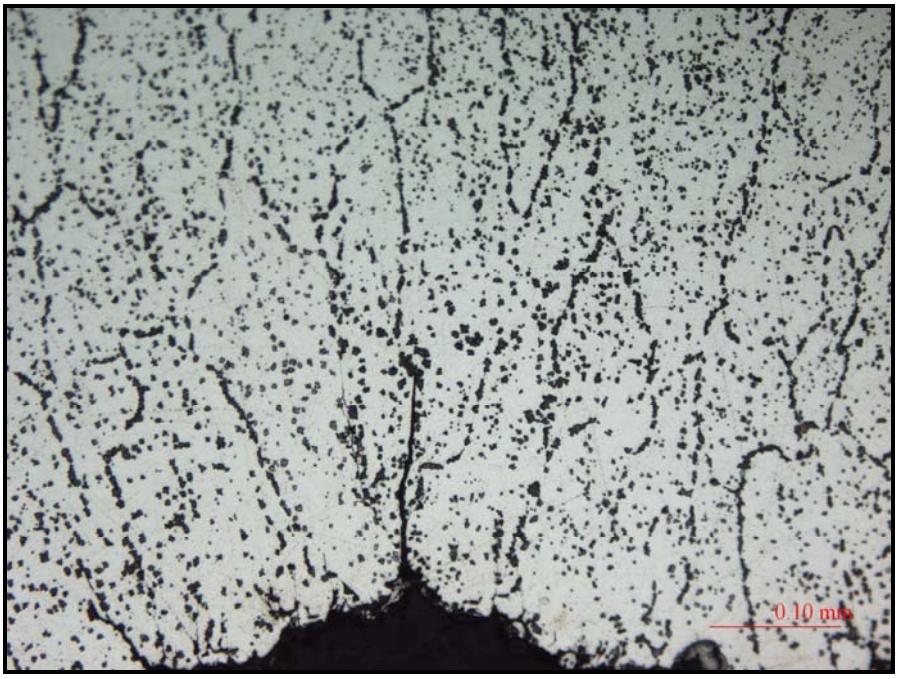

Figure 285: Shows the crack in the neck forming fold propagating from the ID to the OD in plane 2 of section 2. Magnification: 200X Etchant: Keller's Etch

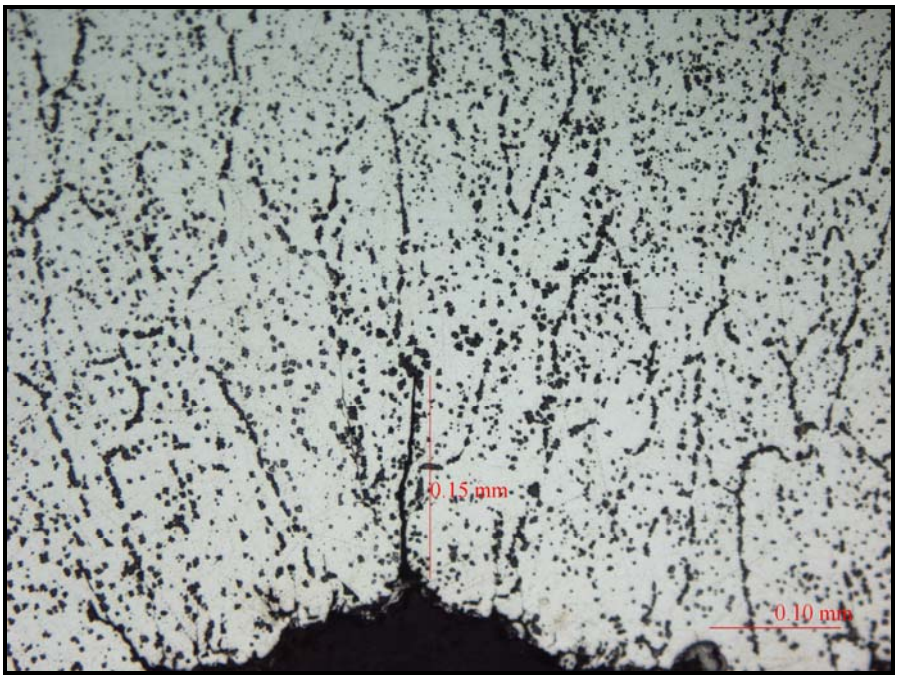

Figure 286: Shows the crack in the neck forming fold propagating from the ID to the OD in plane 2 of section 2. The crack is 0.15 mm deep. Magnification: 200X Etchant: Keller's Etch

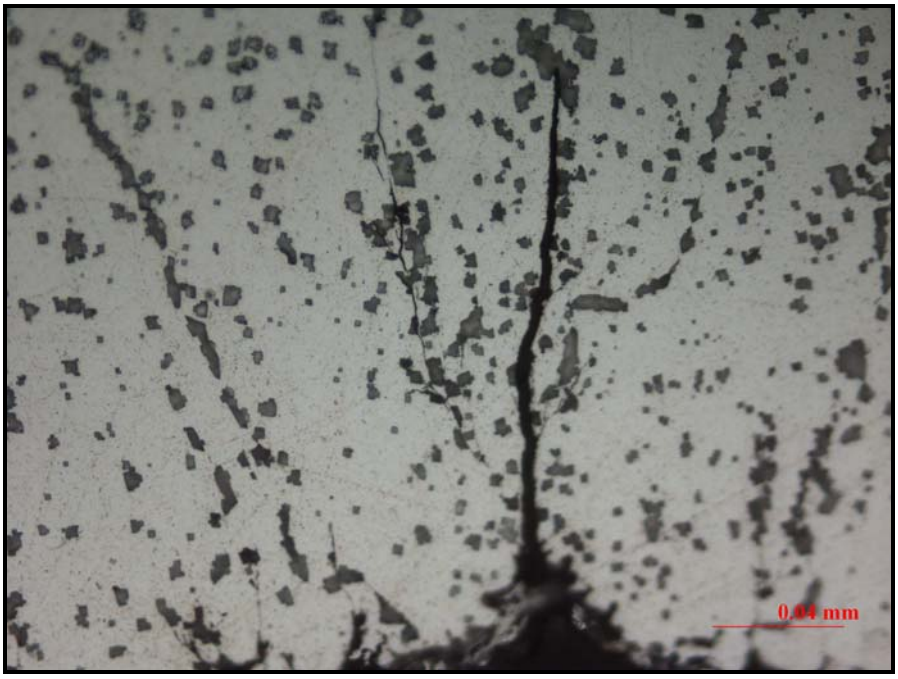

Figure 287: Shows the crack in the neck forming fold propagating from the ID to the OD in plane 2 of section 2. Magnification: 500X Etchant: Keller's Etch